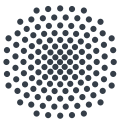

Universität Stuttgart

Quantum Fluctuations and Appearance of Supersolidity in Confined Ultracold Atomic Gases

Von der Fakultät Mathematik und Physik der Universität Stuttgart
zur Erlangung der Würde eines Doktors der Naturwissenschaften
(Dr. rer. nat.) genehmigte Abhandlung

vorgelegt von

Tobias Ilg

aus Tuttlingen

Hauptberichter:	Prof. Dr. Hans Peter Büchler
Mitberichter:	Prof. Dr. Jörg Main
Prüfungsvorsitzender:	Prof. Dr. Tilman Pfau
Tag der mündlichen Prüfung:	30.06.2023

Institut für Theoretische Physik III
Universität Stuttgart

2023

Abstract

In this thesis, we study phenomena in weakly interacting dilute bosonic gases, which evade a mean-field treatment such that the description requires the inclusion of quantum fluctuations. While the beyond-mean-field corrections for the uniform weakly interacting Bose gas with short-range interactions were already derived in the 1950s, the recent observation of droplets in both dipolar quantum gases as well as in Bose-Bose mixtures sparked new interest in the field. For these systems, the interplay of attractive and repulsive interactions leads to a vanishing mean-field contribution. The beyond-mean-field effects become dominant and stabilize the gas against the collapse. Thus, for a quantitative description of the experimental observations, the beyond-mean-field corrections have to be determined with high precision. Despite the inhomogeneous and anisotropic character of the droplets, the analysis has mostly been based on the local-density approximation. In dipolar Bose gases, the stabilization of the gas due to quantum fluctuations not only leads to the formation of droplets but also allows for a supersolid phase, first observed in one-dimensional geometries. The confinement in combination with the anisotropic long-range dipolar interactions leads to a roton spectrum in the superfluid. By increasing the relative strength of the dipolar interaction, the system exhibits a roton instability, which results in the formation of arrays of droplets. These arrays are phase coherent and feature an additional Goldstone mode due to the spontaneously broken translational symmetry, demonstrating their genuine supersolidity. The theoretical description of the supersolid state relies on the extended Gross-Pitaevskii equation. While this allows for reliable results in finite size systems, accessing the thermodynamic limit is difficult. In addition, it is well-established that quantum fluctuations strongly influence spontaneous symmetry breaking in one dimension, which puts into question whether the use of the extended Gross-Pitaevskii formalism is justified for one-dimensional supersolids.

In this work, we investigate the beyond-mean-field corrections in confined geometries and test the validity of the local-density approximation in a harmonic trap with a model system. For a one-dimensional geometry, we derive the excitation spectrum across the phase transition from a superfluid to a supersolid in the thermodynamic limit and demonstrate its stability. We also investigate the influence of quantum fluctuations on the formation of the one-dimensional supersolid and show that for current experimental parameters, the use of the extended Gross-Pitaevskii equation is justified. The chapters cover the following content:

- In Chapter 1, we give an introduction to the recent advances in the field of ultracold dipolar quantum gases.

- In Chapter 2, we discuss the general concepts of scattering theory which are relevant to describe interactions in ultracold bosonic gases. We introduce a two-channel model to describe short-range interactions, and briefly discuss scattering of dipolar particles.
- In Chapter 3, we review two fundamental approaches to obtain beyond-mean-field corrections and exemplarily apply them to the three-dimensional weakly interacting Bose gas with contact interactions. We briefly discuss their respective advantages, and give an overview of beyond-mean-field corrections in other systems relevant to this work.
- In Chapter 4, we use the two-channel model to describe scattering in confined geometries. We derive the confinement-induced resonance for a one-dimensional geometry with periodic boundary conditions and use our approach to reproduce the already known results for the two-dimensional geometry with periodic boundary conditions as well as the results for a harmonic confinement.
- In Chapter 5, we study the behavior of the beyond-mean-field corrections of a weakly interacting Bose gas in a dimensional crossover from three to low dimensions. In a box with periodic boundary conditions, we derive an analytical solution and show that the leading contribution of the confinement-induced resonance is of beyond-mean-field order. In addition, we use a model system to investigate the crossover in a harmonic confinement to show the limitations of the local-density approximation. The work for this chapter was conducted in collaboration with Dmitry Petrov and Luis Santos.
- In Chapter 6, we use an effective Hamiltonian for a dipolar Bose gas, which includes beyond-mean-field corrections in the local-density approximation, to study the excitation spectrum across the phase transition from a superfluid to a supersolid in a one-dimensional geometry. We demonstrate a stable excitation spectrum with two Goldstone modes and an amplitude mode in the low-energy regime. Our results suggest that there exists an experimentally accessible parameter regime for dysprosium atoms where the supersolid phase exhibits a stable excitation spectrum in the thermodynamic limit, and the transition into the supersolid phase is of second order, driven by the roton instability.
- In Chapter 7, we investigate the influence of quantum fluctuations on the formation of the one-dimensional supersolid. The analysis is based on an effective low-energy description, which takes into account the two coupled Goldstone modes of the supersolid. We show that in one dimension, the quantum phase transition from a superfluid to a supersolid is shifted from the position where the local formation of a structure takes place. We also show that for current experimental parameters, this shift is extremely small and thus confirm that the use of the extended Gross-Pitaevskii equation is justified. The work for this chapter was conducted in collaboration with Chris Bühler.

- In Chapter 8, we present the ideas of two unfinished projects that require further numerical investigations. In the first part, we derive a formalism to obtain the beyond-mean-field corrections for a self-bound droplet. In the second part, we connect the parameters of a two-dimensional Hubbard model to the microscopic scattering length and include the influence of the confinement-induced resonance.

List of Publications

This thesis has resulted in the following publications:

- **Tobias Ilg**, Jan Kumlin, Luis Santos, Dmitry S. Petrov, and Hans Peter Büchler, "Dimensional crossover for the beyond-mean-field correction in Bose gases", Physical Review A **98**, 051604(R) (2018)

- **Tobias Ilg**, Hans Peter Büchler, "Ground-state stability and excitation spectrum of a one-dimensional dipolar supersolid", Physical Review A **107**, 013314 (2023)

- Chris Bühler, **Tobias Ilg**, Hans Peter Büchler, "Quantum fluctuations in one-dimensional supersolids", Physical Review Research **5**, 033092 (2023)

Contents

Abstract **i**

List of Publications **v**

1 Introduction **1**

2 Interactions in the Ultracold **7**

2.1 Scattering in Free Space: General Concepts 8
2.1.1 Scattering Amplitude 9
2.2 Isotropic Short-Range Potentials 11
2.2.1 Partial-Wave Decomposition 11
2.3 Effective Interactions 14
2.3.1 Pseudopotential 14
2.3.2 Feshbach model 16
2.4 Dipolar Interactions 20
2.4.1 Scattering Properties and Pseudopotential 22

3 Bose Gases Beyond Mean-Field **23**

3.1 3D Contact Gas: Methods 24
3.1.1 Bogoliubov Theory 24
3.1.2 Field-Theoretic Approach 30
3.2 Beyond-Mean-Field Corrections in Other Systems 35
3.2.1 1D Contact Gas 35
3.2.2 2D Contact Gas 36
3.2.3 3D Dipolar Gas 37

4 Scattering in Confined Geometries **41**

4.1 Introduction 41
4.2 Periodic Boundary Conditions 42
4.2.1 One-Dimensional Geometry 42
4.2.2 Two-Dimensional Geometry 45
4.3 Harmonic Confinement 46
4.3.1 One-Dimensional Geometry 46
4.3.2 Two-Dimensional Geometry 48

5 Dimensional Crossover for the Beyond-Mean-Field Corrections 51

5.1 Introduction . . . 51
5.2 Periodic Boundary Conditions . . . 52
5.2.1 General Setup . . . 52
5.2.2 Crossover to Two Dimensions . . . 55
5.2.3 Crossover to One Dimension . . . 58
5.3 Crossover for a Harmonic Confinement . . . 60
5.4 Comment: Dipoles in the One-Dimensional Regime . . . 63
5.5 Conclusion . . . 65

6 Bogoliubov Theory for a Dipolar One-Dimensional Supersolid 67

6.1 Introduction . . . 67
6.2 Setup . . . 69
6.3 Excitations in the Superfluid Phase . . . 73
6.3.1 Roton Instability . . . 75
6.3.2 Comment on the Depletion . . . 76
6.4 Supersolid Regime . . . 77
6.4.1 Ground State . . . 77
6.4.2 Excitations in the Supersolid . . . 82
6.5 Conclusion . . . 84

7 Quantum Fluctuations in One-Dimensional Supersolids 85

7.1 Introduction . . . 85
7.2 Low-Energy Description of One-Dimensional Supersolids . . . 87
7.2.1 Effective Lagrangian . . . 87
7.2.2 Hamilton Description . . . 88
7.3 Correlations . . . 90
7.4 Superfluid-to-Supersolid Phase Transition . . . 91
7.4.1 Connection to Microscopic Parameters . . . 92
7.5 Supersolid-to-Solid Phase Transition . . . 95
7.6 Conclusion . . . 96

8 Miscellaneous 97

8.1 Beyond-Mean-field Correction in a Self-Bound Quantum Droplet . . . 97
8.1.1 Ground-State Energy of the Self-Bound State . . . 99
8.1.2 Bogoliubov Theory for the Self-Bound State . . . 101
8.2 Microscopic Derivation of Hubbard Parameters for Two-Dimensional Lattices . . . 105
8.2.1 Feshbach Model in Two Dimensions . . . 106
8.2.2 Scattering in an Optical Lattice . . . 107

Appendix 113

A Scattering in Confined Geometries 115

A.1 Periodic Boundary Conditions: 1D . . . 115
A.2 Periodic Boundary Conditions: 2D . . . 115
A.3 Harmonic Confinement: 1D . . . 117
A.4 Harmonic Confinement: 2D . . . 117

B Dimensional Crossover 119

B.1 Crossover to One Dimension . . . 119
B.1.1 3D Regime . . . 121
B.2 Harmonic Confinement . . . 122
B.2.1 Bogoliubov Theory in the 1D Geometry . . . 122
B.2.2 Expansion in the One-Dimensional Regime . . . 124
B.3 Harmonic Confinement and Dipolar Interactions . . . 128

C Bogoliubov Theory for a Dipolar One-Dimensional Supersolid 131

C.1 Ground-State Energy . . . 131
C.2 Excitations . . . 132

D Quantum Fluctuations in One-Dimensional Supersolids 135

D.1 Transformation Matrix . . . 135

Ausführliche Zusammenfassung in deutscher Sprache 137

Bibliography 145

Acknowledgments 161

1 | Introduction

A state of matter which results purely from the quantum statistics of its constituents and does not rely on interactions already attracted the interest of physicists almost one hundred years ago. In a paper sent to Albert Einstein in 1924, the Indian physicist Satyendranath Bose was able to derive Planck's radiation law without relying on results from classical physics [1]. Einstein extended the theory to massive particles which obey the same statistics as photons [2, 3]. This allowed him to show that at low enough temperatures, a uniform ideal gas of these particles exhibits a phase transition to a phase where the particles macroscopically occupy the state of lowest energy. While this phase is today known as a *Bose-Einstein condensate* (BEC), it is remarkable that Einstein's prediction preceded our modern formulation of quantum mechanics as well as the division of particles into classes of fermions and bosons.

Although the theoretical descriptions of BECs that we use today, such as the first microscopic description of weakly interacting bosons by Bogoliubov [4], the field-theoretic approaches by Beliaev [5, 6] as well as Hugenholtz and Pines [7], and the mean-field description in terms of a macroscopic wave function by Gross and Pitaevskii [8, 9], were developed in the middle of the last century, experimentally preparing this quantum state of matter remained unthinkable for decades.

Only with the improvement of laser-based trapping and cooling techniques in the 1980s, which were honored by a Nobel Prize for Claude Cohen-Tannoudji, Steven Chu, and William Daniel Phillips in 1997 [10–12], the required temperatures for a gas of bosons to condense came within reach. Finally, in 1995 the first BEC was produced at Boulder by Eric Cornell and Carl Wieman [13] and shortly afterwards independently by the group of Wolfgang Ketterle at MIT [14]. The successful realization of a BEC not only earned Cornell, Wieman and Ketterle the Nobel Prize in 2001, but more importantly led to the ever-growing research field of ultracold atoms.

Since then, ultracold-atom experiments became a playground to investigate quantum many-body phenomena and helped to deepen our understanding on a fundamental level [15]. In particular, the use of Feshbach resonances [16–18], which allow to tune the interaction strength between the particles, and the use of optical potentials, which provide the means to control the dimensionality and to realize optical lattices, offers a level of experimental control which is hardly found in other platforms. In the meantime, the coherence of condensates has been shown by overlapping two BECs [19], while the appearance of vortices by stirring a BEC with a laser beam clearly indicates their superfluidity [20]. Tight optical traps allow for the investigation of low-dimensional systems and to enter the strongly interacting regime which, for example, led to the observation

of the strongly correlated Tonks-Girardeau gas [21–24]. BECs in optical lattices have been used to demonstrate the quantum phase transition from a superfluid to a Mott insulator [25], and are in general a promising platform for quantum simulations [26–29]. As producing BECs has become routine in today's laboratories, they are not only used for quantum simulations but also quantum sensing [30, 31] and, bringing the story back to Einstein himself, can be used to test the foundations of general relativity [32, 33], even in space [34].

The list of achievements is of course much longer than this introduction can capture. Of special interest for this work, however, are *dipolar* BECs, on which we will focus in the following. For alkali atoms such as rubidium (^{87}Rb) and sodium (^{23}Na), which were used for the first realizations of a BEC [13, 14], the magnetic dipole moment is small compared to the van der Waals forces. Thus, for low temperatures and densities, the interactions between the atoms are fully characterized by the s-wave scattering length and can be described by short-range contact potentials. For BECs consisting of dipolar atoms, on the other hand, the anisotropic and long-range dipolar interactions prevent a simple description in terms of the scattering length. It has been shown, however, that the interactions in these systems are accurately described by a combination of a short-range interaction characterized by an s-wave scattering length, and the dipolar interaction potential [35, 36]. The anisotropy of the dipolar interaction and the ability to tune its influence by manipulating the s-wave scattering length leads to a plethora of new phenomena [37–40]. As a thorough understanding of the interactions in ultracold Bose gases is crucial for this thesis, we will review the fundamental concepts of scattering theory in Chapter 2.

With the condensation of chromium (^{52}Cr) with a magnetic moment of $6\mu_\mathrm{B}$ (μ_B is the Bohr magneton), the first realization of a dipolar BEC has been achieved in 2004 in Stuttgart by the group of Tilman Pfau [41]. Since then, also atoms with a larger magnetic moment such as erbium (^{168}Er) [42] with a magnetic moment of $7\mu_\mathrm{B}$ and dysprosium (^{164}Dy) [43], which has the largest magnetic moment of any bosonic species ($10\mu_\mathrm{B}$), have been condensed. Note that for polar molecules the (electric) dipolar interaction strength is orders of magnitudes larger [37], but the condensation of polar molecules, while within reach, has not yet been achieved.

In 2016 the interest in dipolar BECs rose to new heights with the first observation of the formation of stable and dense droplets in a dipolar BEC of ^{164}Dy in Stuttgart [44–46], while later also droplets of ^{162}Dy [47] and of ^{168}Er [48] have been reported. To understand the significance of this observation, let us briefly return to the theoretical description of these weakly interacting systems. The aforementioned mean-field description in terms of the Gross-Pitaevskii equation [8, 9] was sufficient to describe experimental observations with high accuracy for many years. In the droplet regime, however, mean-field theory predicts a collapse of the BEC and no stable ground state is expected [39, 40]. So why do these droplets appear? Shortly after their discovery, the stabilization mechanism of these droplets was traced back to beyond-mean-field corrections, which prevent a collapse of the gas [45]. It should be noted that this stabilization mechanism was first proposed

for binary mixtures [49], and later droplets in binary mixtures have also been experimentally observed [50, 51]. For a uniform BEC in three dimensions with short-range interactions, these beyond-mean-field corrections were first derived by Lee, Huang, and Yang [52, 53] and are usually referred to as LHY corrections. The beyond-mean-field corrections were later also obtained for a uniform three-dimensional dipolar BEC [54] where the short-range interaction dominates over the dipolar interaction. If the dipolar interaction becomes dominant, however, the system exhibits an instability for long wavelengths referred to as *phonon instability* [37], which leads to complex beyond-mean-field corrections, indicating the breakdown of the current description. Methods to obtain the beyond-mean-field corrections in weakly interacting Bose gases will be discussed in detail in Chapter 3.

The influence of the LHY corrections for contact-interacting BECs became observable in recent years through the depletion of the condensate [55], and corrections to the mean-field result of the ground-state energy [56] as well as of the excitation spectrum [57, 58] have been measured. While for these instances the LHY terms provide a correction to the mean-field result, for the dipolar droplets the mean-field contribution vanishes and the beyond-mean-field corrections become dominant and thus crucial for their stability. Hence, a precise knowledge of the beyond-mean-field corrections in the droplets is essential for their theoretical description. The current description, however, is not without flaws. Since the dipolar beyond-mean-field corrections are only known in the uniform case, but the droplets are finite in their size, the description relies on the assumption that the system can be locally treated as uniform (local-density approximation). The beyond-mean-field corrections then contribute an additional term to the Gross-Pitaevskii equation, leading to the *extended* Gross-Pitaevskii equation [39, 40, 45]. In the droplet regime the dipolar interaction dominates over the short-range interaction such that the use of the local-density approximation entails the already mentioned inconsistencies due to the phonon instability. Since the imaginary part of the beyond-mean-field corrections is typically small in the droplet regime, it is usually ignored. Nevertheless, a self-consistent treatment is still missing. In Chapter 5, we analyze the beyond-mean-field corrections for contact interactions in confined systems in a dimensional crossover, which allows us to test the validity of the local-density approximation in these systems. In Chapter 8, we propose a formalism to improve the description of the beyond-mean-field corrections in the droplet state.

Although the first dipolar droplets were observed in a trap, one should not forget that due to the interplay between the repulsive short-range interaction and the attractive part of the dipolar interaction, the droplet state is self-bound [47, 59–63]. Nevertheless, the presence of a trap can be very beneficial as it can strongly modify the excitation spectrum as a result of the anisotropy of the dipolar interaction. In a trap, dipolar BECs can feature a roton spectrum [64–66], similar to the spectrum of superfluid helium [67–71]. While the roton spectrum shows the typical linear behavior for long wavelengths, it also features a minimum at finite momentum, the depth and position of which can be tuned in dipolar BECs. This minimum introduces a new length scale for the self-

organization, and in 2017 it became clear that the ground state of a dipolar gas can consist of multiple droplets [72, 73]. Thus, trapped dipolar BECs became promising candidates to realize the *supersolid* phase [74].

A supersolid inherits the properties of a superfluid, as it can sustain a frictionless flow, as well as the density modulation of a solid [75]. On a theoretical level, it is usually defined as a state that spontaneously breaks the $U(1)$ symmetry, leading to off-diagonal long-range order of the single-particle density matrix [76, 77], as well as the translational symmetry, leading to diagonal long-range order. Note that this is not the most general definition, as in one dimension spontaneous symmetry breaking is strongly influenced by quantum fluctuations [78–80]. However, quasi-diagonal and quasi-off-diagonal long-range order can survive [81–85], making a modulated superfluid and thus supersolid state possible, even in one dimension. The discussion of the influence of quantum fluctuations on the supersolid state in one dimension will be the focus of Chapter 7.

First discussed in 1957, and initially thought to be impossible due to the seemingly contradicting properties of the supersolid [77], no rigorous proof was given that would preclude its existence. Thus, interest for this exotic state of matter was unbroken in the following years [86–89]. The possibility of a supersolid ground state was then shown in 1970 by Anthony James Leggett who derived an upper bound for the superfluid fraction [90].

For a long time, the quest to experimentally observe the supersolid state of matter focused on solid helium (^{4}He) [75, 91–93]. While supersolid properties of ^{4}He were reported in 2004 [94], the results later had to be retracted [95] such that to this date there is no compelling evidence for supersolidity in ^{4}He. Supersolid properties have been observed for superfluids with cavity-mediated interactions [96, 97] as well as in spin-orbit coupled BECs [98]. So far, in all these experimental realizations the external light field determines the periodicity of the system.

By contrast, the density modulation in dipolar BECs purely results from the interactions between the particles. While the first droplet arrays were not phase coherent [72], later experiments showed global phase coherence between the droplets; first in the group of Giovanni Modugno in Pisa [99] and shortly afterwards in the group of Tilman Pfau in Stuttgart [100] and in the group of Francesca Ferlaino in Innsbruck [101]. The observation of the Goldstone modes due to the two spontaneously broken continuous symmetries [102–105] then confirmed the genuine supersolidity of these arrays [106], while later also higher excitations were experimentally studied [107–109].

These experimental efforts were accompanied by a thorough theoretical investigation of the supersolid state and its excitations [74, 85, 100, 101, 110–128]. As for the droplets, the theoretical description strongly relies on the extended Gross-Pitaevskii equation. Numerical studies within the experimental three-dimensional setting are in good agreement with the experimental observations [39, 40], but accessing the thermodynamic limit, and thus studying the nature of the quantum phase transition from the superfluid to the supersolid, is difficult with these approaches [74, 127]. In Chapter 6, we present an analytical study of the quantum phase transition in a one-dimensional

geometry and investigate the excitation spectrum across the transition.

Of course the interest in the supersolid state did not stop with the first observation of this phase in dipolar quantum gases. The realization and investigation of two-dimensional supersolids [118–120, 129, 130], the influence of the finite temperature in these systems [123], as well as the development of a self-consistent description of beyond-mean-field corrections is just a selection of topics under study. This highlights that dipolar quantum gases are a versatile platform and offer exciting possibilities for the future to study quantum many-body phenomena.

2 | Interactions in the Ultracold

While the exact interatomic potential between neutral atoms in general is complicated, especially at short distances, cold atom experiments operate in a regime where the different length scales of the problem separate. This simplifies the description of interactions tremendously. What are these important length scales for our discussion? One is given by the *range* of the interaction. To get an estimate for the range, let us forget about the short-range details of the interactions for a moment and consider the interaction between atoms at larger distances. For neutral atoms (without a dipole moment), the interaction can then be described by a van der Waals potential,

$$V_{\mathrm{vdW}}(r) = -\frac{C_6}{r^6}, \tag{2.1}$$

where r is the distance between the particles. The coefficient C_6 determines the strength of the interaction and gives rise to a characteristic length scale, the *van der Waals length*,

$$R_{\mathrm{vdW}} = \left(\frac{mC_6}{\hbar^2}\right)^{1/4}, \tag{2.2}$$

with m the mass of the particles and $\hbar$ the reduced Planck constant. The density n of the gas introduces another important scale, the *mean interparticle distance*

$$d = n^{-1/3}. \tag{2.3}$$

While the van der Waals length is typically of the order of a few nanometers, much larger than the distances where short-range details of the interaction play a role, the densities we are interested in are very low ($10^{14}\,\mathrm{cm}^{-3}$ to $10^{15}\,\mathrm{cm}^{-3}$). Thus, we are in the *dilute* regime,

$$d \gg R_{\mathrm{vdW}}. \tag{2.4}$$

Processes involving more than two particles can therefore be safely neglected in the following. The temperature of the gas gives rise to the *de Broglie wavelength*,

$$\lambda_T = \sqrt{\frac{2\pi\hbar^2}{mk_{\mathrm{B}}T}}, \tag{2.5}$$

where k_{B} is the Boltzmann constant. For temperatures in the nano- to millikelvin regime, the de Broglie wavelength greatly exceeds the van der Waals length,

$$\lambda_T \gg R_{\mathrm{vdW}}, \tag{2.6}$$

which we refer to as the *ultracold* regime. If the de Broglie wavelength becomes comparable to the interparticle distance

$$d \sim \lambda_T, \tag{2.7}$$

the gas is *degenerate*, meaning that the gas cannot be considered classically but obeys quantum statistics.

Throughout this work, we will be interested in the regime

$$\lambda_T \gtrsim d \gg R_{\mathrm{vdW}}, \tag{2.8}$$

and also the following short introduction to scattering theory will focus on this regime.

This chapter lays the foundation to understand how to describe the interactions in the ultracold quantum many-body systems, which will be discussed in the following chapters. In the beginning of this chapter, we want to review important concepts that are necessary to describe binary collisions at low energies. We will mainly focus on scattering in three dimensions, but also highlight the differences that occur in lower dimensions. The focus will be on isotropic short-range interactions, that feature universal scattering properties at low energies. Due to these universal scattering properties, we will afterwards discuss how to efficiently describe isotropic short-range interactions and introduce the pseudopotential as well as a minimal two-channel model. At the end of this chapter, we will briefly discuss the dipolar interaction and how it affects the scattering properties.

2.1 | Scattering in Free Space: General Concepts

With this section, we want to provide a short overview of the low-energy scattering between particles. We will introduce all relevant quantities and terminologies that are used throughout this work, however, we refer the reader to standard textbooks for an in-depth introduction to scattering theory (e.g. [131]). The focus of this section is on scattering in three dimensions. We will comment on the peculiarities of scattering in lower dimensions whenever necessary, since this will become important when discussing scattering in confined geometries in Chapter 4.

In the following, we consider the collision of two identical bosons of mass m in the center-of-mass frame without an external potential. We start our discussion with a general interaction potential $V(\boldsymbol{r})$ that vanishes sufficiently fast, $rV(\boldsymbol{r}) \to 0$ for $r \to \infty$. Here, $r = |\boldsymbol{r}|$ denotes the distance between the particles. In the center-of-mass frame, the problem reduces to a single particle with reduced mass $m/2$ interacting with the potential $V(\boldsymbol{r})$. We are interested in scattering states with energy $E > 0$ that are asymptotically free, and which are described by the (stationary) Schrödinger equation

$$[H_0 + V(\boldsymbol{r})]\Psi_k(\boldsymbol{r}) = E_{\boldsymbol{k}}\Psi_{\boldsymbol{k}}(\boldsymbol{r}). \tag{2.9}$$

Here, $H_0 = p^2/m$ is the Hamiltonian for the free particle and the Schrödinger equation has a solution for every $E_{\boldsymbol{k}} = \hbar^2\boldsymbol{k}^2/m$, where $\boldsymbol{k}$ is the wave vector of the incoming

wave. The formal solution of the Schrödinger equation (2.9) is given by the Lippmann-Schwinger equation,

$$\Psi_{\boldsymbol{k}}(\boldsymbol{r}) = e^{i\boldsymbol{k}\cdot\boldsymbol{r}} + \int d^3r'\, G_{\boldsymbol{k}}(\boldsymbol{r}-\boldsymbol{r}')V(\boldsymbol{r}')\Psi_{\boldsymbol{k}}(\boldsymbol{r}'), \tag{2.10}$$

where $G_{\boldsymbol{k}}(\boldsymbol{r})$ is the Green's function defined through

$$\left(\frac{\hbar^2\Delta}{m} + E_{\boldsymbol{k}}\right) G_{\boldsymbol{k}}(\boldsymbol{r}) = \delta(\boldsymbol{r}). \tag{2.11}$$

The solution for the Green's function is readily obtained in Fourier space,

$$G_{\boldsymbol{k}}(\boldsymbol{q}) = \frac{1}{E_{\boldsymbol{k}} - E_{\boldsymbol{q}}}\,. \tag{2.12}$$

To obtain a representation in position space that obeys causality, we shift the pole in Eq. (2.12), $E_{\boldsymbol{k}} \to \lim\limits_{\eta\to 0^+} E_{\boldsymbol{k}} + i\eta$, and perform an inverse Fourier transformation. This yields the *retarded* Green's function,

$$G^+_{\boldsymbol{k}}(\boldsymbol{r}) = \int \frac{d^3q}{(2\pi)^3} \frac{e^{i\boldsymbol{q}\cdot\boldsymbol{r}}}{E_{\boldsymbol{k}} - E_{\boldsymbol{q}} + i\eta} = -\frac{m}{4\pi\hbar^2}\frac{e^{ikr}}{r}, \tag{2.13}$$

where $k = |\boldsymbol{k}|$. In principle, the Lippmann-Schwinger equation in Eq. (2.10) can be solved iteratively leading to the *Born Series* for the wave function. Truncating the Born series after n iterations is then referred to as the *n-th Born approximation*. However, we are mostly interested in the outcome of a scattering event, meaning in the limit $r \to \infty$, while the behavior of the wave function at short distances is of minor interest. The same is true for the many-body systems in dilute cold atom experiments. There, the mean interparticle distance d is large compared to the range of the interaction such that the particles are far apart when they engage in the next scattering event.

2.1.1 | Scattering Amplitude

The far-field behavior of the wave function is determined by the behavior of the Green's function at large distances, as can be seen in Eq. (2.10). We expand $G^+_{\boldsymbol{k}}(\boldsymbol{r}-\boldsymbol{r}')$ for $r \to \infty$ to obtain

$$\Psi_{\boldsymbol{k}}(\boldsymbol{r}) \overset{r\to\infty}{=} e^{i\boldsymbol{k}\cdot\boldsymbol{r}} + f(\boldsymbol{k},\boldsymbol{k}')\frac{e^{ikr}}{r}, \tag{2.14}$$

with $\boldsymbol{k}' = k\boldsymbol{r}/r$ and we have introduced the *scattering amplitude* $f(\boldsymbol{k},\boldsymbol{k}')$,

$$f(\boldsymbol{k},\boldsymbol{k}') = -\frac{m}{4\pi\hbar^2}\int d^3r'\, e^{-i\boldsymbol{k}'\cdot\boldsymbol{r}'}V(\boldsymbol{r}')\Psi_{\boldsymbol{k}}(\boldsymbol{r}'). \tag{2.15}$$

The asymptotic form of the wave function at large distances consists of an incoming plane wave and an outgoing spherical wave. All information about the scattering event is contained in the scattering amplitude. Like the wave function, the scattering amplitude can be computed iteratively by inserting the Lippmann-Schwinger equation from Eq. (2.10) in Eq. (2.15),

$$f(\boldsymbol{k},\boldsymbol{k}') = -\frac{m}{4\pi\hbar^2}\int d^3r \Bigg[e^{i(\boldsymbol{k}-\boldsymbol{k}')\cdot\boldsymbol{r}}\, V(\boldsymbol{r}) + \int d^3r' e^{-i\boldsymbol{k}'\cdot\boldsymbol{r}} V(\boldsymbol{r}) G_{\boldsymbol{k}}(\boldsymbol{r}-\boldsymbol{r'}) V(\boldsymbol{r'}) e^{i\boldsymbol{k}\cdot\boldsymbol{r}'} + \dots \Bigg]. \tag{2.16}$$

This results in an expansion in the interaction potential equivalent to the standard perturbation theory in quantum mechanics and is called Born series of the scattering amplitude. Accordingly, the scattering amplitude in lowest order is simply the Fourier transform of the interaction potential $V(\boldsymbol{r})$ [see first line of Eq. (2.16)]. We will see, however, that an expansion in lowest order can be misleading as the Born series does not necessarily converge.

Before we analyze the properties of the scattering amplitude in detail for isotropic short-range potentials, we first want to comment on the form of the scattering amplitude in lower dimensions, which will be crucial to understand the scattering in confined systems in Chapter 4. We will use the following conventions throughout the rest of this work.

Scattering Amplitude in 2D

We can follow the previous discussion and adapt it for lower-dimensional systems. While the form of the Lippmann-Schwinger equation remains unchanged in lower dimensions, the real space representation of the retarded Green's function, which is the determining factor of the far-field behavior, changes drastically. In two dimensions, the retarded Green's function becomes

$$G^{+}_{\boldsymbol{k}_\rho}(\boldsymbol{\rho}) = -\frac{m}{\hbar^2}\,\frac{i}{4}\,H_0^{(1)}(k_\rho\rho), \tag{2.17}$$

where $\boldsymbol{\rho}$ is a two-dimensional vector with $\rho = |\boldsymbol{\rho}|$, $\boldsymbol{k}_\rho$ is the two-dimensional wave vector with $|\boldsymbol{k}_\rho| = k_\rho$ and $H_0^{(1)}$ is the Hankel function of zeroth order and of the first kind. Accordingly, the Lippmann-Schwinger equation in the far-field reads

$$\begin{aligned}\Psi_{\boldsymbol{k}_\rho}(\boldsymbol{\rho}) &= e^{i\boldsymbol{k}_\rho\cdot\boldsymbol{\rho}} + \int d^2\rho'\, G^{+}_{\boldsymbol{k}_\rho}(\boldsymbol{\rho}-\boldsymbol{\rho'}) V(\boldsymbol{\rho'}) \Psi_{\boldsymbol{k}_\rho}(\boldsymbol{\rho'}) \\ &\overset{\rho\to\infty}{=} e^{i\boldsymbol{k}_\rho\cdot\boldsymbol{\rho}} + f(\boldsymbol{k}_\rho,\boldsymbol{k}'_\rho)\frac{e^{ik_\rho\rho}}{\sqrt{\rho}},\end{aligned} \tag{2.18}$$

with $\boldsymbol{k}'_\rho = k_\rho \boldsymbol{\rho}/\rho$ and where we have define the scattering amplitude as

$$f_{2\mathrm{D}}(\boldsymbol{k}_\rho, \boldsymbol{k}'_\rho) = -\frac{m}{4\hbar^2}\sqrt{\frac{2i}{\pi k_\rho}} \int d^2\rho'\, e^{-i\boldsymbol{k}'_\rho \cdot \boldsymbol{\rho}'} V(\boldsymbol{\rho}') \Psi_{\boldsymbol{k}_\rho}(\boldsymbol{\rho}'). \tag{2.19}$$

Scattering Amplitude in 1D

In one dimension, the retarded Green's function of a free particle is a plane wave,

$$G^+_{k_z}(z) = \frac{m}{2\hbar^2}\frac{1}{ik_z} e^{ik_z|z|}. \tag{2.20}$$

In the far field, the wave function is thus a superposition of the incoming and the scattered plane wave,

$$\begin{aligned} \Psi_{k_z}(z) &= e^{ik_z z} + \int dz'\, G^+_{k_z}(z - z') V(z') \Psi_{k_z}(z') \\ &\overset{z\to\infty}{=} e^{ik_z z} + f_{1\mathrm{D}}(k_z) e^{ik_z z}, \end{aligned} \tag{2.21}$$

where we have introduced the scattering amplitude

$$f_{1\mathrm{D}}(k_z) = \frac{m}{2i\hbar^2 k_z} \int dz' e^{-ik_z z'} V(z') \Psi_{k_z}(z'). \tag{2.22}$$

2.2 | Isotropic Short-Range Potentials

While the discussion so far was kept very general, in the following we want to focus on the special case of a spherical potential $V(\boldsymbol{r}) = V(r)$ of range R which decays at large distances with a power law behavior $\sim r^{-n}$. This is motivated by the van der Waals potential in Eq. (2.1) between neutral atoms. In particular, we are interested in the low-energy behavior of the scattering amplitude. As in the previous section, we will discuss the main ideas for the three-dimensional case and comment on low-dimensional systems afterwards.

2.2.1 | Partial-Wave Decomposition

For a spherical potential, the wave function $\Psi_{\boldsymbol{k}}(\boldsymbol{r})$ and hence the scattering amplitude $f(\boldsymbol{k}, \boldsymbol{k}')$ can be decomposed in partial waves of angular momentum l. Since $V(r)$ is spherically symmetric, the different angular momentum subspaces decouple and the problem can be solved in each sector independently. We will not discuss the decomposition in detail here (see e.g. [131]), but only discuss the result and its implications in the low-energy regime. The scattering amplitude can be written in terms of the partial scattering amplitudes f_l as

$$f(k, \theta) = \sum_{l=0} (2l + 1)\, f_l(k)\, P_l(\cos\theta), \tag{2.23}$$

where θ is the angle between $\boldsymbol{k}$ and $\boldsymbol{k}'$, $k = |\boldsymbol{k}| = |\boldsymbol{k}'|$, and $P_l(x)$ are the Legendre polynomials. For low energies $kR \ll 1$, the partial scattering amplitudes behave as

$$f_l \overset{k\to 0}{\sim} \begin{cases} k^{2l} & l < (n-3)/2 \\ k^{n-3} & \text{otherwise,} \end{cases} \tag{2.24}$$

which has important implications for the scattering at low energies.

Consider the case $n \leq 3$ first. All partial waves show the same k-behavior at low-energies and must be taken into account, which makes a general treatment hard for these so called *long-range* potentials. For the already mentioned dipolar interaction ($n = 3$) the situation is even worse. Since it is long-range, we must in principle take into account all partial waves, however, due to its anisotropy the angular momentum subspaces can not be treated independently and the different partial waves couple. We will briefly comment on the scattering amplitude for dipolar interactions in Sec. 2.4.

If $n > 3$, as in the case of a van der Waals interaction ($n = 6$), the scattering amplitude in the low-energy regime is dominated by the $l = 0$ (s-wave) contribution to the scattering amplitude and the potential is considered *short-range*. Notably, in the low-energy regime f only depends on the magnitude k of the momentum and on a single parameter, the *scattering length* a_s. It takes the form

$$f(k) \overset{kR\ll 1}{=} -\frac{1}{\frac{1}{a_s} + ik + \mathcal{O}(k^2)}. \tag{2.25}$$

The implications of Eq. (2.25) are remarkable. For low energies, scattering at short-range potentials is universal. The exact short-range details of the interaction potential do not appear in the scattering amplitude and scattering is fully determined by the scattering length. Hence, two different potentials that share the same scattering length will produce the same low-energy scattering, which reduces the complexity of calculations for ultracold atomic gases tremendously. The true complicated potential can be replaced by any much simpler short-range potential as long as it has the same scattering length. The scattering amplitude in Eq. (2.25) also shows, that in the limit $k \to 0$, the wave function has a node at $r = a_s$,

$$\Psi_{\boldsymbol{k}\to 0}(\boldsymbol{r}) = 1 - \frac{a_s}{r}. \tag{2.26}$$

For positive scattering lengths, this behavior is the same as for scattering on a hard sphere of radius a_s, which gives an intuitive interpretation of the scattering length.

For the van der Waals interaction, the energy scale below which $l \neq 0$ contributions are irrelevant can be deduced form the height of the centrifugal barrier of the effective radial potential

$$V_{\text{eff}} = \frac{\hbar^2 l(l+1)}{mr^2} - \frac{C_6}{r^6}. \tag{2.27}$$

The height is of the order of the van der Waals energy $E_{\mathrm{vdW}} = \hbar^2/mR_{\mathrm{vdW}}^2$ for $l = 1$. As discussed in the beginning of this chapter, we are interested in extremely low temperatures which means $\lambda_T \gg R_{\mathrm{vdW}}$ such that the typical energies involved are much smaller than the centrifugal barrier. For the discussion of many-body systems in the later chapters, only taking into account the s-wave contributions is therefore well-justified.

The scattering length between atoms can be precisely measured in current experiments [132, 133], and can be seen as a given parameter for our discussion. For any short-range potential we use in the following, we then have to make sure that it reproduces the correct scattering length. Importantly, the scattering length between atoms can also be tuned by an external magnetic field by means of a Feshbach resonance [134–137], a concept which we will discuss in more detail in Sec. 2.3.2.

Universal Scattering in 2D

In lower dimensions, scattering remains universal for short-range potentials and low energies ($kR \ll 1$). This becomes apparent when considering the low-energy behavior of the scattering amplitude in two dimensions, which is given by [138]

$$f_{\mathrm{2D}}(k_\rho) = -\sqrt{\frac{2\pi i}{k_\rho}}\frac{1}{i\pi - \ln(k_\rho^2 a_{\mathrm{2D}}^2 e^{2\gamma}/4)}, \tag{2.28}$$

where $\gamma \approx 0.577$ is the Euler-Mascheroni constant and a_{2D} denotes the scattering length in two dimensions. Again, the scattering length is the characteristic length scale for scattering in two dimensions. While in three dimensions the scattering amplitude is finite in the limit $k \to 0$, it should be noted that f_{2D} diverges in this limit.

Universal Scattering in 1D

Just like in two and three dimensions, the scattering of low-energy particles in one dimension is fully characterized by a single length scale, the one-dimensional scattering length a_{1D} [139],

$$f_{\mathrm{1D}}(k_z) = -\frac{1}{1 + ik_z a_{\mathrm{1D}}}. \tag{2.29}$$

Compared to two dimensions, the scattering amplitude does not diverge for $k_z \to 0$, but loses its dependence on a_{1D}.

Since scattering is universal in the low-energy regime, the true interaction potential between the particles can be replaced by an arbitrary short-range potential which shares the same scattering length. The goal of the next section is to find an interaction which reduces the complexity of calculations, and to connect the parameters of the interaction to the corresponding scattering length.

2.3 | Effective Interactions

In the previous section we have seen that for short-range potentials, the scattering amplitude is uniquely characterized by the scattering length for low energies. The exact potential between atoms is difficult to determine precisely and calculating the scattering length becomes cumbersome. Even small errors can lead to vastly different scattering lengths. However, since the scattering length can be measured precisely in experiments [132, 133], it is more sensible to treat the scattering length as a given parameter in our theories. We can then replace the exact interaction by an interaction potential which depends on additional parameters. Ideally, the potential is chosen such that it allows for the exact and analytic evaluation of the scattering amplitude. The parameters of the potential can then be linked to the (measured) scattering length.

In this section, we will introduce the commonly used *pseudopotential*, which only depends on a single parameter, the *coupling constant* g. While the connection between the coupling constant and the scattering length is easily obtained in three dimensions, determining the coupling constant in confined geometries becomes difficult.

A convenient approach to connect the coupling constant to the scattering length is to use a Feshbach model where the interaction of the particles is described using multiple scattering channels. We give a brief overview over Feshbach models before we introduce a minimal two-channel model. This will allow us to easily connect the coupling constant in confined geometries to the scattering length a_s, which will be the focus of Chapter 4.

2.3.1 | Pseudopotential

A common choice for the interaction potential is given by [140–144]

$$V_\mathrm{pseudo}(\boldsymbol{r}) = g\delta(\boldsymbol{r})\frac{\partial}{\partial r}r, \tag{2.30}$$

where g is the coupling constant. Since this potential contains a derivative and a zero-range potential described by the delta-distribution, it is often called pseudopotential in the literature. The term $\partial_r r$ serves a crucial purpose. Since a simple delta potential leads to a spectrum that is unbound from below [145], it is ill-defined in three dimensions and needs to be regularized. When acting on regular wave functions $\psi_\mathrm{reg.}(\boldsymbol{r})$ at $r = 0$, the additional $\partial_r r$ has no influence

$$V_\mathrm{pseudo}(\boldsymbol{r})\psi_\mathrm{reg.}(\boldsymbol{r}) = g\delta(\boldsymbol{r})\left[\psi_\mathrm{reg.}(\boldsymbol{r}) + r\partial_r\psi_\mathrm{reg.}(\boldsymbol{r})\right] = g\psi_\mathrm{reg.}(0) = g\delta(\boldsymbol{r})\psi_\mathrm{reg.}(\boldsymbol{r}). \tag{2.31}$$

When acting on functions with an $1/r$ divergence at $r = 0$, the pseudopotential circumvents divergences that a simple delta potential would produce. This is crucial for spherical waves, which play a significant role in three-dimensional scattering as seen in Sec. 2.1.1,

To illustrate this point and at the same time connect g to the scattering length, we

consider the Ansatz

$$\psi(\boldsymbol{r}) = e^{i\boldsymbol{k}\cdot\boldsymbol{r}} + f(k)\frac{e^{ikr}}{r}, \tag{2.32}$$

and insert it into the Lippmann-Schwinger equation for the pseudopotential,

$$\begin{aligned} e^{i\boldsymbol{k}\cdot\boldsymbol{r}} + f(k)\frac{e^{ikr}}{r} &= e^{i\boldsymbol{k}\cdot\boldsymbol{r}} + \int d^3r'\, G^+_{\boldsymbol{k}}(\boldsymbol{r}-\boldsymbol{r}')V_{\text{pseudo}}(\boldsymbol{r}')\left[e^{i\boldsymbol{k}\cdot\boldsymbol{r}'} + f(k)\frac{e^{ikr'}}{r'}\right] \\ &= e^{i\boldsymbol{k}\cdot\boldsymbol{r}} + g\, G^+_{\boldsymbol{k}}(\boldsymbol{r})\left[1 + ikf(k)\right]. \end{aligned} \tag{2.33}$$

The term $\partial_r r$ regularizes the influence of the spherical wave, which would otherwise cause a divergence. We can solve Eq. (2.33) for the scattering amplitude,

$$f(k) = -\frac{1}{\frac{4\pi\hbar^2}{mg} + ik}, \tag{2.34}$$

and by comparing to Eq. (2.25), we obtain

$$g = \frac{4\pi\hbar^2 a_s}{m}. \tag{2.35}$$

As shown above, the pseudopotenial allows for the analytic evaluation of the entire Born series, and Eq. (2.35) allows us to connect the coupling constant to the scattering length. It is important to point out that for the calculation above we have not restricted the discussion to low energies, meaning the pseudopotenial reproduces the scattering amplitude in Eq. (2.25) for all values of $\boldsymbol{k}$.

We briefly want to comment on the fact that in literature, especially in context of mean-field theory for weakly interacting bosons, the regularization is neglected and only the delta potential is discussed. In a lowest-order expansion like mean-field theory, only the lowest-order contribution to the scattering amplitude, the first Born approximation, plays a role. Higher Born approximations contain higher orders in the interaction potential [see Eq. (2.16)] and can be neglected. Within first Born approximation, however, the delta potential shows no divergences,

$$f_{1\text{B}}(\boldsymbol{k},\boldsymbol{k}') = -\frac{m}{4\pi\hbar^2}\int d^3r\, g\delta(\boldsymbol{r})e^{i(\boldsymbol{k}-\boldsymbol{k}')\cdot\boldsymbol{r}} = -\frac{mg}{4\pi\hbar^2}, \tag{2.36}$$

and a regularization is not necessary. As already mentioned in the introduction in Chapter 1, in the past years experiments pushed mean-field theory to its limits and higher-order contributions need to be included. To obtain a consistent expansion, also higher terms in the Born series need to be included. For the pure delta potential the second Born approximation contains a characteristic divergence,

$$f_{2\text{B}}(\boldsymbol{k},\boldsymbol{k}') = -\frac{m}{4\pi\hbar^2}\left(g + \frac{mg^2}{\hbar^2}\int\frac{d^3q}{(2\pi)^3}\frac{1}{k^2 - q^2 + i\eta}\right), \tag{2.37}$$

where we have Fourier transformed the last term. The ultraviolet divergence in the second term of Eq. (2.37) will play an important role when discussing Bogoliubov theory in Sec. 3.1.1.

Zero-Range Potentials in Lower Dimensions

As we have seen in Sec. 2.2, scattering remains universal in lower dimensions. Like in three dimensions, we can therefore replace the true interaction potential by a zero-range potential as long as it reproduces the correct scattering length.

In contrast to three dimensions, in one dimension the delta potential

$$V_{1\mathrm{D}}(z) = g_{1\mathrm{D}}\delta(z) \tag{2.38}$$

is well-defined, which means that no regularization is needed. For the potential $V_{1\mathrm{D}}(z)$ we can directly evaluate the Born series,

$$\begin{aligned} f(k) &= \frac{m}{2i\hbar^2 k}\int dz' e^{ikz'}\Psi_k(z') = \left(\frac{mg_{1\mathrm{D}}}{2i\hbar^2 k}\right) + \left(\frac{mg_{1\mathrm{D}}}{2i\hbar^2 k}\right)^2 + \left(\frac{mg_{1\mathrm{D}}}{2i\hbar^2 k}\right)^3 + \dots \\ &= \sum_{n=1}^{\infty}\left(\frac{mg_{1\mathrm{D}}}{2i\hbar^2 k}\right)^n = -\frac{1}{1 - ik\frac{2\hbar^2}{mg_{1\mathrm{D}}}}\,, \end{aligned} \tag{2.39}$$

where we have used the geometric series in the last step. By comparing Eq. (2.39) to Eq. (2.22), we connect the coupling constant $g_{1\mathrm{D}}$ to the scattering length in one dimension,

$$g_{1\mathrm{D}} = -\frac{2\hbar^2}{ma_{1\mathrm{D}}}. \tag{2.40}$$

While in three dimensions a positive scattering length results in a positive coupling constant, the opposite is true in one dimension.

Just as in three dimensions, the delta potential needs a regularization in the two-dimensional case. While in three dimensions the term $\partial_r r$ cures the divergencies, obtaining a regularized zero-range potential in two dimensions is much more tedious. Since we will never actually use the regularized pseudopotential in two dimensions, we waive to include a discussion here but refer the reader to [139].

It is important to point out that the regularization of the delta potential strongly depends on the dimensionality of the system, which makes a systematic treatment challenging. This is a big advantage of the two-channel model which we will introduce in the next section. There, the basic procedure can be easily adapted for lower dimensions or confined geometries.

2.3.2 | Feshbach model

In general, the interaction potential between colliding particles depends on internal degrees of freedom (e.g. spin or angular momentum) of the individual atoms. In our discussion so far, we excluded the coupling to different interaction potentials (and therefore final states) and only considered scattering in a single *channel*. However, during a scattering event different channels can couple, opening the possibility to tune the interaction using a *Feshbach resonance*, a phenomenon which was independently discovered by

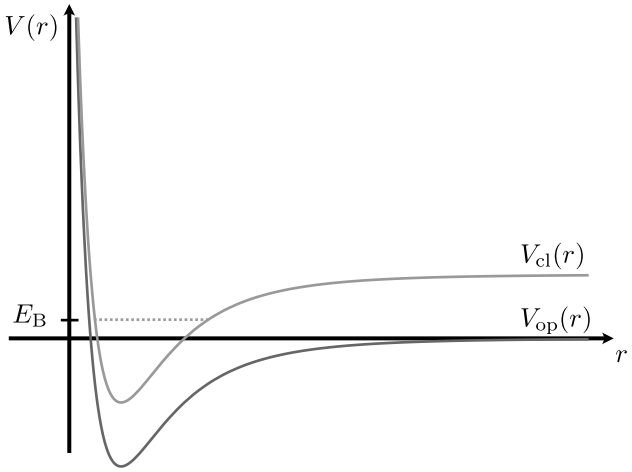

Figure 2.1: Two-channel model to describe a Feshbach resonance.

Herman Feshbach [134, 135] and Ugo Fano [136, 137]. This makes ultracold atom experiments a powerful platform to explore quantum many-body physics. Since we will use a strongly simplified model in the following, we only briefly want to comment on Feshbach resonances here but will refer the reader to [15, 18, 146] for an in-depth discussion.

The mechanism behind a Feshbach resonance is readily understood by introducing one additional channel to our discussion. A two-channel model consists of an *open* and a *closed* channel, where open and closed refers to the dissociation energy of the respective interaction potential. In the open channel, the dissociation energy $V_{\mathrm{op}}(r \to \infty)$ is smaller than the energy E of the colliding particles. In line with the previous sections, we set $V_{\mathrm{op}}(r \to \infty) = 0$. For the closed channel the dissociation energy is larger than the energy E, $V_{\mathrm{cl}}(r \to \infty) > E$, and it supports a bound state of energy E_{B}. This situation is sketched in Fig. 2.1. During the scattering event, the particles can couple to this bound (molecular) state, which drastically alters the scattering properties of the open channel, depending on the energy of the bound state. The energy of the bound state can be influenced, inter alia, if the molecular state and the atom pair have different magnetic moments. Using the Zeeman effect, the energy of the bound state with respect to the dissociation energy of the open channel can then be precisely tuned in a magnetic field B, which alters the scattering length in the open channel. A careful study of the two-channel model then yields the well-known formula for the scattering length as a function of the magnetic field [147],

$$a_{\mathrm{s}} = a_{\mathrm{bg}} \left(1 - \frac{\Delta B}{B - B_0} \right), \tag{2.41}$$

where a_{bg} is the background scattering length far from the resonance position B_0 and ΔB describes the width of the resonance. This opens the possibility to change the interaction strength in cold atom experiments, a powerful tool to explore quantum many-body physics.

Minimal Two-Channel Model

As discussed above, two-channel (or multi-channel) models are commonly used to theoretically predict the behavior of the scattering length as a function of an additional parameter, usually the magnetic field. Our use-case for the two-channel model, however, is much simpler. We only want to describe an interaction characterized by a *given* scattering length a_s. We can therefore use a strongly simplified version to describe the (short-range) interaction between two particles.

In the following, we consider two free particles of equal mass m in three dimensions which *only* interact via the coupling to the closed channel. The coupling between the open and the closed channel can then be readily understood if expressed by the field operators of the particles $\Psi(\boldsymbol{x})$ and the field operator of the molecular state $\Phi(\boldsymbol{z})$,

$$H_\mathrm{int} = \bar{g} \int d^3x\, d^3y\, \alpha_\Lambda(\boldsymbol{x}-\boldsymbol{y}) \Psi(\boldsymbol{x}) \Psi(\boldsymbol{y}) \Phi^\dagger \left(\frac{\boldsymbol{x}+\boldsymbol{y}}{2} \right) + \mathrm{h.c.}\,, \tag{2.42}$$

where $\bar{g}$ is the coupling strength between the two channels. The field operators obey the bosonic commutation relations,

$$\left[\Psi(\boldsymbol{x}), \Psi^\dagger(\boldsymbol{y})\right] = \delta(\boldsymbol{x}-\boldsymbol{y}), \qquad \left[\Phi(\boldsymbol{x}), \Phi^\dagger(\boldsymbol{y})\right] = \delta(\boldsymbol{x}-\boldsymbol{y}), \tag{2.43}$$

while all other commutators vanish. The function $\alpha_\Lambda(\boldsymbol{r})$ characterizes the coupling between the open and the closed channel. It has a (cut-off) range Λ such that $\alpha_\Lambda(\boldsymbol{r}) \to \delta(\boldsymbol{r})$ for $\Lambda \to 0$, e.g. $\alpha_\Lambda(\boldsymbol{x}) = e^{-\boldsymbol{x}^2/2\Lambda^2}/(2\pi\Lambda^2)^{3/2}$. By restricting our discussion to the Fock space containing either two particles or a single molecule and projecting onto position space, we end up with a pair of coupled Schrödinger equations for the open and closed channel,

$$\left[E + \frac{\hbar^2}{2m}\Delta_{\boldsymbol{x}} + \frac{\hbar^2}{2m}\Delta_{\boldsymbol{y}} \right] \psi(\boldsymbol{x},\boldsymbol{y}) = \bar{g} \int d^3z\; \alpha_\Lambda(\boldsymbol{x}-\boldsymbol{y}) \phi(\boldsymbol{z}) \delta\left(\boldsymbol{z} - \frac{\boldsymbol{x}+\boldsymbol{y}}{2} \right), \tag{2.44a}$$

$$\left[E - \nu_0 + \frac{\hbar^2}{2M}\Delta_{\boldsymbol{z}} \right] \phi(\boldsymbol{z}) = \bar{g} \int d^3x\, d^3y\; \alpha_\Lambda(\boldsymbol{x}-\boldsymbol{y}) \psi(\boldsymbol{x},\boldsymbol{y}) \delta\left(\boldsymbol{z} - \frac{\boldsymbol{x}+\boldsymbol{y}}{2} \right). \tag{2.44b}$$

Here, $M = 2m$ is the mass of the molecule, which is described by the wave function $\phi(\boldsymbol{z})$ and $\psi(\boldsymbol{x},\boldsymbol{y})$ is the wave function of the two particles in the open channel. The energy E is given by the kinetic energy of the two particles in the open channel, $E = \hbar^2(\boldsymbol{k}_1^2 + \boldsymbol{k}_2^2)/2m$, where $\hbar\boldsymbol{k}_i$ is the momentum of particle i. In addition, we have introduced the (bare) detuning ν_0 of the molecular state. In this model, the particles do not feel any interaction in the respective channels ($V_\mathrm{op}(\boldsymbol{r}) = V_\mathrm{cl}(\boldsymbol{r}) = 0$).

In what follows, we connect the parameters $\bar{g}$ and ν_0 of the two-channel model to the scattering length a_s in the low-energy regime. To simplify, we introduce relative and center-of-mass coordinates,

$$\boldsymbol{r} = \boldsymbol{x} - \boldsymbol{y}, \qquad \boldsymbol{R} = \frac{\boldsymbol{x}+\boldsymbol{y}}{2}, \tag{2.45}$$

which allows us to separate the center-of-mass motion from the relative motion with the Ansatz

$$\psi(\boldsymbol{r}, \boldsymbol{R}) = e^{i\boldsymbol{K}\cdot\boldsymbol{R}}\,\psi(\boldsymbol{r}), \qquad \phi(\boldsymbol{R}) = e^{i\boldsymbol{K}\cdot\boldsymbol{R}}\,\phi_c, \tag{2.46}$$

where $\boldsymbol{K} = \boldsymbol{k}_1 + \boldsymbol{k}_2$. Inserting the Ansatz from Eq. (2.46) into Eq. (2.44), we obtain

$$\left[\frac{\hbar^2\boldsymbol{k}^2}{m} + \frac{\hbar^2}{m}\Delta\right]\psi(\boldsymbol{r}) = \overline{g}\phi_c\alpha_\Lambda(\boldsymbol{r}), \tag{2.47a}$$

$$\left[\frac{\hbar^2\boldsymbol{k}^2}{m} - \nu_0\right]\phi_c = \overline{g}\int d^3r\,\psi(\boldsymbol{r})\alpha_\Lambda(\boldsymbol{r}), \tag{2.47b}$$

where we have introduced the relative momentum $\boldsymbol{k} = \hbar(\boldsymbol{k}_1 - \boldsymbol{k}_2)/2$. Inspired by the low-energy behavior of the wave function in the open channel, we make the Ansatz

$$\psi_{\boldsymbol{k}}(\boldsymbol{r}) = e^{i\boldsymbol{k}\cdot\boldsymbol{r}} + \beta\int d^3r'\,\alpha_\Lambda(\boldsymbol{r}')G_{\boldsymbol{k}}(\boldsymbol{r}-\boldsymbol{r}'), \tag{2.48}$$

where $G_{\boldsymbol{k}}(\boldsymbol{r})$ is the retarded Green's function introduced in Eq. (2.12) and we drop the superscript (+) for a shorter notation. The factor β can be connected to the scattering amplitude via the far-field behavior of the Ansatz (2.48),

$$f(\boldsymbol{k}, \boldsymbol{k}') = -\frac{m}{4\pi\hbar^2}\beta\int d^3r'\,\alpha_\Lambda(\boldsymbol{r}')e^{i\boldsymbol{k}'\cdot\boldsymbol{r}'}, \tag{2.49}$$

with $\boldsymbol{k}' = k\boldsymbol{r}/r$. Inserting the Ansatz into Eq. (2.47) yields

$$\beta = \bar{g}\phi_c\,, \tag{2.50a}$$

$$\left(\frac{\hbar^2k^2}{m} - \nu_0\right)\phi_c = \bar{g}\left[\int d^3r\,\alpha_\Lambda(\boldsymbol{r})e^{i\boldsymbol{k}\cdot\boldsymbol{r}} + \beta\int d^3r\,d^3r'\,\alpha_\Lambda(\boldsymbol{r})\alpha_\Lambda(\boldsymbol{r}')G_{\boldsymbol{k}}(\boldsymbol{r}-\boldsymbol{r}')\right], \tag{2.50b}$$

which allows us to obtain a closed expression for β,

$$\beta = \frac{\bar{g}^2}{\frac{\hbar^2k^2}{m} - \nu_0 - \bar{g}^2\overline{G}(\boldsymbol{k})}. \tag{2.51}$$

Here, we have introduced

$$\overline{G}(\boldsymbol{k}) = \int d^3r\,d^3r'\,\alpha_\Lambda(\boldsymbol{r})\alpha_\Lambda(\boldsymbol{r}')G_{\boldsymbol{k}}(\boldsymbol{r}-\boldsymbol{r}') = \frac{m}{\hbar^2}\int\frac{d^3q}{(2\pi)^2}\frac{\hat{\alpha}_\Lambda^2(\boldsymbol{q})}{\boldsymbol{k}^2 - \boldsymbol{q}^2 + i\eta}, \tag{2.52}$$

where $\hat{\alpha}_\Lambda(\boldsymbol{q})$ is the Fourier transform of $\alpha_\Lambda(\boldsymbol{r})$.

With the scattering amplitude in Eq. (2.49) and β from Eq. (2.51) we have found a solution for the scattering problem for arbitrary energies. To make a connection to the

universal low-energy behavior of the scattering amplitude from Eq. (2.25), we expand the integrals in Eq. (2.49) and Eq. (2.52) for $k\Lambda \ll 1$,

$$\int d^3r'\, \alpha_\Lambda(\boldsymbol{r}') e^{i\boldsymbol{k}'\cdot\boldsymbol{r}'} \overset{k\Lambda\ll 1}{=} 1 + \mathcal{O}(k^2)\,, \tag{2.53a}$$

$$\int d^3r\, d^3r'\, \alpha_\Lambda(\boldsymbol{r})\alpha_\Lambda(\boldsymbol{r}') G_{\boldsymbol{k}}(\boldsymbol{r}-\boldsymbol{r}') \overset{k\Lambda\ll 1}{=} -\frac{m}{4\pi\hbar^2}\left(\frac{1}{\sqrt{\pi}\Lambda} + ik\right) + \mathcal{O}(k^2). \tag{2.53b}$$

This allows us to write the scattering amplitude in its well-known form,

$$f(k) = -\frac{1}{-\frac{4\pi\hbar^2}{m}\frac{\nu}{\bar{g}^2} + ik + \mathcal{O}(k^2)}, \tag{2.54}$$

where we have introduced the physical detuning

$$\nu = \nu_0 + \bar{g}^2\overline{G}(0) = \nu_0 - \frac{m\bar{g}^2}{4\pi^{3/2}\hbar^2\Lambda}. \tag{2.55}$$

Hence, the parameters of our model are connected to the scattering length via

$$a_\mathrm{s} = -\frac{m}{4\pi\hbar^2}\frac{\bar{g}^2}{\nu}. \tag{2.56}$$

A short note on the connection to the delta potential: For $\Lambda \to 0$, we recover the delta potential in the open channel, which is known to be unphysical in three dimensions and needs to be regularized (see Sec. 2.3.1). For the two-channel model introduced here, this regularization is straightforward. The physical detuning ν is connected to the scattering length and therefore has to remain finite also in the limit $\Lambda \to 0$. In turn, this means that the bare detuning ν_0 entering into the microscopic theory has to diverge in order to ensure a finite detuning ν in Eq. (2.55), similar to the situation in interacting quantum field theories.

The connection between the bare detuning ν_0 and the physically observable detuning ν in Eq. (2.55), as well as the connection to the scattering length in Eq. (2.56) will become important in Chapter 4, where we use the minimal two-channel model to solve the scattering problem for various confinements.

2.4 | Dipolar Interactions

In our discussion so far, we have focused on isotropic short-range interactions, which will help us to understand quantum fluctuations in many-body systems in Chapter 5. While contact interactions allow for fascinating many-body physics on their own, atoms such as dysprosium and erbium with a strong dipolar moment have attracted a lot of interest in recent years [37, 39, 40]. The anisotropic long-range character of the dipolar interaction allows to observe a variety of new phenomena such as quantum droplets or supersolids in cold atomic gases. Due to the anisotropy of the dipolar interaction, the systems

can show very different behavior depending on the exact trapping potential. The particles not only interact via the dipolar interaction but also via a short-range interaction characterized by the scattering length a_s. Tuning the scattering length therefore allows to control the relative strength between the dipolar and the short-range interaction. The tunable strength in combination with the anisotropic long-range character offer a level of control, which makes dipolar gases the ideal playground to explore interesting many-body physics. In this section, we will discuss the dipolar interaction and its most important properties. For an elaborate discussion of the dipolar interaction and the phenomena resulting from it, we refer the reader to [37, 39, 40].

For two dipoles pointing in the (normalized) directions $\boldsymbol{e}_1$ and $\boldsymbol{e}_2$ at relative distance $\boldsymbol{r}$, the interaction potential reads

$$V_\mathrm{dd}(\boldsymbol{r}) = \frac{C_\mathrm{dd}}{4\pi}\frac{(\boldsymbol{e}_1\cdot\boldsymbol{e}_2)r^2 - 3(\boldsymbol{e}_1\cdot\boldsymbol{r})(\boldsymbol{e}_2\cdot\boldsymbol{r})}{r^5}. \tag{2.57}$$

The coupling constant C_dd characterizes the strength of the interaction and depends on whether the particles possess a magnetic or electric dipole moment. For this work, we solely focus on magnetic atoms with a magnetic dipole moment μ, which results in $C_\mathrm{dd} = \mu^2\mu_0$ where μ_0 is the vacuum magnetic permeability. In addition, the dipoles are aligned ($\boldsymbol{e}_1 = \boldsymbol{e}_2 = \boldsymbol{e}$), which simplifies Eq. (2.57) greatly,

$$V_\mathrm{dd}(\boldsymbol{r}) = \frac{C_\mathrm{dd}}{4\pi}\frac{1-3\cos^2\theta}{r^3}. \tag{2.58}$$

Here, θ is the angle between the polarization axis and the relative position of the particles, $\boldsymbol{e}\cdot\boldsymbol{r}/r = \cos\theta$. Depending on the orientation of the dipoles, the dipolar interaction can be attractive, repulsive, or even vanish at the so called magic angle $\theta_\mathrm{m} = \arccos(1/\sqrt{3})$. For this work, we are particularly interested in the attractive head-to-tail configuration ($\theta = 0$) for the dimensional crossover in Sec. 5.4 and in the repulsive side-by-side orientation ($\theta = \pi/2$) for the one-dimensional supersolid in Chapter 6.

The Fourier transform of Eq. (2.58) [37]

$$V_\mathrm{dd}(\boldsymbol{k}) = C_\mathrm{dd}\left(\cos^2\alpha - \frac{1}{3}\right), \tag{2.59}$$

where α is the angle between the polarization axis and $\boldsymbol{k}$, reveals another interesting characteristic. Despite the r-dependence of the dipolar interaction in Eq. (2.58), the Fourier transform in Eq. (2.59) does not depend on the magnitude of $\boldsymbol{k}$ and the $\boldsymbol{k}$-dependence only enters via α. Also note that $V_\mathrm{dd}(\boldsymbol{k}=0) = 0$. As we will see in Sec. 3.2.3, due to the lack of a k-dependence the excitations in a dipolar three-dimensional BEC, despite being direction dependent, are very similar compared to a contact gas. The situation drastically changes when the particles are confined to a trap, which will be the focus of Chapter 6.

2.4.1 | Scattering Properties and Pseudopotential

We have discussed the scattering properties of particles interacting via an isotropic short-range interaction in detail in Sec. 2.2. There, we have seen that the s-wave scattering amplitude describes the scattering event fully for $\boldsymbol{k} \to 0$ and all higher partial waves vanish. For potentials which behave as r^{-3} at large distances this is not true anymore and in principle all partial waves contribute. In addition, the anisotropy of the dipolar interaction causes the partial waves to couple. Hence, the dipolar interaction cannot be replaced by a pseudopotential and be characterized by a scattering length.

It turns out that for magnetic atoms, the interactions in the low-energy regime can be well described by a combination of a contact interaction and a dipolar interaction,

$$V(\boldsymbol{r}) = \frac{4\pi\hbar^2 a_s}{m}\delta(\boldsymbol{r}) + \frac{3\hbar^2 a_{\mathrm{dd}}}{m}\frac{1-3\cos^2\theta}{r^3}, \tag{2.60}$$

where we have introduced the dipolar scattering length $a_{\mathrm{dd}} = m\mu^2\mu_0/12\pi\hbar^2$. Note that we intentionally did not include the renormalization of the delta distribution since Eq. (2.60) should only be understood as producing the correct scattering amplitude in first Born approximation. To be more precise: Full numerical investigations show that the first Born approximation of Eq. (2.60), which becomes

$$f_{1\mathrm{B}}(\boldsymbol{k}) = \begin{cases} -a_{\mathrm{s}}\left[1+\varepsilon_{\mathrm{dd}}(3\cos^2\alpha - 1)\right] \equiv -a_{\mathrm{s}}\, d(\alpha) & \text{for} \quad \boldsymbol{k} \neq 0 \\ -a_{\mathrm{s}} & \text{for} \quad \boldsymbol{k} = 0 \end{cases} \tag{2.61}$$

reproduces the exact scattering amplitude with high accuracy away from shape resonances [35, 36]. Here, we have introduced $\varepsilon_{\mathrm{dd}} = a_{\mathrm{dd}}/a_{\mathrm{s}}$, which characterizes the relative strength of the dipolar interaction compared to the contact interaction.

While this is very useful to study three-dimensional systems with dipolar interactions, the fact that the potential (2.60) only reproduces the scattering amplitude in a perturbative sense makes investigations where corrections to the Born approximation become important extremely challenging. For the investigation of confined dipolar systems in Chapter 6, for example, we *must* choose a regime where corrections due to the confinement-induced resonance, a concept which we will discuss in detail in Chapter 4, do not play a role.

This concludes our overview of scattering in the low-energy regime. In the next chapter, we review two approaches to obtain beyond-mean-field corrections in weakly interacting Bose gases. For these approaches, a fundamental understanding of scattering theory is crucial.

3 | Bose Gases Beyond Mean-Field

With the experimental progress in the field of ultracold atomic gases, we have come to the point where a perturbative lowest-order theoretical description does not explain certain phenomena properly. For a long time, a mean-field description which assumes all particles to be in the lowest energy state was enough to describe experiments adequately. The corresponding description in terms of the *Gross-Pitaevskii* equation [8, 9] is a classical field equation and neglects quantum fluctuations entirely. For systems interacting via a short-range contact interaction not only the depletion of the condensed state became observable [55], but also corrections to the mean-field result of the ground-state energy [56] as well as of the excitation spectrum [57, 58] have been measured. On a theoretical level, a perturbation expansion of these systems is not trivial. Due to their diluteness, the interactions are dominated by two-particle processes, where the particles scatter off each other and a standard quantum-mechanical perturbation series in terms of the interaction potential is not appropriate. In the weakly interacting regime, the characteristic kinetic energy of the system is much larger than the characteristic interaction energy. For a three-dimensional gas of density n this translates to

$$\frac{\hbar^2 n^{1/3}}{m} \gg ng, \tag{3.1}$$

where $g = 4\pi\hbar^2 a_\mathrm{s}/m$ is the coupling constant introduced in Sec. 2.3.1 and m is the mass of the bosons. The scattering in the low-energy regime can be fully described in terms of the scattering length a_s (see Sec. 2.2.1). The condition in Eq. (3.1) then provides a suitable small expansion parameter, the so called *gas parameter* $\sqrt{na_\mathrm{s}^3} \ll 1$. The next-order corrections to the mean-field result for the three-dimensional contact gas were first derived by Lee, Huang and Yang [52, 53] and are referred to as LHY corrections. In two-dimensions, obtaining the beyond-mean-field behavior has been the focus of intensive studies in the past [148–154], while in one dimension it is well understood from the exact result of a contact gas by Lieb and Liniger [155, 156]. As we will see, on a theoretical level the difficulty stems from the correct renormalization of the contact interaction. Also note that a description in terms of mean-field theory inherently assumes the presence of off-diagonal long-range order and in this sense, the beyond-mean-field corrections only influence the short-range part of the correlations and should not be confused with quantum fluctuations that affect spontaneous symmetry breaking in lower-dimensional systems. In one dimension, however, it is well established that fluctuations prevent the appearance of off-diagonal long-range order even at zero temperature [78–80]. In the weakly interacting regime, however, quasi-long-range order can survive [84], which justifies the use of mean-field theory. One can understand this phenomenon as locally

there is still a high number of particles in the condensate and quantum fluctuations only suppress the coherence between these local condensates on large distances. The effect of quantum fluctuations on one-dimensional supersolids and the applicability of mean-field theory will be the main focus of Chapter 7.

In this chapter we want to discuss two common methods to obtain beyond-mean-field corrections in the weakly interacting regime, which we will use throughout this work. Since the remainder of this work relies on a deep understanding of these methods, we dedicate the entire chapter to them. We mainly focus on three-dimensional systems to discuss the strengths and weaknesses of the two approaches. We start with a discussion of Bogoliubov theory [4] and afterwards we briefly introduce the approach of Hugenholtz and Pines [7], which allows for an elegant treatment of the dimensional crossover in Chapter 5. To conclude this chapter, we will briefly discuss the beyond-mean-field corrections for the one- and two-dimensional contact gas as well as for the three-dimensional dipolar gas.

3.1 | 3D Contact Gas: Methods

We start by investigating a dilute weakly interacting gas of bosons at temperature $T = 0$. The particles interact via an isotropic short-range interaction characterized by the scattering length a_s.

3.1.1 | Bogoliubov Theory

In this section, we will use Bogoliubov theory [4] to derive the ground-state energy and excitation spectrum of weakly interacting bosons of mass m. Bogoliubov theory has become a cornerstone in describing weakly interacting systems, such that an elaborate discussion can be found in many textbooks. In this short summary of the most important concepts, we loosely follow the excellent explanation of Noziére and Pines [157].

On a microscopic level, the Hamiltonian describing N interacting bosons in a box of volume Ω consists of the single-particle Hamiltonian

$$H_0 = \sum_{\boldsymbol{k}} \epsilon_0(\boldsymbol{k}) a^\dagger_{\boldsymbol{k}} a_{\boldsymbol{k}}, \tag{3.2}$$

with the dispersion relation $\epsilon_0(\boldsymbol{k}) = \frac{\hbar^2 k^2}{2m}$ and the two-body interaction

$$H_\mathrm{I} = \frac{1}{2\Omega} \sum_{\boldsymbol{k},\boldsymbol{k}',\boldsymbol{q}} V(\boldsymbol{q}) a^\dagger_{\boldsymbol{k}+\boldsymbol{q}} a^\dagger_{\boldsymbol{k}'-\boldsymbol{q}} a_{\boldsymbol{k}'} a_{\boldsymbol{k}}, \tag{3.3}$$

where $a^{(\dagger)}_{\boldsymbol{k}}$ are the annihilation (creation) operators of a particle with momentum $\boldsymbol{k}$ and $V(\boldsymbol{q})$ is the two-body potential in momentum space. The creation and annihilation operators obey the usual bosonic commutation relations

$$\left[a_{\boldsymbol{k}}, a^\dagger_{\boldsymbol{k}'}\right] = \delta_{\boldsymbol{k},\boldsymbol{k}'}, \tag{3.4}$$

where $\delta_{\boldsymbol{k},\boldsymbol{k}'}$ is the Kronecker delta and all remaining commutators vanish. For now, let us not specify the interaction and remain in this general framework. Then, the microscopic Hamiltonian is given by

$$H = H_0 + H_\mathrm{I} = \sum_{\boldsymbol{k}} \epsilon_0(\boldsymbol{k}) a^\dagger_{\boldsymbol{k}} a_{\boldsymbol{k}} + \frac{1}{2\Omega} \sum_{\boldsymbol{k},\boldsymbol{k}',\boldsymbol{q}} V(\boldsymbol{q}) a^\dagger_{\boldsymbol{k}+\boldsymbol{q}} a^\dagger_{\boldsymbol{k}'-\boldsymbol{q}} a_{\boldsymbol{k}'} a_{\boldsymbol{k}}. \tag{3.5}$$

Note that while we formulate the Hamiltonian for a three-dimensional box, adapting the approach to lower dimensions is straightforward.

The general microscopic Hamiltonian poses an extremely difficult quantum many-body problem, but for weak interactions and low temperatures the treatment simplifies drastically. In what follows, we only consider the temperature $T = 0$. In absence of interactions, all bosons occupy the lowest energy state $\boldsymbol{k} = 0$, the *condensate mode*, such that $N_0 = N$, where N_0 is the number of particles in the condensate mode. We can then write the ground state as the Fock state

$$|N_{\boldsymbol{k}=0}, 0_{\boldsymbol{k}_1}, 0_{\boldsymbol{k}_2}, \ldots\rangle \,. \tag{3.6}$$

This changes in the presence of interactions and the condensate mode depletes. For weak interactions, however, we expect the majority of particles to remain in the condensate mode which means $N'/N \ll 1$, where $N' = N - N_0$ is the number of excited particles. In this case, the action of the operators $a_0^{(\dagger)}$ on a state with N_0 condensed particles,

$$\begin{aligned} a_0 \,|N_0, \ldots\rangle &= \sqrt{N_0}\,|N_0 - 1, \ldots\rangle \\ a_0^\dagger \,|N_0, \ldots\rangle &= \sqrt{N_0 + 1}\,|N_0 + 1, \ldots\rangle \,, \end{aligned} \tag{3.7}$$

reveals an important property of the system. Since N_0 is large, a state differing by ± 1 particles in the condensed state will have a huge overlap with the original state $|N_0, \ldots\rangle$, especially in the thermodynamic limit. This means

$$\begin{aligned} a_0 \,|N_0, \ldots\rangle &\approx \sqrt{N_0}\,|N_0, \ldots\rangle \\ a_0^\dagger \,|N_0, \ldots\rangle &\approx \sqrt{N_0}\,|N_0, \ldots\rangle \,. \end{aligned} \tag{3.8}$$

In the thermodynamic limit a_0 and $a_0^\dagger$ have the same action on the state $|N_0, \cdots\rangle$. Hence, they commute and we can replace them by the number $\sqrt{N_0}$ in our discussion, $a_0^{(\dagger)} \to \sqrt{N_0}$. This replacement is referred to as the *Bogoliubov prescription*. Two important points should be kept in mind: First, the Bogoliubov prescription is only determined up to a constant phase, which does not change any physical property of the system. The ground state of the system randomly chooses *one* phase, and thus spontaneously breaks the continuous gauge symmetry, leading to a Goldstone mode [102–105]. Second, the Bogoliubov prescription inherently implies off-diagonal long-range order of the one-particle density matrix,

$$\langle \psi^\dagger(\boldsymbol{r}) \psi(0) \rangle \overset{\boldsymbol{r}\to\infty}{=} n_0, \tag{3.9}$$

where $n_0 = N_0/\Omega$ and the bosonic field operators are given by

$$\psi(\boldsymbol{r}) = \frac{1}{\sqrt{\Omega}} \sum_{\boldsymbol{k}} e^{i\boldsymbol{k}\cdot\boldsymbol{r}} a_{\boldsymbol{k}} \qquad \text{and} \qquad \psi^\dagger(\boldsymbol{r}) = \frac{1}{\sqrt{\Omega}} \sum_{\boldsymbol{k}} e^{-i\boldsymbol{k}\cdot\boldsymbol{r}} a^\dagger_{\boldsymbol{k}}. \tag{3.10}$$

This means that the use of the Bogoliubov prescription is in principle not justified in one dimension. We will comment on the one-dimensional Bose gas in Sec. 3.2.1.

With the Bogoliubov prescription, the Hamiltonian in Eq. (3.5) splits into different orders of N_0,

$$\begin{aligned} H = &\sum_{\boldsymbol{k}} \epsilon_0(\boldsymbol{k}) a^\dagger_{\boldsymbol{k}} a_{\boldsymbol{k}} \\ &+ \frac{N_0^2 V(0)}{2\Omega} \\ &+ {\sum_{\boldsymbol{k}}}' \left[\frac{N_0}{\Omega} [V(0) + V(\boldsymbol{k})] a^\dagger_{\boldsymbol{k}} a_{\boldsymbol{k}} + \frac{N_0 V(\boldsymbol{k})}{2\Omega} \left(a^\dagger_{\boldsymbol{k}} a^\dagger_{-\boldsymbol{k}} + a_{\boldsymbol{k}} a_{-\boldsymbol{k}} \right) \right] \\ &+ {\sum_{\boldsymbol{k},\boldsymbol{q}}}' \frac{V(\boldsymbol{q})}{2\Omega} \sqrt{N_0} \left(a^\dagger_{\boldsymbol{k}+\boldsymbol{q}} a_{\boldsymbol{q}} a_{\boldsymbol{k}} + a^\dagger_{\boldsymbol{k}+\boldsymbol{q}} a^\dagger_{-\boldsymbol{q}} a_{\boldsymbol{k}} \right) \\ &+ {\sum_{\boldsymbol{k},\boldsymbol{k}',\boldsymbol{q}}}' \frac{V(\boldsymbol{q})}{2\Omega} a^\dagger_{\boldsymbol{k}+\boldsymbol{q}} a^\dagger_{\boldsymbol{k}'-\boldsymbol{q}} a_{\boldsymbol{k}'} a_{\boldsymbol{k}}, \end{aligned} \tag{3.11}$$

where the primed sum indicates the absence of the condensate mode. The fourth and fifth line describe interactions where only a single or no condensed particles are involved, respectively. In the dilute, weakly interacting regime, those contributions can be ignored within our order of approximation. The second line is the lowest-order contribution to the ground-state energy, the *mean-field energy*. The remaining terms, however, show a crucial problem stemming from the Bogoliubov prescription: Our initial problem was to find a solution for N interacting bosons, but Eq. (3.11) only contains the number of condensed particles N_0. Since the condensate mode is treated classically, the Hamiltonian in Eq. (3.11) does not conserve the particle number anymore. A convenient way to restore the particle number conservation was introduced by Hugenholtz and Pines [7]. For now, we will only use their results, but their approach will be the main focus of Sec. 3.1.2. We introduce the grand canonical description

$$H' = H - \mu \hat{N}', \tag{3.12}$$

where $\hat{N}' = {\sum_k}' a^\dagger_{\boldsymbol{k}} a_{\boldsymbol{k}}$ is the particle number operator for the excited particles. Surprisingly, the chemical potential μ still fulfills the thermodynamic relation [7]

$$\mu = \frac{\partial E}{\partial N}, \tag{3.13}$$

where E is the ground-state energy. This allows us to search the ground state of H' in Eq. (3.12) for a fixed chemical potential and afterwards use Eq. (3.13) to obtain the

ground-state energy as a function of a fixed particle number N. In addition, we do not need to distinguish between the particle number N and the condensate number N_0 as the difference will only become relevant for higher-order corrections.

Under these considerations, we obtain the quadratic Hamiltonian

$$H' = \frac{N^2 V(0)}{2\Omega} + \frac{1}{2}\sum_{\boldsymbol{k}}{}' : \begin{pmatrix} a_{\boldsymbol{k}}^\dagger \\ a_{-\boldsymbol{k}} \end{pmatrix} \left[\begin{pmatrix} \chi & 0 \\ 0 & \chi \end{pmatrix} + \begin{pmatrix} \eta & \eta \\ \eta & \eta \end{pmatrix} \right] \begin{pmatrix} a_{\boldsymbol{k}} \\ a_{-\boldsymbol{k}}^\dagger \end{pmatrix} :, \tag{3.14}$$

where $: \hat{O} :$ is the normal ordered operator $\hat{O}$ and we have introduced

$$\chi = \epsilon_0(\boldsymbol{k}) + nV(0) - \mu \qquad \text{and} \qquad \eta = nV(\boldsymbol{k}). \tag{3.15}$$

Here, $n = N/\Omega$ is the particle density. To diagonalize the quadratic Hamiltonian in Eq. (3.14), we make use of a Bogoliubov transformation and introduce the new operators $b_{\boldsymbol{k}}^{(\dagger)}$, which are connected to $a_{\boldsymbol{k}}^{(\dagger)}$ by

$$a_{\boldsymbol{k}} = u_{\boldsymbol{k}} b_{\boldsymbol{k}} - v_{\boldsymbol{k}} b_{-\boldsymbol{k}}^\dagger \qquad \text{and} \qquad a_{\boldsymbol{k}}^\dagger = u_{\boldsymbol{k}} b_{\boldsymbol{k}}^\dagger - v_{\boldsymbol{k}} b_{-\boldsymbol{k}}. \tag{3.16}$$

The real Bogoliubov amplitudes $u_{\boldsymbol{k}}$ and $v_{\boldsymbol{k}}$ have to fulfill the condition $u_{\boldsymbol{k}}^2 - v_{\boldsymbol{k}}^2 = 1$ such that the transformation is canonical and the new operators satisfy the bosonic commutation relations

$$\left[b_{\boldsymbol{k}}, b_{\boldsymbol{k}'}^\dagger \right] = \delta_{\boldsymbol{k},\boldsymbol{k}'}\,, \tag{3.17}$$

while all other commutators vanish. A short calculation then leads to the amplitudes

$$u_{\boldsymbol{k}}^2 = \frac{1}{2}\left[\frac{\epsilon_0(\boldsymbol{k}) + n_0 V(\boldsymbol{k})}{\epsilon(\boldsymbol{k})} + 1 \right], \qquad v_{\boldsymbol{k}}^2 = \frac{1}{2}\left[\frac{\epsilon_0(\boldsymbol{k}) + n_0 V(\boldsymbol{k})}{\epsilon(\boldsymbol{k})} - 1 \right], \tag{3.18}$$

where

$$\epsilon(\boldsymbol{k})^2 = \chi^2 + 2\chi\eta \tag{3.19}$$

is the excitation spectrum. The diagonal Hamiltonian then reads

$$H' = E + \sum_{\boldsymbol{k}}{}' \epsilon(\boldsymbol{k}) b_{\boldsymbol{k}}^\dagger b_{\boldsymbol{k}}\,, \tag{3.20}$$

with the ground-state energy

$$E = \frac{N^2 V(0)}{2\Omega} + \frac{1}{2}\sum_{\boldsymbol{k}}{}' \epsilon(\boldsymbol{k}) - \chi - \eta. \tag{3.21}$$

Both, the ground-state energy and the excitation spectrum still depend on the chemical potential μ. In lowest order, the chemical potential is given by

$$\mu^{(1)} = \frac{d}{dN}\frac{N^2 V(0)}{2\Omega} = nV(0), \tag{3.22}$$

and the excitation spectrum becomes gapless,

$$\epsilon(\boldsymbol{k}) = \sqrt{\epsilon_0(\boldsymbol{k})^2 + 2nV(\boldsymbol{k})\epsilon_0(\boldsymbol{k})}\,, \tag{3.23}$$

as required by the famous Hugenholtz-Pines relation [7]. In the thermodynamic limit, we end up with the energy density

$$\frac{E}{\Omega} = \frac{n^2 V(0)}{2} + \frac{1}{2}\int \frac{d^3k}{(2\pi)^3}\left[\epsilon(\boldsymbol{k}) - \epsilon_0(\boldsymbol{k}) - nV(\boldsymbol{k})\right]. \tag{3.24}$$

As we have seen during the discussion of the scattering problem in Chapter 2, in the low-energy regime the scattering of particles becomes universal. Thus, we can replace the true interatomic potential $V(\boldsymbol{k})$ by a much simpler potential, as long as it reproduces the same scattering properties. A common choice is the delta interaction, which produces the correct scattering properties *only* in first Born approximation. Its Fourier transform is given by

$$V(\boldsymbol{k}) = g = \frac{4\pi\hbar^2 a_\mathrm{s}}{m}. \tag{3.25}$$

Inserting the potential from Eq. (3.25) into the excitation spectrum Eq. (3.23) yields the famous Bogoliubov excitation spectrum for the quasi-particles,

$$\epsilon(\boldsymbol{k}) = \sqrt{\frac{\hbar^2 k^2}{2m}\left(2ng + \frac{\hbar^2 k^2}{2m}\right)}\,. \tag{3.26}$$

For low momenta, the spectrum is linear,

$$\epsilon(\boldsymbol{k}) \overset{k\to 0}{=} \hbar|k|c, \tag{3.27}$$

where $c = \sqrt{ng/m}$ is the sound velocity, while for large momenta, we recover the spectrum of a free particle $\epsilon \sim k^2$.

While the potential in Eq. (3.25) yields the correct Bogoliubov spectrum, inserting Eq. (3.25) into the ground-state energy in Eq. (3.24) reveals a fundamental problem: The integral does not converge due to an ultraviolet diverging term of the form

$$\sim \int \frac{d^3k}{(2\pi)^3}\frac{1}{k^2}. \tag{3.28}$$

The reason behind this divergence within Bogoliubov theory is not obvious and explanations in literature are often vague. Two important points need to be kept in mind: First, Bogoliubov theory is not a standard perturbation expansion in $V(\boldsymbol{k})$. In the language of quantum field theory, the Bogoliubov transformation can be seen as way to sum an entire class of interaction diagrams, namely those connected diagrams with an internal momentum pair $(\boldsymbol{k}, -\boldsymbol{k})$ and repetitions of it [158]. Second, the use of the delta potential

can be misleading. As already discussed in Sec. 2.3.1, the delta potential is not a physical potential and needs to be regularized. Interestingly, however, $V(\boldsymbol{k})$ in Eq. (3.25) coincides with the low-energy T-matrix, which accounts for *all* ladder-diagrams of the interaction. Using the Bogoliubov transformation in Eq. (3.16) and inserting $V(\boldsymbol{k})$ combines the summation of two types of diagrams but unfortunately also leads to diagrams being counted more than once. This causes the energy to diverge. A detailed discussion of this double counting can be found in [157] or in a previous work [159]. Luckily, it turns out that this double counting is easily fixed by adding the term

$$\int \frac{d^3k}{(2\pi)^3} \frac{n^2 g^2}{4\epsilon_0(\boldsymbol{k})} \tag{3.29}$$

to the ground-state energy.

We also want to briefly discuss the most common argument to cure the divergence. As we go beyond the mean-field approximation, also higher orders in the scattering amplitude become important. However, if we use the simple delta potential in Eq. (3.25), we have to keep in mind that we have determined the coupling constant g only within first Born approximation [see Eq. (2.36)]. Within mean-field theory, this leading order expansion is sufficient. For the energy in Eq. (3.24) higher orders in a_s appear, which means we also have to include corrections for g on the mean-field level for a consistent expansion in na_s^3. Using the second Born approximation for the delta interaction in Eq. (2.37) means we have to use

$$V(0) = g\left(1 + g\int \frac{d^3k}{(2\pi)^3} \frac{1}{2\epsilon_0(\boldsymbol{k})}\right) \tag{3.30}$$

for the mean-field energy, which exactly provides the term in Eq. (3.29).

Both methods lead to the same result, a consistent expansion in terms of the scattering length a_s. While the diagrammatic approach makes the physical problem very clear, the latter regularization highlights an important property of beyond-mean-field corrections: They are on the same level of accuracy as the second Born approximation, which will become important for the discussion of the dimensional crossover in Chapter 5.

Including the renormalization, we obtain the well-known result

$$\begin{aligned} \frac{E}{\Omega} &= \frac{n^2 g}{2} + \frac{1}{2}\int \frac{d^3k}{(2\pi)^3}\left[\epsilon(\boldsymbol{k}) - \epsilon_0(\boldsymbol{k}) - ng + \frac{n^2 g^2}{2\epsilon_0(\boldsymbol{k})}\right] \\ &= \frac{2\pi\hbar^2 a_\mathrm{s}}{m} n^2 \left(1 + \frac{128}{15\sqrt{\pi}}\sqrt{na_\mathrm{s}^3}\right), \end{aligned} \tag{3.31}$$

which was first obtained by Lee, Huang and Yang (LHY) [52, 53]. Note that to obtain the LHY correction, we integrate over *all* momenta in Eq. (3.31) but as discussed in Chapter 2, scattering is only universal in the low-energy regime. However, the dominant contribution the LHY correction stems from momenta $k \sim 1/\xi_h$, where $\xi_h = \sqrt{\hbar^2/2mng}$ is the healing length such that $ka_\mathrm{s} \sim \sqrt{na_\mathrm{s}^3} \ll 1$ and the error is negligible.

As we have seen in this section, Bogoliubov theory is a straightforward method to obtain the excitation spectrum of the weakly interacting Bose gas but to obtain the beyond-mean-field correction of the ground-state energy, a manual regularization is necessary. This makes its use for the dimensional crossover in Chapter 5 not ideal. In the following section, we will discuss the field-theoretic approach of Hugenholtz and Pines [7], which will allow us to cure divergences systematically.

3.1.2 | Field-Theoretic Approach

While Bogoliubov theory is the most widely known approach to treat the weakly interacting Bose gas, we have seen in the previous section that its simplicity comes with a cost: Divergencies have to be cured manually and the reason behind the divergencies is not obvious from the approach.

A less known method to treat dilute Bose gases relies on methods from quantum field theory. While these methods are much more involved than Bogoliubov theory, they allow for a consistent treatment and provide a good understanding of the underlying divergencies. First developed by Beliaev for a weakly interacting Bose gas at zero temperature, he was able to reproduce the LHY correction [5, 6], while the approach of Hugenholtz and Pines [7] in 1959 allowed them to verify corrections to the LHY result, which were first obtained by Wu [160]. In addition, Hugenholtz and Pines were able to connect the chemical potential to the proper self-energies, which is known as the Hugenholtz-Pines theorem and results in a gapless excitation spectrum.

In the following, we give a brief introduction of the approach of Hugenholtz and Pines. For an elaborate discussion, we refer the reader to the original publications [5–7], the detailed discussion in [161] or a previous work [159].

We start with the same Hamiltonian as in the previous section, but expressed in terms of the field operators,

$$\psi(\boldsymbol{r}) = \frac{1}{\sqrt{\Omega}} \sum_{\boldsymbol{k}} e^{i\boldsymbol{k}\cdot\boldsymbol{r}} a_{\boldsymbol{k}} \qquad \text{and} \qquad \psi^\dagger(\boldsymbol{r}) = \frac{1}{\sqrt{\Omega}} \sum_{\boldsymbol{k}} e^{-i\boldsymbol{k}\cdot\boldsymbol{r}} a_{\boldsymbol{k}}^\dagger, \tag{3.32}$$

which results in

$$\begin{aligned} H &= H_0 + H_{\text{int}} \\ &= -\frac{\hbar^2}{2m} \int d^3r\, \Psi^\dagger(\boldsymbol{r}) \nabla^2 \Psi(\boldsymbol{r}) + \frac{1}{2} \int\int d^3r\, d^3r'\, \Psi^\dagger(\boldsymbol{r}) \Psi^\dagger(\boldsymbol{r}') \tilde{V}(\boldsymbol{r}-\boldsymbol{r}') \Psi(\boldsymbol{r}') \Psi(\boldsymbol{r}). \end{aligned} \tag{3.33}$$

The field operators obey the bosonic commutation relations

$$\left[\psi(\boldsymbol{r}), \psi^\dagger(\boldsymbol{r}')\right] = \delta(\boldsymbol{r}-\boldsymbol{r}'), \tag{3.34}$$

while the remaining commutators are identical to zero. As in the Bogoliubov approach, we replace the operators of the condensate mode $a_0^{(\dagger)} \to \sqrt{N_0}$, which results in

$$\psi(\boldsymbol{r}) \to \sqrt{n_0} + \frac{1}{\sqrt{\Omega}} {\sum_{\boldsymbol{k}}}' e^{i\boldsymbol{k}\cdot\boldsymbol{r}} a_{\boldsymbol{k}}, \tag{3.35}$$

where n_0 is the density of condensed particles. With the Bogoliubov prescription, the Hamiltonian in Eq. (3.33) splits into different orders of n_0 and does not conserve the particle number anymore. We introduce a Lagrange multiplier, the chemical potential μ, to impose the subsidiary condition

$$N = N_0 + {\sum_{\boldsymbol{k}}}' \langle \Phi_{\text{int}}(n_0) | a^\dagger_{\boldsymbol{k}} a_{\boldsymbol{k}} | \Phi_{\text{int}}(n_0) \rangle \ , \tag{3.36}$$

where $|\Phi_{\text{int}}(n_0)\rangle$ is the interacting ground state. Then, the grand canonical Hamiltonian reads

$$H'(n_0, \mu) = H_0 + H_{\text{int}}(n_0) - \mu N'. \tag{3.37}$$

As shown by Hugenholtz and Pines [7], the thermodynamic relation

$$\mu = \frac{dE}{dN} \tag{3.38}$$

still holds after the Bogoliubov prescription and allows us to obtain the ground-state energy for a fixed particle number N.

So far, the procedure is very similar to the Bogoliubov approach of the previous section. To make use of the standard methods of quantum field theory, we introduce the two-point Green's function

$$iG(x, y) = \langle \Phi_{\text{int}} | \mathcal{T} \left[\Psi(x) \Psi^\dagger(y) \right] | \Phi_{\text{int}} \rangle \, , \tag{3.39}$$

where $\mathcal{T}$ is the time-ordering operator and x, y are four-vectors. Like the field operators, separating the condensate mode splits the Green's function

$$iG(x, y) = n_0 + iG'(x, y) \tag{3.40}$$

such that $G'(x, y)$ does not contain any condensate operators anymore. In Fourier space this results in

$$iG'(\boldsymbol{k}, t_2 - t_1) = \langle \Phi_{\text{int}} | \mathcal{T} \left[a_{\boldsymbol{k}}(t_1) a^\dagger_{\boldsymbol{k}}(t_2) \right] | \Phi_{\text{int}} \rangle \qquad \text{for} \qquad \boldsymbol{k} \neq 0. \tag{3.41}$$

The goal is then to connect all relevant physical observables to G', which can be evaluated with the standard methods of quantum field theory. While the connection to the particle number is straightforward,

$$N = \langle \Phi_{\text{int}} | \hat{N} | \Phi_{\text{int}} \rangle = N_0 + \lim_{\eta \to 0^+} {\sum_{\boldsymbol{k}}}' iG'(\boldsymbol{k}, \eta) = N_0 + \lim_{\eta \to 0^+} \Omega \int \frac{d^4k}{(2\pi)^4} \, iG'(k) e^{ik_0 \eta}, \tag{3.42}$$

the connection to the ground-state energy requires effort but yields

$$E = \frac{1}{2} \mu N + \lim_{\eta \to 0^+} \frac{\Omega}{2} \int \frac{d^4k}{(2\pi)^4} \left(\hbar k_0 + \frac{\hbar^2 \boldsymbol{k}^2}{2m} \right) iG'(k) e^{ik_0 \eta}. \tag{3.43}$$

Note that in this section k is a four-vector with zero-component k_0 and not $|\boldsymbol{k}|$. In the following, the limit $\eta \to 0^+$ will be implicit. It is important to point out that Eq. (3.43) for the ground-state energy is a differential equation since $\mu = dE/dN$, which appears on both sides of Eq. (3.43). In the low-density limit, however, we will see that we can use a lower-order expression for μ on the right-hand side to obtain the correct expansion of E.

The relations above show that the remaining task is to determine the Green's function G'. To do so, we want to point out that after the Bogoliubov prescription, *any* annihilation operator in H' destroys the non-interacting ground state $|\Phi_0\rangle$, in which all particles are in the condensate mode [see Eq.(3.6)]. In the language of quantum field theory $|\Phi_0\rangle$ acts as the non-interacting vacuum and all standard methods from quantum field theory become applicable. We waive to include the detailed procedure here since a much more elaborate discussion can be found in any standard textbook on many-body physics, e.g. [161–163] only to name a few. When comparing the treatment to other physical systems, however, one should keep in mind that here, the particle number is not conserved and additional proper self-energies Σ have to be introduced to correctly include the condensate. Without going into too much detail, these proper self-energies can be represented as

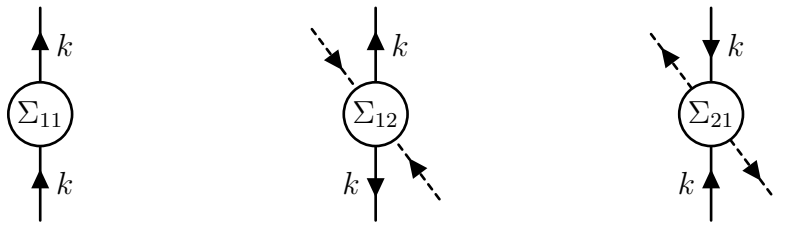

, (3.44)

where a solid line represents the free propagator of non-condensed particles, while each dashed line contributes a factor $\sqrt{n_0}$ and represents the condensate. The non-conservation of particles becomes apparent in Σ_{12} and Σ_{21}, which describe the excitation of two particles with opposite momenta from the condensate or the creation of two condensed particles from two particles with opposite momenta, respectively.

The Green's function G' can then be expressed in terms of the proper self-energies resulting in

$$G'(k) = \frac{k_0 + \left(\epsilon_0(\boldsymbol{k}) - \mu\right)/\hbar + S(k) - A(k)}{\left[k_0 - A(k)\right]^2 - \left[\left(\epsilon_0(\boldsymbol{k}) - \mu\right)/\hbar + S(p)\right]^2 + \Sigma_{12}(k)\Sigma_{21}(k)}, \tag{3.45}$$

where

$$S(k) = \frac{1}{2}\left[\Sigma_{11}(k) + \Sigma_{11}(-k)\right] \qquad \text{and} \qquad A(k) = \frac{1}{2}\left[\Sigma_{11}(k) - \Sigma_{11}(-k)\right]. \tag{3.46}$$

For a resting uniform gas Eq. (3.45) simplifies since $\Sigma_{12} = \Sigma_{21}$. In addition, also the chemical potential can be directly related to the proper self-energies,

$$\mu = \hbar\left[\Sigma_{11}(0) - \Sigma_{12}(0)\right], \tag{3.47}$$

which is known as the Hugenholtz-Pines theorem [7]. It is important to note that Eq. (3.13) holds for all orders of perturbation theory, which means different orders of the ground-state energy can be treated independently. Thus, the problem reduces to finding consistent expressions for the proper self energies.

In lowest order, the proper self-energies and in turn the chemical potential vanish. We recover the propagator of a free particle

$$G'^{(0)}(k) = \frac{1}{k_0 - \epsilon_0(\boldsymbol{k})/\hbar + i\eta},$$

which results in

$$E^{(0)} - \frac{1}{2}\mu N = 0 \tag{3.48}$$

as the integral on the right-hand side of Eq. (3.43) vanishes. By solving this differential equation,

$$E^{(0)} - \frac{1}{2}\frac{dE^{(0)}}{dN}N = 0 \qquad \Leftrightarrow \qquad E^{(0)} = \alpha N^2, \tag{3.49}$$

we make an important observation: The differential equation leaves terms of the order N^2 undetermined. This will be crucial as divergences within Bogoliubov theory exactly appeared in terms $\sim N^2$ [see Eq. (3.29)].

For the first non-trivial order of the proper self-energies, a variety of diagrams share the same order in n_0, which we all have to take into account. Those are precisely the diagrams that describe scattering between particles such that for low-energies $\boldsymbol{k}a_\mathrm{s} \ll 1$, they can be connected to the low-energy scattering amplitude Eq. (2.25),

$\Sigma^{(1)}_{11}(k) =$  $\overset{|\boldsymbol{k}|a_\mathrm{s}\ll 1}{\approx} -\dfrac{8\pi\hbar n_0}{m} f(0)$ (3.50a)

$\Sigma^{(1)}_{12}(k) =$ 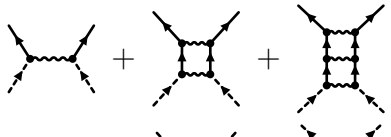 $\overset{|\boldsymbol{k}|a_\mathrm{s}\ll 1}{\approx} -\dfrac{4\pi\hbar n_0}{m} f(0)$ (3.50b)

$\Sigma^{(1)}_{21}(k) =$ 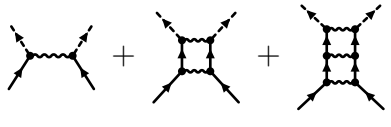 $\overset{|\boldsymbol{k}|a_\mathrm{s}\ll 1}{\approx} -\dfrac{4\pi\hbar n_0}{m} f(0),$ (3.50c)

where $f(0) = -a_\mathrm{s}$. Using the Hugenholtz-Pines theorem from Eq. (3.47) then allows us to obtain the mean-field chemical potential

$$\mu^{(1)} = g n_0, \tag{3.51}$$

where we make use of the coupling constant $g = 4\pi\hbar^2 a_\mathrm{s}/m$. The chemical potential in Eq. (3.51) fixes the mean-field energy to

$$E^{(1)} = E_\mathrm{mf} = \frac{ng}{2}N. \tag{3.52}$$

Note that we have replaced $N_0 \to N$, consistent with Eq. (3.49) and with the discussion below. The proper self-energies in Eq. (3.50) also allow us to obtain the corrections to the mean-field result. We obtain the Green's function

$$G'(\boldsymbol{k}) = \frac{u_{\boldsymbol{k}}^2}{k_0 - \epsilon_{\boldsymbol{k}}/\hbar + i\eta} - \frac{v_{\boldsymbol{k}}^2}{k_0 + \epsilon_{\boldsymbol{k}}/\hbar - i\eta}, \tag{3.53}$$

where

$$u_{\boldsymbol{k}}^2 = \frac{1}{2}\left[\frac{\epsilon_0(\boldsymbol{k}) + n_0 g}{\epsilon(\boldsymbol{k})} + 1\right] \qquad \text{and} \qquad v_{\boldsymbol{k}}^2 = \frac{1}{2}\left[\frac{\epsilon_0(\boldsymbol{k}) + n_0 g}{\epsilon(\boldsymbol{k})} - 1\right] \tag{3.54}$$

coincide with the Bogoliubov amplitudes for the pseudopotential [see Eq. (3.18)]. Here, $\epsilon(\boldsymbol{k})$ is the excitation spectrum,

$$\epsilon(\boldsymbol{k})^2 = \epsilon_0(\boldsymbol{k})^2 + 2n_0 g\epsilon_0(\boldsymbol{k})\,. \tag{3.55}$$

The Green's function in Eq. (3.53) allows us to obtain corrections to mean-field theory. First, let us consider the quantum depletion of the condensate. By inserting Eq. (3.53) into Eq. (3.42), we obtain the fractional depletion

$$\begin{aligned}\frac{n - n_0}{n} &= \frac{1}{n}\int \frac{d^4k}{(2\pi)^4} iG'(k)e^{ik_0\eta} = \frac{1}{n}\int \frac{d^3k}{(2\pi)^3} v_{\boldsymbol{k}}^2 \\ &= \frac{8}{3\sqrt{\pi}}\frac{(n_0 a_\mathrm{s})^{3/2}}{n} < \frac{8}{3}\left(\frac{na_\mathrm{s}^3}{\pi}\right)^{1/2} \ll 1,\end{aligned} \tag{3.56}$$

where in the first line, we have closed the integration contour in the upper half-plane. As the depletion is small, we can safely assume $n_0 \approx n$ in the following.

Inserting the Green's function into Eq. (3.43) and again closing the contour of the k_0-integration in the upper half-plane, yields the differential equation

$$\begin{aligned}\varepsilon^{(2)} - \frac{n}{2}\frac{d\varepsilon^{(2)}}{dn} &= \frac{1}{2}\int \frac{d^3k}{(2\pi)^3}\left[\epsilon_0(\boldsymbol{k}) - \epsilon(\boldsymbol{k})\right] v_{\boldsymbol{k}}^2 \\ &= \frac{1}{4}\int \frac{d^3k}{(2\pi)^3}\left[\frac{2\epsilon_0(\boldsymbol{k})^2 + 3\epsilon_0(\boldsymbol{k})ng}{\sqrt{\epsilon_0(\boldsymbol{k})^2 + 2\epsilon_0(\boldsymbol{k})ng}} - 2\epsilon_0(\boldsymbol{k}) - ng\right] \\ &\equiv \frac{l(n)}{2},\end{aligned} \tag{3.57}$$

where we have introduced the energy density $\varepsilon = E/\Omega$. The solution to this differential equation is then given by

$$\varepsilon^{(2)}(n) = -n^2 \int_0^n dn' \, \frac{l(n')}{n'^3}. \tag{3.58}$$

Note that the first-order differential equation (3.57) requires an additional constraint for a unique solution. The mean-field result in Eq. (3.52) has to be the leading order for a consistent expansion in the weakly interacting regime. For a three-dimensional gas, this means that corrections have to decay faster than n^2 for $n \to 0$. Hence, we have set the lower limit of the integration in Eq. (3.58) to zero, such that the integral itself vanishes for $n \to 0$. By performing the n'-integration, we end up with

$$\varepsilon^{(2)}(n) = \frac{1}{2} \int \frac{d^3k}{(2\pi)^3} \left[\epsilon(\boldsymbol{k}) - \epsilon_0(\boldsymbol{k}) - \frac{4\pi\hbar^2 a_\mathrm{s} n}{m} + \frac{(4\pi\hbar^2 a_\mathrm{s} n/m)^2}{2\epsilon_0(\boldsymbol{k})} \right], \tag{3.59}$$

such that we recover the correct ground-state energy including the LHY correction,

$$\frac{E}{\Omega} = \varepsilon^{(1)} + \varepsilon^{(2)} = \frac{2\pi\hbar^2 a_\mathrm{s}}{m} n^2 \left(1 + \frac{128}{15\sqrt{\pi}} \sqrt{n a_\mathrm{s}^3} \right). \tag{3.60}$$

Within this field-theoretic approach a manual regularization of the ground-state energy is not necessary. In fact, the correct choice of the lower integration limit in Eq. (3.57) provides the required term to cure the divergence in Bogoliubov theory. The lower integration limit, however, requires the knowledge of the correct mean-field energy $\sim n^2$. While this is not a problem for the three-dimensional or pure one- or two-dimensional gas, the correct mean-field term in the low-dimensional regime of a confined system is not obvious, as we will see in Chapter 5.

3.2 | Beyond-Mean-Field Corrections in Other Systems

We conclude this chapter by giving a brief overview of the beyond-mean-field corrections in systems we will need in later chapters. This includes the one- and two-dimensional contact gas, as well as the three-dimensional dipolar gas.

3.2.1 | 1D Contact Gas

Quantum fluctuations prevent the appearance of off-diagonal long-range order for the one-dimensional Bose gas [81–84, 149], and the use of mean-field theory, which inherently assumes the presence of a condensate, is in principle not justified. The one-dimensional Bose gas with a delta interaction, however, is well understood from the exact solution of the Lieb-Liniger model [155, 156]. The interaction strength is characterized by comparing

the characteristic kinetic energy $\hbar^2 n_{1\mathrm{D}}^2/m$ to the characteristic interaction energy $n_{1\mathrm{D}} g_{1\mathrm{D}}$, where $n_{1\mathrm{D}} = N/L$ is the one-dimensional density, L is the quantization length and the coupling constant $g_{1\mathrm{D}}$ is connected to the scattering length $a_{1\mathrm{D}}$ via $g_{1\mathrm{D}} = -2\hbar^2/m a_{1\mathrm{D}}$ [see Eq. (2.40)]. In contrast to the three-dimensional system, this means that the interaction strength *decreases* for an *increasing* density. In the strongly interacting regime,

$$\frac{\hbar^2 n_{1\mathrm{D}}^2}{m} \ll n_{1\mathrm{D}} g_{1\mathrm{D}} \qquad \Leftrightarrow \qquad \frac{1}{|n_{1\mathrm{D}} a_{1\mathrm{D}}|} \gg 1, \tag{3.61}$$

and one recovers the Tonks-Girardeau gas, a gas of impenetrable bosons [21, 22]. Surprisingly, in the weakly interacting regime where $1/|n_{1\mathrm{D}} a_{1\mathrm{D}}| \ll 1$, Lieb and Liniger found that Bogoliubov theory still provides an accurate description for the ground-state energy and the excitation spectrum. This can be understood as the one-body density matrix still exhibit quasi-long-range order [81–84],

$$\langle \Psi^\dagger(x)\Psi(0)\rangle \sim |x|^{-1/2K}, \tag{3.62}$$

where $K = \pi\hbar n_{1\mathrm{D}}/(mc)$ and $c^2 = n_{1\mathrm{D}} g_{1\mathrm{D}}/m$ is the sound velocity. In the weakly interacting regime $K \gg 1$ such that fluctuations only suppress coherence on large distances.

Within Bogoliubov theory no divergences appear for the ground-state energy since $V(z) = g_{1\mathrm{D}}\delta(z)$ is a true physical potential and does not need a regularization, as discussed in Sec. 2.3.1. Adapting Eq. (3.24) to one dimension one obtains

$$\frac{E}{L} = -\frac{\hbar^2}{m a_{1\mathrm{D}}} n_{1\mathrm{D}}^2 \left(1 - \frac{4\sqrt{2}}{3\pi}\frac{1}{\sqrt{|n_{1\mathrm{D}} a_{1\mathrm{D}}|}}\right) \tag{3.63}$$

in the weakly interacting regime. On first sight it might be confusing that the beyond-mean-field corrections scale as $\sim n_{1\mathrm{D}}^{3/2}$, which is *lower* than the mean-field energy. However, this is consistent with our discussion of weak interactions since the mean-field result has to become the dominant contribution for $n_{1\mathrm{D}} \to \infty$. Note that the absence of a true condensate becomes apparent if we try to calculate the depletion of the condensate [see Eq. (3.56)],

$$\frac{n_{1\mathrm{D}} - n_0}{n_{1\mathrm{D}}} = \frac{1}{2n_{1\mathrm{D}}}\int_{-\infty}^{\infty}\frac{dk}{(2\pi)}\left[\frac{\epsilon_0(k) + n_0 g_{1\mathrm{D}}}{\sqrt{\epsilon_0(k)^2 + 2n_0 g_{1\mathrm{D}}\epsilon_0(k)}} - 1\right] \sim \ln\left(\frac{\xi}{L}\right)^{-\frac{1}{K}}, \tag{3.64}$$

which results in a diverging depletion in the thermodynamic limit $L \to \infty$. The influence of quantum fluctuations on the appearance of order will be discussed in more detail in Chapter 7.

3.2.2 | 2D Contact Gas

In two dimensions, off-diagonal long-range order only survives at temperature $T = 0$. While the beyond-mean-field corrections for the three- and one-dimensional Bose gas

were obtained in the late 1950s [52, 53] and early 1960s [22, 155, 156], respectively, obtaining the beyond-mean-field correction for the two-dimensional Bose gas turned out to be much harder. Problems of a consistent expansion arise due to a logarithmic dependence of the chemical potential μ on the two-dimensional density n_{2D}. Hence, even obtaining the chemical potential in lowest-order becomes difficult. A detailed discussion goes far beyond the scope of this work, but intensive studies led to the ground-state energy of the form [150–154],

$$\frac{E}{A} = \frac{2\pi\hbar^2 n_{\mathrm{2D}}^2/m}{\ln(\frac{1}{n_{\mathrm{2D}}a_{\mathrm{2D}}^2}) + \ln\left[\ln(\frac{1}{n_{\mathrm{2D}}a_{\mathrm{2D}}^2})\right] - \ln(e^{2\gamma}\pi\sqrt{e})}. \tag{3.65}$$

Here, A is the quantization area, a_{2D} is the scattering length in two dimensions introduced in Sec. 2.2.1, and $\gamma \approx 0.577$ is the Euler-Mascheroni constant. Form the ground-state energy in Eq. (3.65) it also becomes clear, that the small parameter in the weakly interacting regime is given by [148]

$$\frac{1}{|\ln(n_{\mathrm{2D}}a_{\mathrm{2D}}^2)|} \ll 1. \tag{3.66}$$

For the discussion of the dimensional crossover in Chapter 5, Eq. (3.65) and Eq. (3.66) will be sufficient to compare our results.

3.2.3 | 3D Dipolar Gas

With the field-theoretic approach introduced in Sec. 3.1.2, obtaining the beyond-mean-field correction for a dipolar Bose gas is straightforward. Instead of the scattering amplitude from Eq. (2.25) for an isotropic short-range potential, we make use of the scattering amplitude for dipolar particles introduced in Eq. (2.61). We obtain

$$\frac{E}{\Omega} = \frac{2\pi\hbar^2 a_{\mathrm{s}} n^2}{m} + \frac{1}{2}\int \frac{d^3k}{(2\pi)^3}\left[\epsilon(\boldsymbol{k}) - \epsilon_0(\boldsymbol{k}) - \frac{4\pi\hbar^2 a_{\mathrm{s}} d(\theta) n}{m} + \frac{(4\pi\hbar^2 a_{\mathrm{s}} d(\theta) n/m)^2}{2\epsilon_0(\boldsymbol{k})}\right], \tag{3.67}$$

where θ is the angle between the polarization and $\boldsymbol{k}$. The dipolar interaction also affects the excitation spectrum, which is now given by

$$\epsilon(\boldsymbol{k})^2 = \epsilon_0(\boldsymbol{k})^2 + \frac{8\pi\hbar^2 a_{\mathrm{s}} d(\theta) n}{m}\epsilon_0(\boldsymbol{k}). \tag{3.68}$$

The spectrum is still linear for $\boldsymbol{k} \to 0$, but the sound velocity depends on θ. Since the dipolar scattering amplitude does not depend on the absolute value of $\boldsymbol{k}$, evaluating the integral yields a similar result compared to Eq. (3.31),

$$\frac{E}{\Omega} = \frac{2\pi\hbar^2 a_{\mathrm{s}}}{m} n^2 \left[1 + \frac{128}{15\sqrt{\pi}}\sqrt{n a_{\mathrm{s}}^3}\mathcal{Q}_5(\varepsilon_{\mathrm{dd}})\right], \tag{3.69}$$

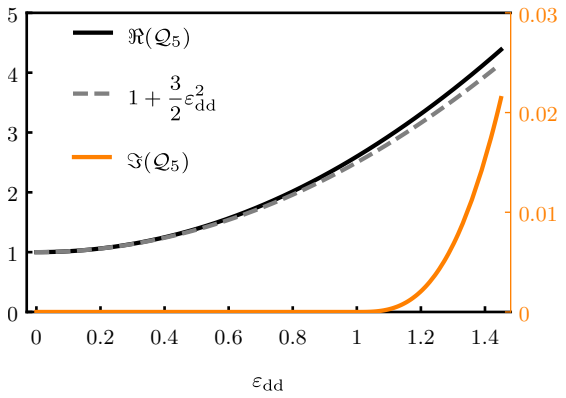

Figure 3.1: Real (black line) and imaginary (orange line) part of the function $\mathcal{Q}_5(\varepsilon_{\rm dd})$. The dashed gray line shows the series expansion of $\mathcal{Q}_5$ around $\varepsilon_{\rm dd} = 0$ up to order $\varepsilon_{\rm dd}^2$.

where

$$\mathcal{Q}_5(\varepsilon_{\rm dd}) = \frac{1}{2}\int_0^\pi d\theta\, \sin(\theta)\left[1+\varepsilon_{\rm dd}\left(3\cos^2(\theta)-1\right)\right]^{5/2} \tag{3.70}$$

stems from the angular dependence of the scattering amplitude. The beyond-mean-field correction for the weakly interacting dipolar gas was first obtained by Lima and Pelster using Bogoliubov theory [54]. Importantly, the function $\mathcal{Q}_5(\varepsilon_{\rm dd})$ becomes complex for $\varepsilon_{\rm dd} > 1$. This means that the gas shows an instability if the dipolar interaction is stronger than the contact repulsion. We show the real and imaginary part of $\mathcal{Q}_5(\varepsilon_{\rm dd})$ in Fig. 3.1. For $\varepsilon_{\rm dd} = 0$ the dipolar interaction is absent and we recover the LHY correction since $\mathcal{Q}_5(0) = 1$. In the range $0 < \varepsilon_{\rm dd} < 1$, the function $\mathcal{Q}_5(\varepsilon_{\rm dd})$ is real and often approximated by

$$\mathcal{Q}_5(\varepsilon_{\rm dd}) \approx 1 + \frac{3}{2}\varepsilon_{\rm dd}^2. \tag{3.71}$$

While this approximation gives accurate results for $\varepsilon_{\rm dd} \gtrapprox 0$, deviations from the exact result become apparent for $\varepsilon_{\rm dd} > 1$. Here, $\mathcal{Q}_5$ picks up an imaginary part, which indicates an instability of the system as the dipolar interaction dominates over the contact repulsion. Close to $\varepsilon_{\rm dd} = 1$, this imaginary part is extremely small. Since a consistent treatment for $\varepsilon_{\rm dd} > 1$ is still missing and the imaginary part is small, it is usually ignored.

How does the imaginary part of the energy arise? In Fig. 3.2, we plot the (dimensionless) squared excitation spectrum $\epsilon(\boldsymbol{k})^2/(ng)^2$ from Eq. (3.68) in the k_x-k_z-plane for $\varepsilon_{\rm dd} = 1.1$. Here, $g = 4\pi\hbar^2 a_{\rm s}/m$ is the coupling constant and $\xi_h = \sqrt{\hbar^2/2mng}$ the healing length. For $\varepsilon_{\rm dd} > 1$, the excitation spectrum shows a *phonon instability*, meaning it becomes imaginary for $\boldsymbol{k} \to 0$. This is highlighted by the orange region in Fig. 3.2 where $\epsilon^2 < 0$. Integrating over the orange region in Eq. (3.67) precisely results in the imaginary

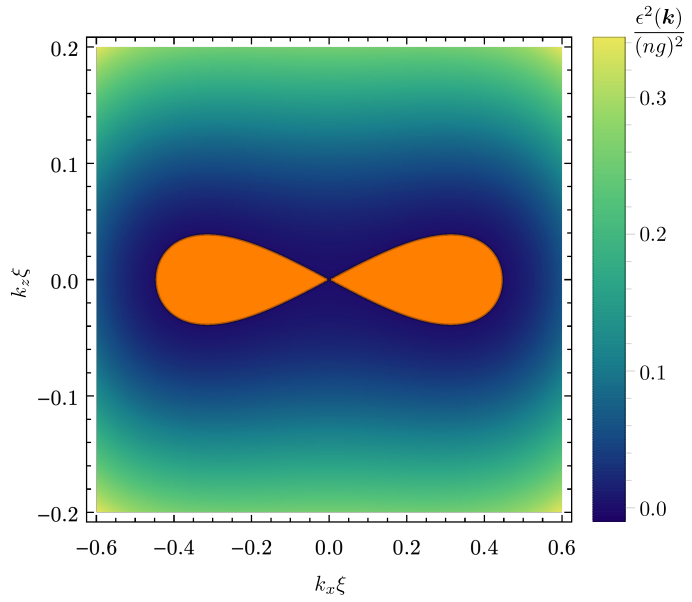

Figure 3.2: Squared dimensionless excitation spectrum in the k_x-k_z-plane. In the orange region $\epsilon^2 < 0$ and the system shows a phonon instability.

contribution of $\mathcal{Q}_5$. Note that the dominant contribution comes from $\theta = \pi/2$, which are excitations orthogonal to the polarization of the gas.

The beyond-mean-field correction for the 3D dipolar Bose gas in Eq. (3.69) plays a fundamental role in the description of dipolar droplets and supersolid states. While a mean-field description predicts a collapse of the dipolar gas, the repulsive beyond-mean-field correction $\sim n^{5/2}$ stabilizes these systems [45, 49]. However, for the trapped finite-size systems, the actual beyond-mean-field term is not known and the description relies on the local-density approximation. Therefore, it is important to investigate whether the use of the local-density approximation is even justified, which we will investigate for a trapped contact gas in Chapter 5. Since for dipolar droplets and supersolid states $\varepsilon_{\mathrm{dd}} > 1$, the use of local-density approximation also leads to imaginary contributions to the ground-state energy in the description of these systems. Hence, future work is required to investigate the beyond-mean-field corrections beyond the instability and in trapped geometries for dipolar quantum gases.

This concludes our discussion on beyond-mean-field effects in weakly interacting Bose gases. We will use the methods and results introduced in this chapter throughout the rest of this work.

4 | Scattering in Confined Geometries

In this chapter, we will derive the confinement-induced resonance for a one-dimensional geometry with periodic boundary conditions. To illustrate the power of our approach, we will also provide alternative derivations for the quasi-two-dimensional geometry with periodic boundary conditions, as well as for the low-dimensional description of scattering in a harmonic confinement.

4.1 | Introduction

In our discussion in Chapter 2, we have only considered scattering in free space in three or lower dimensions. In ultracold atom experiments, however, particles are often confined by traps of various geometries. To investigate effects of low-dimensional systems, the particles are kept at low energies, i.e. low temperatures, and occupy the ground state of the transverse confinement. Let $E_\perp$ be the energy scale for a transverse excitation. If the energy of the particles is smaller than $E_\perp$, transverse excitations are frozen out, and the system enters the low-dimensional regime. As long as the scattering length a_s is much smaller than the transverse length scale $l_\perp$, the scattering processes are still characterized by the scattering length in three dimensions. This can be understood in context of virtual excitations: While at the end of a scattering event the particles are still in the transverse ground state, during the interaction transverse states can be virtually excited. This does not mean that low-dimensional models for the systems at hand do not provide the correct physical behavior, but we have to make sure to connect the parameters characterizing the interaction in these models (i.e. $a_\mathrm{1D}, a_\mathrm{2D}$) to the microscopic parameters in the experiment (i.e. a_s).

To connect the scattering length in lower dimensions to the microscopic scattering length a_s will be the main goal of this chapter. The necessity for this investigation became clear to us during our work on beyond-mean-field corrections in quasi-low-dimensional Bose gases, which we will discuss in context of a dimensional crossover in Chapter 5. There, we will see that beyond-mean-field corrections in the quasi-low-dimensional regime naturally include terms for which a thorough understanding of scattering in confined geometries is crucial. We will use the minimal two-channel model introduced in Sec. 2.3.2, which allows us to systematically renormalize all occurring divergencies and solve the low-energy scattering problem for various confinements. We start our discussion with the easiest "confinement" which will allow for analytical results in dimensional crossover in Chapter 5: periodic boundary conditions for one- and two-dimensional geometries. For the two-dimensional geometry with periodic boundary conditions, the

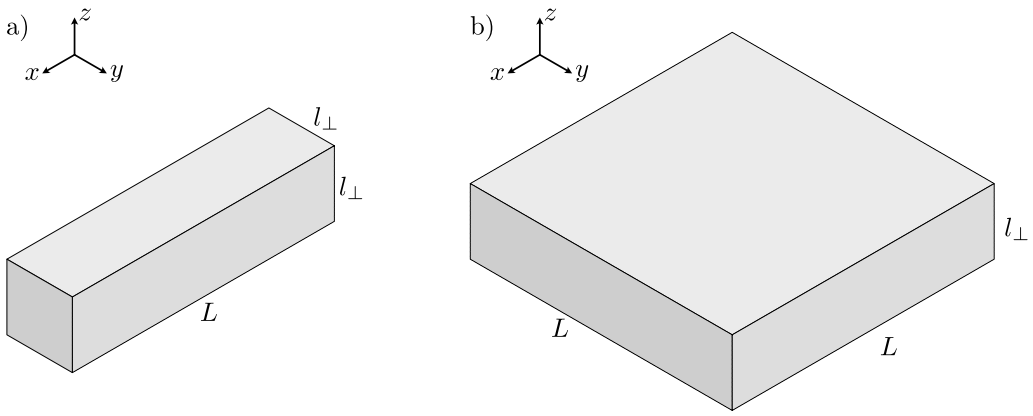

Figure 4.1: Sketch of the two geometries under consideration

connection between a_{2D} and a_s was first obtained by Lammers *et al.* [164]. For the one-dimensional geometry, however, the connection between a_{1D} and a_s has not been established before to our knowledge. Afterwards, we will discuss a harmonic trapping potential, where in the one-dimensional geometry the connection between a_{1D} and a_s was first derived by Olshanii [165], and for the two-dimensional geometry the connection between a_{2D} and a_s was first obtained by Petrov *et al.* [138]. While for many of the discussed confinements the connection to the scattering length has been established before, we still want to discuss them in detail here to illustrate the power of the minimal two-channel model and provide an alternative derivation.

4.2 | Periodic Boundary Conditions

We start our discussion with the simplest way to introduce discrete transverse energy levels. We impose periodic boundary conditions, which restrict the allowed wave vectors of the particles, but the Hamiltonian remains unaffected. In the following, we consider a box of volume $L_x \times L_y \times L_z$. Then, the allowed wave vectors are

$$k_i = \frac{2\pi}{L_i} n_i \qquad \text{where} \qquad n_i \in \mathbb{Z} \qquad \text{and} \qquad i \in \{x, y, z\}. \tag{4.1}$$

Depending on the energy of the particles and the length L_i, the particles can occupy excited states with $n_i \neq 0$. In Fig. 4.1, we sketch the two geometries which we will discuss in the following.

4.2.1 | One-Dimensional Geometry

We consider two particles of mass m interacting via a short-range interaction characterized by the scattering length a_s in the quasi-one-dimensional regime. The one-

dimensional system is sketched in Fig. 4.1 a). We set $L_x = L$ and $L_{y,z} = l_\perp$ with $L \gg l_\perp$. In addition, we require $\frac{\hbar^2}{mL^2} \ll E \ll \frac{\hbar^2}{ml_\perp^2}$, where E is the energy of the particles such that the transverse degrees of freedom are frozen out. Along the axial direction the spectrum can be considered continuous. Hence, the allowed wave vectors take the form

$$k_x \in \mathbb{R}, \qquad k_{y,z} = \frac{2\pi}{l_\perp} n_{y,z} \qquad \text{with} \qquad n_{y,z} \in \mathbb{Z}. \tag{4.2}$$

Our goal is to determine the scattering amplitude for the given geometry and connect it to the scattering length a_s. We describe the short-range interaction by the two-channel model discussed in Sec. 2.3.2. In the center-of-mass frame of the two particles, the coupled Schrödinger equations in Eq. (2.47) remain unchanged,

$$\left[\frac{\hbar^2 \boldsymbol{k}^2}{m} + \frac{\hbar^2}{m}\Delta\right] \psi(\boldsymbol{r}) = \overline{g}\phi_c \alpha_\Lambda(\boldsymbol{r}), \tag{2.47a revisited}$$

$$\left[\frac{\hbar^2 \boldsymbol{k}^2}{m} - \nu_0\right] \phi_c = \overline{g} \int d^3r\, \psi(\boldsymbol{r}) \alpha_\Lambda(\boldsymbol{r}), \tag{2.47b revisited}$$

since the confinement only influences the allowed values of $\boldsymbol{k}$. To solve the coupled Schrödinger equations, we take into account that the energy of the particles is much smaller than the transverse level spacing. Therefore, $\boldsymbol{k} = (k_x, 0, 0)^\mathrm{T}$ and the Ansatz has the same form as before,

$$\psi_{k_x}(\boldsymbol{r}) = e^{ik_x x} + \beta_\mathrm{1D} \int d^3r'\, \alpha_\Lambda(\boldsymbol{r}') G_x(\boldsymbol{r} - \boldsymbol{r}')\,. \tag{4.3}$$

However, the boundary conditions affect the solution of the Green's function in Eq. (2.11), which now becomes

$$\begin{aligned} G_x(\boldsymbol{r}) &= \frac{m}{\hbar^2} \int \frac{dq_x}{2\pi} \sum_{q_y,q_z} \frac{1}{l_\perp^2} \frac{e^{i\boldsymbol{q}\cdot\boldsymbol{r}}}{k_x^2 - \boldsymbol{q}^2 + i\eta} \\ &= \frac{m}{2\hbar^2 l_\perp^2} \frac{1}{ik_x} e^{ik_x|x|} + \frac{m}{\hbar^2} \int \frac{dq_x}{2\pi} \sum_{(q_y,q_z)\neq(0,0)} \frac{1}{l_\perp^2} \frac{e^{i\boldsymbol{q}\cdot\boldsymbol{r}}}{k_x^2 - \boldsymbol{q}^2 + i\eta}, \end{aligned} \tag{4.4}$$

where we separated the term $q_y = q_z = 0$ and performed the q_x-integration. While the incoming wave is restricted to the transverse ground state, the solution of the Green's function requires to take into account the entire transverse spectrum. Note that the far-field behavior of the Green's function is dominated by the first term in Eq. (4.4) ($q_y = q_z = 0$). This allows us to connect β_1D to the scattering amplitude f_1D from Eq. (2.22),

$$\psi_{k_x}(\boldsymbol{r}) \overset{x\to\infty}{=} e^{ik_x x} + f_\mathrm{1D}(k_x) e^{ik_x x} \tag{4.5}$$

where

$$f_{1\mathrm{D}}(k_x) = \frac{m}{2\hbar^2 l_\perp^2}\frac{1}{ik_x}\beta_{1\mathrm{D}}\int d^3r' \alpha_\Lambda(\boldsymbol{r}')e^{-ik_x x'}. \tag{4.6}$$

To obtain $\beta_{1\mathrm{D}}$ and therefore $f_{1\mathrm{D}}$, we follow the same procedure as in Sec. 2.3.2, which yields

$$f_{1\mathrm{D}}(k_x) = \frac{m}{2\hbar^2 l_\perp^2}\frac{1}{ik_x}\frac{\overline{g}^2}{\frac{\hbar^2 k_x^2}{m} - \nu_0 - \overline{g}^2\overline{G}_{1\mathrm{D}}(k_x)}\int d^3r' \alpha_\Lambda(\boldsymbol{r}')e^{-ik_x x'}, \tag{4.7}$$

where

$$\begin{aligned}\overline{G}_{1\mathrm{D}}(k_x) &= \int d^3r\, d^3r' \alpha_\Lambda(\boldsymbol{r})\alpha_\Lambda(\boldsymbol{r}')G_{k_x}(\boldsymbol{r}-\boldsymbol{r}') = \frac{m}{\hbar^2}\frac{1}{l_\perp^2}\sum_{q_x,q_y}\int\frac{dq_z}{2\pi}\frac{\hat{\alpha}_\Lambda^2(\boldsymbol{q})}{k_x^2 - \boldsymbol{q}^2 + i\eta} \\ &= -\frac{im}{2\hbar^2 l_\perp^2 k_x} + \frac{m}{\hbar^2 l_\perp^2}\sum_{(q_x,q_y)\neq(0,0)}\int\frac{dq_z}{2\pi}\frac{\hat{\alpha}_\Lambda^2(\boldsymbol{q})}{k_x^2 - \boldsymbol{q}^2 + i\eta} \\ &= -\frac{im}{2\hbar^2 l_\perp^2 k_x} + \overline{G}'_{1\mathrm{D}}(k_x).\end{aligned} \tag{4.8}$$

Here, $\hat{\alpha}_\Lambda(\boldsymbol{q})$ denotes the Fourier transform of $\alpha_\Lambda(\boldsymbol{r})$, and we separated the mode $q_x = q_y = 0$ in the last step.

So far, the scattering amplitude still depends on the cut-off Λ and $\overline{G}'_{1\mathrm{D}}$ diverges for $\Lambda \to 0$. However, we have to keep in mind that ν_0 is the bare detuning and also diverges for $\Lambda \to 0$. With the connection between the bare detuning ν_0 and the physical detuning ν established in Eq. (2.55), we can write the scattering amplitude in terms of the scattering length $a_{1\mathrm{D}}$ [see Eq. (2.29)],

$$f_{1\mathrm{D}}(k_x) = -\frac{1}{1 + ik_x\frac{2\hbar^2 l_\perp^2}{m}\left[\frac{\nu}{\overline{g}^2} + \overline{G}'_{1\mathrm{D}}(0) - \overline{G}(0)\right] + O(k_x^2)} = -\frac{1}{1 + ik_x a_{1\mathrm{D}}}. \tag{4.9}$$

Thus, the effective scattering length $a_{1\mathrm{D}}$ is given by

$$a_{1\mathrm{D}} = \frac{2\hbar^2 l_\perp^2}{m}\left[\frac{\nu}{\overline{g}^2} + \overline{G}'_{1\mathrm{D}}(0) - \overline{G}(0)\right]. \tag{4.10}$$

The relation between the physical detuning ν and the scattering length a_s is given in Eq. (2.56). The term $\overline{G}(0)$ cancels the divergence of $\overline{G}'_{1\mathrm{D}}(0)$, resulting in a cut-off independent result. A short calculation (see Appendix A.1) leads to the final result,

$$a_{1\mathrm{D}} = -\frac{1}{2\pi}\frac{l_\perp^2}{a_\mathrm{s}}\left(1 - C_{1\mathrm{D}}\frac{a_\mathrm{s}}{l_\perp}\right), \tag{4.11}$$

with

$$C_{1\mathrm{D}} = \int dvdw \frac{1}{\sqrt{v^2+w^2}} - \sum_{v,w}{}' \frac{1}{\sqrt{v^2+w^2}} \approx 3.899. \tag{4.12}$$

This expression describes the confinement-induced resonance for a setup with periodic boundary conditions.

4.2.2 | Two-Dimensional Geometry

We repeat the same procedure as in the previous section but for a quasi-two-dimensional geometry as sketched in Fig. 4.1 b). Since we have already discussed how to treat periodic boundary conditions, we will keep this discussion short and only provide the crucial steps in obtaining the effective scattering length $a_{2\mathrm{D}}$. Again, we are interested in energies $\frac{\hbar^2}{mL^2} \ll E \ll \frac{\hbar^2}{ml_\perp^2}$, resulting in

$$k_{x,y} \in \mathbb{R}, \qquad k_z = \frac{2\pi}{l_\perp} n_z \qquad \text{with} \qquad n_z \in \mathbb{Z}. \tag{4.13}$$

For the coupled Schrödinger equations we make the Ansatz

$$\psi_{\boldsymbol{k}_\rho}(\boldsymbol{r}) = e^{i\boldsymbol{k}_\rho\cdot\boldsymbol{r}} + \beta_{2\mathrm{D}} \int d^3r'\, \alpha_\Lambda(\boldsymbol{r}') G_\rho(\boldsymbol{r}-\boldsymbol{r}'), \tag{4.14}$$

where $\boldsymbol{k}_\rho = (k_x, k_y, 0)^{\mathrm{T}}$ and

$$G_\rho(\boldsymbol{r}) = \frac{m}{\hbar^2}\frac{1}{l_\perp}\sum_{q_z}\int \frac{dq_x\, dq_y}{(2\pi)^2} \frac{e^{i\boldsymbol{q}\cdot\boldsymbol{r}}}{\boldsymbol{k}_\rho^2 - \boldsymbol{q}^2 + i\eta}. \tag{4.15}$$

Analogous to before, analyzing the far-field behavior of the $q_z = 0$ term of the Green's function allows us to connect $\beta_{2\mathrm{D}}$ to the scattering amplitude and we obtain

$$f_{2\mathrm{D}}(k_\rho) = -\frac{m}{4\hbar^2}\sqrt{\frac{2i}{\pi k_\rho}}\frac{1}{l_\perp}\beta_{2\mathrm{D}} = -\frac{m}{4\hbar^2}\sqrt{\frac{2i}{\pi k_\rho}}\frac{1}{l_\perp}\frac{\overline{g}^2}{\frac{\hbar^2 k_\rho^2}{m} - \nu_0 - \overline{g}^2\overline{G}_{2\mathrm{D}}(k_\rho)}, \tag{4.16}$$

with

$$\overline{G}_{2\mathrm{D}}(k_\rho) = \frac{m}{\hbar^2}\frac{1}{l_\perp}\sum_{q_z}\int \frac{dq_x\, q_y}{(2\pi)^2} \frac{\hat{\alpha}_\Lambda^2(\boldsymbol{q})}{\boldsymbol{k}_\rho^2 - \boldsymbol{q}^2 + i\eta}. \tag{4.17}$$

By replacing the bare detuning ν_0 with the physical detuning ν from Eq. (2.55) and connecting it to the scattering length [see Eq. (2.56)], we arrive at

$$f_{2\mathrm{D}}(k_\rho) = -\sqrt{\frac{2\pi i}{k_\rho}}\frac{1}{\frac{l_\perp}{a_{\mathrm{s}}} - \frac{4\pi\hbar^2 l_\perp^2}{m}\left[\overline{G}_{2\mathrm{D}}(k_\rho) - \overline{G}(0)\right]} = -\sqrt{\frac{2\pi i}{k_\rho}}\frac{1}{i\pi - \ln\left(k_\rho^2 l_\perp^2 e^{-l_\perp/a_{\mathrm{s}}}\right) + O(k_\rho^2)}, \tag{4.18}$$

where we have used (see Appendix A.2)

$$\overline{G}_{2\mathrm{D}}(k_\rho) - \overline{G}(0) \overset{k_\rho \Lambda \ll 1}{=} \frac{m}{4\pi\hbar^2 l_\perp} \left[-i\pi + \ln(k_\rho^2 l_\perp^2)\right]. \tag{4.19}$$

To connect the scattering length a_s to the effective scattering length $a_{2\mathrm{D}}$, we compare Eq. (4.18) to the universal low-energy scattering amplitude in Eq. (2.28) and obtain

$$a_{2\mathrm{D}} = 2 l_\perp e^{-\frac{l_\perp}{2a_\mathrm{s}}} e^{-\gamma}. \tag{4.20}$$

This result was first obtained in [164].

For quasi-one-dimensional and quasi-two-dimensional systems shown in Fig. 4.1, $a_{1\mathrm{D}}$ and $a_{2\mathrm{D}}$ fully characterize the short-range interactions in the low-energy regime. While periodic boundary conditions are a useful starting point for our investigation, as they nicely illustrate the general procedure, harmonic traps have a larger significance due to their experimental realization. We will adapt our approach for a harmonic confinement in the next section.

4.3 | Harmonic Confinement

While periodic boundary conditions altered the transverse level spectrum and allowed us to investigate confined geometries, the single-particle Hamiltonian remained that of a free particle. In this section, we add a harmonic confinement with trap frequency ω to the transverse direction of the single-particle Hamiltonian, which introduces a characteristic energy scale $\hbar\omega$ for transverse excitations. As in the previous section, we will investigate the scattering properties of two particles interacting via a short-range interaction. We are interested in the low-energy limit, meaning that the energy of the particles is much lower than required to excite a transverse state.

4.3.1 | One-Dimensional Geometry

We start our discussion with the one-dimensional geometry, where the transverse confinement is described by $H_\perp = \frac{m\omega^2}{2}(y^2 + z^2)$. As for periodic boundary conditions, we treat the problem in the center-of-mass frame but due to the rotational symmetry, we choose cylindrical coordinates, which yields

$$\left[\frac{\hbar^2 k_x^2}{m} + \hbar\omega\,(n+1) + \frac{\hbar^2}{m}\Delta - \frac{m\omega^2}{4}\rho^2\right]\psi(\boldsymbol{r}) = \overline{g}\phi_c\alpha_\Lambda(\boldsymbol{r}) \tag{4.21a}$$

$$\left[\frac{\hbar^2 k_x^2}{m} + \hbar\omega\,(n+1) - \nu_0\right]\phi_c = \overline{g}\int d^3r\,\alpha_\Lambda(\boldsymbol{r})\psi(\boldsymbol{r}), \tag{4.21b}$$

where $\boldsymbol{\rho} = (y,z)^\mathrm{T}$. The eigenstates of the two-dimensional harmonic oscillator $\varphi_{n,l}(\boldsymbol{\rho})$ are then characterized by the quantum numbers $n \in \mathbb{N}_0$ and $l \in \{-n, n+2, \cdots, n-2, n\}$.

In the low-energy regime, the Ansatz takes the form

$$\psi(\boldsymbol{r}) = e^{ik_x x}\varphi_{0,0}(y,z) + \beta^h_{1\mathrm{D}} \int d^3r'\, \alpha_\Lambda(\boldsymbol{r}')G_{x,0,0}(\boldsymbol{r},\boldsymbol{r}'), \tag{4.22}$$

where

$$G_{x,0,0}(\boldsymbol{r},\boldsymbol{r}') = \frac{m}{\hbar^2}\int \frac{dq_x}{2\pi}\sum_{n,l}^{\infty} \frac{e^{iq_x(x-x')}\varphi_{n,l}(y,z)\varphi_{n,l}(y',z')}{k_x^2 - q_x^2 - n/l_\perp^2 + i\eta}, \tag{4.23}$$

and we have introduced the oscillator length $l_\perp = \sqrt{\hbar/m\omega}$. The $n = l = 0$ term determines the far-field behavior and in complete analogy to our discussion of periodic boundary conditions we obtain

$$\psi(\boldsymbol{r}) \overset{x\to\infty}{=} \left[e^{ik_x x} + f^h_{1\mathrm{D}}(k_x)\, e^{ik_x x}\right]\varphi_{0,0}(\boldsymbol{\rho}). \tag{4.24}$$

Here, we have introduced the scattering amplitude with the scattering amplitude

$$f^h_{1\mathrm{D}}(k_x) = \frac{m}{2\hbar^2}\frac{1}{ik_x}\frac{1}{\sqrt{2\pi l_\perp^2}}\beta^h_{1\mathrm{D}} = \frac{m}{2\hbar^2}\frac{1}{ik_x}\frac{1}{2\pi l_\perp^2}\frac{\overline{g}^2}{\frac{\hbar^2k_x^2}{m} - \nu_0 - \overline{G}^h_{1\mathrm{D}}(0)}, \tag{4.25}$$

where

$$\begin{aligned}
\overline{G}^h_{1\mathrm{D}}(k_x) &= \frac{m}{\hbar^2}\int d^3r\, d^3r' \int \frac{dq_x}{2\pi}\sum_{n,l}^{\infty}\frac{\alpha_\Lambda(\boldsymbol{r})\alpha_\Lambda(\boldsymbol{r}')\varphi_{n,l}(\boldsymbol{\rho})\varphi_{n,l}(\boldsymbol{\rho}')e^{iq_x(x-x')}}{k_x^2 - q_x^2 - n/l_\perp^2 + i\eta} \\
&= \frac{m}{4\pi\hbar^2 l_\perp^2}\frac{1}{ik_x} + \frac{m}{\hbar^2}\int d^3r\, d^3r' \int \frac{dq_x}{2\pi}\sum_{(n,l)\neq(0,0)}^{\infty}\frac{\alpha_\Lambda(\boldsymbol{r})\alpha_\Lambda(\boldsymbol{r}')\varphi_{n,l}(\boldsymbol{\rho})\varphi_{n,l}(\boldsymbol{\rho}')e^{iq_x(x-x')}}{k_x^2 - q_x^2 - n/l_\perp^2 + i\eta} \\
&= \frac{m}{4\pi\hbar^2 l_\perp^2}\frac{1}{ik_x} + \overline{G}'^h_{1\mathrm{D}}(k_x).
\end{aligned} \tag{4.26}$$

The divergence appearing in $\overline{G}'^h_{1\mathrm{D}}(0)$ is canceled by replacing the bare detuning ν_0 with the physical detuning ν from Eq. (2.55) and we obtain

$$f^h_{1\mathrm{D}}(k_x) = -\frac{1}{1 + ik_x\frac{4\pi\hbar^2 l_\perp^2}{m}\left[\frac{\nu}{\overline{g}^2} + \overline{G}'^h_{1\mathrm{D}}(0) - \overline{G}(0)\right] + O(k_x^2)} = -\frac{1}{1 + ik_x a^h_{1\mathrm{D}}}, \tag{4.27}$$

where we have introduced the effective scattering length

$$a^h_{1\mathrm{D}} = \frac{4\pi\hbar^2 l_\perp^2}{m}\left[\frac{\nu}{\overline{g}^2} + \overline{G}'^h_{1\mathrm{D}}(0) - \overline{G}(0)\right]. \tag{4.28}$$

To connect $a_{1\mathrm{D}}^h$ to the scattering length a_s, we use Eq. (2.56). Evaluating $\overline{G}_{1\mathrm{D}}^{\prime h}(0) - \overline{G}(0)$ after a short calculation then yields (see Appendix A.3)

$$a_{1\mathrm{D}}^h = -\frac{l_\perp^2}{a_\mathrm{s}} \left(1 - \frac{C_{1\mathrm{D}}^h}{\sqrt{2}} \frac{a_\mathrm{s}}{l_\perp} \right), \tag{4.29}$$

where

$$C_{1\mathrm{D}}^h = \lim_{s\to\infty} \left(\int_0^s ds' \frac{1}{\sqrt{s'}} - \sum_{s'=1}^{s} \frac{1}{\sqrt{s'}} \right) \approx 1.4603\,. \tag{4.30}$$

This well-known result was first obtained by Olshanii [165] and coined the phrase confinement-induced resonance, which can be very misleading. At $a_\mathrm{s} = \sqrt{2} l_\perp / C_{1\mathrm{D}}^h$, the one-dimensional coupling constant $g_{1\mathrm{D}} = -2\hbar^2/m a_{1\mathrm{D}}$ [see Eq. (2.40)] diverges. In three dimensions, a diverging coupling constant corresponds to a diverging scattering length [see Eq. (2.35)], which corresponds to a diverging scattering amplitude. A diverging scattering amplitude indicates the appearance of a new bound state, which is referred to as a resonance. In one dimension, however, a diverging coupling constant does not indicate a resonance. As $a_{1\mathrm{D}}^h$ vanishes, the scattering amplitude $f_{1\mathrm{D}}^h$ in Eq. (4.27) remains finite. Hence, one should keep in mind that a confinement-induced resonance is not actually a resonance but only a zero crossing of the one-dimensional scattering length.

4.3.2 | Two-Dimensional Geometry

We conclude our discussion of scattering in confined geometries by investigating a two-dimensional geometry with a tight harmonic trap in the z-direction. Scattering is then described by

$$\left[\frac{\hbar^2 \boldsymbol{k}_\rho^2}{m} + \hbar\omega \left(n + \frac{1}{2} \right) + \frac{\hbar^2}{m}\Delta - \frac{m\omega^2}{4} z^2 \right] \psi(\boldsymbol{r}) = \overline{g} \phi_c \alpha_\Lambda(\boldsymbol{r}) \tag{4.31a}$$

$$\left[\frac{\hbar^2 \boldsymbol{k}_\rho^2}{m} + \hbar\omega \left(n + \frac{1}{2} \right) - \nu_0 \right] \phi_c = \overline{g} \int d^3 r\, \alpha_\Lambda(\boldsymbol{r}) \psi(\boldsymbol{r}), \tag{4.31b}$$

where $\boldsymbol{k}_\rho = (k_x, k_y)^\mathrm{T}$. For the low-energy regime, we make the Ansatz

$$\psi(\boldsymbol{r}) = e^{i\boldsymbol{k}_\rho \cdot \boldsymbol{\rho}} \varphi_0(z) + \beta_{2\mathrm{D}}^h \int d^3 r'\, \alpha_\Lambda(\boldsymbol{r'}) G_{k_\rho,0}(\boldsymbol{r}, \boldsymbol{r'}), \tag{4.32}$$

with $\boldsymbol{\rho} = (x, y)^\mathrm{T}$, and $\varphi_n(z)$ are the eigenstates of the one-dimensional harmonic oscillator. The far-field behavior of the Green's function

$$G_{k_\rho,0}(\boldsymbol{r}, \boldsymbol{r'}) = \frac{m}{\hbar^2} \int \frac{d^2 q}{(2\pi)^2} \sum_{n=0}^{\infty} \frac{e^{i\boldsymbol{q}\cdot(\boldsymbol{\rho}-\boldsymbol{\rho'})} \varphi_n(z) \varphi_n(z')}{\boldsymbol{k}_\rho^2 - \boldsymbol{q}^2 - n/l_\perp^2 + i\eta} \tag{4.33}$$

allows us to write the wave function as

$$\psi(\boldsymbol{r}) \overset{\boldsymbol{\rho}\to\infty}{=} \left[e^{i\boldsymbol{k}_{\boldsymbol{\rho}}\cdot\boldsymbol{\rho}} + f^h_{\mathrm{2D}}(k_\rho)\frac{e^{ik_\rho\rho}}{\sqrt{\rho}}\right]\varphi_0(z). \tag{4.34}$$

Here, we have introduced the scattering amplitude

$$f^h_{\mathrm{2D}}(k_\rho) = -\frac{m}{4\hbar^2}\sqrt{\frac{2i}{\pi k_\rho}}\left(\frac{1}{2\pi l_\perp^2}\right)^{\frac{1}{4}}\beta^h_{\mathrm{2D}} = -\frac{m}{4\hbar^2}\sqrt{\frac{2i}{\pi k_\rho}}\sqrt{\frac{1}{2\pi l_\perp^2}}\frac{\overline{g}^2}{\frac{\hbar^2\boldsymbol{k}_\rho^2}{m} - \nu_0 - \overline{g}^2\overline{G}^h_{\mathrm{2D}}(k_\rho)} \tag{4.35}$$

where

$$\overline{G}^h_{\mathrm{2D}}(k_\rho) = \int d^3r\, d^3r'\, \alpha_\Lambda(\boldsymbol{r})\alpha_\Lambda(\boldsymbol{r}')G_{k_\rho,0}(\boldsymbol{r},\boldsymbol{r}'). \tag{4.36}$$

In terms of the physical detuning, the quasi-two-dimensional scattering amplitude simplifies to

$$f^h_{\mathrm{2D}}(k_\rho) = -\frac{m}{4\hbar^2}\sqrt{\frac{2i}{\pi k_\rho}}\frac{1}{\sqrt{2\pi l_\perp^2}}\frac{\overline{g}^2}{\frac{\hbar^2\boldsymbol{k}_\rho^2}{m} - \nu - \overline{g}^2\left[\overline{G}^h_{\mathrm{2D}}(k_\rho) - \overline{G}(0)\right]}\,. \tag{4.37}$$

Without loss of generality, we choose $\alpha_\Lambda(\boldsymbol{r}) = e^{-\boldsymbol{\rho}/2\Lambda^2}\delta(x)/2\pi\Lambda^2$. This allows us to evaluate the summation over the harmonic oscillator modes in $\overline{G}^h_{\mathrm{2D}}(k_\rho) - \overline{G}(0)$ analytically (for details see Appendix A.4). We are left with an integration in momentum space and obtain

$$\overline{G}^h_{\mathrm{2D}}(k_\rho) - \overline{G}(0) = \frac{m}{4\pi\hbar^2}\frac{1}{\sqrt{2\pi l_\perp^2}}\left[\overline{C}^h_{\mathrm{2D}} - i\pi + \ln\left(k_\rho^2 l_\perp^2/2\right)\right], \tag{4.38}$$

where

$$\overline{C}^h_{\mathrm{2D}} = \int_0^\infty du\, 2u\left(\frac{\sqrt{\pi}}{u} - \frac{\sqrt{\pi}\Gamma(u^2)}{\Gamma(u^2+\frac{1}{2})} + \frac{1}{u^2(1+u)}\right) \approx 1.938\,. \tag{4.39}$$

The scattering amplitude takes the form

$$\begin{aligned} f^h_{\mathrm{2D}}(k_\rho) &= -\sqrt{\frac{2\pi i}{k_\rho}}\frac{1}{i\pi - \ln\left[(k_\rho l_\perp)^2 e^{\overline{C}^h_{\mathrm{2D}} - \sqrt{2\pi}l_\perp/a_{\mathrm{s}}}/2\right] + O(k_\rho^2)} \\ &= -\sqrt{\frac{2\pi i}{k_\rho}}\frac{1}{i\pi - \ln\left[(k_\rho a^h_{\mathrm{2D}})^2 e^{2\gamma}/4\right]}\,, \end{aligned} \tag{4.40}$$

where the effective scattering length is given by

$$a^h_{\mathrm{2D}} = \sqrt{2}l_\perp e^{-\gamma - \overline{C}^h_{\mathrm{2D}}/2}e^{-\sqrt{2\pi}l_\perp/2a_{\mathrm{s}}}. \tag{4.41}$$

	Periodic Boundary Conditions	**Harmonic Confinement**
1D	$a_{1\mathrm{D}} = -\frac{1}{2\pi}\frac{l_\perp^2}{a_\mathrm{s}}\left(1 - C_{1\mathrm{D}}\frac{a_\mathrm{s}}{l_\perp}\right)$	$a_{1\mathrm{D}}^h = -\frac{l_\perp^2}{a_\mathrm{s}}\left(1 - \frac{C_{1\mathrm{D}}^h}{\sqrt{2}}\frac{a_\mathrm{s}}{l_\perp}\right)$ [165]
2D	$a_{2\mathrm{D}} = 2l_\perp e^{-\frac{l_\perp}{2a_\mathrm{s}}} e^{-\gamma}$ [164]	$a_{2\mathrm{D}}^h = \sqrt{2}l_\perp e^{-\gamma - \overline{C}_{2\mathrm{D}}^h/2} e^{-\sqrt{2\pi}l_\perp/2a_\mathrm{s}}$ [138]

Table 4.1: Effective scattering length for different geometries. For periodic boundary conditions $l_\perp$ refers to the size of the box in the transverse direction(s) while for the harmonic confinement $l_\perp = \sqrt{\hbar/m\omega}$ is the oscillator length.

The effective scattering length $a_{2\mathrm{D}}^h$ was first derived in [138]. To make the connection to our result clear, we want to point out that the constant B found in Refs. [138, 166] is connected to $\overline{C}_{2\mathrm{D}}^h$ by

$$B = 2\pi e^{-\overline{C}_{2\mathrm{D}}^h} \approx 0.905\,. \tag{4.42}$$

With the results of this sections, we are now able to describe the interactions in the confinements relevant to Chapter 5. To conclude, we summarize the connection between the effective scattering length of the respective geometry and the scattering length a_s in Table 4.1.

5 | Dimensional Crossover for the Beyond-Mean-Field Corrections

In this chapter, we will investigate the behavior of the beyond-mean-field corrections of a weakly interacting Bose gas in the crossover from three to low dimensions. For a box with periodic boundary conditions, we are able to derive analytic solutions for the ground-state energy throughout the entire crossover. This investigation shows that the leading-order contribution of the confinement-induced resonance is of beyond-mean-field order. We also provide corrections to the three- and low-dimensional limits. Afterwards, we investigate the crossover for a model system with short- and long-range interactions in a harmonic confinement, which allows us to investigate the limitations of the local-density approximation. In addition, we show that for a harmonic confinement and a one-dimensional geometry dipoles aligned parallel to the tube show a drastically different behavior than a contact gas in the one-dimensional regime.

5.1 | Introduction

As we have seen in Chapter 3, beyond-mean-field corrections of uniform systems are an interesting research field on their on and pose hard challenges to overcome in a theoretical description. While for the uniform cases discussed before, the beyond-mean-field corrections are well understood by now, experiments are typically performed in a trap and the description becomes more difficult. For weak traps, the density varies only slowly such that locally we expect that the system can be treated as uniform (local-density approximation), and shows a three-dimensional character. For tight traps and low energies on the other hand, a quasi-low-dimensional description seems adequate.

In recent years, dipolar condensates and binary Bose-Bose mixtures attracted a lot of interest due to the appearance of quantum droplets [44–51, 59–63, 72, 167–175]. Both systems feature tunable competing interactions that can lead to a cancellation of the mean-field interaction such that the beyond-mean-field corrections become relevant. Hence, the beyond-mean-field effects not only lead to a small correction as discussed for uniform systems in Chapter 3, but are crucial to understand the stability of these quantum droplets [45, 49]. For these anisotropic and inhomogeneous systems, which are highly sensitive to the exact behavior of the beyond-mean-field correction, the theoretical description heavily relies on the use of the local-density approximation.

The above discussion naturally rises important questions. Are there corrections to the local-density approximation and up to which point is its use justified? Also the

opposite regime needs to be understood better. Are there corrections to the quasi-low-dimensional description due to the presence of the transverse degrees of freedom, and how are the different regimes connected?

To answer these questions is the main goal of this chapter, which is based on the publication [176] that resulted from a collaboration with Dmitry Petrov and Luis Santos. Note that during the same time we became aware of very related results by Zin et al. [177]. The main focus of this chapter is on contact interactions and we make use of the field-theoretic approach by Hugenholtz and Pines [7] introduced in Sec. 3.1.2. We start with a short discussion of the theoretical foundation before we discuss the dimensional crossover for periodic boundary conditions and afterwards also consider a harmonic confinement. The numerical analysis required for the full crossover in a harmonic confinement was provided by Luis Santos. With all this machinery at hand, we conclude the chapter by a short section on the dipolar case, which was first discussed in Ref. [178], and provide the analytical correction in the quasi-one-dimensional regime.

5.2 | Periodic Boundary Conditions

We start our discussion with the simplest confinement that introduces a discrete transverse level spacing: Periodic boundary conditions. While periodic boundary conditions are not a realistic description of an experimental setup, they will allow us to obtain a deeper understanding of beyond-mean-field corrections in general since we are able to derive simple analytic expressions for the ground-state energy through the crossover.

5.2.1 | General Setup

In this chapter, we consider a one-component weakly interacting Bose gas of mass m where the short-range interaction between the particles is characterized by the scattering length a_s. The gas is confined along one or two directions by a box potential with length $l_\perp$ and we impose periodic boundary conditions. This introduces a transverse level spacing $E_\perp = \hbar^2/ml_\perp^2$ as the transverse wave vectors are discrete, $k_\perp = 2\pi j/l_\perp$ with $j \in \mathbb{Z}$. The dimensionality of the system is then characterized by comparing $E_\perp$ to the chemical potential $\mu = 4\pi\hbar^2 a_\mathrm{s} n/m$, which naturally gives rise to the dimensionless parameter $\kappa = nl_\perp^2 a_\mathrm{s} \sim \mu/E_\perp$ where n is the density of the system. For $\kappa \gg 1$, the system is in a three-dimensional regime, while for $\kappa \ll 1$ the system becomes effectively low-dimensional since the energy is too low and the transverse degrees of freedom are frozen out.

In addition, we have to keep in mind that within our approach we are limited to weak interactions. As we have seen in Sec. 3, for a three-dimensional system this results in $\sqrt{na_\mathrm{s}^3} \ll 1$. In terms of κ this means $\kappa \ll 1/\lambda^2$, where we have introduced our second important dimensionless quantity $\lambda = a_\mathrm{s}/l_\perp$. On the other hand, we have seen in Sec.3.2.1 that low one-dimensional densities result in the strongly correlated Tonks-Girardeau regime, while the gas becomes weakly interacting for $|n_\mathrm{1D}a_\mathrm{1D}| \gg 1$. For

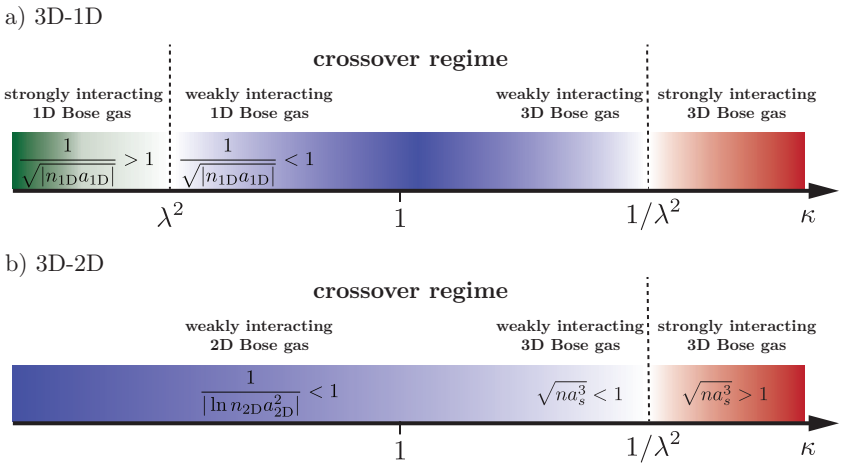

Figure 5.1: Crossover regime from three dimensions to a) one dimension and b) two dimensions: The parameter characterizing the crossovers is $\kappa = na_s l_\perp^2$, which relates the transverse confinement to the chemical potential. The beyond-mean-field predictions are valid in the weakly interacting regime (blue), which requires that $\sqrt{na_s^3} \ll 1$ for three dimensions, $1/|n_{1D}a_{1D}| \ll 1$ for one dimension, and $1/|\ln n_{2D}a_{2D}^2| \ll 1$ for two dimensions. These requirements translate to the conditions $\lambda^2 \ll \kappa \ll 1/\lambda^2$ for the 3D-1D crossover and $\kappa \ll 1/\lambda^2$ for the 3D-2D crossover, where $\lambda = a_s/l_\perp$. Furthermore, it shows that λ is our small parameter and we require $\lambda \ll 1$ for the validity of our results.

our box with periodic boundary conditions, we can write the one-dimensional density as $n_{1D} = nl_\perp^2$. The lowest order of the one-dimensional scattering length is given by $a_{1D} = -l_\perp^2/2\pi a_s$ [see Eq. (4.11)]. Then, $|n_{1D}a_{1D}| \gg 1$ translates to $\kappa \gg \lambda^2$ such that the full crossover in the one-dimensional geometry is given by $\lambda^2 \ll \kappa \ll 1/\lambda^2$. As there is no low-density limit for the weakly interacting regime in two dimensions, for the two-dimensional geometry we only require $\kappa \ll 1/\lambda^2$. For a wide crossover regime, we require $\lambda \ll 1$. Both crossover regimes are illustrated in Fig. 5.1

In terms of the dimensionless parameters κ and λ, the three-dimensional ground-state energy including the beyond-mean-field correction [see Eq. (3.31)] can be written as

$$E_{3D} = \frac{2\pi\hbar^2 a_s}{m} V n^2 \left(1 + \frac{128}{15\sqrt{\pi}}\sqrt{na_s^3}\right) = \frac{2\pi\hbar^2}{m}\frac{V}{l_\perp^4 a_s}\left(\kappa^2 + \lambda\,\frac{128}{15\sqrt{\pi}}\,\kappa^{5/2}\right), \tag{5.1}$$

which naturally gives rise to the energy scale

$$E_0 = \frac{2\pi\hbar^2}{m}\frac{V}{l_\perp^4 a_s}, \tag{5.2}$$

where V is the volume of the box. Note that in the crossover, beyond-mean-field corrections are of order of λ. In this sense, λ is the small expansion parameter in our approach and characterizes the influence of the beyond-mean-field corrections.

To describe the ground-state energy in the crossover regime, we make use of the approach by Hugenholtz and Pines [7] introduced in Sec. 3.1.2. The energy is determined by [see Eq. (3.57)]

$$E - \frac{1}{2}\mu N = \frac{1}{4}\sum_{\boldsymbol{k}\neq 0} \frac{2\epsilon_0(\boldsymbol{k})^2 + 3\epsilon_0(\boldsymbol{k})ng}{\sqrt{\epsilon_0(\boldsymbol{k})^2 + 2\epsilon_0(\boldsymbol{k})ng}} - 2\epsilon_0(\boldsymbol{k}) - ng, \tag{5.3}$$

where $g = 4\pi\hbar^2 a_\mathrm{s}/m$ is the coupling constant. The chemical potential fulfills the thermodynamic relation $\mu = dE/dN$, which makes Eq. (5.3) a linear first-order differential equation. In terms of κ and λ, the differential equation becomes

$$E - \frac{\kappa}{2}\frac{dE}{d\kappa} = \frac{\lambda}{2}E_0 \sum\!\!\!\!\!\!\int \frac{2\varepsilon^2 + 3\varepsilon\kappa}{\sqrt{\varepsilon^2 + 2\varepsilon\kappa}} - 2\varepsilon - \kappa, \tag{5.4}$$

where the notation $\sum\!\!\!\!\!\!\int$ describes a summation over the transversal degrees of freedom and an integration over the unconfined dimensions. In addition, we have introduced the dimensionless single-particle excitation spectrum $\varepsilon = \epsilon_0(\boldsymbol{k})/(4\pi\hbar^2/ml_\perp^2) = \pi(u^2 + v^2 + w^2)/2$, with u, v, and w the three components of the single-particle momentum in dimensionless units, e.g. $u = k_x/(2\pi/l_\perp)$. As discussed in Sec. 3.1.2, the differential equation Eq. (5.4) does not determine the mean-field term $\sim \kappa^2$, which enters as an initial condition for the differential equation. The general solution can then be written as

$$\frac{E}{E_0} = \kappa^2 \left[1 + \lambda\left(A(\kappa^*) - \int_{\kappa^*}^{\kappa} d\kappa'\, h(\kappa')\right)\right], \tag{5.5}$$

with

$$h(\kappa) = \frac{1}{\kappa^3}\sum\!\!\!\!\!\!\int \left[\frac{2\varepsilon^2 + 3\kappa\varepsilon}{\sqrt{\varepsilon^2 + 2\kappa\varepsilon}} - 2\varepsilon - \kappa\right]. \tag{5.6}$$

The constant $A(\kappa^*)$ determines the initial condition of the differential equation and has to be chosen in order to reproduce the correct mean-field term proportional to κ^2, while κ^* denotes an arbitrary value. To properly determine $A(\kappa^*)$, we require that the general solution in Eq. (5.5) produces the correct ground-state energy in Eq. (5.1) in the three-dimensional regime ($\kappa \gg 1$), which leads to

$$A(\kappa^*) = \int_{\kappa^*}^{\infty} d\kappa' \left[h(\kappa') - h_\mathrm{3D}(\kappa')\right] - \int_0^{\kappa^*} d\kappa' h_\mathrm{3D}(\kappa'). \tag{5.7}$$

Here,

$$h_\mathrm{3D}(\kappa) = -\frac{64}{15\sqrt{\pi\kappa}} \tag{5.8}$$

is the corresponding expression to $h(\kappa)$ for a three-dimensional system. The relation in Eq. (5.7) holds for all values of κ^*. We choose $\kappa^* = \kappa$ such that the last term in Eq. (5.7)

exactly provides the correct three-dimensional LHY correction. The ground state in the dimensional crossover is then given by

$$\begin{aligned} E &= E_0\,\kappa^2\,[1+\lambda A(\kappa)] \\ &= E_{3\mathrm{D}} + \kappa^2\lambda\,E_0\int_\kappa^\infty d\kappa'\,\left[h(\kappa')-h_{3\mathrm{D}}(\kappa')\right]. \end{aligned} \tag{5.9}$$

The last term in the integral guarantees that it is convergent and vanishes for $\kappa\to\infty$.

The energy in Eq. (5.9) describes the ground-state energy for all values of κ, and is the starting point of our investigation. In the following two sections, we will analyze the expression in detail for the two- and one-dimensional geometry and derive its asymptotic limits.

5.2.2 | Crossover to Two Dimensions

We start our investigation of the dimensional crossover with the two-dimensional geometry with just a single transverse dimension confined. Then, Eq. (5.6) becomes

$$h(\kappa) = \frac{1}{\kappa^3}\sum_w \int du\,dv\left[\frac{2\varepsilon^2+3\kappa\varepsilon}{\sqrt{\varepsilon^2+2\kappa\varepsilon}} - 2\varepsilon - \kappa\right]. \tag{5.10}$$

By introducing polar coordinates, the integrals $\int du\,dv$ can be evaluated analytically. We obtain

$$h(\kappa) = \frac{1}{\kappa^3}\left[g(0)+2\sum_{w=1}^\infty g\left(\frac{\pi w^2}{2}\right)\right] \quad \text{with} \quad g(q^2) = 2q^2\left(q^2+\kappa-q\sqrt{q^2+2\kappa}\right)-\kappa^2, \tag{5.11}$$

and we are left with a single sum. To evaluate the sum, we replace it with a contour integral,

$$h(\kappa) = \frac{1}{\kappa^3}\left[g(0)+2\sum_{w=1}^\infty g\left(\frac{\pi w^2}{2}\right)\right] = \frac{1}{\kappa^3}\left[g(0) - i\oint_\gamma dw\,g\left(\frac{\pi w^2}{2}\right)\cot(\pi w)\right], \tag{5.12}$$

with poles appearing for $w\in\mathbb{Z}$. The contour γ surrounds the positive real axis and is illustrated in Fig. 5.2. The green crosses corresponds to the poles of the integrand. For the red dashed line, the integrand in Eq. (5.12) decays fast enough and can be neglected. Hence, we are left with an integration over the solid red line. Since the result is real, we realize that only the integration along the branch cut of $\sqrt{q^2+2\kappa}$ contributes. The pole at $w=0$ exactly cancels $g(0)$, which results in

$$h(\kappa) = -\frac{32}{\sqrt{\pi\kappa}}\int_0^1 dq\;q^3\sqrt{1-q^2}\coth(q\sqrt{4\pi\kappa}). \tag{5.13}$$

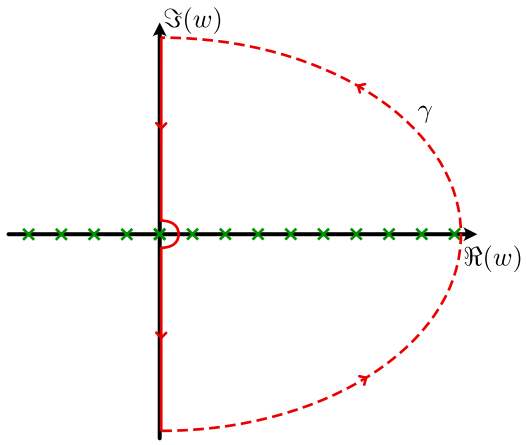

Figure 5.2: Contour γ to replace the sum over transverse modes by an integral. The green crosses correspond to the poles of the integrand while for the dashed part, the integrand drops fast enough and can be neglected. Thus, we are left with an integration over the solid red line.

By expressing $h_{3\mathrm{D}}(\kappa)$ in the same way,

$$h_{3\mathrm{D}}(\kappa) = -\frac{64}{15\sqrt{\pi\kappa}} = -\frac{32}{\sqrt{\pi\kappa}} \int_0^1 dq\, q^3 \sqrt{1-q^2}, \tag{5.14}$$

we can perform the integration over κ' in Eq. (5.9),

$$\begin{aligned} \int_\kappa^\infty d\kappa' \, [h(\kappa') - h_{3\mathrm{D}}(\kappa')] &= -\frac{32}{\sqrt{\pi}} \int_0^1 dq\, q^3 \sqrt{1-q^2} \int_\kappa^\infty d\kappa' \, \frac{\coth(q\sqrt{4\pi\kappa'}) - 1}{\sqrt{\kappa'}} \\ &= \frac{32}{\pi} \int_0^1 dq\, q^2 \sqrt{1-q^2} \ln\left(1 - e^{-\sqrt{16\pi\kappa} q}\right). \end{aligned} \tag{5.15}$$

Hence, the ground-state energy in Eq. (5.9) for the two-dimensional geometry is given by

$$\frac{E_{2\mathrm{D}}}{E_0} = \kappa^2 + \lambda \frac{128}{15\sqrt{\pi}} \kappa^{5/2} + \lambda \kappa^2 \frac{32}{\pi} \int_0^1 dq\, q^2 \sqrt{1-q^2} \, \ln\left(1 - e^{-\sqrt{16\pi\kappa}\, q}\right), \tag{5.16}$$

which describes the system including beyond-mean-field corrections for $\kappa \ll \frac{1}{\lambda^2}$. In the following, we will investigate the three-dimensional ($\kappa \gg 1$) and two-dimensional regime ($\kappa \ll 1$) in detail.

Three-Dimensional Regime

In the three-dimensional regime, we expand Eq. (5.16) for $\kappa \gg 1$ and obtain

$$\frac{E_{2\mathrm{D}}}{E_0} \overset{\kappa \gg 1}{=} \kappa^2 + \lambda \frac{128}{15\sqrt{\pi}} \kappa^{5/2} - \lambda \frac{\pi^{3/2}}{90} \sqrt{\kappa} + O(\lambda \kappa^{-1/2}). \tag{5.17}$$

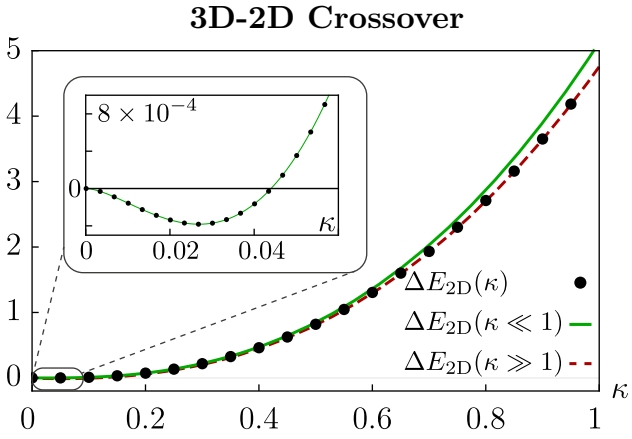

Figure 5.3: Crossover behavior of the beyond-mean-field correction ($\Delta E_{2\mathrm{D}} = (E_{2\mathrm{D}}/E_0 - \kappa^2)/\lambda$) from 3D to 2D with periodic boundary conditions in the transverse direction. Black dots denote the result from the numerical evaluation within the crossover, while the asymptotic behavior for small κ is plotted as a green (solid) line, and the red (dashed) line shows the analytical prediction for large κ.

With the first two terms we recover the three-dimensional result, while the last term describes an attractive correction to the ground-state energy due to the transverse confinement. This correction is non-vanishing even for $\kappa \to \infty$.

Two-Dimensional Regime

In the opposite regime, we expand Eq. (5.16) for $\kappa \ll 1$, which results in

$$\frac{E_{2\mathrm{D}}(\kappa)}{E_0} \overset{\kappa \ll 1}{=} \kappa^2 + \lambda\kappa^2 \ln(\kappa 4\pi\sqrt{e}) + \frac{2\pi}{3}\,\lambda\,\kappa^3 + O(\lambda\kappa^4). \tag{5.18}$$

The third term describes an effective three-body interaction due to quantum fluctuations, while the first two terms provide the ground-state energy of a purely two-dimensional Bose gas. In order to establish the latter connection, we note that the ground-state energy of a two-dimensional Bose gas takes the form [150–154]

$$\frac{E}{A} = \frac{2\pi\hbar^2 n_{2\mathrm{D}}^2/m}{\ln(\frac{1}{n_{2\mathrm{D}}a_{2\mathrm{D}}^2}) + \ln\left[\ln(\frac{1}{n_{2\mathrm{D}}a_{2\mathrm{D}}^2})\right] - \ln(e^{2\gamma}\pi\sqrt{e})}, \tag{5.19}$$

as discussed in Sec. 3.2.2. Here, $n_{2\mathrm{D}} = nl_\perp$ denotes the two-dimensional density and $a_{2\mathrm{D}}$ the two-dimensional scattering length. As discussed in Sec. 4.2, for the two-dimensional geometry with periodic boundary conditions, $a_{2\mathrm{D}}$ is connected to the s-wave scattering length $a_{2\mathrm{D}}$ by

$$a_{2\mathrm{D}} = 2l_\perp e^{-\frac{l_\perp}{2a_s}} e^{-\gamma}, \tag{5.20}$$

which was first obtained in Ref. [164]. By inserting $a_{2\mathrm{D}}$ into Eq. (5.19) and expanding in our small parameter λ, we reproduce the first two terms in Eq. (5.17). Note that the expansion in Eq.(5.17) implies $\kappa \gtrsim \lambda e^{-1/\lambda}$. Otherwise, for exponentially low densities, the two-dimensional small parameter $1/|\ln n_{2\mathrm{D}} a_{2\mathrm{D}}^2| = 1/|\ln(\kappa/\lambda) - 1/\lambda| \ll 1$ [148] is no longer dominated by λ but rather by the logarithm of the densities.

The full crossover behavior of $E_{2\mathrm{D}}$ is shown in Fig. 5.3, where it is most convenient to only show the beyond-mean-field correction $\Delta E_{2\mathrm{D}} = (E_{2\mathrm{D}}/E_0 - \kappa^2)/\lambda$. The black dots show the numerical evaluation of Eq. (5.16). The green solid line shows the asymptotic behavior for $\kappa \ll 1$ [see Eq. (5.17)], which accounts for the negative beyond-mean-field corrections to the ground-state energy as well as the zero-crossing. The asymptotic behavior for $\kappa \gg 1$ [see Eq. (5.18)] is shown as a red dashed line, which already describes the system accurately for $\kappa \approx 1$. Also note that the influence of the correction to the three-dimensional result in Eq. (5.17) only has a minor influence in this regime. This means a three-dimensional description is surprisingly accurate, even for a relatively strong confinement.

5.2.3 | Crossover to One Dimension

Next, we focus on the dimensional crossover from a three-dimensional setup toward a one-dimensional tube with two transverse dimensions confined. Like the Bogoliubov theory, the method used here relies on the existence of a condensate, which is absent in one dimension. In the weakly interacting regime, however, the ground-state energy is well described within the Bogoliubov theory, as the system still exhibits quasi-long-range order [84]. The ground-state energy in the crossover is denoted as $E_{1\mathrm{D}}$, and $h(\kappa)$ becomes

$$h(\kappa) = \frac{1}{\kappa^3} \sum_{w,v} \int du \left[\frac{2\varepsilon^2 + 3\kappa\varepsilon}{\sqrt{\varepsilon^2 + 2\kappa\varepsilon}} - 2\varepsilon - \kappa \right]. \tag{5.21}$$

In contrast to the 2D situation, we first perform the integration over κ' in Eq. (5.9). Then, the expression for the beyond-mean-field correction reduces to

$$\frac{E_{1\mathrm{D}} - E_{3\mathrm{D}}}{E_0} = \lambda \int du \left[\sum_{v,w} f(\epsilon) - \int dv dw\, f(\epsilon) \right], \quad \text{where} \quad f(\epsilon) = \sqrt{\epsilon^2 + 2\kappa\epsilon} - \epsilon - \kappa. \tag{5.22}$$

Again, it is possible to derive an expression in terms of well-known functions by performing the double sum, which is explained in detail in Appendix B.1. We obtain

$$\begin{aligned} \frac{E_{1\mathrm{D}}}{E_0} =& \kappa^2(1 + \lambda C_{1\mathrm{D}}) - \lambda \frac{8}{3\sqrt{\pi}} \kappa^{3/2} + \lambda\kappa^2 \int_0^\infty \frac{d\tau}{\sqrt{\pi\tau}} \\ & \times \left[\vartheta_3\left(0, e^{-\tau}\right)^2 - 1 \right] \left[1 - \frac{e^{-2\tau\kappa/\pi} I_1\left(\frac{2\tau\kappa}{\pi}\right)}{\tau\kappa/\pi} \right]. \end{aligned} \tag{5.23}$$

Here, $\vartheta_3(z,q) = \sum_n q^{n^2}\cos(2nz)$ denotes the Jacobi theta function, while $I_\nu(z)$ is the modified Bessel function. The term involving $C_{1\mathrm{D}}$ is a shift to the mean-field energy due to the confinement defined as

$$C_{1\mathrm{D}} = \int dvdw \frac{1}{\sqrt{v^2+w^2}} - \sum_{v,w}{}' \frac{1}{\sqrt{v^2+w^2}} \approx 3.899,$$

where the summation $\sum'$ omits the term $v=w=0$.

One-Dimensional Regime

Using the properties of Bessel functions, we expand Eq. (5.23) for small values of $\kappa \ll 1$. We obtain the leading corrections for the one-dimensional regime,

$$\frac{E_{1\mathrm{D}}}{E_0} \overset{\kappa\ll 1}{=} \kappa^2\left(1+\lambda C_{1\mathrm{D}}\right) - \lambda\frac{8}{3\sqrt{\pi}}\kappa^{3/2} + \lambda B_{1\mathrm{D}}\kappa^3 + O(\lambda\kappa^4), \tag{5.24}$$

with

$$B_{1\mathrm{D}} = (1/\pi)\sum_{vw}{}'(v^2+w^2)^{-3/2} \approx 2.88. \tag{5.25}$$

These terms account for the attractive part of the beyond-mean-field correction as well as the zero-crossing. Again, we have a very clear interpretation of these results: The term with κ^3 provides an effective three-body interaction, while the other terms account for the ground-state energy of a one-dimensional Bose gas. The latter is well established to take the form [155]

$$\frac{E}{L} = -\frac{\hbar^2}{m a_{1\mathrm{D}}} n_{1\mathrm{D}}^2 \left(1 - \frac{4\sqrt{2}}{3\pi}\frac{1}{\sqrt{|n_{1\mathrm{D}}a_{1\mathrm{D}}|}}\right), \tag{5.26}$$

as discussed in Sec. 3.2.1. To connect this result to our asymptotic form, we note that $a_{1\mathrm{D}}$ is connected to a_s by

$$a_{1\mathrm{D}} = -\frac{1}{2\pi}\frac{l_\perp^2}{a_\mathrm{s}}\left(1 - C_{1\mathrm{D}}\frac{a_\mathrm{s}}{l_\perp}\right),$$

which was derived in Sec. 4.2. Inserting $a_{1\mathrm{D}}$ and $n_{1\mathrm{D}} = n l_\perp^2$ into Eq. (5.26) and expanding in the small parameter $\lambda = a_\mathrm{s}/l_\perp$ then exactly provides the first two terms in Eq. (5.24). We want to emphasize that therefore the approach naturally includes the leading contribution of the confinement-induced resonance or in other words: The confinement-induced resonance is of the same order in λ as the beyond-mean-field corrections of a pure one-dimensional gas.

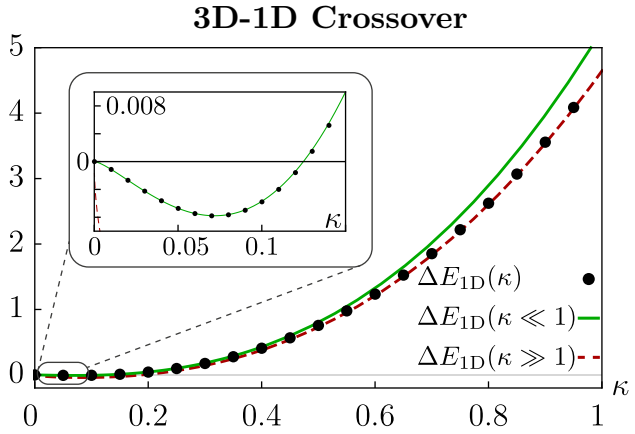

Figure 5.4: Crossover behavior of the beyond-mean-field correction ($\Delta E_{1D} = (E_{1D}/E_0 - \kappa^2)/\lambda$) from 3D to 1D with periodic boundary conditions in the transverse direction. Black dots denote the result from the numerical evaluation within the crossover, while the asymptotic behavior for small κ is plotted as a green (solid) line, and the red (dashed) line shows the analytical prediction for large κ.

Three-Dimensional Regime

In the three-dimensional regime, we again find an attractive correction to the three-dimensional result in Eq. (5.1),

$$\frac{E_{1D} - E_{3D}}{E_0} \overset{\kappa \gg 1}{=} -\sqrt{\kappa}\lambda \frac{A_{1D}}{2\pi^{5/2}} + O(\kappa^{-1/2}), \tag{5.27}$$

with the constant

$$A_{1D} = \sum\nolimits'_{v,w} \left(v^2 + w^2\right)^{-2} \approx 6.0268. \tag{5.28}$$

A detailed derivation of this result is presented in Appendix B.1.

In Fig. 5.4, we show the full crossover behavior of E_{1D}, where we only plot the beyond-mean-field correction, $\Delta E_{1D} = (E_{1D}/E_0 - \kappa^2)/\lambda$. The black dots show the numerical evaluation of Eq. (5.23), while the green solid line shows the asymptotic behavior from Eq. (5.24) for $\kappa \ll 1$, which describes the negative beyond-mean-field correction in one-dimension and also accurately describes the zero-crossing. The red dashed line shows the asymptotic behavior for $\kappa \gg 1$ from Eq. (5.27). As for the two-dimensional geometry, the three-dimensional results describes the system accurately even for surprisingly small values of $\kappa \gtrsim 0.5$.

5.3 | Crossover for a Harmonic Confinement

With the understanding gained from the discussion of the systems confined by periodic boundary conditions in the previous section, we will now investigate the more realistic

setup with a harmonic confinement in the transverse direction. The trapping frequency $\omega_\perp$ is related to the transverse confinement length via $\omega_\perp = \hbar/ml_\perp^2$. It is important to point out that we are not interested in mean-field modifications of the ground-state wave function due to interactions, which was studied previously [179–181]. We are interested in beyond-mean-field corrections for a setup where the condensate remains in the lowest state of the harmonic confinement. Experimentally, this goal can be achieved for bosonic mixtures [49]. On the theoretical level, this goal is conveniently achieved by adding an attractive interaction potential which is dominated by a large range $r_0 \gg l_\perp, l_\perp/\sqrt{\kappa}$ within the tube elongated along x, e.g.,

$$V(x,y,y',z,z') = g\delta(y-y')\delta(z-z')\left(\delta(x) - \frac{1}{\sqrt{\pi r_0^2}}e^{-x^2/r_0^2}\right). \tag{5.29}$$

Note that such a potential does not contribute to the beyond-mean-field corrections, which are dominated by momenta $k \sim 1/\xi_h \propto \sqrt{\kappa}/l_\perp$, due to its large range. However, it guarantees that the condensate remains in the lowest energy state of the transverse confinement within mean-field theory since the lowest-order chemical potential vanishes (see Appendix B.2.1). We will mainly focus our discussion on the dimensional crossover from three to one dimension and only briefly discuss the two-dimensional case afterwards.

The interaction potential in combination with the harmonic confinement leads to the mixing of different transverse modes, and we have to adapt the approach of Hugenholtz and Pines. As we have seen in Sec. 3.1.2 [see Eq. (3.57)], we can express the differential equation for the ground-state energy in terms of the Bogoliubov amplitudes, which can be conveniently derived within Bogoliubov theory, see Appendix B.2.1. The Bogoliubov transformation in general involves many transverse modes,

$$a_{u,\alpha\beta} = \sum_{vw}\left[u_{u,vw}^{\alpha\beta}b_{u,vw} - v_{u,vw}^{\alpha\beta}b_{-u,vw}^\dagger\right], \tag{5.30}$$

where $a_{u,\alpha\beta}$ are the new bosonic operators, and $u_{u,vw}^{\alpha\beta}$ ($v_{u,vw}^{\alpha\beta}$) are the Bogoliubov amplitudes. Then, the ground state within the approach of Hugenholtz and Pines fulfills

$$E_{1\mathrm{D}}^h - \frac{1}{2}\mu N = \frac{L}{2}\int\frac{dk}{2\pi}\sum_{\substack{v,\alpha\\w,\beta}}\left[\tilde{\epsilon}_{k,vw} - \tilde{E}_{k,\alpha\beta}\right]|v_{k,vw}^{\alpha\beta}|^2, \tag{5.31}$$

with $\tilde{\epsilon}_{k,vw} = \frac{\hbar^2k^2}{2m} + \hbar\omega_\perp(v+w)$ the excitation spectrum of a free particle. Here, $v,w \in \{0,1,2,\ldots\}$ denote the quantum numbers for the harmonic oscillator modes of the transverse confinement, and $\tilde{E}_{k,\alpha\beta}$ denotes the Bogoliubov excitation spectrum.

As for periodic boundary conditions, it is convenient to define $\kappa = n_{1\mathrm{D}}a_\mathrm{s}$. The single-particle excitation spectrum in dimensionless units is modified to $\epsilon = \epsilon_0/(4\pi\hbar^2/ml_\perp^2) = \pi/2\left[u^2+(v+w)/2\pi^2\right]$. Then, the term $h(\kappa)$ within the approach of Hugenholtz and Pines takes the form

$$h(\kappa) = \frac{4\pi}{\kappa^3}\int du\sum_{\alpha\beta}\sum_{vw}\left[\epsilon - E_{\alpha\beta}\right]|v_{u,vw}^{\alpha\beta}|^2, \tag{5.32}$$

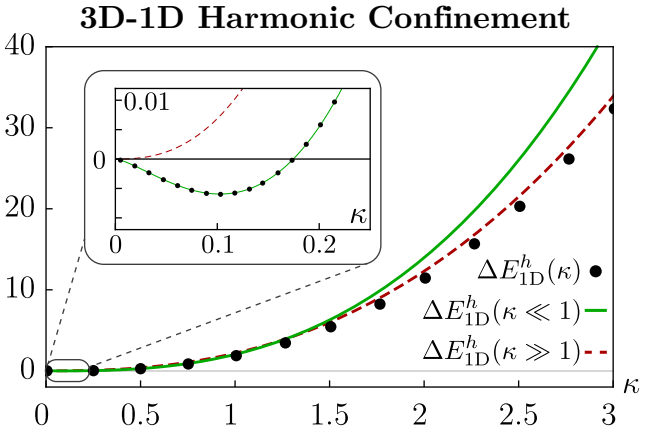

Figure 5.5: Crossover behavior of the beyond-mean-field correction ($\Delta E^h_{1D} = E^h_{1D}/\lambda E^h_0$) from 3D to 1D with a harmonic trapping potential in the transverse direction. Black dots denote the result from the numerical evaluation within the crossover, while the asymptotic behavior for small κ is plotted as a green (solid) line, and the red (dashed) line shows the analytical prediction for large κ. Note that $\Delta E^h_{1D}(\kappa \ll 1)$ includes in addition to the analytical expression Eq. (5.35), the term $B^h_{1D}\kappa^3$.

where $E_{\alpha\beta}$ is the Bogoliubov excitation energy in dimensionless units. In general, the determination of the Bogoliubov excitation spectrum $E_{\alpha\beta}$ and the factors $v^{\alpha\beta}_{u,vw}$ requires a numerical analysis, which was carried out by Luis Santos. The beyond-mean-field correction to the ground-state energy is determined by fixing the correct mean-field term $\propto \kappa^2$. In the previous analysis, we observed that the beyond-mean-field correction includes the modification of the mean-field term through the confinement-induced resonance. This allows us to fix the mean-field term in the one-dimensional regime $\kappa \ll 1$. Alternatively, one would expect that for a very shallow trapping potential the local-density approximation is well justified, which in turn allows us to fix the mean-field term for $\kappa \gg 1$. Our numerical analysis shows that both approaches coincide. The result of this numerical analysis in the full crossover from three to one dimension is shown in Fig. 5.5, where $\Delta E^h_{1D} = E^h_{1D}/\lambda E^h_0$ and $E^h_0 = \hbar\omega_\perp L/a_s$. In the three-dimensional regime with $\kappa \gg 1$, we find excellent agreement between the numerical analysis and the prediction within the local-density approach (red dashed line). The latter is obtained by integrating the 3D LHY result in Eq. (5.1) over the transversal density profile of the condensate,

$$n(\boldsymbol{r}) = n_{1D}\frac{e^{-(y^2+z^2)/l_\perp^2}}{l_\perp^2\pi}. \tag{5.33}$$

This then results in

$$E^h_{1D} = \lambda\frac{512}{75\pi}\,\kappa^{5/2}E^h_0 \quad \text{for} \quad \kappa \gg 1\,. \tag{5.34}$$

Note that the term κ^2 is missing due to our special choice of the interaction potential. In turn, for $\kappa \ll 1$ it is possible to derive the leading corrections to the ground-state energy

by determining the Bogoliubov energy $E_{\alpha\beta}$ and the factors $v^{\alpha\beta}_{u,vw}$ within perturbation theory. It is required to perform the analysis up to second-order perturbation theory for $E_{\alpha\beta}$ and first order for $v^{\alpha\beta}_{u,vw}$, which is straightforward but cumbersome. The perturbation expansion is explained in detail in Appendix B.2.2. Then, the beyond-mean-field correction takes the form

$$\frac{E^h_{1\mathrm{D}}}{\lambda E^h_0} \overset{\kappa\ll 1}{=} \kappa^2 \frac{C^h_{1\mathrm{D}}}{\sqrt{2}} - \frac{4\sqrt{2}}{3\pi}\kappa^{3/2} + \frac{4\sqrt{2}\ln(4/3)}{\pi}\kappa^{5/2} + O(\kappa^3). \tag{5.35}$$

The first term on the right side accounts for the correction to the mean-field term due to the confinement-induced resonance with $C^h_{1\mathrm{D}} \approx 1.4603$ [165], while the second term describes the beyond-mean-field contribution of a purely one-dimensional system. Finally, the term with $\kappa^{5/2}$ provides the leading correction in the crossover. It is highly remarkable that for harmonic confinement a term $\kappa^{5/2}$ appears, which was absent in the previous analysis with periodic boundary conditions. These predictions are fully confirmed with the numerical approach, as can be seen in Fig. 5.5 (green solid line). However, for a correct description of the zero-crossing it is also important to include the next term $B^h_{1\mathrm{D}}\kappa^3$ in the expansion. While $B_{1\mathrm{D}}$ can be determined with the procedure of Appendix B.2.1, this would require to calculate $v^{\alpha\beta}_{u,vw}$ up to second-order perturbation theory, which is very cumbersome. Thus, we determine $B^h_{1\mathrm{D}}$ by a fitting procedure to the numerical evaluation, which predicts $B^h_{1\mathrm{D}} \approx 0.1$.

An analogous calculation can also be performed for the 3D-2D crossover within a harmonic confinement. Here, the crossover parameter takes the form $\kappa = n_{2\mathrm{D}} a_s l_\perp$. Again, we expect the prediction of local-density approximation to be accurate for $\kappa \gg 1$, while for $\kappa \ll 1$ the ground-state energy reduces to the two-dimensional result,

$$E^h_{2\mathrm{D}} = \hbar\omega_\perp \kappa^2 \ln\left(\kappa C^h_{2\mathrm{D}}\right) L^2/l^2_\perp, \tag{5.36}$$

with $C^h_{2\mathrm{D}} \approx 28.69$ [138, 166], including the renormalized scattering length (see Sec. 4.3.2). Repeating the same procedure as in Appendix B.2.1 for the two-dimensional geometry provides a correction $\propto \kappa^3 \ln\kappa$. Obtaining the correct prefactor of this contribution is problematic. This would require a consistent expansion up to order κ^3, and thus to determine the Bogoliubov amplitudes within second order perturbation theory, as we have already seen in the one-dimensional case (see Appendix B.2.2).

5.4 | Comment: Dipoles in the One-Dimensional Regime

Before we conclude this chapter, we briefly want to comment on the one-dimensional regime for dipolar interactions. For this we begin with a short historic context: Our investigation of the dimensional crossover for short-range contact interactions arose after the discussion of the crossover for dipolar interactions, which was analyzed by Edler *et al.* [178] in the group of Luis Santos, who also collaborated on the crossover discussed

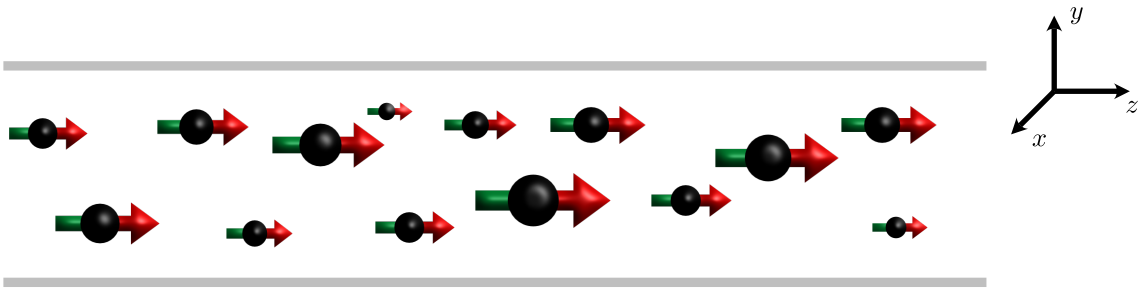

Figure 5.6: Sketch of the dipolar atoms in the trap. The dipoles are aligned in the z direction and strongly confined in the x-y plane.

in the previous sections. In their paper, the crossover was investigated for dipoles in a one-dimensional geometry. The dipoles, which are aligned in the z direction, are strongly confined in the x-y plane by a harmonic confinement, but free along the z direction (see Fig. 5.6). Note that the cancellation of the lowest-order chemical potential is naturally achieved for $\varepsilon_{\mathrm{dd}} = 1$ in this setup. Due to the harmonic confinement and the dipolar interaction, the investigation was performed numerically. With what we have learned from the crossover for short-range interactions, it is worth to briefly revisit the dimensional crossover for dipoles. Now, we have a deeper understanding of the influence of the confinement-induced resonance and the tools to investigate the leading contribution in the one-dimensional regime. The following discussion developed in collaboration with a master student, Christoph Pitzal.

The ground-state energy fulfills the differential equation,

$$E - \frac{1}{2}\mu N = \frac{L}{2}\int \frac{dk}{2\pi} \sum_{n_r,n_r',m} \left[\tilde{\epsilon}_{k,n_r m} - \tilde{E}_{k,n_r' m}\right] |v_{k,n_r m}^{n_r' m}|^2, \tag{5.37}$$

similar to Sec. 5.3. Note that for the dipolar case, we make use of the rotational symmetry around the tube axis and chose a basis for the transverse harmonic oscillator with a well-defined angular momentum. Then, the single-particle spectrum reads

$$\tilde{\epsilon}_{k,n_r,m} = \frac{\hbar^2 k^2}{2M} + \hbar\omega_\perp(2n_r + |m|) \tag{5.38}$$

with the radial quantum number n_r, the orbital quantum number m and the mass of the atoms is denoted by M in this section to avoid any confusion. The dipolar interaction strongly modifies the Bogoliubov amplitudes $v_{k,n_r m}^{n_r' m}$ and the Bogoliubov spectrum $\tilde{E}_{k,n_r m}$. However, the expansion in the regime $\kappa = n_{1\mathrm{D}} a_{\mathrm{s}} \ll 1$ can be performed in complete analogy to Sec. 5.3. A detailed derivation is presented in Appendix B.3. In the one-dimensional regime we obtain

$$\frac{E_{1\mathrm{D}}^{\mathrm{dd}}}{E_0} \overset{\kappa\ll 1}{=} \alpha\kappa^2 - \lambda\frac{2B_{1\mathrm{D}}^{\mathrm{dd}}}{\pi}\kappa^3 + O(\kappa^{7/2}), \tag{5.39}$$

where $B_{1D}^{dd} \approx -27.724$ and $E_0 = \hbar\omega_\perp L/a_s$. Again, we want to point out that within our approach we are not able to determine α. This would either require knowledge of the confinement-induced shift for quasi-one-dimensional bosons, which so far is missing or to fix the mean-field energy in the three-dimensional regime and find an expansion for $\kappa \ll 1$. The latter, however, is extremely challenging and to our knowledge analytically not possible, but was performed numerically in Ref. [178]. Hence, we suspect that the reported linear density dependence of the chemical potential $\Delta\mu_{LHY} \propto -n_{1D}$ by Edler *et al.* is not a unique feature of the dipolar interaction, but arises through the confinement-induced resonance. The next order in the ground-state energy then already scales as κ^3, which differs significantly from the result of a contact-interacting system, see Eq. (5.35). Note that for the dipolar case, to obtain a consistent expansion up to order κ^3 does *not* require to determine the Bogoliubov amplitudes within second-order perturbation theory. Due to the momentum dependence of the dipolar interaction, already the lowest-order expansion provides all terms $\propto \kappa^3$ (see Appendix B.3).

5.5 | Conclusion

We present a detailed study of the beyond-mean-field corrections for a weakly interacting Bose gas in the dimensional crossover. While for a transverse confinement with periodic boundary conditions the analysis can be performed analytically, for a realistic setup with harmonic confinement a numerical analysis is required. We find excellent agreement with the predictions from local-density approximation for $\kappa \gtrsim 1$. Furthermore, we find that the correction to the local-density approximation lowers the ground-state energy. This phenomenon might explain the recently observed systematic shift in the scattering length determined by the stability of the self-bound droplets [47, 59]: The finite extent of the droplets in transverse direction naturally introduces a confinement of the underlying gas and hence a correction to the local-density approximation. A possible way to adapt our approach to these self-bound droplets is presented in Sec. 8.1. In addition, our results show that the full crossover is excellently described by the combination of the leading contribution for $\kappa \ll 1$ and $\kappa \gg 1$, which in general is sufficient to describe the qualitative behavior throughout the crossover. With our approach, we are also able to investigate the quasi-one-dimensional regime for dipolar particles, where the dipoles are aligned parallel to the tube. We find that the leading order beyond the confinement-induced shift already scales as κ^3, which is vastly different from the behavior of a one-dimensional Bose gas with only contact interactions.

6 | Bogoliubov Theory for a Dipolar One-Dimensional Supersolid

In this chapter, we use Bogoliubov theory to study the behavior of the excitation spectrum across the quantum phase transition from a superfluid to a supersolid phase of a dipolar Bose gas confined to a one-dimensional geometry. Since quantum fluctuations are crucial for the stability of the supersolid state, we derive an effective Hamiltonian that includes the beyond-mean-field corrections in a local-density approximation. In the supersolid regime, we extend Bogoliubov theory to include several order parameters which take into account the superfluid as well as the solid structure. We find fast convergence of the ground-state energy in the supersolid with the number of order parameters. The excitation spectrum is stable and shows two Goldstone modes and an amplitude mode in the low-energy regime. Our results suggest that there exists an experimentally achievable parameter regime for dysprosium atoms where the supersolid phase exhibits a stable excitation spectrum in the thermodynamic limit and the transition into the supersolid phase is of second order driven by the roton instability. This chapter is based on the publication [128].

6.1 | Introduction

While we so far mainly discussed short-range interactions to obtain a deeper understanding of beyond-mean-field corrections, we will shift our focus to dipolar atoms confined to a one-dimensional geometry in the following. This is inspired by the recent breakthrough experiments of weakly interacting dipolar Bose gases in elongated traps that demonstrated the appearance of a supersolid phase [99–101].

The supersolid state is characterized by its properties which combine the frictionless flow of a superfluid with the density modulation of a solid [75, 90]. The possibility of such a ground state for interacting bosonic particles has been shown by Leggett [90]. For a long time, the search for a supersolid state of matter focused on solid helium, a system with nearly one atom per unit cell [75, 92, 93]. In contrast, current experiments with dysprosium atoms work in a rather complementary regime and realize supersolid states with several thousand atoms on each lattice site [39, 40]. In this parameter regime, one can expect mean-field theory to describe the one-dimensional supersolid state accurately; a claim which we will investigate in detail in Chapter 7.

The interplay between three ingredients are key for the appearance of a supersolid phase in current experiments: The tunable short-range interaction, the anisotropic mag-

netic dipole-dipole interaction, and the geometry of the system play a fundamental role. For increasing influence of the dipolar interaction, such systems can undergo an instability towards the formation of quantum droplets [44–48, 60, 72, 167–171], as well as self-bound droplets [47, 59–63], or supersolid states [74, 85, 99–101, 106–130, 182–185], depending on the external trapping geometry.

As we will see in this chapter, the formation of the supersolid phase in the one-dimensional geometry is driven by a *roton instability*. The dipolar interaction in combination with the external confinement leads to a roton spectrum for the superfluid [64, 66], similar to the spectrum of superfluid helium [67–70]. By increasing the relative strength of the dipolar interaction, a minimum at finite momentum develops in the excitation spectrum and excitations around this minimum are called rotons. The position of the minimum can be precisely tuned through the strength of the dipolar interaction and the trapping frequency in ultracold atom experiments. When the energy of the roton minimum approaches zero, the system exhibits a roton instability and, depending on exact system parameters, can transition to a supersolid phase.

An important observation was that these states are only stabilized by the leading beyond-mean-field correction, which provides an additional contribution to the energy functional, stabilizing the system at higher densities against a collapse [45]. Such a stabilization has previously been predicted for Bose mixtures [49] and later also experimentally observed [50, 51]. Within the local-density approximation, this additional term can be included into the Gross-Pitaevskii functional and forms the basis for extensive numerical studies of the supersolid state and its excitation spectrum. Such numerical studies within the experimental three-dimensional setting are in good agreement with the experimental observation in dipolar quantum gases [39, 40]. However, predictions about the thermodynamic limit of these systems are often difficult to access in such fully numerical approaches in a finite-size setting [74, 127].

In this chapter, we study whether the supersolid phase exhibits stable excitations in the thermodynamic limit by deriving the low-energy excitation spectrum across the phase transition from the superfluid to the supersolid phase within Bogoliubov theory, which allows for an analytical study of the nature of the quantum phase transition. The analysis is based on Bogoliubov theory (see Sec. 3.1.1) in a one-dimensional setting, where we account for the transverse confinement by a variational ansatz. We make use of the local-density approximation and include the beyond-mean-field contributions within an effective Hamiltonian. Compared to the superfluid where only the mode $k = 0$ is macroscopically occupied, the supersolid phase is described by the macroscopic occupation of additional modes, each mode contributing a higher harmonic to the modulated ground-state wave function. The influence of each harmonic is characterized by a new order parameter and we extend the Bogoliubov theory introduced in Sec. 3.1.1 to systems where more than one mode is macroscopically occupied.

We start with a discussion of our effective Hamiltonian and use it to investigate the superfluid phase afterwards. We discuss the roton excitation spectrum before we then extend our approach to the supersolid regime, where we first calculate the ground-state

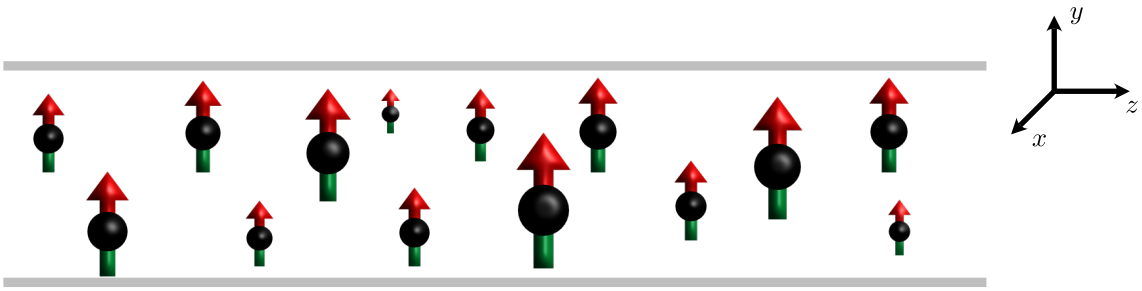

Figure 6.1: Sketch of the dipolar atoms in the trap. The dipoles are aligned in the y direction and strongly confined in the x-y plane.

energy and afterwards derive the excitation spectrum.

6.2 | Setup

Our analysis is based on a simple reduced three-dimensional model [115], which has recently been shown to produce qualitatively accurate predictions [127]. We consider a gas of trapped dipolar bosons with mass m, which are tightly confined in the x-y plane by a harmonic confinement but free along the z direction (see Fig. 6.1). In Chapter 5, we obtained a good understanding of beyond-mean-field effects in confined geometries and saw that the use of the local-density approximation is justified even for relatively strong confinements. In addition we saw that in the low-dimensional regime, the confinement-induced resonance is of beyond-mean-field order. With that in mind, we are interested in a regime where the healing length ξ_h of the superfluid is much smaller than the harmonic oscillator length $l_\perp$ of the transverse confinement,

$$\frac{\xi_h}{l_\perp} \ll 1, \tag{6.1}$$

such that the use of the local-density approximation is justified (see Sec. 5.3) and we are in a regime where the unknown effect of the confinement-induced resonance for dipoles does not play a role. In contrast to the discussion in Sec. 5.4, the dipoles are aligned perpendicular to the tube (y direction), which is important to obtain a roton spectrum in the superfluid (see below). Therefore, the lowest-order chemical potential is non-vanishing, resulting in a ground state which occupies many transverse modes, especially for $\xi_h/l_\perp \ll 1$. For our investigation, however, we are only interested in the low-energy excitations and the stability analysis of the supersolid phase. Under these considerations, the transverse degrees of freedom can be ignored and we make a variational ansatz for

the transverse wave function

$$\psi(x,y) = \frac{1}{\sqrt{\pi}\sigma l_\perp} e^{-\frac{\nu x^2 + y^2/\nu}{2(\sigma l_\perp)^2}}, \tag{6.2}$$

where σ and ν are the dimensionless variational parameters, which are determined by minimizing the ground-state energy. The anisotropic dipolar interaction leads to an anisotropic shape of the wave function, which is characterized by ν, while σ characterizes the width of the cloud. Our theory is then a low-energy description, which is restricted to excitation energies $\epsilon(q)$ that are much lower than the energy of a transverse excitation,

$$\epsilon(q) \ll E_\perp = \frac{\hbar^2}{m l_\perp^2}. \tag{6.3}$$

Within this variational framework, the microscopic Hamiltonian becomes one dimensional and consists of two parts, $H_0 + H_\mathrm{I}$. The single-particle Hamiltonian H_0 consists of the kinetic energy along the tube but also has to take into account the energy of the particles in the transverse trap, which for a single particle is given by

$$\begin{aligned} E_t(\sigma,\nu) &= \int dx\, dy\, \psi^*(x,y) \left[-\frac{\hbar^2}{2m}\left(\partial_x^2 + \partial_y^2\right) + \frac{\hbar^2}{2ml_\perp^2}\left(x^2+y^2\right)\right] \psi(x,y) \\ &= \frac{E_\perp}{4}\left(\frac{1}{\nu} + \nu\right)\left(\frac{1}{\sigma^2} + \sigma^2\right). \end{aligned} \tag{6.4}$$

We obtain

$$H_0 = \sum_q \left[\epsilon_0(q) + E_t(\sigma,\nu)\right] a_q^\dagger a_q, \tag{6.5}$$

where $a_q^\dagger (a_q)$ are the bosonic creation (annihilation) operators of particles with momentum q and $\epsilon_0(q)$ is the dispersion relation $\epsilon_0(q) = \frac{\hbar^2 q^2}{2m}$.

The particles interact via a short-range contact interaction characterized by the s-wave scattering length a_s and the anisotropic magnetic dipole-dipole interaction with strength a_dd, see Sec. 2.4. The dipoles are aligned perpendicular to the z direction. To obtain the interaction potential in momentum space for our one-dimensional description, we integrate over the transverse degrees of freedom using our variational wave function,

$$V(q_z) = \int \frac{dq_x\, dq_y}{(2\pi)^2}\, V_\mathrm{3D}(\boldsymbol{q}) n_\perp^2(q_x, q_y). \tag{6.6}$$

Here, $V_\mathrm{3D}(\boldsymbol{q})$ is the Fourier transform of the pseusopotential from Eq. (2.60) [37],

$$V_\mathrm{3D}(\boldsymbol{q}) = g\left[1 + \varepsilon_\mathrm{dd}\left(3\cos^2\alpha - 1\right)\right], \tag{6.7}$$

where α is the angle between $\boldsymbol{q}$ and the direction of the polarization and $n_\perp(q_x, q_y)$ is the Fourier transform of $|\psi(x,y)|^2$. For $\nu = 1$ we can evaluate the integral in Eq. (6.6) analytically,

$$V(q) \overset{\nu=1}{=} g_{1\mathrm{D}} \left[1 + \varepsilon_{\mathrm{dd}} \left(\frac{3\left(1 - (ql_\perp\sigma)^2\Gamma(0,(ql_\perp\sigma)^2/2)e^{(ql_\perp\sigma)^2/2}/2\right)}{2} - 1 \right) \right], \tag{6.8}$$

where $g_{1\mathrm{D}} = 2\hbar^2 a_{\mathrm{s}}/(m\sigma^2 l_\perp^2)$ and $\Gamma(n,x)$ denotes the incomplete Gamma function. We are unaware of an analytic result for an arbitrary $\nu \neq 1$. It has been shown by Blakie *et al.* [186], however, that Eq. (6.6) is well-approximated by

$$V(q) \approx g_{1\mathrm{D}} \left[1 + \varepsilon_{\mathrm{dd}} \left(\frac{3[1 - Qe^Q\Gamma(0,Q)]}{1+\nu} - 1 \right) \right], \tag{6.9}$$

with $Q = \sqrt{\nu}(q\sigma l_\perp)^2/2$, which we will use in the following. We want to point out again that corrections to $g_{1\mathrm{D}}$ due to the confinement-induced resonance are only relevant for $\xi_h/l_\perp \gg 1$ [165, 176] and therefore can be ignored here. It is also important to note that due to the confinement entering through the shape of $\psi(x,y)$, the potential (6.9) depends on the magnitude of q, in contrast to the three-dimensional case from Eq. (6.7). The q dependence of $V(q)$ will have a significant influence on the excitation spectrum as we will see in Sec. 6.3. The interaction part of the Hamiltonian is then given by

$$H_{\mathrm{I}} = \frac{1}{2L} \sum_{p,k,q} V(q) a_{p+q}^\dagger a_{k-q}^\dagger a_k a_p, \tag{6.10}$$

where L is the quantization volume.

From the microscopic Hamiltonian $H_0 + H_{\mathrm{I}}$ one obtains the mean-field energy, the single-particle Bogoliubov excitation spectrum, as well as the leading beyond-mean-field correction within standard Bogoliubov theory (see Sec. 3.1.1). However, it is well established that for dipolar quantum gases the beyond-mean-field correction plays a crucial role in stabilizing the quantum droplets [39, 40, 45] and needs to be included when describing the excitation spectrum. So far, the analysis is mainly based on numerical studies of the extended Gross-Pitaevskii equation, where the beyond-mean-field term is included within local-density approximation [74, 127]. In analogy, we add a term H_{LHY} to the Hamiltonian such that Bogoliubov theory on this effective Hamiltonian properly accounts for the low-energy excitations within Bogoliubov theory. Note that this method is equivalent to studying the excitation spectrum within the extended Gross-Pitaevskii equation, but more suitable for our analytical study.

We have discussed the beyond-mean-field correction for a three-dimensional dipolar Bose-Einstein condensate in Sec. 3.2.3. There, we have seen that the energy density, which is denoted as u in this chapter to avoid confusions, takes the form [see Eq.(3.69)],

$$u_{\mathrm{LHY}} = \frac{256\sqrt{\pi}\hbar^2}{15m} (n_{3\mathrm{D}} a_{\mathrm{s}})^{5/2} \mathcal{Q}_5(\varepsilon_{\mathrm{dd}}), \tag{6.11}$$

with $\mathcal{Q}_5(\varepsilon_{\rm dd}) = \int_0^1 du(1-\varepsilon_{\rm dd}+3\,\varepsilon_{\rm dd}u^2)^{5/2}$ [see Eq. (3.70)] and $n_{\rm 3D}$ the density of the homogeneous three-dimensional system. This result was first obtained in Refs. [54, 187]. The function $\mathcal{Q}_5(\varepsilon_{\rm dd})$ accounts for the modification due to the additional dipolar interaction to the well-established result for contact interactions derived by Lee, Huang, and Yang (LHY) [52, 53]. As we have seen in Sec. 3.1.1, the LHY correction is dominated by excitations around the momenta $1/\xi_h$, with the characteristic length scale $\xi_h = \hbar/\sqrt{2mn_{\rm 3D}g}$. This implies that the local-density approximation is well justified if the density varies smoothly on this characteristic scale ξ_h, i.e., $l_\perp \gg \xi_h$. Within local-density approximation and using the variational wave function $\psi(x,y)$, we end up with the correction

$$\frac{E_{\rm LHY}}{L} = \frac{256\sqrt{\pi}\hbar^2}{15m}(na_{\rm s})^{5/2}\mathcal{Q}_5(\varepsilon_{\rm dd})\int dx\,dy\,|\psi(x,y)|^5 = \frac{2}{5}\gamma_{\rm QF}n^{5/2}, \tag{6.12}$$

where we have introduced

$$\gamma_{\rm QF} = \frac{256}{15\pi}\frac{\hbar^2}{m(\sigma l_\perp)^3}\mathcal{Q}_5(\varepsilon_{\rm dd})a_{\rm s}^{5/2} \tag{6.13}$$

and $n = N/L$ is the one-dimensional particle density.

The ground-state energy including the LHY correction hence becomes

$$\frac{E}{L} = \min_{\sigma,\nu}\left[n\,E_t(\sigma,\nu) + \frac{1}{2}n^2V(0) + \frac{2}{5}\gamma_{\rm QF}n^{5/2}\right]. \tag{6.14}$$

The correction to the mean-field energy provides a correction in the chemical potential

$$\mu = \frac{dE}{dN} = E_t + nV(0) + \gamma_{\rm QF}n^{3/2}, \tag{6.15}$$

where N is the particle number. Note, that σ and ν are only very weakly depending on the number of particles and within our analysis we self-consistently ignore this small contribution. Accordingly, a correction to the chemical potential affects the compressibility $\varkappa = d\mu/dn$, which gives rise to a modified sound velocity of the superfluid,

$$c^2 = \frac{n\varkappa}{m} = \frac{1}{m}\left(nV(0) + \frac{3}{2}\gamma_{\rm QF}n^{3/2}\right). \tag{6.16}$$

The term $H_{\rm LHY}$ we add to the Hamiltonian is therefore determined such that it reproduces the correct ground-state energy E within mean field as well as the correct sound velocity as the low-momentum limit of the excitation spectrum $\epsilon(q)$ within lowest-order Bogoliubov theory. The contribution to the Hamiltonian which fulfills these conditions can be written as

$$H_{\rm LHY} = \frac{2}{5}\gamma_{\rm QF}\int dz\left[\Psi^\dagger(z)\Psi^\dagger(z)\Psi(z)\Psi(z)\right]^{5/4} \tag{6.17}$$

with

$$\Psi(z) = \frac{1}{\sqrt{L}} \sum_q e^{iqz} a_q, \tag{6.18}$$

as will be demonstrated in the following. The effective Hamiltonian

$$H = H_0 + H_{\mathrm{I}} + H_{\mathrm{LHY}} \tag{6.19}$$

will allow us to determine the low-energy excitation spectrum across the phase transition from the superfluid to the supersolid. The validity of our approach is limited to momenta $q \ll 1/\xi_h$ and energies $\epsilon(q) \ll \mu$ such that the local-density treatment for the term H_{LHY} is justified.

6.3 | Excitations in the Superfluid Phase

We start with the study of the excitation spectrum in the superfluid using the standard Bogoliubov procedure [4], which we have discussed in detail in Sec. 3.1.1 for the three-dimensional case. Since adapting it to one dimension is straightforward, we will keep the discussion short. It is important to point out that even in one dimension, the Bogoliubov theory provides the correct excitation spectrum in the weakly interacting regime as can be seen by a comparison with the exact Lieb-Liniger theory for bosons with contact interactions [155, 156]. One can understand this phenomenon as locally there are still a high number of particles in the condensate, while quantum fluctuations only suppress the coherence between these local condensates on large distances giving rise to the well-established algebraic behavior [82, 84]. As we will see in Chapter 7, Bogoliubov theory also still provides an accurate description in the supersolid regime. In the following, it is convenient to work in the grand canonical ensemble described by the chemical potential μ and self-consistently determine the chemical potential to find the correct particle density n. Within mean-field theory, we replace the operator $a_0^\dagger = \sqrt{Ln}$ by the local particle density. Inserting this ansatz in the grand canonical potential H' provides, as required, the ground-state energy including the LHY correction,

$$H' = E - \mu N, \tag{6.20}$$

and we recover the relation between the particle number n and the chemical potential in Eq. (6.15) by minimizing H'. In the next step, we can use the standard Bogoliubov prescription to derive the excitation spectrum. For this purpose, we write for the bosonic field operator

$$\Psi(z) \to \sqrt{n} + \frac{1}{\sqrt{L}} \sum_{q \neq 0} e^{iqz} a_q = \sqrt{n} + \delta\psi(z). \tag{6.21}$$

Note that within this approach with fixed chemical potential and leading-order expansion, we do not have to distinguish between the particle density n and the condensate

density n_0, as the difference only becomes relevant for the higher-order corrections. Inserting the bosonic field operator into the Hamiltonian and expanding it up to second order in the small fluctuations $\delta\psi$, we end up with a quadratic Hamiltonian H_{B} accounting for the Bogoliubov excitations

$$H_{\mathrm{B}} = \frac{1}{2}\sum_{q\neq 0} :\begin{pmatrix} a_q^\dagger \\ a_{-q}\end{pmatrix}\left[\begin{pmatrix}\chi & 0\\ 0 & \chi\end{pmatrix}+\begin{pmatrix}\eta & \eta\\ \eta & \eta\end{pmatrix}\right]\begin{pmatrix} a_q \\ a_{-q}^\dagger\end{pmatrix}: . \tag{6.22}$$

Here, $:\hat{O}:$ denotes the normal ordered operator $\hat{O}$, and we introduced the two parameters

$$\chi = \epsilon_0(q) + E_t + nV(0) + \gamma_{\mathrm{QF}} n^{3/2} - \mu\,, \tag{6.23a}$$

$$\eta = nV(q) + \frac{3}{2}\gamma_{\mathrm{QF}} n^{3/2}, \tag{6.23b}$$

which contain additional terms of the form $\gamma_{\mathrm{QF}} n^{3/2}$ compared to Eq. (3.15) due to the inclusion of fluctuations within local-density approximation. Note that we do not include the lowest-order contribution of the Bogoliubov prescription in H_{B} since we are only interested in the excitation spectrum.

To obtain the excitation spectrum $\epsilon(q)$, we diagonalize the Hamiltonian (6.22) via the Bogoliubov transformation

$$a_q = u_q b_q + v_q b_{-q}^\dagger\,. \tag{6.24}$$

The amplitudes u_p and v_p have to fulfill the constraint $u_p^2 - v_p^2 = 1$ for the transformation to be canonical. A short calculation yields the diagonal Hamiltonian for the excitation spectrum

$$H_{\mathrm{B}} = \sum_{q\neq 0} \epsilon(q) b_q^\dagger b_q, \tag{6.25}$$

where the Bogoliubov excitation spectrum is given by

$$\epsilon(q)^2 = \chi^2 + 2\chi\eta\,. \tag{6.26}$$

The Bogoliubov excitation spectrum $\epsilon(q)$ depends on the chemical potential. Using the correct chemical potential in Eq. (6.15) including the LHY correction, the excitation spectrum becomes gapless,

$$\epsilon(q)^2 = \epsilon_0(q)^2 + 2\epsilon_0(q)\left[nV(q) + \frac{3}{2}\gamma_{\mathrm{QF}} n^{3/2}\right], \tag{6.27}$$

as required by the famous Hugenholtz and Pines relation [7]. At low momenta, we recover the predicted sound velocity,

$$\begin{aligned}\epsilon(q) &\overset{q\to 0}{=} |q|\sqrt{\frac{\hbar^2}{m}\left(nV(0) + \frac{3}{2}\gamma_{\mathrm{QF}} n^{3/2}\right)} \\ &= \hbar|q|c\,,\end{aligned} \tag{6.28}$$

with c given in Eq. (6.16). Therefore, we demonstrated that our effective approach with the Hamiltonian in Eq. (6.19) is capable to reproduce the ground-state energy including quantum fluctuations within local-density approximation, as well as the correct low-energy excitation spectrum within Bogoliubov theory.

In the following, we will briefly discuss the behavior of the excitation spectrum for a varying influence of the dipolar interaction. As we will see, this can lead to a complex excitation spectrum, which indicates an instability of the system.

6.3.1 | Roton Instability

The competition of the contact repulsion and the attractive part of the dipole-dipole interaction provides a characteristic Bogoliubov excitation spectrum exhibiting a roton-like structure in the tube. In particular, for an increasing strength of the dipole-dipole interaction, the excitation spectrum exhibits a minimum at a finite momentum k_{min}. Eventually, this minimum can reach zero energy and gives rise to an instability of the superfluid. The two different interactions in combination with the transverse trapping potential offer a high level of control over the spectrum. The different parameters are most conveniently expressed by the dimensionless quantities which we have already introduced in Chapter 5,

$$\kappa = n a_s \propto \frac{l_\perp^2}{\xi_h^2}, \qquad \varepsilon_{\mathrm{dd}} = \frac{a_{\mathrm{dd}}}{a_{\mathrm{s}}}, \qquad \text{and} \qquad \lambda = \frac{a_{\mathrm{s}}}{l_\perp}. \tag{6.29}$$

Here, κ controls the dimensionality of the system and in our one-dimensional geometry within local-density approximation we require $\kappa \gg 1$ (see Sec. 5.4). In addition, the condition of a weakly interacting Bose gas requires $\lambda \ll 1$ (see Sec. 5.2.1 [176]). By tuning these three parameters, the position and energy of the roton excitation can be influenced. We are interested in the region where the superfluid becomes unstable at a finite momentum k_{r} and transitions to the supersolid phase. This critical point is determined by the two conditions

$$\epsilon(k_{\mathrm{r}})^2 = 0, \qquad \text{and} \qquad \frac{d\epsilon(q)^2}{dq}\Big|_{q=k_{\mathrm{r}}} = 0, \tag{6.30}$$

which we solve numerically. For our discussion, we consider a parameter regime comparable to recent dysprosium experiments [100, 106]. Throughout this chapter, we set the instability to appear at $\kappa_{\mathrm{c}} = 11.931$ and $\lambda_{\mathrm{c}} = 1/200$ if not stated otherwise, which provides the critical values $\varepsilon_{\mathrm{dd,c}} = 1.34$ and $k_{\mathrm{r}} l_\perp = 1.570$ that allow for a second-order phase transition (see Sec. 6.4.1). Note that the wave vector k_{r} of the roton instability for these parameters satisfies the condition of low momenta with $k_{\mathrm{r}} < 1/\xi_h$. It should also be noted that for $\varepsilon_{\mathrm{dd}} > 1$ the function $\mathcal{Q}_5(\varepsilon_{\mathrm{dd}})$ contains a very small imaginary part. This contribution is an unphysical artifact from local-density approximation since a three-dimensional homogeneous dipolar gas exhibits a phonon instability for $\varepsilon_{\mathrm{dd}} > 1$ [37], which we have discussed in detail in Sec. 3.2.3. Therefore, we drop the imaginary

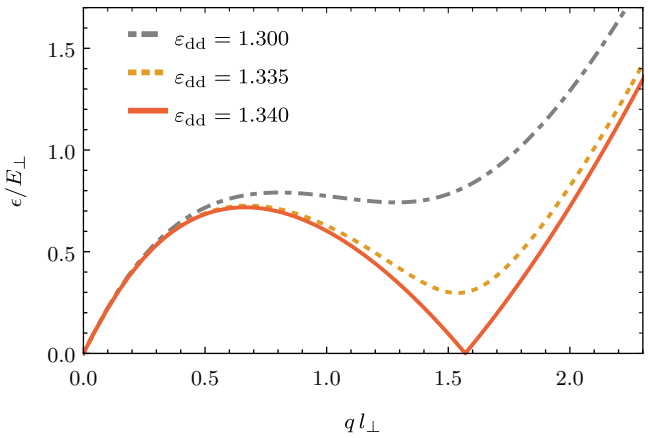

Figure 6.2: Excitation spectrum in the superfluid for different values of $\varepsilon_{\mathrm{dd}}$ for $\kappa_{\mathrm{c}} = 11.931$ and $\lambda_{\mathrm{c}} = 1/200$. By increasing $\varepsilon_{\mathrm{dd}}$ the spectrum develops a minimum, which eventually reaches zero energy at the critical point.

part in the following. In Fig. 6.2 we compare the excitation spectrum from Eq. (6.27) for different values of $\varepsilon_{\mathrm{dd}}$. We want to point out that changing $\varepsilon_{\mathrm{dd}}$ experimentally is achieved by tuning the scattering length a_s, which also affects κ and λ. For $q \to 0$ the spectrum is linear, while for large q we recover the spectrum of a free particle $\epsilon \sim q^2$. Compared to the three-dimensional case in Sec. 3.2.3, the q dependence of the potential (6.9) strongly affects the behavior of the excitation for intermediate momenta. By increasing $\varepsilon_{\mathrm{dd}}$ a minimum develops, which eventually reaches zero energy at the critical point $\varepsilon_{\mathrm{dd,c}}$. For $\varepsilon_{\mathrm{dd}} > \varepsilon_{\mathrm{dd,c}}$ the excitation spectrum becomes imaginary close to the roton momentum, indicating an instability and a breakdown of our current treatment.

6.3.2 | Comment on the Depletion

We briefly want to comment on the validity of Bogoliubov theory approaching the instability. As discussed in Sec. 3.2.1, Bogoliubov theory is applicable for the one-dimensional contact gas in the weakly interacting regime. Correlations only decay algebraically with an exponent $1/2K \ll 1$, which translates to a logarithmically diverging quantum depletion in the thermodynamic limit $\Delta n/n \sim \frac{1}{K}\ln(L/\xi)$ (see Sec. 3.2.1). Since $K \gg 1$, Bogoliubov theory remains valid as quantum fluctuations only suppress coherence on large scales. We propose a similar argument for the dipolar gas close to the critical point. A linear spectrum at the critical point adds an additional logarithmic divergence to the depletion. Overall the depletion then behaves as

$$\Delta n/n \sim \alpha_0 \ln[L/l_\perp] + \alpha_{\mathrm{r}} \ln[E_\perp/\epsilon(k_{\mathrm{min}})], \tag{6.31}$$

with

$$\alpha_0 = \frac{\lambda}{2\pi\kappa}\frac{m l_\perp c}{\hbar} \ll 1, \qquad \text{and} \qquad \alpha_{\mathrm{r}} = \frac{\lambda (k_{\mathrm{r}} l_\perp)^2}{4\pi\kappa}\frac{\hbar}{m l_\perp c_{\mathrm{r}}} \ll 1. \tag{6.32}$$

Here, c_r is the sound velocity of of the roton mode at the critical point. As α_r is small, we still expect Bogoliubov theory to give reliable results, even for small values of the roton gap $\epsilon(k_\mathrm{min})$. Note that this argument is by no means a rigorous proof of the applicability of Bogoliubov theory and should only be understood as a hint for its validity. A rigorous derivation would require one to calculate the correlation functions for a dipolar gas approaching the instability.

In the next section, we will adapt our approach for the supersolid regime and show that the instability in the excitation spectrum is absent.

6.4 | Supersolid Regime

In the following, we first study the ground state in the supersolid phase and afterwards its excitation spectrum.

6.4.1 | Ground State

The roton instability indicates the formation of a new ground state with a density modulation with wavelength close to the corresponding roton momentum. Within our Bogoliubov approach, this is accounted for by the macroscopic occupation of not only the $q = 0$ mode, but also the modes with $q = lk_\mathrm{s}$ with $l \in \mathbb{Z}$. The latter give rise to a density modulation with momentum k_s and break the continuous translational symmetry, resulting in a supersolid. The mean-field ansatz takes the form

$$a_0 \to \sqrt{Ln_0} \qquad \text{and} \qquad a_{\pm lk_\mathrm{s}} \to \frac{\Delta_l}{2}\sqrt{Ln_0}\, e^{\pm il\varphi}, \tag{6.33}$$

with the order parameters Δ_l accounting for the solid structure. The bosonic field operator within mean-field theory is replaced by the condensate wave function

$$\Psi(z) \to \phi(z) \equiv \sqrt{n_0}\left(1 + \sum_{l=1}^{\infty} \Delta_l \cos\left[l\, k_\mathrm{s} z + l\varphi\right]\right). \tag{6.34}$$

We also added a phase φ for the mean field, which illustrates the possibility to freely shift the entire density wave in position. Different to our previous treatment, the zero-momentum mode is not occupied by all particles and the total particle density is given by

$$n = \frac{1}{L}\int dz |\phi(z)|^2 = n_0\left(1 + \sum_{l=1}^{\infty} \frac{\Delta_l^2}{2}\right). \tag{6.35}$$

Note that for only one order parameter, the ansatz in Eq. (6.34) reduces to the cosine-modulated ansatz used in [115]. Inserting the mean-field wave function into the effective

Hamiltonian H, the energy depends on the order parameters Δ_l as well as the wave vector k_s, i.e., $E(\mathbf{\Delta} = (\Delta_1, \Delta_2, \ldots, k_\mathrm{s}))$, which is conveniently expressed by

$$\begin{aligned} E(\mathbf{\Delta}) =& N E_t(\sigma,\nu) - \int dz\, \phi^*(z) \frac{\hbar^2\nabla^2}{2m}\phi(z) \\ &+ \frac{1}{2}\int dz\, dz'\, V(z-z')|\phi(z')|^2|\phi(z)|^2 \\ &+ \frac{2}{5}\gamma_\mathrm{QF}\int dz\, |\phi(z)|^5, \end{aligned} \tag{6.36}$$

where $V(z)$ is the effective 1D interaction potential in real space. We have evaluated the energy analytically for up to four order parameters, which can be found in Appendix C.1. As we will see in the following, including more than four order parameters does not drastically improve our Ansatz. Note that the energy also still depends on the transverse variational parameters σ and ν but not on the phase φ. Varying φ results in displacing the entire modulated state within the tube and accounts for the spontaneously broken continuous translation symmetry, which will give rise to an additional Goldstone mode [105]. Without loss of generality, we set $\varphi = 0$ in the following.

The ground state is obtained by minimizing the energy $E(\mathbf{\Delta})$ with respect to $\mathbf{\Delta}$, σ, and ν, under the constraint of a fixed particle number n in Eq. (6.35), resulting in the parameters $\mathbf{\Delta}_\mathrm{gs}$. The superfluid state is then given by $\Delta_l = 0$, while the phase transition into the supersolid phase is characterized by a finite $\Delta_l \neq 0$. The chemical potential is determined by

$$\mu = \frac{1}{L}\frac{dE(\mathbf{\Delta}_\mathrm{gs})}{dn}. \tag{6.37}$$

Note that $\mathbf{\Delta}_\mathrm{gs}$ also depends on the density n, but in analogy to the treatment in the superfluid phase we neglect the weak density dependence of the transverse degrees of freedom σ and ν.

Since the phase diagram of this model has been studied in [115] and an accurate phase diagram of the microscopic parameters would require to include the transverse degrees of freedom not only variationally [127], we waive to include a phase diagram here. In the following we mainly focus on the parameters κ_c and λ_c that allow for a second-order phase transition. Afterwards, we briefly discuss the behavior of our approach for first-order transitions before we continue with the investigation of the stability in the thermodynamic limit.

Second-Order Phase Transition

As already mentioned in Sec. 6.3.1, for $\kappa_c = 11.931$ and $\lambda_c = 1/200$ the excitation spectrum of the superfluid becomes unstable at $\varepsilon_\mathrm{dd,c} = 1.34$ (red solid line in Fig. 6.2). In Fig. 6.3(a), we show the energy difference per particle,

$$\Delta E_l = \frac{E(\mathbf{\Delta}_\mathrm{gs}) - E(0)}{E_\perp N}, \tag{6.38}$$

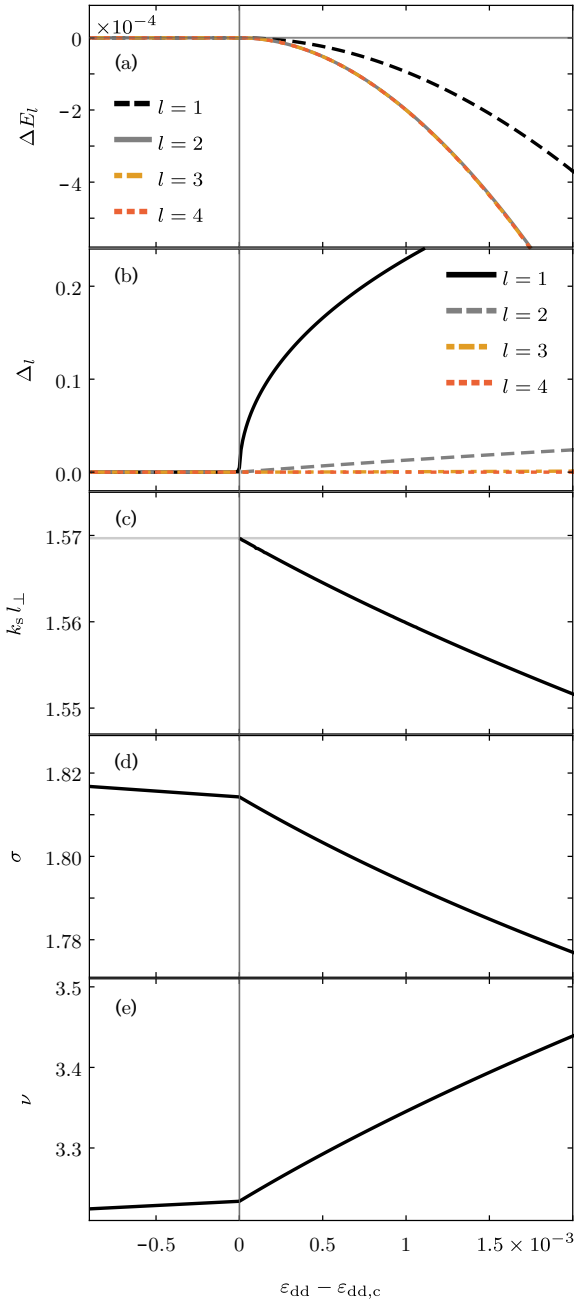

Figure 6.3: Ground state-parameters across the superfluid to supersolid phase transition as a function of $\varepsilon_{\mathrm{dd}}$ for $\kappa_c = 11.931$ and $\lambda_c = 1/200$. (a) Energy difference per particle $\Delta E_l = [E(\mathbf{\Delta}_{\mathrm{gs}}) - E(0)]/(E_\perp N)$ between the ground state of Eq.(6.36) and the superfluid when including $l = 1 \ldots 4$ order parameters. (b) The four order parameters used to obtain ΔE_4 as a function of $\varepsilon_{\mathrm{dd}}$. (c) Wave vector k_{s} for the density modulation in the supersolid state. The gray horizontal line shows the roton momentum k_{r}. (d) Transverse width σ and (e) transverse anisotropy ν of the ground-state wave function.

between the minimized energy in Eq. (6.36) when including l order parameters and the energy of the superfluid, $E(\boldsymbol{\Delta} = 0)$, as a function of $\varepsilon_{\mathrm{dd}}$. As expected, for $\varepsilon_{\mathrm{dd}} < \varepsilon_{\mathrm{dd,c}}$ the energy difference vanishes and the superfluid is the ground state of the system. Increasing $\varepsilon_{\mathrm{dd}}$ beyond $\varepsilon_{\mathrm{dd,c}}$, we find a continuous phase transition into the supersolid phase. While a single order parameter very poorly describes the ground-state energy across the phase transition (black dashed line), the impact of more than two order parameters on the results is negligible within the studied parameter range. It shows that our ansatz converges fast with the number of order parameters. In Fig. 6.3(b), we show the four lowest order parameters Δ_l, which clearly exhibit a continuous behavior consistent with a second-order phase transition. From Fig. 6.3(c) we can see that the density modulation at the critical point appears at the position of the roton instability k_{r} (gray horizontal line), but k_{s} is slightly lowered for increasing $\varepsilon_{\mathrm{dd}}$, i.e., the lattice spacing increases. This behavior can be understood as the side-by-side orientation of the dipoles pushes neighboring droplets further apart for an increasing dipolar strength. Fig. 6.3(d) and (e) show the transverse width and anisotropy of the ground-state wave function. Since $\kappa > 1$, the three-dimensional character of the system leads to the width of the cloud being larger than the harmonic oscillator length ($\sigma > 1$), while the anisotropic dipolar interactions leads to a significant anisotropy of the cloud.

In addition to the continuous transition, we briefly want to comment on first-order transitions within our approach.

First-Order Transition

For the parameters κ_{c} and λ_{c}, a single order parameter does not describe the ground state accurately but predicts the correct type of phase transition, which is not generally true. For first-order transitions, including only a single order parameter can falsely predict a continuous transition, while including more order parameters clearly indicates a discontinuous transition. To show this, we consider the critical values $\kappa_{\mathrm{c}}^{(1)} = 9.982$ and $\lambda_{\mathrm{c}}^{(1)} = 1/220$ in this section. The values are chosen such that the roton instability again appears at $\varepsilon_{\mathrm{dd,c}} = 1.34$, however, since $\kappa_{\mathrm{c}}^{(1)}$ and $\lambda_{\mathrm{c}}^{(1)}$ are smaller compared to the values chosen in the previous section, the term $\lambda\,\kappa^{3/2} \sim H_{\mathrm{LHY}}/N$ is too small and the transition is of first order. This becomes apparent in Fig. 6.4, where we show the system parameters across the phase transition.

For Figs. 6.4(a)-(e), we only include a single order parameter in our approach, which corresponds to a simple cosine-modulated ansatz. The energy difference per particle ΔE_1 in Fig. 6.4(a), the order parameter Δ_1 in Fig 6.4(b), the modulation k_{s} in Fig. 6.4(c), as well as the transverse width σ in Fig. 6.4(d) and the transverse anisotropy ν in Fig. 6.4(e) all indicate a second-order phase transition, analogously to the parameter regime in the previous section. Including more order parameters, the discussion changes drastically. By including more order parameters we find that the ground-state energy can be lowered even for $\varepsilon_{\mathrm{dd}} < \varepsilon_{\mathrm{dd,c}}$ [see Fig. 6.4(f)] indicating a first-order phase transition. For Figs. 6.4(g)-(j) we show the system parameters when including four order parameters. In Fig. 6.4(g), the lowest order parameters Δ_l show a jump to a finite value at $\varepsilon_{\mathrm{dd}} \approx 1.3395$.

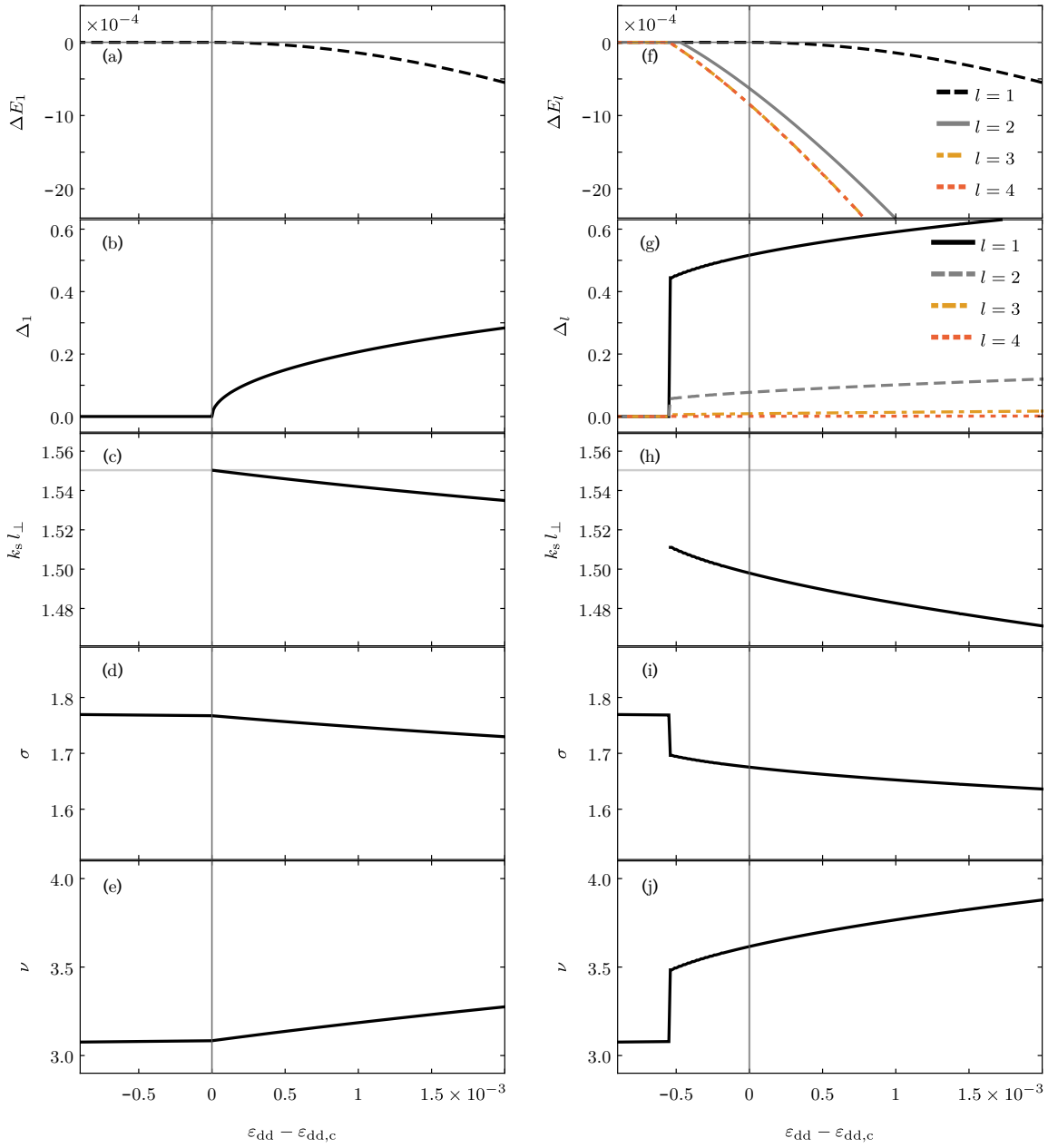

Figure 6.4: Ground-state parameters across the superfluid to supersolid phase transition as a function of $\varepsilon_{\mathrm{dd}}$ for $\kappa_{\mathrm{c}} = 9.982$ and $\lambda_{\mathrm{c}} = 1/220$. For (a)-(e) we only include a single order parameter. (a) Energy difference per particle ΔE_1. (b) Order parameter used to obtain ΔE_1 as a function of $\varepsilon_{\mathrm{dd}}$. (c) Wave vector k_{s} for the density modulation of the supersolid state. (d) Transverse width σ and (e) transverse anisotropy ν of the ground-state wave function. (f) Energy difference per particle ΔE_l when including $l = 1 \ldots 4$ order parameters. For (g)-(j) we include four order parameters to obtain the system parameters' analog to (b)-(e).

This discontinuous behavior also appears in the width in Fig. 6.4(i) and anisotropy in Fig. 6.4(j) of the ground-state wave function. The modulation of the ground state never coincides with the roton momentum (gray horizontal line) [see Fig. 6.4(h)]. The previous discussion shows that a simple cosine-modulated ansatz can falsely predict a continuous transition and can therefore be very misleading.

In the following, we will focus on the second-order phase transition and calculate the excitation spectrum in the supersolid regime.

6.4.2 | Excitations in the Supersolid

To study the excitation spectrum in the supersolid phase, we generalize the procedure introduced in Sec. 3.1.1 to systems with more than one macroscopically occupied mode. Since our results converge very fast with the number of order parameters, it is sufficient to include only two order parameters in the analysis. We again expand the field operator around the mean-field values

$$\Psi(z) = \phi(z) + \delta\psi(z) \tag{6.39}$$

and derive the Hamiltonian up to second order in $\delta\psi(z)$, which leads to a quadratic Hamiltonian in the creation and annihilation operators $a_q^{(\dagger)}$. Due to the broken translational symmetry in the supersolid state, the excitations are only characterized by their quasi-momentum within the first Brillouin zone and couple states with a momentum difference of $\pm l k_\mathrm{s}$. Therefore, the excitations exhibit a behavior similar to the well-known band structure in solids. As we are interested in the low-energy modes, however, we only analyze the lowest band. The Hamiltonian takes the form

$$H_\mathrm{B} = \frac{1}{2} \sum_{q \in 1.\mathrm{BZ}} : \begin{pmatrix} \boldsymbol{a}_+^\dagger \\ \boldsymbol{a}_- \end{pmatrix} \left[\begin{pmatrix} \boldsymbol{\chi} & 0 \\ 0 & \boldsymbol{\chi} \end{pmatrix} + \begin{pmatrix} \boldsymbol{\eta} & \boldsymbol{\eta} \\ \boldsymbol{\eta} & \boldsymbol{\eta} \end{pmatrix} \right] \begin{pmatrix} \boldsymbol{a}_+ \\ \boldsymbol{a}_-^\dagger \end{pmatrix} : \tag{6.40}$$

where

$$\boldsymbol{a}_\pm = \begin{pmatrix} a_{\pm q} \\ a_{\pm(q+k_\mathrm{s})} \\ a_{\pm(q-k_\mathrm{s})} \\ a_{\pm(q+2k_\mathrm{s})} \\ a_{\pm(q-2k_\mathrm{s})} \\ \vdots \end{pmatrix}, \tag{6.41}$$

and the matrices $\boldsymbol{\chi}$ and $\boldsymbol{\eta}$ depend on $\boldsymbol{\Delta}_\mathrm{gs}$ and the chemical potential μ. We obtain the excitation spectrum by diagonalizing the Hamiltonian in Eq.(6.40) via a Bogoliubov transformation

$$a_i = \sum_\alpha u_i^\alpha b_\alpha + v_i^\alpha b_{-\alpha}^\dagger\,, \quad \text{where} \quad i, \alpha \in \{q + l k_\mathrm{s}, l \in \mathbb{Z}\}. \tag{6.42}$$

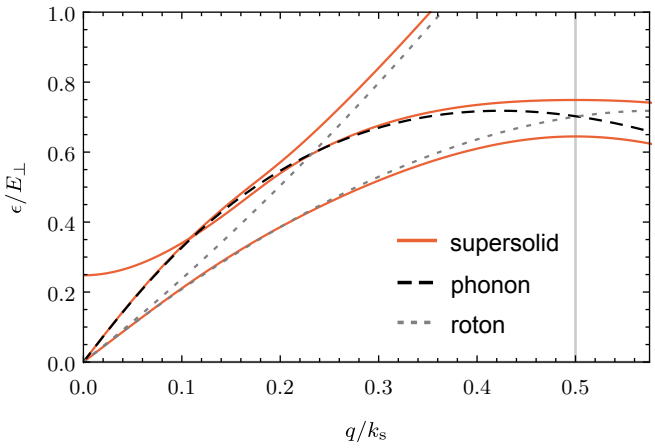

Figure 6.5: Excitation spectrum in the supersolid phase for $\varepsilon_{dd} = 1.3405$, $\lambda_c = 1/200$, and $\kappa_c = 11.931$. The red solid line shows the solution ϵ_s of Eq.(6.43) as a function of $q\,l_\perp$. The gray vertical line indicates the first Brillouin zone. The black and gray dashed lines show the phonon and roton branches at the phase transition, respectively, and are used as a guide to the eye.

Finding the eigenmodes ϵ_s in the supersolid then reduces to finding the eigenvalues of $\boldsymbol{\chi}^2 + 2\boldsymbol{\chi}\boldsymbol{\eta}$,

$$\det\left(\boldsymbol{\chi}^2 + 2\boldsymbol{\chi}\boldsymbol{\eta} - \epsilon_s(q)^2\mathbf{1}\right) = 0, \tag{6.43}$$

which generalizes Eq. (6.26) to systems where more than one mode is macroscopically occupied.

As shown in Sec. 6.4.1, the ground state close to the continuous phase transition is very accurately described by including only the two order parameters Δ_1 and Δ_2. The restriction to two order parameters implies that in our treatment, the modes with momenta $q = 0, \pm k_s, \pm 2k_s$ are macroscopically occupied, while all the remaining modes are *not*. For a consistent expansion in the macroscopically occupied modes (and thus Δ_1 and Δ_2), the matrices $\boldsymbol{\chi}$ and $\boldsymbol{\eta}$ must be restricted to only include the coupling between these modes. Hence, $\boldsymbol{\chi}$ and $\boldsymbol{\eta}$ reduce to 5×5 matrices and the vectors $\boldsymbol{a}_\pm$ are restricted to the 5 lowest momentum modes $q, q \pm k_s, q \pm 2k_s$, with q in the first Brillouin zone. We determine the expression for the matrices $\boldsymbol{\chi}$ and $\boldsymbol{\eta}$ analytically (see Appendix C.2) and calculate the eigenvalues numerically.

In Fig. 6.5, we show the excitation spectrum for $\varepsilon_{dd} = 1.3405$, close to the instability at $\varepsilon_{dd,c} = 1.34$. The three red solid lines show the lowest eigenvalues $\epsilon_s(ql_\perp)/E_\perp$. The remaining two eigenvalues contribute to higher bands and are not shown. We have also added the roton modes (gray dotted lines) and the phonon mode (black dotted line) which were evaluated at the critical point. The gray vertical line indicates the first Brillouin zone. The excitation spectrum contains two gapless modes at $q = 0$, stemming from the broken $U(1)$ and translational symmetry in the supersolid, while the third mode shows a finite gap. The latter corresponds to the amplitude mode of the solid structure.

None of the modes show an instability, which indicates the stability of the supersolid phase in the thermodynamic limit. It is important to point out that restricting the analysis to a single order parameter Δ_1 for the parameters above significantly alters the excitation spectrum. In particular, the amplitude mode is strongly affected. Therefore, it is crucial to accurately describe the ground state in the supersolid phase and derive the excitation spectrum with high accuracy.

6.5 | Conclusion

We present a study of the excitation spectrum of a weakly interacting gas of dipolar bosons in a tight transverse harmonic confinement across the superfluid-to-supersolid phase transition. In a one-dimensional geometry, where the dipoles are aligned perpendicular to the tube, we introduce an effective Hamiltonian which includes beyond-mean-field effects in a local-density approximation and make a variational ansatz for the transverse degrees of freedom. The transverse confinement in combination with the dipolar interaction leads to a roton spectrum in the superfluid. When the roton mode goes soft, more than a single mode becomes macroscopically occupied and we adapt Bogoliubov theory by introducing an order parameter for each additional macroscopically occupied mode. This allows us to determine the ground-state energy and the excitation spectrum across the phase transition. For parameters comparable to current dysprosium experiments, we find that using one order parameter, which corresponds to a simple cosine-modulated ansatz for the ground-state wave function in the supersolid, is not enough to describe the system, neither in the continuous nor in the discontinuous transition regime. However, we show that our ansatz converges fast with the number of order parameters. The excitation spectrum in the supersolid regime close to a continuous transition shows no instabilities, indicating the stability in the thermodynamic limit. In the low-energy regime, we find two gapless modes in agreement with the two broken continuous symmetries as well as a gapped amplitude mode for the solid structure.

7 | Quantum Fluctuations in One-Dimensional Supersolids

Our discussion of the one-dimensional supersolid in Chapter 6 within Bogoliubov theory inherently assumes the presence of diagonal and off-diagonal long-range order. In one-dimension, however, quantum fluctuations prevent the appearance of long-range order in a supersolid even at zero temperature [78–80]. Nevertheless Bogoliubov theory can provide reliable results, as long as quasi-long-range order survives in the system [155, 156]. In this chapter, we derive the quantum critical behavior and study its influence on the superfluid response and properties of the solid. Our analysis is based on an effective low-energy description [188–190] which takes into account the two coupled Goldstone modes of the supersolid. We find that the quantum phase transition from the superfluid to the supersolid is shifted by quantum fluctuations from the position where the local formation of a solid structure takes place. For current experimental parameters with dipolar atomic gases, this shift is extremely small and cannot be resolved yet. Hence, current observations in experiments are expected to be in good agreement with predictions from mean-field theory based on the extended Gross-Pitaevskii formalism.

This chapter is based on the publication [85]. Most of the work for the publication has been conducted by Chris Bühler. The contribution of this thesis mainly concerns the connection between the parameters of our effective low-energy description and the microscopic parameters for an experimentally realistic setup based on dysprosium atoms close to the superfluid-to-supersolid phase transition. With that in mind, we will focus this chapter on the aspects that are relevant to establish this connection and are important to understand the critical behavior close to the phase transition. However, we will also briefly summarize the main results of Ref. [85] to tell a coherent story. For a detailed discussion we refer the reader to Ref. [85] and the Master thesis of Chris Bühler [191].

7.1 | Introduction

In Chapter 6, we have investigated the superfluid-to-supersolid phase transition in the thermodynamic limit in a one-dimensional geometry, motivated by the recent observation of supersolid phases in elongated traps [99–101]. So far, the theoretical description of these experiments is based on mean-field theory within the extended Gross-Pitaevskii formalism and also our approach in Chapter 6 is no exception. It includes the leading beyond-mean-field correction within local-density approximation [39, 40]. These corrections account for the modification of short-range correlations by quantum fluctuations.

The behavior of the beyond-mean-field effects has been studied for superfluids in tight traps [176–178] and has been the focus of the discussion of Chapter 5. Analyses based on the extended Gross-Pitaevskii formalism are in good agreement with the experimental observations in elongated trap geometries, and also predict the stability of the supersolid phase in the thermodynamic limit for a one-dimensional geometry [74, 127, 128, 186] as discussed in Chapter 6.

The properties of the supersolid are usually understood in terms of spontaneous symmetry breaking: The spontaneous breaking of the translational symmetry gives rise to the solid structure (diagonal long-range order) while the superfluid results from the broken $U(1)$ symmetry and is connected to off-diagonal long-range order [75, 90]. Also note that the approach in Chapter 6 inherently assumes the presence of diagonal and off-diagonal long-range order. In one dimension, however, a remarkable property of quantum fluctuations is that they strongly influence both, the spontaneous symmetry breaking and the appearance of order at large distances [9, 78, 79], in addition to the modification of short-range correlations. In particular, it is well established that one-dimensional superfluids only exhibit quasi-long-range order with a characteristic algebraic decay [81–84]. Despite the absence of true off-diagonal long-range order, one-dimensional superfluids can still support a superfluid flow across a weak impurity [192, 193]. Similarly, quantum fluctuations will prevent the appearance of diagonal and off-diagonal long-range order and modify the characteristic properties of the one-dimensional supersolid state.

In this chapter, we study the influence of quantum fluctuations at large distances and the appearance of quasi-long-range order for such one-dimensional supersolid phases in the thermodynamic limit. This allows us to investigate whether the use of the extended Gross-Pitaevskii equation is justified for current experimental parameters. The analysis is based on the effective low-energy theory for a supersolid with many particles within a lattice site [188–190], and allows for the derivation of the algebraic behavior of the characteristic correlation functions. The superfluid is defined by the ability of the system to sustain a dissipationless particle flow across a weak impurity, i.e., absence of a linear relation between flow and pressure [192, 193]. In analogy the solid character is defined by the ability of the system to drag the solid structure with a moving impurity.

We start by introducing the effective low-energy description. Within this approach, we will then derive the characteristic correlation functions of the supersolid and afterwards analyze the superfluid-to-supersolid phase transition through the action of an impurity. We will then estimate the quantum critical regime by connecting the low-energy description to the microscopic parameters in an experiment, for which we will use the effective Hamiltonian of Chapter 6.

7.2 | Low-Energy Description of One-Dimensional Supersolids

We start with the effective low-energy description of a one-dimensional supersolid consisting of weakly interacting bosons of mass m with a large number of atoms per lattice site. Then, the bosonic field operator can be written as

$$\psi(\boldsymbol{x}) = \sqrt{\rho(\boldsymbol{x})}\, e^{i\varphi(\boldsymbol{x})} \tag{7.1}$$

with the phase field φ and the density field

$$\rho(\boldsymbol{x}) = [n + \delta n(\boldsymbol{x})]\, f\left(x - \frac{d}{2\pi} u(\boldsymbol{x})\right), \tag{7.2}$$

while we introduced the notation $\boldsymbol{x} = (x, t)$ for the space-time coordinate. Here, $f(x) = f(x + d)$ is a periodic function with period d and normalized

$$\frac{1}{d}\int_0^d dx\, f(x) = 1. \tag{7.3}$$

It accounts for the local formation of a solid-like structure by droplets, while the displacement field $u(\boldsymbol{x})$ allows for fluctuations in the position of these droplets. The averaged one-dimensional density is denoted by n in this chapter such that each droplet contains $nd \gg 1$ particles, while $\delta n(\boldsymbol{x})$ describes local density fluctuations. Note that within our low-energy description, the fields φ, δn, and u vary only slowly compared to the periodic function $f(x)$.

7.2.1 | Effective Lagrangian

To obtain the low-energy behavior of the supersolid, the goal is to separate the long-wavelength behavior of the system from the underlying rapidly oscillating lattice. This results in an effective Lagrangian for the slowly varying fields φ, δn, and u [188–190],

$$\begin{aligned}\mathcal{L} = &-\hbar\delta n\partial_t\varphi - \frac{\varkappa}{2}(\delta n)^2 - \frac{\lambda_{\mathrm{L}}'}{2}(\partial_x u)^2 - \xi'\delta n\partial_x u \\ &+ \frac{\hbar^2 n}{2m}\left[\frac{n_{\mathrm{L}}}{n}\left(\frac{md}{2\pi\hbar}\partial_t u - \partial_x\varphi\right)^2 - (\partial_x\varphi)^2\right].\end{aligned} \tag{7.4}$$

The second line corresponds to the kinetic energy, where the term $\partial_t u$ accounts for the velocity of the droplet at position x, while the superfluid exhibits a reduced superfluid density $n_{\mathrm{s}} \equiv n - n_{\mathrm{L}}$ due to the formation of a local solid-like structure [90]. Furthermore, the first line includes the conventional coupling between the phase field and the density in a superfluid as well as an expansion of the interaction energy to second order in the

slowly varying fields with parameters $\varkappa$, λ_{L}' and ξ'. The stability of the system naturally requires $\varkappa\lambda_{\mathrm{L}}' - (\xi')^2 > 0$. In the weakly interacting regime, we also require

$$\frac{\hbar^2 n}{m\varkappa} \gg 1, \tag{7.5}$$

such that the kinetic energy of the superfluid is much larger than the interaction energy. Note that in the superfluid, this is the same condition as in Eq. (3.61) since $\varkappa \to g_{1\mathrm{D}}$. In the vicinity of the superfluid-to-supersolid phase transition, we will derive the parameters $\varkappa$, λ_{L}', and ξ within mean-field theory in Sec. 7.4.1.

The Lagrangian in Eq. (7.4) describes a strong coupling between the Bogoliubov mode of the superfluid and the phonon mode of a solid, and it gives rise to two linear sound modes accounting for the two broken symmetries. Furthermore, the Euler-Lagrange equations provide the current conservation

$$\partial_t \delta n = -\partial_x (j_{\mathrm{s}} + j_{\mathrm{n}}), \tag{7.6}$$

with the normal and superfluid current

$$j_{\mathrm{n}} = (n_{\mathrm{L}} d/2\pi)\partial_t u \qquad \text{and} \qquad j_{\mathrm{s}} = (\hbar n_{\mathrm{s}}/m)\partial_x \varphi. \tag{7.7}$$

For $n_{\mathrm{L}}/n \to 0$ the solid structure disappears. Consequently, $\xi' \to 0$ and $\lambda_{\mathrm{L}}' \to 0$, and we recover the effective low-energy description of a superfluid. For $n_{\mathrm{L}}/n \to 1$, we obtain the theory of phonons in a solid with the compressibility $(n^2\varkappa + 4\pi^2\lambda_{\mathrm{L}}'/d^2 - 4\pi n\xi'/d)/m$.

7.2.2 | Hamilton Description

So far, the effective Lagrangian (7.4) contains the coupled slowly varying fields φ, δn, and u. To make use of a canonical transformation which decouples the fields, it is convenient to switch to a Hamiltonian description of the low-energy quantum theory. With the conjugate variables

$$\Pi = \frac{\partial \mathcal{L}}{\partial \dot{\varphi}} = -\hbar \delta n \equiv -\frac{\hbar}{\pi}\partial_x \vartheta\,, \tag{7.8a}$$

$$P = \frac{\partial \mathcal{L}}{\partial \dot{u}} = -\frac{\hbar d n_L}{2\pi}\left(\partial_x \varphi - \frac{md}{2\pi\hbar}\partial_t u\right) \equiv -\frac{\hbar}{\pi}\partial_x w \tag{7.8b}$$

the Hamilton density becomes $\mathcal{H} = \Pi\dot{\varphi} + P\dot{u} - \mathcal{L}$ and we can write the Hamiltonian as

$$H = \frac{\hbar}{2\pi}\int dx \left[v_J \begin{pmatrix}\partial_x\varphi \\ \partial_x w\end{pmatrix} \mathbf{M}_J \begin{pmatrix}\partial_x\varphi \\ \partial_x w\end{pmatrix} + v_N \begin{pmatrix}\partial_x\vartheta \\ \partial_x u\end{pmatrix} \mathbf{M}_N \begin{pmatrix}\partial_x\vartheta \\ \partial_x u\end{pmatrix}\right]. \tag{7.9}$$

Here, we have introduced the two velocities $v_J = \hbar\pi n/m$ and $v_N = \varkappa/\pi\hbar$, with $v_N/v_J \ll 1$ in the weakly interacting regime. The matrices $\mathbf{M}_J$ and $\mathbf{M}_N$ take the form

$$\mathbf{M}_J = \begin{pmatrix} 1 & -\beta \\ -\beta & \beta^2/\gamma \end{pmatrix}, \quad \mathbf{M}_N = \begin{pmatrix} 1 & \xi \\ \xi & \lambda_{\mathrm{L}} \end{pmatrix}, \tag{7.10}$$

with $\beta = 2/nd$, $\gamma = n_\mathrm{L}/n$ and the dimensionless parameters $\lambda_\mathrm{L} = \lambda_\mathrm{L}'\pi^2/\varkappa$ and $\xi = \xi'\pi/\varkappa$. Since $\gamma \leq 1$, $\mathbf{M}_J$ is positive semi-definite. The stability in the thermodynamic limit requires $\mathbf{M}_N$ to be positive semi-definite as well, i.e. $\lambda_\mathrm{L} - \xi^2 \geq 0$. Being conjugate variables, the canonical commutation relations read

$$[\partial_x \vartheta(\boldsymbol{x}), \varphi(\boldsymbol{y})] = i\pi\delta(\boldsymbol{x}-\boldsymbol{y}) = [\partial_x u(\boldsymbol{x}), w(\boldsymbol{y})]\,. \tag{7.11}$$

Canonical Transformation

Using a canonical transformation, we can diagonalize this Hamiltonian into two uncoupled sound modes. The invariance of the commutator in Eq. (7.11) requires the transformation to be of the form

$$\begin{pmatrix}\phi_+\\ \phi_-\end{pmatrix} = \mathbf{Q}\begin{pmatrix}\varphi\\ w\end{pmatrix}, \quad \begin{pmatrix}\theta_+\\ \theta_-\end{pmatrix} = \left(\mathbf{Q}^{-1}\right)^T\begin{pmatrix}\vartheta\\ u\end{pmatrix}. \tag{7.12}$$

Hence, for a diagonal Hamiltonian with uncoupled sound velocities $v_\pm$ the transformation $\mathbf{Q}$ has to fulfill

$$\left(\mathbf{Q}^{-1}\right)^T[v_J\mathbf{M}_J]\,\mathbf{Q}^{-1} = \begin{pmatrix}v_+ & 0\\ 0 & v_-\end{pmatrix} \quad \text{and} \quad \mathbf{Q}\,[v_N\mathbf{M}_N]\,\mathbf{Q}^T = \begin{pmatrix}v_+ & 0\\ 0 & v_-\end{pmatrix}. \tag{7.13}$$

To construct $\mathbf{Q}$, we realize that

$$\mathbf{Q}\,[v_N v_J \mathbf{M}_N\mathbf{M}_J]\,\mathbf{Q}^{-1} = \begin{pmatrix}v_+^2 & 0\\ 0 & v_-^2\end{pmatrix}, \tag{7.14}$$

which means that we can simply find the eigenvectors of $\mathbf{M}_N\mathbf{M}_J$ and fix their length such that Eq. (7.13) is fulfilled. A closed expression for the matrix $\mathbf{Q}$ is given in Appendix D.1. For a detailed derivation, we refer the reader to [191].

With this transformation, we obtain the Hamiltonian

$$H = \frac{\hbar}{2\pi}\int dx \sum_{\sigma\in\{+,-\}} v_\sigma\left[(\partial_x\phi_\sigma)^2 + (\partial_x\theta_\sigma)^2\right] \tag{7.15}$$

with the two sound velocities

$$v_\pm^2 = \frac{v_J v_N}{2}\left[\alpha \pm \sqrt{\alpha^2 - 4\beta^2(\lambda_\mathrm{L}-\xi^2)(1-\gamma)/\gamma}\right] \tag{7.16}$$

and

$$\alpha = 1 - 2\xi\beta + \beta^2\lambda_\mathrm{L}/\gamma. \tag{7.17}$$

With this Hamiltonian, we will consider the characteristic correlation functions next and afterwards introduce perturbations to the simple quadratic theory, which allows us to study the quantum phase transitions in the system.

7.3 | Correlations

For the quadratic diagonal Hamiltonian from Eq. (7.15) obtaining correlation functions for the fields ϕ and θ is straightforward. For an elaborate discussion, we refer the reader to standard textbooks (e.g.[83, 194–196]). In imaginary time ($t \to -i\tau$) we obtain

$$\langle [\theta_\sigma(x,\tau) - \theta_{\sigma'}(0)]^2 \rangle = \langle [\phi_\sigma(x,\tau) - \phi_{\sigma'}(0)]^2 \rangle = \frac{1}{2}\delta_{\sigma,\sigma'} \ln\left(\frac{x^2 + (v_\sigma \tau + \zeta)^2}{\zeta^2}\right), \quad (7.18)$$

with a short-distance cut-off ζ. The first equality can be understood as the Hamiltonian (7.15) is invariant under $\theta \to \phi$, $\phi \to \theta$. The connection to the physical fields is then provided by $\mathbf{Q}$ [see Eq. (7.12)]. For the (equal-time) long-distance behavior of the one-particle density matrix we obtain

$$\langle \psi(x)\psi^\dagger(0) \rangle = n \left(\frac{\zeta}{|x|}\right)^{A/2}, \quad (7.19)$$

resulting in quasi-off-diagonal long-range order for the superfluid, where the algebraic decay is determined by

$$A = [(\mathbf{Q}^{-1})_{11}]^2 + [(\mathbf{Q}^{-1})_{12}]^2 = \frac{v_N}{v_+ + v_-}\left[1 + \sqrt{\frac{\beta^2(\lambda_\mathrm{L} - \xi)}{\gamma(1-\gamma)}}\right]. \quad (7.20)$$

The density-density correlations provide the quasi-long-range diagonal order for the solid,

$$\langle \rho(x)\rho(0) \rangle - n^2 = -\frac{C}{2\pi^2|x|^2} + \eta \left(\frac{\zeta}{|x|}\right)^{B/2} \cos\frac{2\pi x}{d}, \quad (7.21)$$

where we have introduced

$$B = (\mathbf{Q}_{12})^2 + (\mathbf{Q}_{22})^2 = \frac{v_J}{v_+ + v_-}\beta^2 \left[\frac{1}{\gamma} + \sqrt{\frac{1-\gamma}{\gamma\beta^2\,(\lambda_\mathrm{L} - \xi^2)}}\right], \quad (7.22a)$$

$$C = (\mathbf{Q}_{11})^2 + (\mathbf{Q}_{21})^2 = \frac{v_J}{v_+ + v_-}\left[1 + \lambda_\mathrm{L}\,\beta^2 \sqrt{\frac{1-\gamma}{\gamma\beta^2(\lambda_\mathrm{L} - \xi^2)}}\right], \quad (7.22b)$$

and η is a non-universal parameter.

While the correlation functions in Eq. (7.19) and Eq. (7.21) clearly exhibit off-diagonal as well as diagonal quasi-long-range order, respectively, an algebraic behavior of the correlation functions alone does not necessarily indicate the presence of a superfluid and solid behavior of the system. We still need to investigate the systems response to a perturbation to characterize the phase transition.

7.4 | Superfluid-to-Supersolid Phase Transition

In the following, we study the quantum phase transitions in the system. The characteristic property of a superfluid is that it can sustain a superfluid flow, while in a solid a moving localized impurity can drag the solid structure along. A supersolid exhibits both of these properties, as it can sustain a superfluid flow while a moving impurity drags the solid structure along. These conditions provide critical values for the algebraic correlations above and will be studied in the following.

We start with the parameters in the superfluid close to the formation of a solid-like structure, where $\gamma \ll 1$ such that $A \sim \sqrt{v_N/v_J} \ll 1$. This condition is sufficient to sustain a superfluid flow (see Sec. 7.5). Therefore, we first study the transition into the supersolid for increasing γ, resulting in a stronger local solid-like structure.

A local impurity at position x_0 is described by an external potential $V_I \approx g\delta(x - x_0)$ and provides a contribution to the low-energy Hamiltonian

$$H_{\mathrm{I}} = \int dx \rho(x) V_I(x) \sim g_u \cos(u(x_0) + 2\pi x_0/d), \tag{7.23}$$

where we expanded the local solid structure $f(x)$ in Eq. (7.2) into a Fourier series. Note that the impurity can provide additional terms when taking the discrete nature of particles into account [82], but these do not become relevant before superfluidity is lost (see Sec. 7.5). The low-energy description then reduces to a coupled boundary sine-Gordon model [197–202]. A renormalization group analysis provides the flow equation for g_u,

$$\partial_l g_u = (1 - B/4)\, g_u, \tag{7.24}$$

where l is the scaling parameter. Hence, the term in Eq. (7.23) is irrelevant for $B > 4$, which means that the system does not feel the presence of the impurity in the low-energy regime. In turn, the term becomes relevant for $B < 4$ and pins $u(x_0)$ to the minimum of the cosine. Varying the position x_0 of the impurity then results in a change in u, which shifts the entire local solid structure of the system with the impurity. Thus, the system exhibits a solid character for $B < 4$. In Fig. 7.1 the critical line $B = 4$ of the quantum phase transition separating the superfluid from the supersolid is shown for different values of ξ. The parameters $v_J/v_N = 1.0 \times 10^7$ and $\beta = 2.1 \times 10^{-4}$ are fixed to realistic values derived within mean-field theory using an extended Gross-Pitaevskii approach for an experimentally realistic setup (see Sec 7.4.1). The black dashed line shows the asymptotic behavior of B close to the phase transition, which is given by

$$B \;\sim\; \beta^2 \sqrt{\frac{v_J}{v_N}} \frac{1}{\sqrt{\gamma \beta^2 \lambda_{\mathrm{L}}}} \quad \text{for} \quad \gamma \to 0\,. \tag{7.25}$$

The transition always takes place at a finite and non-vanishing value of γ and is therefore shifted from the local formation of a solid structure at $\gamma = 0$.

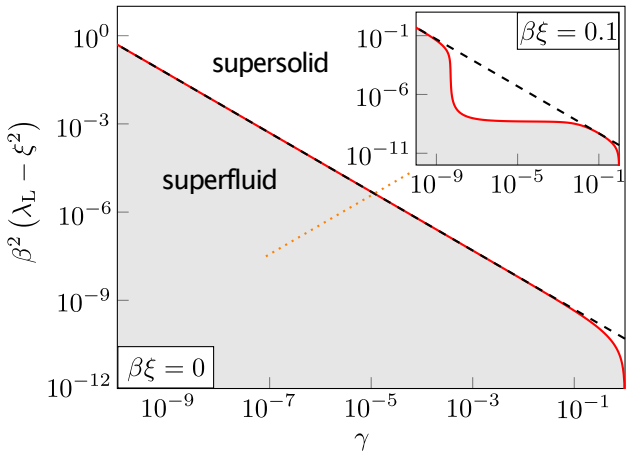

Figure 7.1: Critical line $B = 4$ (red solid line) as a function of γ and $\beta^2(\lambda - \xi^2)$ at $\beta\xi = 0$ for fixed $v_J/v_N \approx 1.0 \times 10^7$ and $\beta \approx 2.1 \times 10^{-4}$. The black dashed line shows the asymptotic behavior of B for $\gamma \to 0$. In the gray shaded region $B > 4$ and the system does not feel the impurity (superfluid), while in the white region $B < 4$ the perturbation becomes relevant (supersolid). The orange dotted line shows the path across the phase transition for experimentally realistic parameters. In the inset, we fix $\beta\xi = 0.1$ while v_J/v_N and β remain unchanged. This figure was created by Chris Bühler.

7.4.1 | Connection to Microscopic Parameters

In the following, we analyze the quantum critical region for an experimentally realistic setup based on dysprosium atoms. For this, we consider the reduced three-dimensional model of dipolar bosons of mass m in a transverse harmonic trap of oscillator length $l_\perp$ introduced in Chapter 6 [128, 186].

Let us briefly recapitulate the procedure of Chapter 6. In a mean-field approach, we include quantum fluctuations in local-density approximation and use a variational ansatz $\psi(y,z) = \frac{1}{\sqrt{\pi}\sigma} e^{-(\nu y^2 + z^2/\nu)/\sigma^2}$ for the wave function in the transverse direction. The variational parameters σ and ν are determined by minimizing the ground-state energy. In the supersolid regime, we use the mean-field ansatz

$$\phi(x) = \frac{\sqrt{n}}{\sqrt{1 + \sum_{l=1}^{\infty} \Delta_l^2/2}} \left(1 + \sum_{l=1}^{\infty} \Delta_l \cos\left[l\, k_s x\right]\right) \qquad \text{(6.34 revisited)}$$

for the longitudinal direction, with the order parameters Δ_l, the wave vector k_s of the modulation and the one-dimensional density n. With the mean-field ansatz, we can

write the energy as

$$\begin{aligned} E(\boldsymbol{\Delta}) =& NE_t(\sigma,\nu) - \int dx\, \phi^*(x)\frac{\hbar^2\nabla^2}{2m}\phi(x) \\ &+ \frac{1}{2}\int dx\, dx'\, V(x-x')|\phi(x')|^2|\phi(x)|^2 \\ &+ \frac{2}{5}\gamma_{\mathrm{QF}}\int dx\, |\phi(x)|^5, \end{aligned} \qquad \text{(6.36 revisited)}$$

where the first line contains the kinetic energy and the energy contribution of the transverse trap. The second line takes into account the interaction between the particles while the third line includes quantum fluctuations within local-density approximation. The ground state is obtained by minimizing Eq. (6.36) with respect to Δ_l and k_s as well as σ and ν.

From the ground state we can extract all relevant quantities of our model. Within mean-field theory, Leggetts upper bound for the superfluid fraction [90] is completely saturated [203],

$$\frac{n_{\mathrm{s}}}{n} = \left[\left(\frac{k_{\mathrm{s}}}{2\pi}\int_0^{2\pi/k_{\mathrm{s}}} dx\, |\phi(x)|^2\right)\left(\frac{k_{\mathrm{s}}}{2\pi}\int_0^{2\pi/k_{\mathrm{s}}} dx\, \frac{1}{|\phi(x)|^2}\right)\right]^{-1}, \tag{7.26}$$

such that we obtain

$$\gamma = \frac{n_{\mathrm{L}}}{n} = 1 - \frac{n_{\mathrm{s}}}{n}. \tag{7.27}$$

The parameters $\varkappa$, ξ' and λ' of our model characterize the effective potential of the supersolid,

$$\mathcal{V} = \frac{\varkappa}{2}(\delta n)^2 + \frac{\lambda'_{\mathrm{L}}}{2}(\partial_x u)^2 + \xi'\delta n\partial_x u\,, \tag{7.28}$$

and account for energy contributions to variations in the density ($\varkappa$), the lattice spacing (λ'_L) and combinations of both (ξ'). We can investigate those energy contributions with the ground state of Eq. (6.36) and thus obtain $\varkappa$, λ'_{L} and ξ'. To do so, we calculate the ground-state energy in our dimensionless units for a given $\kappa = na_{\mathrm{s}}$, $\varepsilon_{\mathrm{dd}} = a_{\mathrm{dd}}/a_s$ and $\lambda = a_s/l_\perp$, where a_{s} is the scattering length and a_{dd} is the dipolar length. This then provides us with the ground-state parameters $\boldsymbol{\Delta}_{\mathrm{gs}}$ and k_{s} as well as the chemical potential μ. For a fixed chemical potential and $\boldsymbol{\Delta}_{\mathrm{gs}}$, we can then expand $E(\boldsymbol{\Delta}_{\mathrm{gs}}) - \mu N$ up to second order in the variations of k_{s} and κ,

$$\frac{[E(\boldsymbol{\Delta}_{\mathrm{gs}}) - \mu N]a_{\mathrm{s}}}{L} = \frac{\hbar^2}{ml_\perp^2}\left[C_0 + C_\varkappa(\delta\kappa)^2 + C_{\lambda'_{\mathrm{L}}}(l_\perp\delta k_s)^2 + C_{\xi'}(\delta\kappa)(l_\perp\delta k_s)\right], \tag{7.29}$$

where L is the quantization volume and we obtain the expansion coefficient $C_\varkappa$, $C_{\lambda'_{\mathrm{L}}}$ and $C_{\xi'}$ numerically. Variations in κ we can directly connect to δn since $\delta\kappa = a_{\mathrm{s}}\delta n$, while a

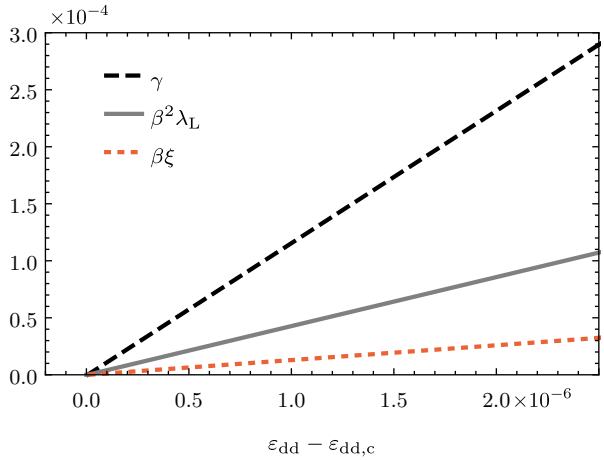

Figure 7.2: System parameters γ, $\beta\xi$ and $\beta^2\lambda_{\mathrm{L}}$ as a function of $\varepsilon_{\mathrm{dd}}$ for $\kappa_c = 11.931$ and $\lambda_c = 1/200$. For $\gamma \to 0$, we find that ξ and λ_{L} vanish.

variation in the wave vector k_s is connected to $\partial_x u$. To establish the latter connection, we note that a (slowly varying) linear displacement field $\partial_x u = \delta a = \text{const.}$ changes the periodicity of the system, which translates to $k_s \to k_s - (\delta a) = k + \delta k_s$.

Comparing the effective potential from Eq. (7.28) to the expansion in Eq. (7.29), we obtain the parameters

$$\varkappa = \frac{2\hbar^2 a_{\mathrm{s}}}{m l_\perp^2} C_\varkappa, \qquad \lambda_{\mathrm{L}}' = \frac{2\hbar^2}{m a_{\mathrm{s}}} C_{\lambda_L'}, \qquad \xi' = -\frac{\hbar^2}{m l_\perp} C_{\xi'}, \tag{7.30}$$

resulting in the dimensionless parameters

$$\lambda_{\mathrm{L}} = \frac{\lambda_{\mathrm{L}}' \pi^2}{\varkappa} = \frac{\pi^2 C_{\lambda_{\mathrm{L}}'}}{\lambda^2 C_\varkappa}, \qquad \xi = \frac{\xi' \pi}{\varkappa} = -\frac{\pi C_{\xi'}}{2\lambda C_\varkappa},$$

$$\beta = \frac{2}{nd} = \frac{(k_s l_\perp)\lambda}{\pi\kappa}, \qquad \frac{v_J}{v_N} = \frac{\hbar^2\pi^2 n}{m\varkappa} = \frac{\pi^2\kappa}{2\lambda^2 C_\varkappa}. \tag{7.31}$$

We focus our analysis on the parameter regime of Chapter 6 in which mean-field theory predicts a second-order phase transition (see Sec. 6.4.1). For $\kappa_c = 11.931$ and $\lambda_c = 1/200$ the local formation of a droplets appears at $\varepsilon_{\mathrm{dd,c}} = 1.34$. As the ground state converges very fast with the number of order parameters (see Fig. 6.3), we include two order parameters in our ansatz (6.34). For such a set of parameters, we obtain $v_J/v_N \approx 1.0 \times 10^7$ and $\beta \approx 2.1 \times 10^{-4}$. In Fig. 7.2, we show the parameters γ, $\beta\xi$, and $\beta^2\lambda_{\mathrm{L}}$ as a function of $\varepsilon_{\mathrm{dd}} - \varepsilon_{\mathrm{dd,c}}$ close to the phase transition. As predicted above, we find that ξ and λ_{L} vanish for $\gamma \to 0$. The behavior of the parameter $B/4$ is shown in Fig. 7.3. Indeed, we find that the quantum phase transition to the supersolid at $B/4 = 1$ (gray vertical line) is shifted by quantum fluctuations from the position where a local solid structure forms at $\varepsilon_{\mathrm{dd,c}} = 1.34$ (black vertical line). However, this region is extremely small with

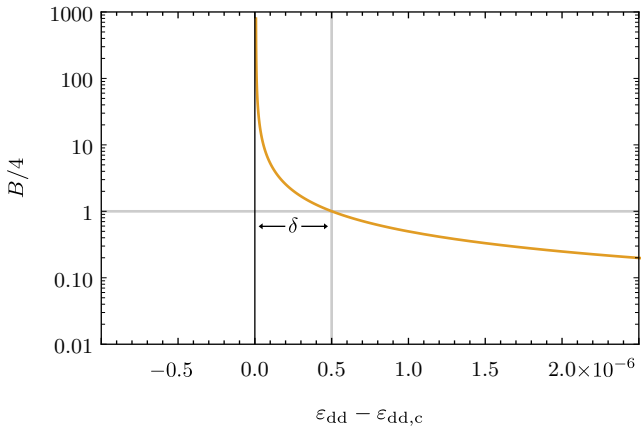

Figure 7.3: Superfluid-to-supersolid transition for increasing dipolar strength. We show $B/4$ as a function of $\varepsilon_{\mathrm{dd}} - \varepsilon_{\mathrm{dd,c}}$, where $\varepsilon_{\mathrm{dd,c}} = 1.34$ marks the local formation of droplets. To obtain B, we use the parameters of Fig. 7.2. The system transitions to the supersolid at $B/4 = 1$ (gray vertical line), which is shifted compared to the local formation of a solid structure at $\gamma = 0$ (black vertical line).

$\delta \approx 5 \times 10^{-7}$ and beyond current control on the experimental parameters. Therefore, the transition from the superfluid into the supersolid phase is excellently described by mean-field theory within the extended Gross-Pitaevskii approach for current experimental setups.

7.5 | Supersolid-to-Solid Phase Transition

For completeness, we also want to briefly summarize the results obtained for the transition from the supersolid to the solid, which appears for $\gamma \to 1$. In this regime, the different droplets are only connected by a very weak superfluid link, giving rise to a Josephson junction between each droplet. Such a Josephson junction can only support a superfluid flow if $A < 1$ in Eq. (7.20) [197]. For experimentally realistic setups with $v_N/v_J \ll 1$ and the asymptotic behavior

$$A \sim \frac{1}{\sqrt{1-\gamma}} \sqrt{\frac{v_N}{v_J}} \quad \text{for} \quad \gamma \to 1, \tag{7.32}$$

we find that this transition can only appear for $\gamma \approx 1$. This simple criterion provides an upper bound on the transition from the supersolid into the solid. However, this transition can be preempted at commensurate fillings with an integer number of particles within each droplet, i.e., $nd = 2/\beta \in \mathbb{N}$. Then, the microscopic interaction between the particles also generates a term [82]

$$H_{\mathrm{M}} = g_M \iint dx\, dt \cos\left(2\vartheta(\boldsymbol{x}) + 2u(\boldsymbol{x})/\beta\right), \tag{7.33}$$

which becomes relevant for

$$D = (\mathbf{Q}_{11} + \mathbf{Q}_{12}/\beta)^2 + (\mathbf{Q}_{21} + \mathbf{Q}_{22}/\beta)^2 < 2\,, \tag{7.34}$$

and pins the number of particles in each droplet to the integer value $2/\beta$. It describes the quantum phase transition into a Mott insulator with an excitation gap for adding/removing a particle from a droplet. However, the droplets can still fluctuate in position giving rise to a phononic sound mode characteristic for a solid. Since $D = A^{-1}$ for $\gamma \to 1$, the Mott transition at commensurate fillings occurs earlier than the transition of a single Josephson junction.

7.6 | Conclusion

We present a study on the influence of quantum fluctuations on a one-dimensional supersolid. We obtain quasi-long-range order for the off-diagonal one-particle density matrix as well as diagonal order for the density-density correlation functions and determine the exponents for the algebraic decay. We find that the quantum phase transition from the superfluid to the supersolid is shifted by quantum fluctuations from the position where a local solid structure forms. Close to the superfluid-to-supersolid phase transition, we connect the parameters of our effective low-energy description to the microscopic parameters of current dysprosium experiments with many atoms per lattice site. For these systems we find that the shift is extremely small, which means that the supersolid is accurately described by the extended Gross-Pitaevskii equation.

8 | Miscellaneous

In this chapter, we present two projects with promising ideas that were not completed. For both projects it became clear that an elaborate numerical investigation is necessary to confirm our intuition. However, the topic of quantum fluctuations in cold atomic gases poses many interesting research questions that can be addressed without relying on extensive numerics. While working on these projects, the interest in dipolar supersolids exploded in the community. Therefore, I decided to dedicate my time to this new interesting research topic and not spend my time programming. Nevertheless, both projects deserve to be mentioned here such that hopefully someone can finish them in the future.

The ideas for both projects stem from our investigation of the dimensional crossover discussed in Chapter 5. In the first part of this chapter, we adapt the approach of Hugenholtz and Pines [7] with the goal to derive the beyond-mean-field correction for self-bound states.

In the second part of this chapter, we focus on short-range interactions in optical lattices, in particular for a two-dimensional geometry with a harmonic trapping in the transverse direction. For this setup, we make the connection between the Hubbard parameters of a single band two-dimensional Hubbard model and the scattering length a_s in three dimensions. The connection to the investigation of the dimensional crossover might not be immediately obvious. There, however, it became clear that a thorough understanding of scattering in confined geometries and the concept of the confinement-induced resonance is crucial. With the Feshbach model discussed in Sec. 2.3.2, we have a powerful tool to connect the effective scattering a_2D to the scattering length a_s. We follow the same procedure as in [204, 205], where the connection of the Hubbard parameters to the scattering length a_s has been established for a three-dimensional lattice.

8.1 | Beyond-Mean-field Correction in a Self-Bound Quantum Droplet

Quantum droplets form in a regime, where the competition of an attractive and repulsive interaction leads to a cancellation of the mean-field energy such that the beyond-mean-field corrections become crucial to understand the stability of these systems [45, 49]. Since the beyond-mean-field effects become the leading order of the description, they have to be determined with high precision to allow for quantitative statements about the experiments. It is important to note that these quantum droplets do not rely on

an external trapping potential, but also appear self-bound [47, 59–62, 171]. However, the current description, which relies on the local-density approximation, fails to predict the critical atom number of these self-bound states and shows a systematic shift in the scattering length [47]. From the discussion of the dimensional crossover in Chapter 5, we have seen that although the local-density approximation is surprisingly accurate even for tightly confined systems, there are corrections to it, which might explain this discrepancy. Our results obtained from the dimensional crossover, however, cannot be directly applied to the self-bound dipolar systems.

In this section, we want to adapt the procedure introduced in Chapter 5 to dipolar self-bound states. For a better description of the experimental results we propose the following modifications to our prior analysis: The self-bound dipolar droplets observed in the experiments are highly elongated in the direction of the dipole axis (z-axis). In the transverse directions the density profile resembles a Gaussian. Since these droplets are self-bound, no external potential is necessary and the grand-canonical Hamiltonian describing the system reads

$$H' = \int d^3r\, \Psi^\dagger(\boldsymbol{r}) \left(-\frac{\hbar^2 \Delta}{2m_p} - \mu \right) \Psi(\boldsymbol{r}) + \int d^3r\, d^3r'\, \Psi^\dagger(\boldsymbol{r}) \Psi^\dagger(\boldsymbol{r}') V(\boldsymbol{r} - \boldsymbol{r}') \Psi(\boldsymbol{r}') \Psi(\boldsymbol{r}), \tag{8.1}$$

where m_p is the mass of the particles and μ is the chemical potential. The interaction potential $V(\boldsymbol{r} - \boldsymbol{r}')$ includes the long-range dipolar interaction in addition to the short-range contact interaction [see Eq. (2.60)].

The main idea is now not to expand the field operators $\Psi(\boldsymbol{r})$ in terms of plane waves, which would be the obvious choice to diagonalize the non-interacting Hamiltonian, but instead to expand it in terms of the harmonic oscillator wave functions to account for the experimentally observed Gaussian shape of the droplets,

$$\Psi(\boldsymbol{r}) = \frac{1}{\sqrt{L}} \sum_{k,\boldsymbol{u}} R_{nm}(\rho) e^{im\phi} e^{ikz} a_{k,\boldsymbol{u}}\,. \tag{8.2}$$

Here, $\boldsymbol{u} = (n, m)$ with $n \in \mathbb{N}_0$, $m \in \mathbb{Z}$ and $R_{nm}(\rho)$ is the radial wave function of the two-dimensional harmonic oscillator. In the following, we use cylindrical coordinates with the radial distance $\rho^2 = x^2 + y^2$ and azimuthal angle ϕ.

The harmonic oscillator wave functions introduce a length scale l, which characterizes the extent of the droplets but is *not* given by an external potential. The goal is then to derive the beyond-mean-field correction for this setup and treat l as a variational parameter. For a given l, we can derive the ground-state energy E as well as the chemical potential μ including beyond-mean-field corrections. This procedure is detailed in this section. The challenging numerical task is then to use the beyond-mean-field correction for the chemical potential in the extended Gross-Pitaevskii equation and find the ground state and its energy in a finite system. Note that this procedure is usually performed with the result from the local-density approximation. Here, however, this procedure has to be repeated for varying l until the ground-state energy of the droplet is minimized.

The deviations from the local-density approximation will be small, but hopefully provide a shift to the critical atom number.

8.1.1 | Ground-State Energy of the Self-Bound State

To obtain the beyond-mean-field correction for the self-bound state, we repeat the procedure introduced in Sec. 3.1.2. We start by inserting the field operators from Eq. (8.2) into the Hamiltonian in Eq. (8.1). Not being eigenfunctions to the non-interacting part of the Hamiltonian, the choice of this basis produces an off-diagonal non-interacting Hamiltonian in the annihilation (creation) operators $a_{k,\boldsymbol{u}}^{(\dagger)}$,

$$H_0 = \sum_{k,\boldsymbol{u},\boldsymbol{v}} T^{\boldsymbol{uv}}(k) a_{k,\boldsymbol{u}}^\dagger a_{k,\boldsymbol{v}} \,, \quad \text{with} \tag{8.3a}$$

$$\begin{aligned} T^{(n,m)(n',m')}(k) = \Bigg[& \left(\frac{\hbar^2 k^2}{2m_p} + \frac{\hbar\omega}{2}(2n + |m|) \right) \delta_{n,n'} \\ & - \frac{\hbar\omega}{2} \sqrt{2n + |m| + 1 + n(n + |m|)} \delta_{n',n+1} \\ & - \frac{\hbar\omega}{2} \sqrt{n(n + |m|)} \delta_{n',n-1} \Bigg] \delta_{m,m'} \,, \end{aligned} \tag{8.3b}$$

where $\omega = \hbar/m_p l^2$. Keep in mind that ω is *not* the trap frequency but characterizes the extent of the droplets in the transverse directions and is a variational parameter of our approach.

Due to the cylindrical symmetry of the problem, the interaction between the particles conserves the angular momentum and can be expressed as

$$H_\mathrm{I} = \frac{1}{2} \sum_{k,p,q} \sum_{\substack{\boldsymbol{u},\boldsymbol{u}' \\ \boldsymbol{v},\boldsymbol{v}'}} V_{\boldsymbol{u},\boldsymbol{u}'}^{\boldsymbol{v},\boldsymbol{v}'}(q) a_{k-q,\boldsymbol{u}}^\dagger a_{p+q,\boldsymbol{u}'}^\dagger a_{p,\boldsymbol{v}'} a_{k,\boldsymbol{v}}, \tag{8.4}$$

where the interaction matrix elements are given by

$$\begin{aligned} V_{(n,m),(n',m')}^{(r,l),(r',l')}(k) = & \frac{2\pi}{L} \int dk_\rho k_\rho V(k_\rho, k) \int d\rho \rho J_{m-l}(k_\rho \rho) R_{n,m}(\rho) R_{r,l}(\rho) \\ & \times \int d\rho' \rho' J_{m'-l'}(k_\rho \rho') R_{n'm'}(\rho') R_{r',l'}(\rho') \delta_{m+m',l+l'}, \end{aligned} \tag{8.5}$$

with $J_m(x)$ the Bessel function of the first kind.

The state $(k, n, m) = (0, 0, 0)$ is macroscopically occupied, which allows us to perform the Bogoliubov prescription $a_{0,\mathbf{0}}^{(\dagger)} \to \sqrt{N_0}$ (see Sec. 3.1.1), where N_0 is the number of condensate particles. We keep terms up to the quadratic order in the operators and the

Hamiltonian reads

$$\begin{aligned} H' = \quad & \frac{N_0^2}{2L} V_{\mathbf{0},\mathbf{0}}^{\mathbf{0},\mathbf{0}}(0) \\ & + \sqrt{N_0} \sum_{\boldsymbol{u}}{}' \left[T^{\boldsymbol{u}\mathbf{0}}(0) a_{0,\boldsymbol{u}}^\dagger + T^{\mathbf{0}\boldsymbol{u}}(0) a_{0,\boldsymbol{u}} \right] + N_0^{3/2} \sum_{\boldsymbol{u}}{}' V_{\boldsymbol{u},\mathbf{0}}^{\mathbf{0},\mathbf{0}}(0) \left[a_{0,\boldsymbol{u}}^\dagger + a_{0,\boldsymbol{u}} \right] \\ & + \sum_{k,\boldsymbol{u},\boldsymbol{v}}{}' \left[\xi_{\boldsymbol{u}}^{\boldsymbol{v}}(k) a_{k,\boldsymbol{u}}^\dagger a_{k,\boldsymbol{v}} + \frac{1}{2} \eta_{\boldsymbol{u}}^{\boldsymbol{v}}(k) \left(a_{k,\boldsymbol{u}}^\dagger a_{-k,\boldsymbol{v}}^\dagger + a_{k,\boldsymbol{u}} a_{k,\boldsymbol{v}} \right) \right], \end{aligned} \tag{8.6}$$

where L is a quantization length. For a shorter notation, we have introduced the matrix elements

$$\xi_{\boldsymbol{u}}^{\boldsymbol{v}}(k) = T^{\boldsymbol{u}\boldsymbol{v}}(k) - \mu \delta^{\boldsymbol{u},\boldsymbol{v}} + N_0 \left(V_{\boldsymbol{u},\mathbf{0}}^{\mathbf{0},\boldsymbol{v}}(k) + V_{\boldsymbol{u},\mathbf{0}}^{\boldsymbol{v},\mathbf{0}}(0) \right) , \tag{8.7a}$$

$$\eta_{\boldsymbol{u}}^{\boldsymbol{v}}(k) = N_0 V_{\boldsymbol{u},\boldsymbol{v}}^{\mathbf{0},\mathbf{0}}(k), \tag{8.7b}$$

and the primed sum indicates the absence of the condensate mode. The first line of Eq. (8.6) contains the mean-field energy while the third line contains the expected quadratic contributions. In contrast to Sec. 3.1.1, however, the second line contains terms which are linear in the creation and annihilation operators. At first sight this seems problematic, as we usually expand our Hamiltonian around an energy minimum and those terms are absent. The droplet state minimizes the energy so why do those terms appear? We know that the droplets are stabilized by beyond-mean-field corrections and that the shape of our wave function matches the experimental observations very well. Hence, our Ansatz is a good guess for the extended Gross-Pitaevskii equation, which includes beyond-mean-field terms, and therefore it minimizes the energy. Thus, if we would self-consistently include higher order terms in Eq. (8.6), the linear terms would be absent. The beyond-mean-field terms are small which implies that the linear terms here are small as well and we will not include them in the following discussion.

We are interested in the ground-state energy E of the system or to be more precise in corrections to the mean-field result. By closely following the procedure of Hugenholtz and Pines [7] introduced in Sec. 3.1.2, we obtain a differential equation, which connects the ground-state energy E to the Green's function,

$$E - \frac{1}{2}\mu N = \frac{1}{2} \lim_{\eta \to 0^+} \int \frac{d\omega}{2\pi} \sum_{k,\boldsymbol{u},\boldsymbol{v}}{}' \left[\hbar\omega \delta^{\boldsymbol{u},\boldsymbol{v}} + T^{\boldsymbol{u}\boldsymbol{v}}(k) \right] i G_{\boldsymbol{u}\boldsymbol{v}}(k,\omega) e^{i\omega\eta}, \tag{8.8}$$

where $G_{\boldsymbol{u}\boldsymbol{v}}(k,w)$ is the Fourier transform of the Green's function

$$i G_{\boldsymbol{u}\boldsymbol{v}}(k, t'-t) = \langle \Phi_{\text{int}} | \mathcal{T} [a_{k,\boldsymbol{u}}(t) a_{k,\boldsymbol{v}}^\dagger(t')] | \Phi_{\text{int}} \rangle , \tag{8.9}$$

$|\Phi_{\text{int}}\rangle$ is the ground state of the interacting system and $\mathcal{T}$ is the time-ordering operator. Note that Eq. (8.8) is the exact ground-state energy of the system but we will determine the Green's function perturbatively.

For the beyond-mean-field correction, it is sufficient to express the Green's function in terms of the Bogoliubov amplitudes $u^{\alpha}_{k,\boldsymbol{u}}$ and $v^{\alpha}_{k,\boldsymbol{u}}$, which determine the Bogoliubov transformation

$$a_{k,\boldsymbol{u}} = \sum_{\boldsymbol{\alpha}}{}' \left[u^{\boldsymbol{\alpha}}_{k,\boldsymbol{u}} b_{k,\boldsymbol{\alpha}} + v^{\boldsymbol{\alpha}}_{k,\boldsymbol{u}} b^{\dagger}_{-k,\boldsymbol{\alpha}} \right]. \tag{8.10}$$

Inserting the transformation (8.10) into the Green's function (8.9) and performing a Fourier transformation yields

$$G_{\boldsymbol{uv}}(k,\omega) = \sum_{\boldsymbol{\alpha}} \left[\frac{u^{\boldsymbol{\alpha}}_{k,\boldsymbol{u}} (u^{\boldsymbol{\alpha}}_{k,\boldsymbol{v}})^*}{\omega - E_{\boldsymbol{\alpha}}(k)/\hbar + i\varepsilon} - \frac{v^{\boldsymbol{\alpha}}_{k,\boldsymbol{u}} (v^{\boldsymbol{\alpha}}_{k,\boldsymbol{v}})^*}{\omega + E_{\boldsymbol{\alpha}}(k)/\hbar - i\varepsilon} \right]. \tag{8.11}$$

Here, we have used that the time evolution of the new operators $b_{k,\boldsymbol{\alpha}}(t)$ is determined by the Bogoliubov excitation spectrum $E_{\boldsymbol{\alpha}}(k)$ of the interacting system and can be written as

$$b_{k,\boldsymbol{\alpha}}(t) = e^{-iE_{\boldsymbol{\alpha}}(k)t/\hbar} b_{k,\boldsymbol{\alpha}}. \tag{8.12}$$

By inserting the Green's function from Eq. (8.11) into the differential equation for the ground-state energy from Eq. (8.8) and closing the ω integration in the upper half-plane, we obtain

$$E - \frac{1}{2}\mu N = \frac{1}{2} \sum_{k,\boldsymbol{u},\boldsymbol{v},\boldsymbol{\alpha}}{}' \left[T^{\boldsymbol{uv}}(k) - E_{\boldsymbol{\alpha}}(k)\delta^{\boldsymbol{u},\boldsymbol{v}} \right] v^{\boldsymbol{\alpha}}_{k,\boldsymbol{u}} (v^{\boldsymbol{\alpha}}_{k,\boldsymbol{v}})^*, \tag{8.13}$$

which generalizes the differential equation of Hugenholtz and Pines from Eq. (3.57) to non-diagonal single-particle Hamiltonians.

To solve this differential equation, we still need to determine the Bogoliubov amplitudes $u^{\boldsymbol{\alpha}}_{k,\boldsymbol{u}}$ and $v^{\boldsymbol{\alpha}}_{k,\boldsymbol{u}}$, as well as the Bogoliubov excitation spectrum $E_{\boldsymbol{\alpha}}(k)$, which we will do in the following.

8.1.2 | Bogoliubov Theory for the Self-Bound State

Using the Hamiltonian from Eq. (8.6), we will make use of Bogoliubov theory to calculate the excitation spectrum $E_{\boldsymbol{\alpha}}(k)$ and the Bogoliubov amplitudes $u^{\boldsymbol{\alpha}}_{k,\boldsymbol{u}}$ and $v^{\boldsymbol{\alpha}}_{k,\boldsymbol{u}}$. This is most conveniently achieved by following the same procedure as in Appendix B.2.1 and adapting it for our Hamiltonian here.

We start with the evaluation of the Heisenberg equation for the annihilation operator, which results in

$$i\hbar \dot{a}_{k,\boldsymbol{u}} = [a_{k,\boldsymbol{u}}, H'] = \sum_{\boldsymbol{v}}{}' \left[\xi^{\boldsymbol{v}}_{\boldsymbol{u}}(k) a_{k,\boldsymbol{v}} + \eta^{\boldsymbol{v}}_{\boldsymbol{u}}(k) a^{\dagger}_{-k,\boldsymbol{v}} \right]. \tag{8.14}$$

This allow us to rewrite the second time derivative as

$$(i\hbar)^2\ddot{a}_{k,\boldsymbol{u}} = \sum_{\boldsymbol{v},\boldsymbol{w}}{}' \Big[\left(\xi^{\boldsymbol{v}}_{\boldsymbol{u}}(k)\xi^{\boldsymbol{w}}_{\boldsymbol{v}}(k) - \eta^{\boldsymbol{v}}_{\boldsymbol{u}}(k)\eta^{\boldsymbol{w}}_{\boldsymbol{v}}(k)\right) a_{k,\boldsymbol{w}} + \left(\xi^{\boldsymbol{v}}_{\boldsymbol{u}}(k)\xi^{\boldsymbol{w}}_{\boldsymbol{v}}(k) - \eta^{\boldsymbol{v}}_{\boldsymbol{u}}(k)\eta^{\boldsymbol{w}}_{\boldsymbol{v}}(k)\right) a^\dagger_{-k,\boldsymbol{w}} \Big]. \tag{8.15}$$

Next, we add and subtract $(i\hbar)^2\ddot{a}^\dagger_{-k,\boldsymbol{u}}$ to and from Eq. (8.15) and make use of the Bogoliubov transformation (8.10) to obtain two equations, which determine the excitation spectrum $E_{\boldsymbol{\alpha}}(k)$ and the amplitudes $u^{\boldsymbol{\alpha}}_{k,\boldsymbol{u}}$ and $v^{\boldsymbol{\alpha}}_{k,\boldsymbol{u}}$

$$E^2_{\boldsymbol{\alpha}}(k) f^{+,\boldsymbol{\alpha}}_{k,\boldsymbol{u}} = \sum_{\boldsymbol{v},\boldsymbol{w}} h^{-,\boldsymbol{v}}_{\boldsymbol{u}}(k) h^{+,\boldsymbol{w}}_{\boldsymbol{v}}(k) f^{+,\boldsymbol{\alpha}}_{k,\boldsymbol{w}}, \tag{8.16a}$$

$$E^2_{\boldsymbol{\alpha}}(k) f^{-,\boldsymbol{\alpha}}_{k,\boldsymbol{u}} = \sum_{\boldsymbol{v},\boldsymbol{w}} h^{+,\boldsymbol{v}}_{\boldsymbol{u}}(k) h^{-,\boldsymbol{w}}_{\boldsymbol{v}}(k) f^{-,\boldsymbol{\alpha}}_{k,\boldsymbol{w}}. \tag{8.16b}$$

Here, we have introduced

$$f^{(\pm),\boldsymbol{\alpha}}_{k,\boldsymbol{u}} = u^{\boldsymbol{\alpha}}_{k,\boldsymbol{u}} \pm v^{\boldsymbol{\alpha}}_{k,\boldsymbol{u}}, \tag{8.17a}$$

$$h^{\pm,\boldsymbol{v}}_{\boldsymbol{u}}(k) = \xi^{\boldsymbol{v}}_{\boldsymbol{u}}(k) \pm \eta^{\boldsymbol{v}}_{\boldsymbol{u}}(k), \tag{8.17b}$$

and the amplitudes $f^{\pm,\boldsymbol{\alpha}}_{k,\boldsymbol{u}}$ are connected via

$$f^{+,\boldsymbol{\alpha}}_{k,\boldsymbol{u}} = \sum_{\boldsymbol{v}} \frac{h^{-,\boldsymbol{v}}_{\boldsymbol{u}}(k)}{E_{\boldsymbol{\alpha}}(k)} f^{-,\boldsymbol{\alpha}}_{k,\boldsymbol{v}}. \tag{8.18}$$

For the Bogoliubov transformation to be canonical, they have to satisfy

$$\delta_{\boldsymbol{\alpha},\boldsymbol{\beta}} = \sum_{\boldsymbol{u}} f^{+,\boldsymbol{\alpha}}_{k,\boldsymbol{u}} f^{-,\boldsymbol{\beta}}_{k,\boldsymbol{u}} = \frac{1}{E_{\boldsymbol{\alpha}}(k)} \sum_{\boldsymbol{u},\boldsymbol{v}} h^{-,\boldsymbol{v}}_{\boldsymbol{u}}(k) f^{-,\boldsymbol{\alpha}}_{k,\boldsymbol{v}} f^{-,\boldsymbol{\beta}}_{k,\boldsymbol{u}}. \tag{8.19}$$

The equations above fully characterize the excitation spectrum and corrections to the mean-field energy of a self-bound state.

To Be Done:

Within our approach for a self-bound state, we have derived the differential equation for the ground-state energy in Eq. (8.13) as well as a set of equations, that allow to determine the excitation spectrum and the Bogoliubov amplitudes [see Eq. (8.16)]. Thus, we have introduced the theoretical framework for the description of the self-bound state. To proceed, the excitation spectrum and the Bogoliubov amplitudes have to be determined numerically, similarly to the discussion in Sec. 5.3. The excitation spectrum $E_{\boldsymbol{\alpha}}(k)$ and

the amplitudes $v^{\boldsymbol{\alpha}}_{k,\boldsymbol{u}}$ then allow to extract the beyond-mean-field correction from the differential equation (8.13). The beyond-mean-field correction of the chemical potential can then be used in the extended Gross-Pitaevskii equation to find the ground state of the finite system. This procedure has to be repeated for varying l until the ground-state energy of the droplet is minimized.

Both, the numerical determination of the beyond-mean-field correction and the following minimization of the extended Gross-Pitaevskii equation are cumbersome but promising, and will hopefully be implemented in the future.

8.2 | Microscopic Derivation of Hubbard Parameters for Two-Dimensional Lattices

The Hubbard Model is a perfect toy model for strongly correlated many-body systems and ultracold atoms in optical lattices represent a suitable platform for simulating these quantum many-body systems [15, 25, 27, 28]. To understand the experimental results, however, precise knowledge of the connection between the Hubbard parameters and the microscopic experimental parameters is crucial. For deep three-dimensional lattices, weak interactions and low energies where the influence of higher bands can be neglected, the on-site interaction U can be derived by assuming a delta-interaction between the particles $V(\boldsymbol{r}) = 4\pi\hbar^2 a_\mathrm{s}\delta(\boldsymbol{r})/m$ (see Sec. 2.3.1), such that U becomes [26]

$$U = \frac{4\pi\hbar^2 a_\mathrm{s}}{m}\int d^3r\,|\mathrm{w}_0^{\mathrm{3D}}(\boldsymbol{r})|^4, \tag{8.20}$$

where $\mathrm{w}_n^{\mathrm{3D}}(\boldsymbol{r})$ are the Wannier functions with band index n. More generally, for a three-dimensional lattice and particles interacting via a Feshbach resonance the connection to the microscopic parameters has been derived by Hans Peter Büchler [204, 205]. The main idea behind this derivation is to compare the scattering amplitude in the optical lattice to the scattering amplitude of the Hubbard model and fix the Hubbard parameters such that both scattering amplitudes match.

Adapting this approach for experiments with two-dimensional lattices is straightforward. While the optical lattice potential is restricted to the plane, the particles are kept in the plane by a tight harmonic trapping potential in the transverse direction. One can then simply follow the same procedure as in Ref. [204] to calculate the scattering amplitude for this setup and fix the Hubbard parameters of the two-dimensional Hubbard model such that it reproduces the same scattering properties. However, this requires a careful numerical investigation of the scattering amplitude.

As for the three-dimensional case, for low energies and deep lattices, it is tempting to simply modify Eq. (8.20) for the new geometry,

$$U_{\mathrm{2D}} = \frac{4\pi\hbar^2 a_\mathrm{s}}{m}\int d^2\rho\,dz\,|\mathrm{w}_0^{\mathrm{2D}}(\boldsymbol{\rho})|^4|\varphi_0(z)|^4, \tag{8.21}$$

where $\varphi_0(z)$ is the ground-state wave function of the transverse harmonic oscillator. For a strong transverse confinement, however, Eq. (8.21) may not be precise enough as the scattering between the particles can be affected by the confinement-induced resonance due to the transverse trap [138, 165] (see Sec. 4.3.2).

In this section, we want to investigate how to include the effect of the confinement-induced resonance in the description of a pure two-dimensional lattice and how this affects the on-site interaction U. As we describe the interaction in the two-dimensional lattice with a Feshbach resonance, we first need to revisit the Feshbach model from Sec. 2.3.2 and connect the parameters of the two-dimensional Feshbach model to the scattering amplitude in two dimensions. By comparing the two-dimensional scattering

amplitude to the scattering amplitude obtained for a transverse harmonic confinement [see Eq.(4.40)], we can connect the parameters of the two-dimensional Feshbach model to the microscopic scattering length a_s. Using the two-dimensional Feshbach model, we will then follow the procedure in Ref. [204] for a two-dimensional optical lattice and derive the scattering amplitude on the lattice, which can in turn be connected to the scattering amplitude of the two-dimensional Hubbard model.

8.2.1 | Feshbach Model in Two Dimensions

In the following, we will briefly repeat the procedure of Sec. 2.3.2 for the two-dimensional case. The interaction between the particles is described by the coupled Schrödinger equations

$$\left[\frac{\hbar^2 \boldsymbol{k}_\rho^2}{m} + \frac{\hbar^2}{m}\Delta\right]\psi(\boldsymbol{\rho}) = \overline{g}\phi_c\alpha_\Lambda(\boldsymbol{\rho}), \tag{8.22a}$$

$$\left[\frac{\hbar^2 \boldsymbol{k}_\rho^2}{m} - \nu_0\right]\phi_c = \overline{g}\int d^2\rho\,\psi(\boldsymbol{\rho})\alpha_\Lambda(\boldsymbol{\rho}), \tag{8.22b}$$

where $\boldsymbol{k}_\rho$ and $\boldsymbol{\rho}$ are two-dimensional vectors. Without loss of generality, we choose $\alpha_\Lambda(\boldsymbol{\rho}) = e^{-\boldsymbol{\rho}/2\Lambda^2}/2\pi\Lambda^2$ in the following. We make the Ansatz

$$\psi(\boldsymbol{\rho}) = e^{i\boldsymbol{k}_\rho\cdot\boldsymbol{\rho}} + \beta_\mathrm{2D}\int d\rho'\alpha_\Lambda(\boldsymbol{\rho}')G_\mathrm{2D}(\boldsymbol{\rho}-\boldsymbol{\rho}'), \tag{8.23}$$

where the Green's function is conveniently expressed as

$$G_\mathrm{2D}(\boldsymbol{\rho}) = \frac{m}{\hbar^2}\int\frac{d^2q}{(2\pi)^2}\frac{e^{i\boldsymbol{q}\cdot\boldsymbol{\rho}}}{\boldsymbol{k}_\rho^2 - \boldsymbol{q}^2 + i\eta}. \tag{8.24}$$

From the far-field behavior of our Ansatz and following the same procedure as in Sec. 2.3.2, we obtain the scattering amplitude

$$f_\mathrm{2D}(k_\rho) = -\frac{m}{4\hbar^2}\sqrt{\frac{2i}{\pi k_\rho}}\beta_\mathrm{2D} = -\frac{m}{4\hbar^2}\sqrt{\frac{2i}{\pi k_\rho}}\frac{\overline{g}^2}{\frac{\hbar^2\boldsymbol{k}_\rho^2}{m} - \nu_0 - \overline{g}^2\overline{G}_\mathrm{2D}(k_\rho)}. \tag{8.25}$$

Here, we have introduced

$$\begin{aligned}\overline{G}_\mathrm{2D}(k_\rho) &= \frac{m}{\hbar^2}\int\frac{d^2q}{(2\pi)^2}\frac{\hat{\alpha}_\Lambda(\boldsymbol{q})^2}{k_\rho^2 - q^2 + i\eta}\\ &\overset{k_\rho\Lambda\ll 1}{=} \frac{m}{4\pi\hbar^2}\left[\gamma - i\pi + \ln(k_\rho^2\Lambda^2)\right] + O(k_\rho^2\Lambda^2),\end{aligned} \tag{8.26}$$

where γ is the Euler-Mascheroni constant. As in the three-dimensional case, $\overline{G}_\mathrm{2D}(k_\rho)$ diverges for $\Lambda \to 0$, which is not surprising. For $\Lambda \to 0$, we recover a delta potential

in the open channel, which needs to be regularized in two dimensions [139]. In the following, it is beneficial to extract the divergence and write

$$\overline{G}_{2\mathrm{D}} \overset{k_\rho \Lambda \ll 1}{=} \frac{m}{4\pi\hbar^2}\left(\ln(k_\rho^2 \bar{l}^2) - i\pi\right) + \overline{G}_{2\mathrm{D}}(i/\bar{l}), \tag{8.27}$$

where $\bar{l}$ is an arbitrary length scale to separate the Λ-behavior such that

$$\begin{aligned}\overline{G}_{2\mathrm{D}}(i/\bar{l}) &= \frac{m}{\hbar^2}\int \frac{d^2q}{(2\pi)^2}\frac{\hat{\alpha}_\Lambda(\boldsymbol{q})^2}{-1/\bar{l}^2 - q^2 + i\eta} \\ &\overset{\Lambda/\bar{l}\ll 1}{=} \frac{m}{4\pi\hbar^2}\left[\gamma + \ln\left(\Lambda^2/\bar{l}^2\right)\right].\end{aligned} \tag{8.28}$$

Hence, we arrive at the two-dimensional scattering amplitude

$$f_{2\mathrm{D}}(k_\rho) = -\sqrt{\frac{2\pi i}{k_\rho}}\frac{1}{i\pi - \ln(k_\rho^2/\bar{l}^2) - \frac{4\pi\hbar^2}{m}\frac{\nu}{\overline{g}^2} + O(k_\rho^2)} \tag{8.29}$$

where we have introduced the physical detuning

$$\nu = \nu_0 + \overline{g}^2\overline{G}_{2\mathrm{D}}(i/\bar{l}) \tag{8.30}$$

in complete analogy to Eq. (2.55).

By comparing the scattering amplitude from Eq. (8.29) to the universal low-energy scattering amplitude in two dimensions from Eq. (2.19), it is possible to connect the parameters of the Feshbach model to the two-dimensional scattering length $a_{2\mathrm{D}}$. Since we are ultimately interested in the connection to the microscopic scattering length a_s for a tight harmonic confinement, we can also directly compare the scattering amplitude from Eq. (8.29) to the scattering amplitude in a transverse harmonic trap [see Eq. (4.40)], which yields

$$\frac{\nu}{\overline{g}^2} = \frac{m}{4\pi\hbar^2}\left(\ln(l_\perp^2/2\bar{l}^2) + \overline{C}_{2\mathrm{D}}^h - \sqrt{2\pi}\frac{l_\perp}{a_\mathrm{s}}\right). \tag{8.31}$$

We can now use the two-dimensional Feshbach model to describe interactions in the lattice. The connection of the bare detuning ν_0 to the physical detuning ν in Eq. (8.30) and thus the connection to the microscopic scattering length a_s in Eq. (8.31) will be crucial for the following calculations.

8.2.2 | Scattering in an Optical Lattice

To obtain the scattering amplitude in the optical lattice, we closely follow the procedure and notation of Ref. [204], where we refer the reader to for a detailed discussion. We completely focus on two dimensions, such that all occurring vectors are two-dimensional in the following section.

Two-Channel Model in an Optical Lattice

In presence of an optical lattice, the particles a and b of equal mass m_p interacting via the Feshbach resonance discussed in Sec. 8.2.1 can be described by

$$\left[E + \frac{\hbar^2}{2m_p}\left(\Delta_{\boldsymbol{x}} + \Delta_{\boldsymbol{y}}\right) - U(\boldsymbol{x}) - U(\boldsymbol{y})\right]\psi(\boldsymbol{x},\boldsymbol{y}) = \overline{g}\int d^2z\, \alpha_\Lambda(\boldsymbol{r})\phi(\boldsymbol{z})\delta(\boldsymbol{z}-\boldsymbol{R}), \quad (8.32a)$$

$$\left[E - \nu_0 + \frac{\hbar^2}{4m_p}\Delta_{\boldsymbol{z}} - 2U(\boldsymbol{z})\right]\phi(\boldsymbol{z}) = \overline{g}\int d^2x\, d^2y\ \alpha_\Lambda(\boldsymbol{r})\psi(\boldsymbol{x},\boldsymbol{y})\delta(\boldsymbol{z}-\boldsymbol{R}), \quad (8.32b)$$

where $U(\boldsymbol{x}) = U_0\sum_{i=1}^{2}\sin^2(k_L x_i)$ is the optical lattice potential with lattice constant $d = \pi/k_L$. In addition, we have introduced the relative and center-of-mass coordinates $\boldsymbol{r} = \boldsymbol{x} - \boldsymbol{y}$ and $\boldsymbol{R} = (\boldsymbol{x}+\boldsymbol{y})/2$, respectively. In the periodic potential, the single particle problem is best described in terms of the Bloch wave functions

$$\psi^a_{n,\boldsymbol{k}_a}(\boldsymbol{x}), \qquad \psi^b_{m,\boldsymbol{k}_b}(\boldsymbol{y}), \qquad \phi^M_{s,\boldsymbol{K}}(\boldsymbol{z}), \quad (8.33)$$

where n, m and s label the Bloch bands with band energy

$$E^a_n(\boldsymbol{k}_a), \qquad E^b_m(\boldsymbol{k}_b), \qquad E^M_s(\boldsymbol{K}), \quad (8.34)$$

respectively, and the superscript M denotes the molecular state. Here, we have introduced the quasimomenta $\boldsymbol{k}_a$, $\boldsymbol{k}_b$ and the total momentum $\boldsymbol{K} = \boldsymbol{k}_a + \boldsymbol{k}_b$, which is conserved due to the discrete translational invariance. Note that we measure energies with respect to the lowest Bloch band in the following ($E^a_0(0) + E^b_0(0) = 0$). As the Bloch functions form a complete basis, we can expand $\psi(\boldsymbol{x},\boldsymbol{y})$ and $\phi(\boldsymbol{z})$ for a given $\boldsymbol{K}$ as

$$\psi(\boldsymbol{x},\boldsymbol{y}) = \frac{1}{\sqrt{N}}\sum_{n,m}\sum_{q}\varphi^{nm}(\boldsymbol{q})\psi^a_{n,\boldsymbol{q}}(\boldsymbol{x})\psi^b_{m,\boldsymbol{K}-\boldsymbol{q}}(\boldsymbol{y}), \quad (8.35a)$$

$$\phi(\boldsymbol{z}) = \sum_s R^s\phi_{s,\boldsymbol{K}}(\boldsymbol{z}), \quad (8.35b)$$

where N is the number of unit cells. By inserting the expansion into the coupled Schrödinger equations (8.32) and projecting onto the Bloch basis we obtain

$$\left[E - E_{nm}(\boldsymbol{q})\right]\varphi^{nm}(\boldsymbol{q}) = \sum_s w\, h^{nm}_s(\boldsymbol{q})R^s, \quad (8.36a)$$

$$\left[E - \nu - E^M_s(\boldsymbol{K})\right]R^s = \frac{w}{N}\sum_{n,m}\sum_{\boldsymbol{q}} h^s_{nm}(\boldsymbol{q})\varphi^{nm}(\boldsymbol{q}) - \overline{g}^2\overline{G}_{2\mathrm{D}}(i/\bar{l})R^s, \quad (8.36b)$$

where we have replaced the bare detuning ν_0 with the physical detuning ν from Eq. (8.30). In addition, we have introduced

$$E_{nm}(\boldsymbol{q}) = E_n^a(\boldsymbol{q}) + E_m^b(\boldsymbol{K}-\boldsymbol{q}) \qquad \text{and} \tag{8.37a}$$

$$h_s^{nm}(\boldsymbol{q}) = \sqrt{NV_0}\int d^2x\, d^2y\, \left[\psi^a_{n,\boldsymbol{q}}(\boldsymbol{x})\psi^b_{m,\boldsymbol{K}-\boldsymbol{q}}(\boldsymbol{y})\right]^* \alpha_\Lambda(\boldsymbol{r})\phi_{s,\boldsymbol{K}}(\boldsymbol{R}), \tag{8.37b}$$

with $w = \overline{g}/\sqrt{V_0}$, the volume of the unit cell V_0 and $h^s_{nm}(\boldsymbol{q}) = [h_s^{nm}(\boldsymbol{q})]^*$. In the following, we consider a wide resonance, which means $\nu \to \infty$, $\overline{g} \to \infty$ with $\nu/\overline{g}^2$ given by Eq. (8.31). Thus, E and $E_s^M(\boldsymbol{K})$ in the second line of Eq. (8.36) can be neglected.

Scattering Amplitude

To obtain the scattering solutions on the lattice, we make the Ansatz

$$\varphi^{nm}(\boldsymbol{q}) = \varphi_0^{nm}(\boldsymbol{q}) + \frac{\lambda^{nm}(\boldsymbol{q},\boldsymbol{k},\boldsymbol{K})}{E - E_{nm}(\boldsymbol{q})}, \tag{8.38}$$

in complete analogy to scattering in free space. Here, $\varphi_0^{nm}(\boldsymbol{q})$ is an incoming wave in the lowest Bloch band with relative momentum $\boldsymbol{q}$ and center of mass momentum $\boldsymbol{K}$. We are interested in the low-energy behavior $E \to 0$ of the incoming wave to connect λ^{nm} to the scattering length. Inserting the Ansatz (8.38) into the coupled equations (8.36) yields

$$\lambda^{nm}(\boldsymbol{q},\boldsymbol{k},\boldsymbol{K}) = \sum_s h_s^{nm}(\boldsymbol{q})R^s, \tag{8.39a}$$

$$R^s = W\sum_t \chi_t^s(E)R^t - \frac{w}{\nu}h^s_{00}(\boldsymbol{k}), \tag{8.39b}$$

where we have introduced $W = -w^2/\nu$ and the matrix

$$\chi_t^s(E) = \sum_{n,m}\int_{1.\mathrm{BZ}} \frac{d^2q}{v_0}\left[\frac{h^s_{nm}(\boldsymbol{q})h_t^{nm}(\boldsymbol{q})}{E - E_{nm}(\boldsymbol{q})}\right] - \frac{\overline{g}^2}{w^2}\overline{G}(i/\bar{l})\delta_{t,s}, \tag{8.40}$$

with $v_0 = (2\pi)^2/V_0$ the volume of the first Brillouin zone.

To obtain a closed expression for the scattering amplitude, it is convenient to introduce the eigenvectors R^s_α for the matrix χ_t^s and the corresponding eigenvalues χ_α. We can then expand R^s in terms of the eigenfunctions R^s_α,

$$R^s = \sum_\alpha C^\alpha R^s_\alpha, \tag{8.41}$$

and determine the prefactors C^α from Eq. (8.39b) by making use of the orthogonality of the eigenfunctions R^s_α. This results in

$$C^\alpha = -\frac{w}{\nu}\frac{\sum_s R^s_\alpha h^s_{00}(\boldsymbol{k})}{1 - W\chi_\alpha}, \tag{8.42}$$

such that from Eq. (8.39a) we obtain the scattering amplitude, which in the low-energy limit reads

$$\lambda \equiv \lambda^{00}(0,0,0) = W\sum_\alpha \frac{|w_\alpha|^2}{1 - W\chi_\alpha} \approx W\frac{|w_0|^2}{1 - W\chi_0}, \tag{8.43}$$

where we have introduced

$$w_\alpha = \sum_s h^{00}_s(0) R^s_\alpha. \tag{8.44}$$

Connection to the Hubbard Model

We can now use the scattering amplitude from Eq. (8.43) to fix the on-site interaction U of the Hubbard model. For the Hubbard model, the scattering amplitude takes the well-known form [206, 207]

$$\lambda_{\mathrm{HM}} = \frac{U}{1 - UG(E)} \qquad \text{with} \qquad G(E) = \int \frac{d^2q}{v_0}\frac{1}{E - E_{00} + i\eta}. \tag{8.45}$$

By comparing the scattering amplitude from Eq. (8.43) to the scattering amplitude λ_{HM} from the Hubbard model, we obtain

$$U = \frac{1}{\lambda^{-1} + G(0)} \approx \frac{W|w_0|^2}{1 + W\left(|w_0|^2 G(0) - \chi_0\right)}, \tag{8.46}$$

which can be evaluated numerically. The dominant contribution to U is provided by $W|w_0|^2$, while $|w_0|^2G(0) - \chi_0$ describes a correction for stronger interactions. To estimate this correction, we make a perturbation expansion in the low-energy regime. To do so, we write

$$\begin{aligned}\chi^s_t(E) &= \sum_{n,m}\int_{1.\mathrm{BZ}} \frac{d^2q}{v_0}\left[\frac{h^s_{nm}(\boldsymbol{q})h^{nm}_t(\boldsymbol{q})}{E - E_{nm}(\boldsymbol{q})}\right] - \frac{\overline{g}^2}{w^2}\overline{G}(i/\bar{l})\delta_{t,s} \\ &\approx \overline{\chi}^s_t + \delta\chi^s_t - \frac{\overline{g}^2}{w^2}\overline{G}(i/\bar{l})\delta_{t,s}\end{aligned} \tag{8.47}$$

where we have introduced

$$\overline{\chi}^s_t = \int_{1.\mathrm{BZ}} \frac{d^2q}{v_0}\left[\frac{h^s_{00}(0)h^0_t(0)}{E - E_{nm}(\boldsymbol{q})}\right], \tag{8.48a}$$

$$\delta\chi^s_t = {\sum_{nm}}' \int_{1.\mathrm{BZ}} \frac{d^2q}{v_0}\left[\frac{h^s_{nm}(\boldsymbol{q})h^{nm}_t(\boldsymbol{q})}{E - E_{nm}(\boldsymbol{q})}\right], \tag{8.48b}$$

and the primed sum indicates the absence of the term $(n, m) = (0, 0)$. In the low-energy regime $E \to 0$, the dominant contribution to χ_t^s comes from $\overline{\chi}_t^s$, while the remaining terms are considered as a small perturbation. The (unperturbed) eigenfunctions of $\overline{\chi}_t^s$ are then simply given by

$$\overline{R}_0^s = \frac{h_{00}^s(0)}{\sqrt{\sum_u |h_{00}^u(0)|^2}}, \tag{8.49}$$

with the (unperturbed) eigenvalue

$$\chi_0^{(0)} = \sum_t \int \frac{d^2q}{v_0} \frac{h_t^{00}(0) h_{00}^t(0)}{E - E_{00}} = |w_0|^2 G(E). \tag{8.50}$$

Within first order perturbation theory, the correction to the unperturbed eigenvalue $\chi_0^{(0)}$ becomes

$$\begin{aligned} \chi_0^{(1)} &= \frac{1}{\sqrt{\sum_u |h_{00}^u(0)|^2}} \sum_{s,t} \sum_{n,m}{}' \int \frac{d^2q}{v_0} \left[\frac{h_t^{nm}(\boldsymbol{q}) h_{00}^t(0) h_{nm}^s(\boldsymbol{q}) h_s^{00}(0)}{E - E_{nm}} \right] - \frac{\overline{g}^2}{w^2} \overline{G}(i/\bar{l}) \\ &\equiv \delta\chi_0^{(1)} - \frac{\overline{g}^2}{w^2} \overline{G}(i/\bar{l})\,. \end{aligned} \tag{8.51}$$

Using our perturbation expansion $\chi_0 = \chi_0^{(0)} + \chi_0^{(1)}$, we can write U as

$$\begin{aligned} \frac{1}{U} &= \frac{1}{|w_0|^2} \left(\frac{1}{W} - \chi_0^{(1)} \right) \\ &= \frac{mV_0}{4\pi\hbar^2 |w_0|^2} \left[\sqrt{2\pi} \frac{l_\perp}{a_\mathrm{s}} + \ln(2) - \overline{C}_{2\mathrm{D}}^h + C_\mathrm{L} \right], \end{aligned} \tag{8.52}$$

where we have made use of the connection between the parameters of the Feshbach model and the scattering length from Eq. (8.31). In addition to the constant $\overline{C}_{2\mathrm{D}}^h$ resulting from the transverse harmonic confinement, also the constant

$$C_\mathrm{L} = \frac{4\pi\hbar^2}{m} \left(\overline{G}_{2\mathrm{D}}(i/l_\perp) - \frac{1}{V_0} \delta\chi_0^{(1)} \right) \tag{8.53}$$

appears within this order of approximation, which needs to be evaluated numerically. For deep latices, the separation of the first excited Bloch band scales as $\sqrt{E_r U_0}$ [26], where $E_r = \hbar^2 k_L^2 / 2m_p$ is the recoil energy. Thus, $C_\mathrm{L} \sim \ln(E_\perp / \sqrt{U_0 E_r})$ with $E_\perp = \hbar^2 / m_p l_\perp^2$, and C_L is not expected to be negligibly small due to the logarithmic behavior.

Unfortunately, this means that for a two-dimensional optical lattice and transverse harmonic confinement, we cannot simply include the correction to the confinement-induced resonance since within this order of approximation, also higher bands contribute to U through C_L.

To Be Done:

While all relevant renormalization steps have been performed here and an expression for U has been derived that includes the effect of the confinement-induced resonance, the additional constant C_{L} still needs to be evaluated. Afterwards, the result of our perturbation expansion in Eq. (8.52) has to be compared to Eq. (8.46). For a complete analysis, however, also repeating the procedure for the full three-dimensional setup is required to analyze the influence of the transverse trap.

Appendix

A | Scattering in Confined Geometries

In this Appendix, we briefly want to outline the calculations required to obtain the confinement-induced resonance for different geometries.

A.1 | Periodic Boundary Conditions: 1D

To obtain the constant $C_{1\mathrm{D}}$, we need to evaluate

$$\overline{G}'_{1\mathrm{D}}(0) - \overline{G}(0) = \frac{m}{\hbar^2}\left(\int \frac{dq^3}{(2\pi)^3}\frac{\hat{\alpha}_\Lambda^2(\boldsymbol{q})}{\boldsymbol{q}^2 + i\eta} - \frac{1}{l_\perp^2}\sum_{q_x,q_y}{}' \int \frac{dq_z}{2\pi}\frac{\hat{\alpha}_\Lambda^2(\boldsymbol{q})}{\boldsymbol{q}^2 + i\eta}\right). \tag{A.1}$$

As the difference $\overline{G}'_{1\mathrm{D}}(0) - \overline{G}(0)$ remains finite, we take the limit $\Lambda \to 0$, such that $\hat{\alpha}_\Lambda(\boldsymbol{q}) \to 1$ and we can perform the q_z integration,

$$\overline{G}'_{1\mathrm{D}}(0) - \overline{G}(0) = \frac{m}{2\hbar^2}\left(\int \frac{dq^2}{(2\pi)^2}\frac{1}{\sqrt{q_x^2+q_y^2}} - \frac{1}{l_\perp^2}\sum_{q_x,q_y}{}' \frac{1}{\sqrt{q_x^2+q_y^2}}\right). \tag{A.2}$$

Substituting $q_x = 2\pi v/l_\perp$ and $q_y = 2\pi w/l_\perp$, we obtain the final result

$$\begin{aligned}\overline{G}'_{1\mathrm{D}}(0) - \overline{G}(0) &= \frac{m}{4\pi\hbar^2 l_\perp}\left(\int dv dw \frac{1}{\sqrt{v^2+w^2}} - \sum_{v,w}{}' \frac{1}{\sqrt{v^2+w^2}}\right) \\ &= \frac{m}{4\pi\hbar^2 l_\perp} C_{1\mathrm{D}},\end{aligned} \tag{A.3}$$

with $C_{1\mathrm{D}}$ introduced in Eq. (4.12).

A.2 | Periodic Boundary Conditions: 2D

As the two-dimensional low-energy scattering amplitude diverges for $\boldsymbol{k}_\rho \to 0$, evaluating

$$\overline{G}_{2\mathrm{D}}(k_\rho) - \overline{G}(0) = \frac{m}{\hbar^2}\left(\frac{1}{l_\perp}\sum_{q_z}\int \frac{dq_x\, q_y}{(2\pi)^2}\frac{\hat{\alpha}_\Lambda^2(\boldsymbol{q})}{\boldsymbol{k}_\rho^2 - \boldsymbol{q}^2 + i\eta} + \int \frac{dq^3}{(2\pi)^3}\frac{\hat{\alpha}_\Lambda^2(\boldsymbol{q})}{\boldsymbol{q}^2 + i\eta}\right) \tag{A.4}$$

requires some effort. Without loss of generality, we choose $\alpha(\boldsymbol{r}) = \delta(z)e^{-(x^2+y^2)/2\Lambda^2}/2\pi\Lambda^2$ such that $\hat{\alpha}(\boldsymbol{q}) = e^{-(q_x^2+q_y^2)\Lambda^2/2}$. Using Mathematica, we can perform the q_z summation and integration,

$$\overline{G}_{\mathrm{2D}}(k_\rho) - \overline{G}(0) = \frac{m}{2\hbar^2}\int \frac{dq_x\, dq_y}{(2\pi)^2}\left(\frac{\cot(l_\perp\sqrt{k_\rho^2 - q_\rho^2}/2)}{\sqrt{k_\rho^2 - q_\rho^2}} + \frac{1}{q_\rho}\right)e^{-q_\rho^2\Lambda^2}, \tag{A.5}$$

where $\boldsymbol{q_\rho} = (q_x, q_y)^T$. While $\overline{G}(0)$ cures the ultraviolet divergence of $\overline{G}_{\mathrm{2D}}$, the integral diverges for $k_\rho \to 0$, which is expected for the two-dimensional scattering amplitude [see Eq. (2.28)]. To extract the characteristic $\sim \ln(k^2)$ behavior, we introduce polar coordinates and add and subtract

$$\frac{1 + \frac{k_\rho^2 l_\perp^2}{4}}{\left(\frac{k_\rho^2 l_\perp^2}{4} - \frac{q_\rho^2 l_\perp^2}{4}\right)\left(1 + \frac{q_\rho^2 l_\perp^2}{4}\right)}, \tag{A.6}$$

which behaves as $\overline{G}_{\mathrm{2D}}$ for $k_\rho = 0$ and $q_\rho \ll 1$ but also converges for $q_\rho \to \infty$. With $q_\rho = 2u/l_\perp$ we obtain

$$\begin{aligned}\overline{G}_{\mathrm{2D}}(k_\rho) - \overline{G}(0) = \frac{m}{2\pi\hbar^2 l_\perp}\int du\, u e^{-4u^2\Lambda^2/l_\perp^2}\Bigg[&\frac{1 + \frac{k_\rho^2 l_\perp^2}{4}}{\left(\frac{k_\rho^2 l_\perp^2}{4} - u^2\right)(1+u^2)} \\ &+ \frac{1}{u} + \frac{\cot\left(\sqrt{\frac{k_q^2 l_\perp^2}{4} - u^2}\right)}{\sqrt{\frac{k_\rho^2 l_\perp^2}{4} - u^2}} - \frac{1 + \frac{k_\rho^2 l_\perp^2}{4}}{\left(\frac{k_\rho^2 l_\perp^2}{4} - u^2\right)(1+u^2)}\Bigg].\end{aligned} \tag{A.7}$$

As the first line already provides the leading k_ρ contribution,

$$\int du\, u e^{-4u^2\Lambda^2/l_\perp^2}\left[\frac{1 + \frac{k_\rho^2 l_\perp^2}{4}}{\left(\frac{k_\rho^2 l_\perp^2}{4} - u^2\right)(1+u^2)}\right] = \frac{1}{2}\left[-i\pi + \ln\left(\frac{k_\rho^2 l_\perp^2}{4}\right)\right], \tag{A.8}$$

we set $k_\rho = 0$ for the second line

$$\int du\, u e^{-4u^2\Lambda^2/l_\perp^2}\left[\frac{1}{u} - \frac{\coth(u)}{u} + \frac{1}{u^2(1+u^2)}\right] \overset{\Lambda\to 0}{=} \ln(2) \tag{A.9}$$

to obtain the final result

$$\overline{G}_{\mathrm{2D}}(k_\rho) - \overline{G}(0) = \frac{m}{4\pi\hbar^2 l_\perp}\left(-i\pi + \ln(k_\rho^2 l_\perp^2)\right). \tag{A.10}$$

A.3 | Harmonic Confinement: 1D

As $\overline{G}(0)$ cures the divergence of $\overline{G}'^h_{\mathrm{1D}}(0)$, we can take the limit $\Lambda \to 0$ and obtain

$$\overline{G}'^h_{\mathrm{1D}}(0) - \overline{G}(0) = \frac{m}{\hbar^2}\left(\int \frac{d^3q}{(2\pi)^3}\frac{1}{\boldsymbol{q}^2 - i\eta} + \int \frac{dq_x}{2\pi}\sum_{(n,l)\neq(0,0)}^{\infty}\frac{|\varphi_{n,l}(0)|^2}{-q_x^2 - n/l_\perp^2 + i\eta}\right), \quad \text{(A.11)}$$

but need to keep the correct limiting procedure introduced by the functions α_Λ in mind. With the property of the harmonic oscillator wave functions,

$$|\varphi_{n,l}(0)|^2 = \begin{cases} \frac{1}{2\pi l_\perp^2} & \text{for} \quad l = 0 \\ 0 & \text{for} \quad l \neq 0 \end{cases} \quad \text{(A.12)}$$

the sum over l vanishes and we can perform the q_x integration for both terms. In polar coordinates this yields

$$\overline{G}'^h_{\mathrm{1D}}(0) - \overline{G}(0) = \frac{m}{4\pi\hbar^2}\left(\int dq_\rho - \frac{1}{l_\perp}\sum_{n=2,4,\ldots}\frac{1}{\sqrt{n}}\right). \quad \text{(A.13)}$$

Using $n = 2s'$ and $q_\rho^2 = 2s'/l_\perp^2$ to ensure the correct limiting procedure, we obtain the final result

$$\begin{aligned}\overline{G}'^h_{\mathrm{1D}}(0) - \overline{G}(0) &= \frac{m}{4\pi\hbar^2}\frac{1}{\sqrt{2}l_\perp}\lim_{s\to\infty}\left(\int_0^s ds'\,\frac{1}{\sqrt{s'}} - \sum_{s'=1}^{s}\frac{1}{\sqrt{s'}}\right) \\ &= \frac{m}{4\pi\hbar^2}\frac{1}{\sqrt{2}l_\perp}C^h_{\mathrm{1D}},\end{aligned} \quad \text{(A.14)}$$

with C^h_{1D} introduced in Eq. (4.30).

A.4 | Harmonic Confinement: 2D

As in Appendix A.2, we choose $\alpha(\boldsymbol{r}) = \delta(z)e^{-(x^2+y^2)/2\Lambda^2}/2\pi\Lambda^2$ for the evaluation of $\overline{G}^h_{\mathrm{2D}}(\boldsymbol{k}_\rho) - \overline{G}(0)$, which then can be written as

$$\overline{G}^h_{\mathrm{2D}}(\boldsymbol{k}_\rho) - \overline{G}(0) = \frac{m}{\hbar^2}\left(\int \frac{dq_x\,dq_y}{(2\pi)^2}\sum_n \frac{e^{-q_\rho^2\Lambda^2}|\varphi_n(0)|^2}{k_\rho^2 - q_\rho^2 - n/l_\perp^2 + i\eta} + \int \frac{d^3q}{(2\pi)^3}\frac{1}{\boldsymbol{q}^2 - i\eta}\right), \quad \text{(A.15)}$$

where $\boldsymbol{q}_\rho = (q_x, q_y)^T$. The harmonic oscillator eigenfunctions take the form

$$|\varphi_n(0)|^2 = \frac{1}{\sqrt{2\pi l_\perp^2}}\frac{1}{2^n n!}H_n(0)^2, \quad \text{(A.16)}$$

where the Hermite polynomials evaluated at zero can be written as

$$H_n(0) = \begin{cases} 0 & \text{for odd } n \\ (-2)^{n/2}(n-1)!! & \text{for even } n\,. \end{cases} \tag{A.17}$$

With the help of Mathematica, we can then perform the summation in $\overline{G}^h_{\mathrm{2D}}$ as well as the q_z integration in $\overline{G}(0)$ to obtain

$$\overline{G}^h_{\mathrm{2D}}(k_\rho) - \overline{G}(0) = \frac{m}{2\hbar^2}\int \frac{dq_x dq_y}{(2\pi)^2} e^{-q_\rho^2\Lambda^2}\left(\frac{1}{q_\rho} - \frac{l_\perp}{\sqrt{2}}\frac{\Gamma(l_\perp^2(q_\rho^2-k_\rho^2)/2)}{\Gamma(\frac{1}{2}+l_\perp^2(q_\rho^2-k_\rho^2)/2)}\right), \tag{A.18}$$

where $\Gamma(x)$ is the gamma function. Similar to Appendix A.2, we need to extract the diverging contribution for $k_\rho \to 0$. We add and subtract

$$\frac{1}{\sqrt{\pi}}\frac{1+\frac{k_\rho^2 l_\perp^2}{2}}{\left(\frac{k_\rho^2 l_\perp^2}{2} - \frac{q_\rho^2 l_\perp^2}{2}\right)\left(1+\frac{q_\rho^2 l_\perp^2}{2}\right)}, \tag{A.19}$$

which behaves as $\overline{G}^h_{\mathrm{2D}}$ for $k_\rho = 0$ and $q_\rho \ll 1$ but also converges for $q_\rho \to \infty$. In polar coordinates and using $q_\rho = \sqrt{2}u/l_\perp$, we obtain

$$\begin{aligned}\overline{G}^h_{\mathrm{2D}}(k_\rho) - \overline{G}(0) =& \frac{m}{4\pi\hbar^2}\frac{\sqrt{2}}{l_\perp}\int du\, u e^{-2u^2\Lambda^2/l_\perp^2}\left[\frac{1}{\sqrt{\pi}}\frac{1+\frac{k_\rho^2 l_\perp^2}{2}}{\left(\frac{k_\rho^2 l_\perp^2}{2}-u^2\right)(1+u^2)}\right. \\ &\left. + \frac{1}{u} - \frac{\Gamma(u^2-\frac{k_\rho^2 l_\perp^2}{2})}{\Gamma(\frac{1}{2}+u^2-\frac{k_\rho^2 l_\perp^2}{2})} - \frac{1}{\sqrt{\pi}}\frac{1+\frac{k_\rho^2 l_\perp^2}{2}}{\left(\frac{k_\rho^2 l_\perp^2}{2}-u^2\right)(1+u^2)}\right].\end{aligned} \tag{A.20}$$

The first line provides the leading k_ρ behavior,

$$\int du\, u\, e^{-2u^2\Lambda^2/l_\perp^2}\frac{1}{\sqrt{\pi}}\frac{1+\frac{k_\rho^2 l_\perp^2}{2}}{\left(\frac{k_\rho^2 l_\perp^2}{2}-u^2\right)(1+u^2)} \overset{k_\rho\Lambda\ll 1}{=} \frac{1}{2\sqrt{\pi}}\left[-i\pi + \ln\left(\frac{k_\rho^2 l_\perp^2}{2}\right)\right]. \tag{A.21}$$

Thus, we set $k_\rho = 0$ in the second line, which yields

$$\int du\, u\, e^{-2u^2\Lambda^2/l_\perp^2}\left[\frac{1}{u} - \frac{\Gamma(u^2)}{\Gamma(\frac{1}{2}+u^2)} + \frac{1}{\sqrt{\pi}}\frac{1}{u^2(1+u^2)}\right] = \frac{\overline{C}^h_{\mathrm{2D}}}{2\sqrt{\pi}}, \tag{A.22}$$

with $\overline{C}^h_{\mathrm{2D}}$ introduced in Eq. (4.39). Hence, we obtain

$$\overline{G}^h_{\mathrm{2D}}(k_\rho) - \overline{G}(0) = \frac{m}{4\pi\hbar^2}\frac{1}{\sqrt{2\pi l_\perp^2}}\left(\overline{C}^h_{\mathrm{2D}} - i\pi + \ln\left(k_\rho^2 l_\perp^2/2\right)\right). \tag{A.23}$$

B | Dimensional Crossover

B.1 | Crossover to One Dimension

In the following, we will briefly sketch the derivation of the function describing the entire crossover regime in the 3D-1D crossover. We start with the general expression from Eq. (5.9),

$$\frac{E - E_{\mathrm{3D}}}{E_0} = \kappa^2 \lambda \int_{\kappa}^{\infty} d\kappa' \, \left[h(\kappa') - h_{\mathrm{3D}}(\kappa') \right], \tag{5.9 revisited}$$

and perform the integration over κ' first. The upper boundary of the integration vanishes and we obtain

$$\frac{E_{\mathrm{1D}} - E_{\mathrm{3D}}}{E_0} = \lambda \int du \left[\sum_{n,m} f(\varepsilon) - \int dv dw f(\varepsilon) \right] \tag{B.1}$$

where

$$f(\varepsilon) = \sqrt{\varepsilon^2 + 2\varepsilon\kappa} - \varepsilon - \kappa. \tag{B.2}$$

We proceed by rewriting the integration over u by deforming the integration path into the complex plane. For this consider the contours γ_1 and γ_2 in Fig. B.1. Both closed loops vanish independently as no poles are enclosed. For the dashed part of γ_1 and γ_2, $f(\varepsilon)$ decays fast enough such that they do not contribute to the integral. We can therefore replace the integration over the real axis by an integration over the imaginary axis. By realizing that γ_1 and γ_2 contribute equally and using that the result is real, we obtain the identity

$$\int_{-\infty}^{\infty} du \, \left[\sqrt{\varepsilon^2 + 2\varepsilon\kappa} - \varepsilon - \kappa \right] = -\frac{4\kappa^{3/2}}{\sqrt{\pi}} \int_0^1 dt \, \frac{\sqrt{t(1-t)}}{\sqrt{t + \frac{\pi}{4\kappa}(v^2 + w^2)}}. \tag{B.3}$$

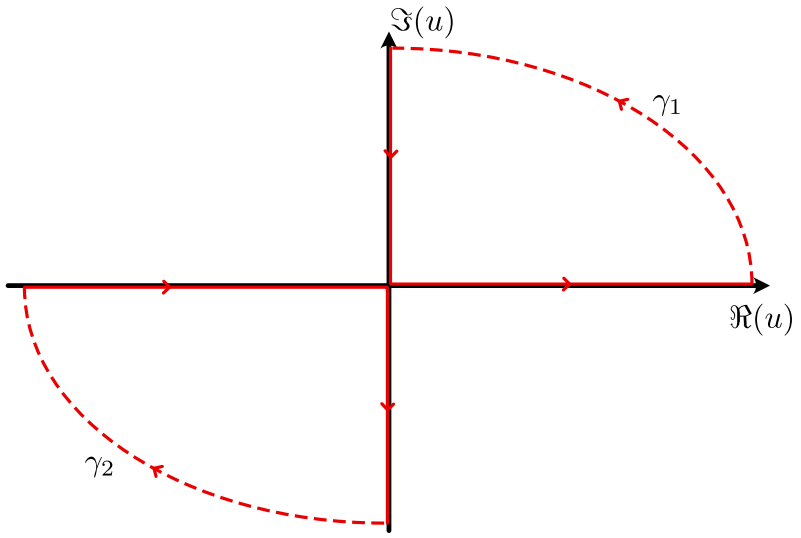

Figure B.1: The contours γ_1 and γ_2 used to obtain the identity in Eq. (B.3). Both loops do not contain any poles such that the integrations along γ_1 and γ_2 vanish independently. For the dashed part, the integrand decays fast enough such that it does not contribute to the integral.

This allows us now to nicely separate the different contributions to the ground-state energy,

$$\begin{aligned}
&\int dv\,dw \frac{1}{\sqrt{t+\frac{\pi}{4\kappa}(v^2+w^2)}} - \sum_{v,w} \frac{1}{\sqrt{t+\frac{\pi}{4\kappa}(v^2+w^2)}} \\
&= -\frac{1}{\sqrt{t}} + \sum_{v,w}{}' \frac{1}{\sqrt{\frac{\pi}{4\kappa}(v^2+w^2)}} - \sum_{v,w}{}' \frac{1}{\sqrt{t+\frac{\pi}{4\kappa}(v^2+w^2)}} \\
&\quad + \int dv\,dw \frac{1}{\sqrt{\frac{\pi}{4\kappa}(v^2+w^2)}} - \sum_{v,w}{}' \frac{1}{\sqrt{\frac{\pi}{4\kappa}(v^2+w^2)}} \Bigg\} = \sqrt{\frac{4\kappa}{\pi}} C_{\mathrm{1D}} \\
&\quad + \int dv\,dw \int \frac{1}{\sqrt{t+\frac{\pi}{4\kappa}(v^2+w^2)}} - \int dv\,dw \frac{1}{\sqrt{\frac{\pi}{4\kappa}(v^2+w^2)}} \Bigg\} = -8\sqrt{t}\kappa.
\end{aligned} \tag{B.4}$$

Hence, we arrive at

$$\begin{aligned}
\frac{E-E_{\mathrm{3D}}}{\lambda E_0} &= -\frac{8}{3\sqrt{\pi}}\kappa^{3/2} + C_{\mathrm{1D}}\kappa^2 - \frac{128}{15\sqrt{\pi}}\kappa^{5/2} \\
&\quad + \frac{8\kappa^2}{\pi}\int_0^1 dt\,\sqrt{t(1-t)}\left[\sum_{v,w}{}' \frac{1}{\sqrt{v^2+w^2}} - \sum_{v,w}{}' \frac{1}{\sqrt{v^2+w^2+\frac{4\kappa t}{\pi}}}\right].
\end{aligned} \tag{B.5}$$

As a last step, we want to get rid of the double summation. Therefore, we use $1/\sqrt{A} = \int_0^\infty d\tau\, e^{-\tau A}/\sqrt{\tau}$ to write

$$\sum_{v,w}{}' \left[\frac{1}{\sqrt{v^2+w^2}} - \frac{1}{\sqrt{v^2+w^2+\frac{4\kappa t}{\pi}}} \right] = \int_0^\infty \frac{d\tau}{\sqrt{\pi\tau}} \sum_{v,w}{}' e^{-\tau(v^2+w^2)}(1-e^{-\tau 4\kappa t/\pi}) \\ = \int_0^\infty \frac{d\tau}{\sqrt{\pi\tau}} \left(\vartheta_3(0,e^{-\tau})^2 - 1\right)\left(1-e^{-\tau 4\kappa t/\pi}\right), \tag{B.6}$$

where we have made use of the definition of the Jacobi theta function $\vartheta_3(z,q) = \sum_n q^{n^2}\cos(2nz)$. Finally, we perform the integration over t,

$$\int_0^1 dt\sqrt{t(1-t)}\left(1-e^{-4\tau\kappa t/\pi}\right) = \frac{\pi}{8}\left(1 - \frac{e^{-\frac{2\tau\kappa}{\pi}} I_1(\frac{2\tau\kappa}{\pi})}{\tau\kappa/\pi}\right), \tag{B.7}$$

and arrive at the final result

$$\frac{E_{1\mathrm{D}}}{E_0} = \kappa^2(1+\lambda C_{1\mathrm{D}}) - \lambda\frac{8}{3\sqrt{\pi}}\kappa^{3/2} + \lambda\kappa^2\int_0^\infty \frac{d\tau}{\sqrt{\pi\tau}}\left[\vartheta_3\left(0,e^{-\tau}\right)^2 - 1\right]\left[1 - \frac{e^{-\frac{2\tau\kappa}{\pi}} I_1\left(\frac{2\tau\kappa}{\pi}\right)}{\tau\kappa/\pi}\right]. \tag{B.8}$$

B.1.1 | 3D Regime

Using the relation $\vartheta_3\left(0,e^{-\pi x}\right) = \vartheta_3\left(0,e^{-\pi/x}\right)/\sqrt{x}$, which is straightforward to prove using the Poisson summation formula, we find a suitable expression to perform the analytic expansion for $\kappa \gg 1$,

$$\kappa^2\int_0^\infty \frac{d\tau}{\sqrt{\pi\tau}}\left[\vartheta_3\left(0,e^{-\tau}\right)^2 - 1\right]\left[1 - \frac{e^{-\frac{2\tau\kappa}{\pi}} I_1\left(\frac{2\tau\kappa}{\pi}\right)}{\tau\kappa/\pi}\right] \\ = \kappa^2\int_0^\infty \frac{d\tau}{\sqrt{\pi\tau}}\left[\vartheta_3\left(0,e^{-\tau}\right)^2 - \frac{\pi}{\tau}\right]\left[1 - \frac{e^{-\frac{2\kappa\pi}{\tau}} I_1\left(\frac{2\pi\kappa}{\tau}\right)}{\pi\kappa/\tau}\right] \\ \left.\kappa^2\int_0^\infty \frac{d\tau}{\sqrt{\pi\tau}}\left[1 - \frac{e^{-\frac{2\kappa\pi}{\tau}} I_1\left(\frac{2\pi\kappa}{\tau}\right)}{\pi\kappa/\tau}\right]\right\} = \frac{128}{15\sqrt{\pi}}\kappa^{5/2} \tag{B.9}$$

$$\left. + \kappa^2\int_0^\infty \frac{d\tau}{\sqrt{\pi\tau}}\left[\vartheta_3\left(0,e^{-\tau}\right)^2 - \frac{\pi}{\tau} - 1\right]\right\} = -\kappa^2 C_{1\mathrm{D}} \tag{B.10}$$

$$\left. + \kappa^2\int_0^\infty \frac{d\tau}{\sqrt{\pi\tau}}\frac{\pi}{\tau}\left[\frac{e^{-\frac{2\kappa\pi}{\tau}} I_1\left(\frac{2\pi\kappa}{\tau}\right)}{\pi\kappa/\tau}\right]\right\} = \frac{8}{3\sqrt{\pi}}\kappa^{3/2} \tag{B.11}$$

$$- \kappa^2\int_0^\infty \frac{d\tau}{\sqrt{\pi\tau}}\left[\vartheta_3\left(0,e^{-\tau}\right)^2 - 1\right]\left[\frac{e^{-\frac{2\kappa\pi}{\tau}} I_1\left(\frac{2\pi\kappa}{\tau}\right)}{\pi\kappa/\tau}\right] \tag{B.12}$$

We see that Eq. (B.9) provides the correct 3D result while Eq. (B.10) cancels the correction to the mean-field shift due to the confinement-induced resonance and Eq. (B.11) cancels the 1D beyond-mean-field correction. The last term [Eq. (B.12)] can now be expanded in the small parameter τ/κ,

$$\begin{aligned} &-\kappa^2 \int_0^\infty \frac{d\tau}{\sqrt{\pi\tau}} \left[\vartheta_3\left(0, e^{-\tau}\right)^2 - 1\right] \left[\frac{e^{-\frac{2\kappa\pi}{\tau}} I_1\left(\frac{2\pi\kappa}{\tau}\right)}{\pi\kappa/\tau}\right] \\ &\approx -\kappa^2 \int_0^\infty \frac{d\tau}{\sqrt{\pi\tau}} \left[\vartheta_3\left(0, e^{-\tau}\right)^2 - 1\right] \sqrt{\frac{2}{\pi}} \left(\frac{\tau}{2\kappa\pi}\right)^{3/2} \\ &= -\sqrt{\kappa} \frac{A_{1\mathrm{D}}}{2\pi^{5/2}} \end{aligned} \tag{B.13}$$

which provides the leading correction for large $\kappa \gg 1$ with $A_{1\mathrm{D}} = {\sum_{v,w}}' \left(v^2 + w^2\right)^{-2} \approx 6.0268$.

B.2 | Harmonic Confinement

B.2.1 | Bogoliubov Theory in the 1D Geometry

In the following, we study a system where the mean-field energy is canceled by a second type of interaction, and the ground state remains always in the lowest harmonic mode of the transverse confinement within mean-field theory. Then, we can derive the Bogoliubov excitation spectrum in analogy to the situation with periodic boundary conditions and perform a perturbation expansion for small values of $\kappa = n_{1\mathrm{D}} a_\mathrm{s}$. We express the bosonic field operator in eigenstates of the non-interacting theory,

$$\psi(\boldsymbol{r}) = \frac{1}{\sqrt{L}} \sum_{v,w} \int \frac{dk}{2\pi} e^{ikx} \varphi_v(y) \varphi_w(z) b_{k,vw} \tag{B.14}$$

where

$$\varphi_w(z) = \frac{1}{\sqrt{2^w w!\, l_\perp \sqrt{\pi}}} H_w(z/l_\perp) e^{-z^2/2l_\perp^2} \tag{B.15}$$

are the eigenfunctions of the harmonic oscillator with the Hermite polynomials H_w and the oscillator length $l_\perp = \sqrt{\hbar/m\omega_\perp}$. The quantum many-body Hamiltonian takes the form

$$H = \sum_k \sum_{v,w} \tilde{\epsilon}_{k,vw} b^\dagger_{k,vw} b_{k,vw} + \frac{1}{2L} \sum_{\substack{k,k',\\ q}} \sum_{\substack{i,i',w,w',\\ j,j',v,v'}} V^{ij,i'j'}_{vw,v'w'}(q) b^\dagger_{k,vw} b^\dagger_{k',v'w'} b_{k'-q,i'j'} b_{k+q,vw}, \tag{B.16}$$

with the excitation spectrum $\tilde{\epsilon}_{k,vw} = \frac{\hbar^2 k^2}{2m} + \hbar\omega_\perp(v+w)$ and the interaction potential

$$\begin{aligned} V^{ij,i'j'}_{vw,v'w'}(q) = \int dx\, dy\, dy'\, dz\, dz'\, V(x,y,y',z,z') e^{iqx} \\ \times \varphi_v(y)\varphi_{v'}(y')\varphi_w(z)\varphi_{w'}(z')\varphi_{i'}(y')\varphi_i(y)\varphi_j(z)\varphi_{j'}(z'). \end{aligned} \tag{B.17}$$

In order to achieve the cancellation of the mean-field energy, we add an attractive interaction with a very long range. The combined interaction potential is suitably chosen as

$$V(x,y,y',z,z') = g\delta(y-y')\delta(z-z')\left(\delta(x) - \frac{1}{\sqrt{\pi r_0^2}} e^{-x^2/r_0^2}\right). \tag{B.18}$$

The first term is the contact interaction with $g = 4\pi\hbar^2 a_\mathrm{s}/m$, whereas the attractive second part will not contribute to the beyond-mean-field corrections due to its long-range character. The mean-field part, however, is strongly influenced by the additional interaction, as $\mu = V^{00,00}_{00,00}(0) = 0$. Following the standard approach by Bogoliubov, we replace the lowest state $b_{0,00}$ by a macroscopic occupation $\sqrt{N_0}$. Then, we express the condensate fraction by

$$N_0 = N - {\sum_{k,vw}}' b^\dagger_{k,vw} b_{k,vw}, \tag{B.19}$$

which is equivalent to switching to a grand canonical description as in Sec. 3.1.1. In leading order in N, we obtain

$$\begin{aligned} H =& \sum_k \sum_{vw} \tilde{\epsilon}_{k,vw} b^\dagger_{k,vw} b_{k,vw} \\ &+ \frac{n_{1\mathrm{D}}}{2} {\sum_{\substack{k,v,w,\\ v',w'}}}' \left[2V_{vw,v'w'} b^\dagger_{k,vw} b_{k,v'w'} + V_{vw,v'w'} b^\dagger_{k,vw} b^\dagger_{-k,v'w'} + V_{vw,v'w'} b_{k,vw} b_{-k,v'w'} \right], \end{aligned} \tag{B.20}$$

where we have introduced

$$V_{vw,v'w'} = g \int dy\, dz\, \varphi_v(y)\varphi_{v'}(y)\varphi_0(y)^2 \varphi_w(z)\varphi_{w'}(z)\varphi_0(z)^2 \tag{B.21}$$

and the primed sum indicates the absence of the condensate mode.

In Sec. 3.1.1, we have detailed the standard approach which allows to easily obtain the Bogoliubov amplitudes and the Bogoliubov spectrum. For the harmonic confinement and with regard to a perturbative treatment for small $\kappa = n_{1\mathrm{D}} a_\mathrm{s}$ in the next section, we want to follow a slightly different approach: We start with the Heisenberg equation

$$i\hbar \dot{b}_{k,vw} = [b_{k,vw}, H] = \tilde{\epsilon}_{k,vw} b_{k,vw} + n_{1\mathrm{D}} \sum_{v',w'} V_{vw,v'w'} (b_{k,v'w'} + b_{-k,v'w'}). \tag{B.22}$$

Then, the second time derivative simplifies to

$$\begin{aligned}(i\hbar)^2\ddot{b}_{k,vw} =&\tilde{\epsilon}^2_{k,vw}b_{k,vw} + \tilde{\epsilon}_{k,vw}n_{1\mathrm{D}}\sum_{v'w'}V_{vw,v'w'}\left(b_{k,v'w'} + b^\dagger_{-k,v'w'}\right)\\ &+ n_{1\mathrm{D}}\sum_{v'w'}V_{vw,v'w'}\left(\tilde{\epsilon}_{k,v'w'}b_{k,v'w'} - \tilde{\epsilon}_{k,v'w'}b^\dagger_{-k,v'w'}\right).\end{aligned} \tag{B.23}$$

Adding and subtracting the adjoint of Eq. (B.23) and making use of the Bogoliubov transformation

$$b_{k,vw} = \sum_{\alpha,\beta} u^{\alpha\beta}_{k,vw}a_{k,\alpha\beta} + v^{\alpha\beta}_{k,vw}a^\dagger_{-k,\alpha\beta}, \tag{B.24}$$

we obtain two equations for the excitation spectrum $\tilde{E}_{k,\alpha\beta}$,

$$\tilde{E}^2_{k,\alpha\beta}f^{+,\alpha\beta}_{k,vw} = \tilde{\epsilon}^2_{k,vw}f^{+,\alpha\beta}_{k,vw} + 2\tilde{\epsilon}_{k,vw}n_{1\mathrm{D}}\sum_{v'w'}V_{vw,v'w'}f^{+,\alpha\beta}_{k,v'w'} \tag{B.25a}$$

$$\tilde{E}^2_{k,\alpha\beta}f^{-,\alpha\beta}_{k,vw} = \tilde{\epsilon}^2_{k,vw}f^{-,\alpha\beta}_{k,vw} + 2n_{1\mathrm{D}}\sum_{v'w'}\tilde{\epsilon}_{k,v'w'}V_{v'w',vw}f^{-,\alpha\beta}_{k,v'w'}, \tag{B.25b}$$

where we have introduced

$$f^{\pm,\alpha\beta}_{k,vw} = u^{\alpha\beta}_{k,vw} \pm v^{\alpha\beta}_{k,vw}. \tag{B.26}$$

Both equations are connected by the relation $f^{+,\alpha\beta}_{k,vw} = \frac{\tilde{\epsilon}_{k,vw}}{\tilde{E}_{k,\alpha\beta}}f^{-,\alpha\beta}_{k,vw}$. As the Bogoliubov transformation has to be canonical, the Bogoliubov functions satisfy

$$\delta_{\alpha,\gamma}\delta_{\beta,\delta} = \sum_{vw} f^{+,\alpha\beta}_{k,vw}f^{-,\gamma\delta}_{k,vw}, \tag{B.27}$$

which determines the normalization of the Bogoliubov functions $f^{\pm,\alpha\beta}_{k,vw}$. The numerical solution of Eq. (B.25) provides the excitation spectrum $\tilde{E}_{k,\alpha\beta}$, the Bogoliubov function $f^{\pm,\alpha\beta}_{k,vw}$ and hence the amplitude $v^{\alpha\beta}_{k,vw}$. This allows us to determine the beyond-mean-field correction by the approach of Hugenholtz and Pines (see Sec. 3.1.2),

$$E^h_{1\mathrm{D}} - \frac{1}{2}\mu N = \frac{L}{2}\int\frac{dk}{2\pi}\sum_{\substack{v,\alpha\\ w,\beta}}\left[\tilde{\epsilon}_{k,vw} - \tilde{E}_{k,\alpha\beta}\right]|v^{\alpha\beta}_{k,vw}|^2. \tag{B.28}$$

B.2.2 | Expansion in the One-Dimensional Regime

In general, Eq.(B.25) has to be solved numerically. In the quasi-one-dimensional regime $\kappa = n_{1\mathrm{D}}a_\mathrm{s} \ll 1$, we can perform a perturbation expansion for $\tilde{E}_{k,\alpha\beta}$ and $f^{\pm,\alpha\beta}_{k,vw}$ in κ to obtain the leading contributions. A consistent expansion in κ turns out to be challenging and we will describe the procedure in detail. We introduce the dimensionless single

particle excitation spectrum $\epsilon_{u,vw} = \tilde{\epsilon}_{k,vw}/(4\pi\hbar^2/ml_\perp^2) = \pi[u^2+(v+w)/(2\pi^2)]/2$ and the dimensionless Bogoliubov spectrum $E_{u,\alpha\beta} = \tilde{E}_{k,\alpha\beta}/(4\pi\hbar^2/ml_\perp^2)$, where $u = kl_\perp/(2\pi)$. In what follows, we will discuss the right-hand side of Eq. (5.31) and separate the different contributions,

$$\begin{aligned}
&\frac{L}{2}\int\frac{dk}{2\pi}\sum_{\substack{v,\alpha\\ w,\beta}}\left[\tilde{\epsilon}_{k,vw}-\tilde{E}_{k,\alpha\beta}\right]|v^{\alpha\beta}_{k,vw}|^2\\
=&2\pi E_0^h\lambda\Bigg(\int du\,\left[\epsilon_{u,00}-E_{u,00}\right]|v^{00}_{u,00}|^2+\int du\sum_{v,w}{}'\left[\epsilon_{u,vw}-E_{u,00}\right]|v^{00}_{u,vw}|^2\\
&+\int du\sum_{\alpha,\beta}{}'\left[\epsilon_{u,00}-E_{u,\alpha\beta}\right]|v^{\alpha\beta}_{u,00}|^2+\int du\sum_{v,w}{}'\sum_{\alpha,\beta}{}'\left[\epsilon_{u,vw}-E_{u,\alpha\beta}\right]|v^{\alpha\beta}_{u,vw}|^2\Bigg),
\end{aligned}\tag{B.29}$$

where we have introduced the energy scale $E_0^h = \hbar\omega_\perp L/a_\mathrm{s}$ and $\lambda = a_\mathrm{s}/l_\perp$. For the first term we determine the Bogoliubov spectrum within second order perturbation theory,

$$E^2_{u,00} = \epsilon^2_{u,00} + 2\epsilon_{u,00}\kappa\eta_{00}\eta_{00} + 4\kappa^2\sum_{v,w}{}'\frac{\epsilon_{u,00}\epsilon_{u,vw}\eta^2_{v0}\eta^2_{w0}}{\epsilon^2_{u,00}-\epsilon^2_{u,vw}},\tag{B.30}$$

where we have introduced the overlap of the harmonic oscillator wave functions

$$\eta_{vw} = l_\perp\int dz\,\varphi_v(z)\varphi_w(z)\varphi_0(z)^2 = \begin{cases}\frac{1}{\sqrt{2\pi}}\frac{(-1)^{(v-w)/2}}{2^{v+w}}\frac{(v+w)!}{(\frac{v+w}{2})!}\frac{1}{\sqrt{v!w!}} & v+w=\text{even}\\ 0 & v+w=\text{odd.}\end{cases}\tag{B.31}$$

The momentum dependence of the third term can be neglected, and we can evaluate the remaining sum over the harmonic oscillator modes,

$$\sum_{v,w}{}'\frac{\eta^2_{v0}\eta^2_{w0}}{v+w} = \frac{\ln(4/3)}{8\pi^2}.\tag{B.32}$$

Thus, the Bogoliubov spectrum reads

$$E^2_{u,00} = \epsilon^2_{u,00} + 2\epsilon_{u,00}\left(\frac{\kappa}{2\pi} - \frac{\ln(4/3)}{\pi}\kappa^2\right).\tag{B.33}$$

For the Bogoliubov function $f^{+,00}_{u,00}$ on the other hand, it is sufficient only to include the lowest order $(f^{+,00}_{u,00})^2 = \frac{\epsilon_{u,00}}{E_{u,00}}$. Any higher order will only provide contribution of order $\kappa^{7/2}$ or higher. We obtain the amplitude

$$|v^{00}_{u,00}|^2 = \frac{1}{4}\left(1-\frac{E_{u,00}}{\epsilon_{u,00}}\right)^2\left(f^{+,00}_{u,00}\right)^2 = \frac{1}{4}\left(1-\frac{E_{u,00}}{\epsilon_{u,00}}\right)^2\frac{\epsilon_{u,00}}{E_{u,00}}\tag{B.34}$$

and perform the momentum integration, which yields

$$2\pi\lambda \int du\ \left[\epsilon_{u,00} - E_{u,00}\right] |v^{00}_{u,00}|^2 = \lambda \left(-\frac{\sqrt{2}}{3\pi}\kappa^{3/2} + \frac{\sqrt{2}\ln(4/3)}{\pi}\kappa^{5/2} \right). \tag{B.35}$$

The first term will provide the beyond-mean-field correction of a one-dimensional system, whereas the second is part of the leading correction. In contrast to the situation with periodic boundary conditions, the leading correction to the one-dimensional behavior is not of order κ^3, but the coupling of the condensate mode to higher harmonic oscillator modes leads to a three-dimensional behavior of the form $\kappa^{5/2}$. Terms of order κ^3 appear in our calculations as well but they are not the dominant correction anymore. In the following we will see, that a consistent expansion up to κ^3 would require to calculate the Bogoliubov functions within second order perturbation theory, which makes a consistent expansion very cumbersome.

We will now continue with the second term of Eq. (B.29). As $(v, w) \neq (\alpha, \beta) = (0, 0)$, we need to calculate the perturbative correction to the Bogoliubov function $f^{\pm,00}_{u,vw}$. In our calculation, we determine $f^{+,00}_{u,vw}$ within first order, take care of the normalization in the relevant order and obtain

$$|v^{00}_{u,vw}|^2 = \frac{1}{4}\left(1 - \frac{E_{u,00}}{\epsilon_{u,vw}}\right)^2 (f^{+,00}_{u,vw})^2 = \kappa^2 \frac{\epsilon_{u,00}}{E_{u,00}} \left(1 - \frac{E_{u,00}}{\epsilon_{u,vw}}\right)^2 \left(\frac{\epsilon_{u,vw}\eta_{v0}\eta_{w0}}{\epsilon^2_{u,00} - \epsilon^2_{u,vw}}\right)^2. \tag{B.36}$$

Although we calculated the Bogoliubov spectrum $E_{u,00}$ up to second order, it is sufficient to use only its lowest order as $v^{00}_{u,vw}$ itself contains orders of κ^2 and higher. Again, we can perform the momentum integration and expand the result in orders of κ,

$$2\pi\lambda \int du \sum_{v,w}{}' \left[\epsilon_{u,vw} - \epsilon_{u,00}\right] |v^{00}_{u,vw}|^2 = \lambda \sum_{vw}{}' \eta^2_{v0}\eta^2_{w0} \left(\frac{2\pi^2\kappa^2}{\sqrt{v+w}} - \frac{16\sqrt{2}\pi}{v+w}\kappa^{5/2} + O(\kappa^3) \right). \tag{B.37}$$

The first term of order κ^2 carries the κ-dependence of the amplitude $|v^{00}_{u,vw}|^2$. Hence, evaluating the Bogoliubov functions up to second order immediately yields additional contributions of order κ^3. In the following we will waive to include those. The second term is another contribution to the energy of order $\kappa^{5/2}$ with the same double sum as in Eq. (B.32).

The procedure for the third term of Eq. (B.29) is very similar to the previous one. It is sufficient to calculate the Bogoliubov spectrum $E_{u,\alpha\beta}$ and the amplitudes $v^{\alpha\beta}_{u,00}$ within first order,

$$E^2_{u,\alpha\beta} = \epsilon^2_{u,\alpha\beta} + 2\kappa\epsilon_{u,\alpha\beta}\eta_{\alpha\alpha}\eta_{\beta\beta} \tag{B.38a}$$

$$|v^{\alpha\beta}_{u,00}|^2 = \kappa^2 \frac{\epsilon_{u,\alpha\beta}}{E_{u,\alpha\beta}} \left(1 - \frac{E_{u,\alpha\beta}}{\epsilon_{u,00}}\right)^2 \left(\frac{\epsilon_{u,00}\eta_{\alpha0}\eta_{\beta0}}{\epsilon^2_{u,\alpha\beta} - \epsilon^2_{u,00}}\right)^2. \tag{B.38b}$$

The expansion for small values of $\kappa \ll 1$ and the momentum integration yields another contribution of order κ^2,

$$2\pi\lambda \int du \sum_{\alpha,\beta}{}' \left[\epsilon_{u,00} - E_{u,\alpha\beta}\right] |v^{\alpha\beta}_{u,00}|^2 = -\lambda \sum_{\alpha,\beta}{}' 2\pi^2 \frac{\eta^2_{\alpha 0}\eta^2_{\beta 0}}{\sqrt{\alpha+\beta}}\kappa^2 + O(\kappa^3), \tag{B.39}$$

which exactly cancels the κ^2 contribution of Eq. (B.37).

For the last term in Eq. (B.29), even the lowest order in the Bogoliubov spectrum $E_{u,\alpha\beta}$ and the amplitudes

$$|v^{\alpha\beta}_{u,vw}|^2 = \frac{1}{4}\left(1 - \frac{E_{u,\alpha\beta}}{\epsilon_{u,vw}}\right)^2 \frac{\epsilon_{u,vw}}{E_{u,\alpha\beta}}\delta_{v\alpha}\delta_{w\beta} \tag{B.40}$$

immediately leads to contributions of order κ^3.

In conclusion, we arrive at a differential equation for $\kappa \ll 1$,

$$E^h_{1\mathrm{D}} - \frac{1}{2}\mu N = E^h_{1\mathrm{D}} - \frac{\kappa}{2}\frac{dE^h_{1\mathrm{D}}}{d\kappa} = \lambda E^h_0 \left(-\frac{\sqrt{2}}{3\pi}\kappa^{3/2} - \frac{\sqrt{2}\ln(4/3)}{\pi}\kappa^{5/2} + O(\kappa^3)\right) \tag{B.41}$$

and its solution reads

$$\frac{E^h_{1\mathrm{D}}}{E^h_0} = \lambda\frac{C^h_{1\mathrm{D}}}{\sqrt{2}}\kappa^2 - \lambda\frac{4\sqrt{2}}{3\pi}\kappa^{3/2} + \lambda\frac{4\sqrt{2}\ln(4/3)}{\pi}\kappa^{5/2} + O(\kappa^3). \tag{B.42}$$

Note that the first term of order κ^2 is not determined by the differential equation, but enters as a constraint as the crossover has to include the leading correction to the confinement-induced resonance, which became evident in the study for periodic boundary conditions. For a harmonic confinement, we confirm this by a full numerical evaluation of the ground-state energy in the crossover form 3D to 1D, which was carried out by Luis Santos. This requires the full numerical evaluation of the Bogoliubov excitation spectrum $E_{u,\alpha\beta}$ and the determination of the factors $|v^{\alpha\beta}_{u,vw}|^2$. Inserting the result in Eq. (5.31) and performing the summation and integration numerically allows us to solve the differential equation and obtain the ground-state energy $E^h_{1\mathrm{D}}$ in the full crossover. We can fix the integration constant at large densities ($\kappa \gg 1$) by requiring the correct mean-field term from the local-density approximation. Then, we can derive the behavior in the one-dimensional regime $\kappa \ll 1$. From our numerical calculations, we obtain the leading corrections in Eq. (14) in the main text, and recover the analytical expressions for $C^h_{1\mathrm{D}}$ with an error of 1%. Remarkably, from the 3D result in local-density approximation, the crossover allows us to recover the expected beyond-mean-field correction for a one-dimensional Bose gas, as well as the correction stemming from the regularization of the 1D scattering length due to the transverse confinement.

Finally, we want to comment on the situation in the 2D geometry with harmonic confinement. The analysis of the ground-state energy in the two-dimensional regime is carried out analogously to the 1D scenario. We find that the leading correction to

the beyond-mean-field energy is of order $\kappa^3 \ln(\kappa)$. This is problematic as a consistent expansion up to order κ^3 would require to determine the Bogoliubov functions $f^{\pm,\alpha}_{\boldsymbol{k},w}$ within second order perturbation theory, as we have already seen in the one-dimensional case.

B.3 | Harmonic Confinement and Dipolar Interactions

We briefly want to derive the leading contribution of the beyond-mean-field correction for dipolar bosons in a one-dimensional geometry. As the full crossover for this setup was discussed in detail in [178], we keep the discussion short and only point out the differences compared to the expansion in Appendix B.2.2.

Analog to Appendix B.2.2, we introduce the energy scale $E_0 = \hbar\omega_\perp L/a_\mathrm{s}$ and start by separating the different contributions,

$$\begin{aligned} E^{\mathrm{dd}}_{\mathrm{1D}} - \frac{1}{2}\mu N =& \frac{L}{2}\int \frac{dk}{2\pi} \sum_{n_r,n_r',m} \left[\tilde{\epsilon}_{k,n_r m} - \tilde{E}_{k,n_r' m}\right] |v^{n_r' m}_{k,n_r m}|^2 \\ =& \frac{E_0^h \lambda}{\pi}\Bigg(\int du\, \left[\epsilon_{u,00} - E_{u,00}\right] |v^{00}_{u,00}|^2 + \int du \sum_{n_r}{}' \left[\epsilon_{u,n_r 0} - E_{u,00}\right] |v^{00}_{u,n_r 0}|^2 \\ &+ \int du \sum_{n_r'}{}' \left[\epsilon_{u,00} - E_{u,n_r' 0}\right] |v^{n_r' 0}_{u,00}|^2 + \int du \sum_{n_r,n_r',m}{}' \left[\epsilon_{u,n_r m} - E_{u,n_r' m}\right] |v^{n_r' m}_{u,n_r m}|^2 \Bigg), \end{aligned} \tag{B.43}$$

where $\epsilon = \tilde{\epsilon}/(2\hbar\omega_\perp) = u^2 + n + |m|/2$ and $E_{u,n_r m}$ is the dimensionless Bogoliubov spectrum. The Bogoliubov amplitudes and the excitation spectrum can be derived within Bogoliubov theory. For that, we simply adapt Eq. (B.25) for the dipolar interaction and obtain

$$E^2_{u,n_r m} f^{+,n_r m}_{u,n_r' m} = \epsilon^2_{k,n_r' m} f^{+,n_r m}_{u,n_r' m} + 2\kappa \epsilon_{u,n_r' m} \sum_{n_r''} U_{n_r',n_r'',m} f^{+,n_r m}_{u,n_r'' m} \tag{B.44a}$$

$$E^2_{u,n_r m} f^{-,n_r m}_{k,n_r' m} = \epsilon^2_{u,n_r' m} f^{-,n_r m}_{u,n_r' m} + 2\kappa \sum_{n_r''} \epsilon_{k,n_r''} U_{n_r'',n_r',m} f^{-,n_r m}_{k,n_r'' m}, \tag{B.44b}$$

in dimensionless units, where the interaction potential for $\varepsilon_{\mathrm{dd}} = 1$ is given by [178]

$$U_{n_r,n_r',m} = C_{n_r,n_r',m} F\left(n_r + n_r' + m, 2u^2\right). \tag{B.45}$$

Here,

$$C_{n_r,n_r',m} = 6\frac{(-1)^{n_r+n_r'}}{2^{n_r+n_r'+m+1}} \sqrt{\binom{n_r + n_r' + m}{n_r}\binom{n_r + n_r' + m}{n_r'}} \tag{B.46}$$

and

$$F(j,\sigma) = \sigma^{j+1} e^\sigma \Gamma(-j,\sigma). \tag{B.47}$$

For a lowest-order expansion in κ, we determine both $E_{u,n_r m}$ and $v_{u,n_r m}^{n_r' m}$ in first-order perturbation theory, which yields

$$E_{u,n_r m}^2 = \epsilon_{u,n_r m}^2 + 2\kappa\epsilon_{u,n_r m} U_{n_r,n_r,m} \tag{B.48}$$

and

$$|v_{u,n_r m}^{n_r' m}|^2 = \frac{1}{4}\left(1 - \frac{E_{n_r' m}}{\epsilon_{n_r m}}\right)^2 \begin{cases} \frac{\epsilon_{u,n_r m}}{E_{u,n_r m}} & n_r = n_r' \\ \left(\frac{2\kappa\epsilon_{u,n_r m} U_{n_r,n_r',m}}{\epsilon_{u,n_r' m}^2 - \epsilon_{u,n_r m}^2}\right)^2 \frac{\epsilon_{u,n_r' m}}{E_{u,n_r' m}} & n_r \neq n_r' \,. \end{cases} \tag{B.49}$$

Under these considerations, the first term in Eq. (B.43) becomes

$$\int du\, \left[\epsilon_{u,00} - E_{u,00}\right] |v_{u,00}^{00}|^2 \overset{\kappa \ll 1}{=} -\frac{\kappa^3}{4} \int du \frac{[C_{0,0,0} F(0, 2u^2)]^3}{u^4} + O(\kappa^4), \tag{B.50}$$

while the second term in Eq. (B.43) can be expanded as

$$\begin{aligned} &\int du \sum_{n_r}{}' \left[\epsilon_{u,n_r 0} - E_{u,00}\right] |v_{u,n_r 0}^{00}|^2 \\ &\overset{\kappa \ll 1}{=} \kappa^2 \sum_{n_r=1}^{\infty} \int du\, n_r \left(\frac{C_{n_r,0,0} F(n_r, 2u^2)}{n_r + 2u^2}\right)^2 \\ &\quad + \kappa^3 \sum_{n_r=1}^{\infty} \int du\, \frac{C_{0,0,0} C_{n_r,0,0}^2 F(0, 2u^2) F(n_r, 2u^2)^2 (n + 3u^2)}{u^2 (n + 2u^2)^2} + O(\kappa^4). \end{aligned} \tag{B.51}$$

The expansion of the third term can be written as

$$\begin{aligned} &\int du \sum_{n_r'}{}' \left[\epsilon_{u,00} - E_{u,n_r' 0}\right] |v_{u,00}^{n_r' 0}|^2 \\ &\overset{\kappa \ll 1}{=} -\kappa^2 \sum_{n_r'=1}^{\infty} \int du\, n_r' \left(\frac{C_{n_r',0,0} F(n_r', 2u^2)}{n_r' + 2u^2}\right)^2 \\ &\quad - \kappa^3 \sum_{n_r'=1}^{\infty} \int du\, \frac{C_{n_r',0,0}^2 C_{n_r',n_r',0} F(n_r', 2u^2)^2 F(2n_r', 2u^2)(2n_r' + 3u^2)}{(n_r' + u^2)(n_r' + 2u^2)^2} + O(\kappa^4). \end{aligned} \tag{B.52}$$

The first term of Eq. (B.51) cancels the first term in Eq. (B.52) such that we are left with contributions $\propto \kappa^3$. Hence, we obtain Eq. (5.39) for the ground-state energy

$$\frac{E_{1D}^{dd}}{E_0} \overset{\kappa \ll 1}{=} \alpha\kappa^2 - \lambda \frac{2B_{1D}^{dd}}{\pi} \kappa^3 + O(\kappa^{7/2}), \tag{5.39 revisited}$$

where

$$\begin{aligned} B_{1\mathrm{D}}^{\mathrm{dd}} = &- \int du\, \frac{[C_{0,0,0}F(0,2u^2)]^3}{4u^4} \\ &- \int du \sum_{n_r=1}^{\infty} \frac{C_{0,0,0}C_{n_r,0,0}^2 F(0,2u^2)F(n_r,2u^2)^2(n+3u^2)}{u^2(n+2u^2)^2} \\ &- \int du \sum_{n_r=1}^{\infty} \frac{C_{n_r,0,0}^2 C_{n_r,n_r,0} F(n_r,2u^2)^2 F(2n_r,2u^2)(2n_r+3u^2)}{(n_r+u^2)(n_r+2u^2)^2} \approx -27.724 \end{aligned} \tag{B.53}$$

is evaluated numerically.

C | Bogoliubov Theory for a Dipolar One-Dimensional Supersolid

C.1 | Ground-State Energy

We obtain the energy in the supersolid phase as a function of $\mathbf{\Delta}$ by inserting the mean-field ansatz Eq. (6.34) into the energy functional (6.36). For four order parameters, we evaluate the integrals analytically and obtain

$$E = NE_t + E_{\text{kin}} + E_{\text{int}} + E_{\text{LHY}}, \tag{C.1}$$

where

$$\frac{E_{\text{kin}}}{N} = E_\perp \frac{(k_\text{s} l_\perp)^2}{4} \frac{\Delta_1^2 + 4\Delta_2^2 + 9\Delta_3^2 + 16\Delta_4^2}{1 + \frac{\Delta_1^2}{2} + \frac{\Delta_2^2}{2} + \frac{\Delta_3^2}{2} + \frac{\Delta_4^2}{2}}, \tag{C.2}$$

$$\begin{aligned}\frac{E_{\text{int}}}{N} = \Bigg[& \frac{(2 + \Delta_1^2 + \Delta_2^2 + \Delta_3^2 + \Delta_4^2)^2}{2} nV(0) + (\Delta_1(2 + \Delta_2) + \Delta_3(\Delta_2 + \Delta_4))^2 nV(k_\text{s}) \\ & + \frac{(\Delta_1^2 + 2\Delta_1\Delta_3 + 2\Delta_2(2 + \Delta_4))^2}{4} nV(2k_\text{s}) + (2\Delta_3 + \Delta_1(\Delta_2 + \Delta_4))^2 nV(3k_\text{s}) \\ & + \frac{(\Delta_2^2 + 2\Delta_1\Delta_3 + 4\Delta_4)^2}{4} nV(4k_\text{s}) + (\Delta_2\Delta_3 + \Delta_1\Delta_4)^2 nV(5k_\text{s}) \\ & + \frac{(\Delta_3^2 + 2\Delta_2\Delta_4)^2}{4} nV(6k_\text{s}) + \Delta_3^2\Delta_4^2 nV(7k_\text{s}) \\ & + \frac{\Delta_4^4}{4} nV(8k_\text{s}) \Bigg] \Bigg/ (2 + \Delta_1^2 + \Delta_2^2 + \Delta_3^2 + \Delta_4^2)^2.\end{aligned} \tag{C.3}$$

Close to the phase transition

$$1 + \sum_{l=1}^{4} \Delta_l \cos(lx) > 0 \quad \forall \quad x \tag{C.4}$$

and the absolute value in Eq. (6.36) can be ignored which yields

$$\begin{aligned}\frac{E_{\mathrm{LHY}}}{N} =&\gamma_{\mathrm{QF}} n^{3/2}\Bigg[\frac{2}{5}+\frac{1}{8}\Big(\Delta_1^4(6+4\Delta_2+\Delta_4)+4\Delta_1^3\Delta_3(2+3\Delta_2+3\Delta_4)\\ &+2\Delta_1^2\big\{8+3\Delta_2^3+12\Delta_4^2+6\Delta_2^2(2+\Delta_4)+3\Delta_3^2(4+\Delta_4)\\ &\qquad+6\Delta_2(2+\Delta_3^2+\Delta_4(2+\Delta_4))\big\}\\ &+12\Delta_1\Delta_3\big\{\Delta_2^3+2\Delta_2^2(1+\Delta_4)+\Delta_4(4+\Delta_3^2+\Delta_4^2)\\ &\qquad+\Delta_2(4+\Delta_3^2+2\Delta_4(2+\Delta_4))\big\}\\ &+2\Big\{\Delta_2^3\Delta_3^2+3\Delta_3^4+8\Delta_4^2+3\Delta_4^4+3\Delta_2\Delta_3^2\Delta_4(4+\Delta_4)\\ &\qquad+\Delta_2^4(3+2\Delta_4)+4\Delta_3^2(2+3\Delta_4^2)\Big\}\\ &+2\Delta_2^2\Big\{8+6\Delta_3^2(2+\Delta_4)+3\Delta_4(2+\Delta_4)^2\Big\}\Big)\Bigg]\Big/\Big(1+\frac{\Delta_1^2}{2}+\frac{\Delta_2^2}{2}+\frac{\Delta_3^2}{2}+\frac{\Delta_4^2}{2}\Big)^{\frac{5}{2}}.\end{aligned} \tag{C.5}$$

The ground state is then obtained by minimizing the energy with respect to $\Delta_1,\dots,\Delta_4$, k_{s}, σ and ν.

C.2 | Excitations

We calculate the matrices $\boldsymbol{\chi}$ and $\boldsymbol{\eta}$ by including two order parameters and expanding the Hamiltonian 6.19 up to quadratic order in the creation and annihilation operators. The procedure is straightforward but tedious and we obtain

$$\boldsymbol{\chi}=\boldsymbol{x}+\frac{1}{2}\frac{\gamma_{\mathrm{QF}}n^{3/2}}{(1+\frac{\Delta_1^2}{2}+\frac{\Delta_2^2}{2})^{3/2}}\boldsymbol{\Lambda}\quad\text{and}\quad\boldsymbol{\eta}=\frac{\boldsymbol{h}}{1+\frac{\Delta_1^2}{2}+\frac{\Delta_2^2}{2}}+\frac{3}{4}\frac{\gamma_{\mathrm{QF}}n^{3/2}}{(1+\frac{\Delta_1^2}{2}+\frac{\Delta_2^2}{2})^{3/2}}\boldsymbol{\Lambda} \tag{C.6}$$

where $\boldsymbol{x}$, $\boldsymbol{h}$, and $\boldsymbol{\Lambda}$ are symmetric 5×5 matrices with entries

$$x_{11}=\epsilon_0(q)-\mu+E_t+nV(0), \tag{C.7}$$

$$x_{22}=\epsilon_0(q+k_{\mathrm{s}})-\mu+E_t+nV(0), \tag{C.8}$$

$$x_{33}=\epsilon_0(q-k_{\mathrm{s}})-\mu+E_t+nV(0), \tag{C.9}$$

$$x_{44}=\epsilon_0(q+2k_{\mathrm{s}})-\mu+E_t+nV(0), \tag{C.10}$$

$$x_{55}=\epsilon_0(q-2k_{\mathrm{s}})-\mu+E_t+nV(0), \tag{C.11}$$

$$x_{12}=x_{13}=x_{24}=x_{35}=\frac{\Delta_1\left(\frac{\Delta_2}{2}+1\right)nV\left(k_s\right)}{1+\frac{\Delta_1^2}{2}+\frac{\Delta_2^2}{2}}, \tag{C.12}$$

$$x_{14} = x_{15} = x_{23} = \frac{\left(\frac{\Delta_1^2}{4} + \Delta_2\right) nV\left(2k_s\right)}{1 + \frac{\Delta_1^2}{2} + \frac{\Delta_2^2}{2}}, \tag{C.13}$$

$$x_{25} = x_{34} = \frac{\Delta_1 \Delta_2 nV\left(3k_s\right)}{2\left(1 + \frac{\Delta_1^2}{2} + \frac{\Delta_2^2}{2}\right)}, \tag{C.14}$$

$$x_{45} = \frac{\Delta_2^2 nV\left(4k_s\right)}{4\left(1 + \frac{\Delta_1^2}{2} + \frac{\Delta_2^2}{2}\right)}, \tag{C.15}$$

$$\Lambda_{i,i} = 2\left(\frac{3}{4}\Delta_2\Delta_1^2 + \frac{3\Delta_1^2}{2} + \frac{3\Delta_2^2}{2} + 1\right), \tag{C.16}$$

$$\Lambda_{12} = \Lambda_{13} = \Lambda_{24} = \Lambda_{35} = \frac{3\Delta_1^3}{4} + \frac{3}{2}\Delta_2^2\Delta_1 + 3\Delta_2\Delta_1 + 3\Delta_1, \tag{C.17}$$

$$\Lambda_{14} = \Lambda_{15} = \Lambda_{23} = \frac{3\Delta_2^3}{4} + \frac{3}{2}\Delta_1^2\Delta_2 + 3\Delta_2 + \frac{3\Delta_1^2}{2}, \tag{C.18}$$

$$\Lambda_{25} = \Lambda_{34} = \frac{\Delta_1^3}{4} + \frac{3}{4}\Delta_2^2\Delta_1 + 3\Delta_2\Delta_1, \tag{C.19}$$

$$\Lambda_{45} = \frac{3}{4}\Delta_2\Delta_1^2 + \frac{3\Delta_2^2}{2}, \tag{C.20}$$

$$h_{11} = \frac{\Delta_1^2}{4}\left[nV\left(q - k_s\right) + nV\left(k_s + q\right)\right] + \frac{\Delta_2^2}{4}\left[nV\left(q - 2k_s\right) + nV\left(2k_s + q\right)\right] + nV\left(q\right), \tag{C.21}$$

$$h_{22} = \frac{\Delta_1^2}{4}\left[nV\left(2k_s + q\right) + nV\left(q\right)\right] + \frac{\Delta_2^2}{4}\left[nV\left(q - k_s\right) + nV\left(3k_s + q\right)\right] + nV\left(k_s + q\right), \tag{C.22}$$

$$h_{33} = \frac{\Delta_1^2}{4}\left[nV\left(q - 2k_s\right) + nV\left(q\right)\right] + \frac{\Delta_2^2}{4}\left[nV\left(q - 3k_s\right) + nV\left(k_s + q\right)\right] + nV\left(q - k_s\right), \tag{C.23}$$

$$h_{44} = \frac{\Delta_1^2}{4}\left[nV\left(k_s + q\right) + nV\left(3k_s + q\right)\right] + \frac{\Delta_2^2}{4}\left[nV\left(4k_s + q\right) + nV\left(q\right)\right] + nV\left(2k_s + q\right), \tag{C.24}$$

$$h_{55} = \frac{\Delta_1^2}{4}\left[nV\left(q - 3k_s\right) + nV\left(q - k_s\right)\right] + \frac{\Delta_2^2}{4}\left[nV\left(q - 4k_s\right) + nV\left(q\right)\right] + nV\left(q - 2k_s\right), \tag{C.25}$$

$$h_{12} = \frac{\Delta_1}{2}\left[nV\left(k_s+q\right)+nV\left(q\right)\right]+\frac{\Delta_1\Delta_2}{4}\left[nV\left(q-k_s\right)+nV\left(2k_s+q\right)\right], \tag{C.26}$$

$$h_{13} = \frac{\Delta_1}{2}\left[nV\left(q-k_s\right)+nV\left(q\right)\right]+\frac{\Delta_1\Delta_2}{4}\left[nV\left(q-2k_s\right)+nV\left(k_s+q\right)\right], \tag{C.27}$$

$$h_{14} = \frac{\Delta_1^2}{4}nV\left(k_s+q\right)+\frac{\Delta_2}{2}\left[nV\left(2k_s+q\right)+nV\left(q\right)\right], \tag{C.28}$$

$$h_{15} = \frac{\Delta_1^2}{4}nV\left(q-k_s\right)+\frac{\Delta_2}{2}\left[nV\left(q-2k_s\right)+nV\left(q\right)\right], \tag{C.29}$$

$$h_{23} = \frac{\Delta_2}{2}\left[nV\left(q-k_s\right)+nV\left(k_s+q\right)\right]+\frac{\Delta_1^2}{4}nV\left(q\right), \tag{C.30}$$

$$h_{24} = \frac{\Delta_1}{2}\left[nV\left(k_s+q\right)+nV\left(2k_s+q\right)\right]+\frac{\Delta_1\Delta_2}{4}\left[nV\left(3k_s+q\right)+nV\left(q\right)\right], \tag{C.31}$$

$$h_{25} = \frac{\Delta_1\Delta_2}{4}\left[nV\left(q-k_s\right)+nV\left(q\right)\right], \tag{C.32}$$

$$h_{34} = \frac{\Delta_1\Delta_2}{4}\left[nV\left(k_s+q\right)+nV\left(q\right)\right], \tag{C.33}$$

$$h_{35} = \frac{\Delta_1\Delta_2}{4}\left[nV\left(q-3k_s\right)+nV\left(q\right)\right]+\frac{\Delta_1}{2}\left[nV\left(q-2k_s\right)+nV\left(q-k_s\right)\right], \tag{C.34}$$

$$h_{45} = \frac{\Delta_2^2}{4}nV\left(q\right). \tag{C.35}$$

D | Quantum Fluctuations in One-Dimensional Supersolids

D.1 | Transformation Matrix

The canonical transformation which decouples the Hamiltonian (7.9) is given by [85, 191]

$$\mathbf{Q} = \sqrt[4]{\frac{v_J}{v_N}} \begin{pmatrix} \sqrt{\frac{\gamma\hat{v}_+^2 - \beta^2\lambda(1-\gamma)}{\gamma\hat{v}_+\sqrt{\Delta}}} & -s_{1-}s_{2-}\beta\sqrt{\frac{\hat{v}_+^2-(1-\gamma)}{\gamma\hat{v}_+\sqrt{\Delta}}} \\ -\sqrt{-\frac{\gamma\hat{v}_-^2 - \beta^2\lambda(1-\gamma)}{\gamma\hat{v}_-\sqrt{\Delta}}} & s_{1+}s_{2+}\beta\sqrt{-\frac{\hat{v}_-^2-(1-\gamma)}{\gamma\hat{v}_-\sqrt{\Delta}}} \end{pmatrix}, \tag{D.1a}$$

$$\mathbf{Q}^{-1} = \sqrt[4]{\frac{v_N}{v_J}} \begin{pmatrix} s_{1+}\sqrt{\frac{\gamma\hat{v}_+^2 - \beta^2(\lambda-\xi^2)}{\gamma\hat{v}_+\sqrt{\Delta}}} & s_{1-}\sqrt{-\frac{\gamma\hat{v}_-^2 - \beta^2(\lambda-\xi^2)}{\gamma\hat{v}_-\sqrt{\Delta}}} \\ s_{2+}\sqrt{\frac{\lambda\hat{v}_+^2 - (\lambda-\xi^2)}{\hat{v}_+\sqrt{\Delta}}} & s_{2-}\sqrt{-\frac{\lambda\hat{v}_-^2 - (\lambda-\xi^2)}{\hat{v}_-\sqrt{\Delta}}} \end{pmatrix}. \tag{D.1b}$$

Here, we have introduced the dimensionless velocities $\hat{v}_\sigma = v_\sigma/\sqrt{v_J v_N}$ and

$$\Delta = (1 - 2\xi\beta + \beta^2\lambda/\gamma)^2 - 4\beta^2(\lambda - \xi^2)(1-\gamma)/\gamma. \tag{D.2}$$

The signs $s_{i\sigma}$ are given by

$$s_{i\sigma} = \operatorname{sign}\left[\begin{pmatrix} \frac{1}{2}\left[1 - \beta^2\lambda/\gamma + \sigma\sqrt{\Delta}\right] \\ \xi - \beta\lambda \end{pmatrix}_i\right]. \tag{D.3}$$

Ausführliche Zusammenfassung in deutscher Sprache

Ein Aggregatzustand, welcher rein aus der Quantenstatistik seiner Bestandteile resultiert, zog bereits vor knapp 100 Jahren das Interesse von Physikern auf sich. In einer im Jahre 1924 an Albert Einstein gesendeten Abhandlung demonstrierte der indische Physiker Satyendranath Bose, dass das Plancksche Strahlungsgesetz hergeleitet werden kann ohne auf Resultate aus der klassischen Physik zurückzugreifen [1]. Einstein erweiterte die Theorie auf massebehaftete Teilchen, die der gleichen Statistik wie Photonen genügen [2, 3]. Dies ermöglichte ihm zu zeigen, dass ein homogenes ideales Gas dieser Teilchen bei niedrigen Temperaturen einen Phasenübergang zu einer Phase erlaubt, in welcher der niedrigste Energiezustand makroskopisch besetzt ist. Diese Phase ist heute als *Bose-Einstein-Kondensat* bekannt und es ist erstaunlich, dass Einsteins Vorhersage über die Existenz dieses Zustandes unserer heutigen Formulierung der Quantenmechanik und der Einteilung der Teilchen in Bosonen und Fermionen vorausging.

Obwohl die theoretischen Beschreibungen von Bose-Einstein-Kondensaten die wir heute heranziehen, wie zum Beispiel die erste mikroskopische Beschreibung von schwach wechselwirkenden Bosonen von Bogoliubov [4], die feldtheoretischen Ansätze sowohl von Beliaev [5, 6] als auch von Hugenholtz und Pines [7], sowie die Beschreibung im Sinne einer Molekularfeldtheorie durch eine makroskopische Wellenfunktion von Gross und Pitaevskii [8, 9] bereits in der Mitte des letzten Jahrhunderts entwickelt wurden, blieb die experimentelle Realisierung dieses Zustandes für weitere Jahrzehnte undenkbar.

Erst Fortschritte in der laserbasierten Kühlung und Erzeugung von Fallen in den 1980er Jahren, welche durch den Nobel Preis an Claude Cohen-Tannoudji, Steven Chu und William Daniel Phillips im Jahre 1997 geehrt wurden [10–12], ermöglichten Temperaturen, die für die Kondensation von Bosonen benötigt werden. Schließlich wurden im Jahre 1995 die ersten Bose-Einstein-Kondensate in Boulder von Eric Cornell und Carl Wieman [13] und kurz darauf auch in der Gruppe von Wolfgang Ketterle am MIT [14] erzeugt. Die erfolgreiche Erzeugung eines Bose-Einstein-Kondensates resultierte nicht nur in einem Nobel Preis für Cornell, Wieman und Ketterle im Jahre 2001, sondern führte auch zu einem stetig wachsenden Forschungsfeld, welches sich mit ultrakalten Quantengasen beschäftigt.

Seitdem wurden Experimente mit ultrakalten Atomen zu einer Spielwiese um quantenmechanische Vielteilchenphänomene zu untersuchen und auf fundamentaler Weise zu verstehen [15]. Insbesondere Feshbach-Resonanzen [16–18], welche es erlauben die Wechselwirkungsstärke zwischen den Teilchen zu beeinflussen und die Verwendung von

optischen Potentialen um die Dimension des Gases zu reduzieren oder optische Gitter einzuführen, liefern eine Kontrolle über die Systeme, die kaum eine andere Plattform bieten kann. In der Zwischenzeit wurde die Kohärenz der Kondensate durch das Überlappen zweier Bose-Einstein-Kondensate gezeigt [19], während das Auftreten von Vortices durch das Rühren eines Bose-Einstein-Kondensates mit einem Laserstrahl klar deren Suprafluidität demonstriert [20]. Enge optische Fallen erlauben es niedrigdimensionale Systeme zu untersuchen und das stark wechselwirkende Regime zu erkunden, welches zum Beispiel die experimentelle Realisierung des Tonks-Girardeau Gases ermöglichte [21–24]. Bose-Einstein-Kondensate in optischen Gittern haben es ermöglicht den Phasenübergang einer Supraflüssigkeit zu einem Mott-Isolator zu untersuchen [25] und stellen eine erfolgsversprechende Plattform für Quantensimulationen dar [26–29]. Da das Erzeugen von Bose-Einstein-Kondensaten in heutigen Laboren zur Routine geworden ist, werden diese nicht nur für die Quantensimulation sondern auch für Quantensensoren verwendet [30, 31]. Diese Quantensensoren können unter anderem verwendet werden um die Grundlagen der allgemeinen Relativitätstheorie zu testen [32, 33] und das sogar im Weltraum [34].

Die Liste der Errungenschaften ist natürlich deutlich länger als wir in dieser Zusammenfassung behandeln können. Von besonderem Interesse für diese Arbeit sind allerdings dipolare Bose-Einstein-Kondensate, auf die wir uns im Folgenden konzentrieren. Alkali Atome, wie zum Beispiel Rubidium (^{87}Rb) oder Natrium (^{23}Na), welche für die ersten Realisierungen von Bose-Einstein-Kondensaten verwendet wurden [13, 14], besitzen ein, im Vergleich zu der Van-der-Waals Wechselwirkung, kleines magnetisches Moment, sodass die Wechselwirkung zwischen den Teilchen vollständig durch die s-Wellen-Streulänge beschrieben werden kann. Für Bose-Einstein-Kondensate, welche aus dipolaren Atomen bestehen, wird dies durch die langreichweitigen und anisotropen Eigenschaften der dipolaren Wechselwirkung verhindert. Es wurde allerdings gezeigt, dass die Wechselwirkung durch eine Kombination des dipolaren Potentials und einer kurzreichweitigen Kontaktwechselwirkung, welche durch eine s-Wellen-Streulänge charakterisiert ist, präzise beschrieben werden kann [35, 36]. Die Anisotropie der dipolaren Wechselwirkung in Kombination mit der Möglichkeit deren Einfluss durch das Verändern der s-Wellen-Streulänge zu modifizieren, führt zu einer Fülle neuer Phänomene [37–40]. Da ein tiefgehendes Verständnis über die Wechselwirkungen in ultrakalten Quantengasen unabdingbar für diese Arbeit ist, werden wir die fundamentalen Konzepte der Streutheorie in Kapitel 2 behandeln.

Mit der Kondensierung von Chrom (^{52}Cr) mit einem magnetischen Moment von $6\mu_\mathrm{B}$ (μ_B ist das Bohrsche Magneton) wurde im Jahr 2004 das erste dipolare Bose-Einstein-Kondensat in der Gruppe von Tilman Pfau in Stuttgart erzeugt [41]. Später wurden auch Atome mit einem größeren magnetischen Moment wie zum Beispiel Erbium (^{168}Er) [42] mit einem magnetischen Moment von $7\mu_\mathrm{B}$ oder Dysprosium (^{164}Dy) [43], welches das größte magnetische Moment unter den bosonischen Elementen besitzt ($10\mu_\mathrm{B}$), kondensiert. Wir möchten anmerken, dass die (elektrische) dipolare Wechselwirkungsstärke von polaren Molekülen um einige Größenordnungen größer ist [37], jedoch steht deren

Kondensation zu diesem Zeitpunkt noch aus, ist aber in greifbarer Nähe.

Im Jahr 2016 stieg das Interesse an dipolaren Bose-Einstein-Kondensaten zu neuen Höhen. Grund dafür war die Beobachtung der Bildung von stabilen Tröpfchen in einem dipolaren Bose-Einstein-Kondensat aus ^{164}Dy in Stuttgart [44–46], während später auch Tröpfchen in ^{162}Dy [47] und ^{168}Er [48] beobachtet wurden. Um die Bedeutung dieser Beobachtungen zu verstehen, müssen wir kurz zur theoretischen Beschreibung dieser schwach wechselwirkenden Systeme zurückkehren. Die Beschreibung der Systeme durch die bereits erwähnte Gross-Pitaevskii Gleichung [8, 9] war für viele Jahre ausreichend um die experimentellen Beobachtungen zu verstehen. Im Bereich, in dem die Tröpfchen auftreten, sagt diese Molekularfeldtheorie allerdings den Kollaps des Bose-Einstein-Kondensates voraus und es wird kein stabiler Grundzustand erwartet. Warum also treten diese Tröpfchen auf? Kurz nach deren Entdeckung wurde der Stabilisierungsmechanismus auf Korrekturen zur Molekularfeldtheorie zurückgeführt [45]. Dieser Stabilisierungsmechanismus wurde zuerst für Bose-Bose Mischungen vorhergesagt [49] und später wurden auch Tröpfchen in Bose-Bose Mischungen experimentell beobachtet [50, 51]. Für ein homogenes Bose-Einstein-Kondensat mit kurzreichweitigen Wechselwirkungen wurden diese Korrekturen zur Molekularfeldtheorie von Lee, Huang und Yang hergeleitet [52, 53] und sind typischerweise als LHY Korrekturen bekannt. Später wurden die Korrekturen auch für homogene dipolare Bose-Einstein-Kondensate im Bereich berechnet, in welchem die kurzreichweitige Kontaktwechselwirkung über die langreichweitige dipolare Wechselwirkung dominiert [54]. Falls allerdings die dipolare Wechselwirkung stärker als die Kontaktwechselwirkung ist, tritt im System eine Instabilität bei großen Wellenlängen auf, welche als *Phononinstabilität* bezeichnet wird [37]. Dies führt zu komplexen Korrekturen zur Molekularfeldtheorie und zu einem Zusammenbrechen der derzeitigen Beschreibung. Zwei Methoden, mit denen die Korrekturen zur Molekularfeldtheorie bestimmt werden können, werden wir detailliert in Kapitel 3 behandeln. In Kapitel 8 schlagen wir zudem einen Formalismus vor, mit dem die Beschreibung der Korrekturen zur Molekularfeldtheorie für die Tröpfchen verbessert werden könnte.

Der Einfluss der LHY Korrekturen auf kontaktwechselwirkende Bose-Einstein-Kondensate konnte in den vergangenen Jahren durch die Messungen der Minderung der Anzahl der Kondensatteilchen [55], sowie durch die Messung von Korrekturen zur Grundzustandsenergie [56] und zum Anregungsspektrum [57, 58] bestätigt werden. Für all diese Situationen sorgen die LHY Terme für Korrekturen zum Resultat der Molekularfeldtheorie, während für die dipolaren Tröpfchen der Beitrag der Molekularfeldtheorie verschwindet und somit die Korrekturen zur führenden Ordnung werden und für deren Stabilität sorgen. Für die theoretische Beschreibung der Tröpfchen ist es deshalb notwendig diese Korrekturen sehr genau zu bestimmen. Die derzeitige Beschreibung der Tröpfchen ist jedoch nicht frei von Mängeln. Obwohl die Tröpfchen anisotrop und inhomogen sind, verlässt sich die derzeitige Beschreibung auf die Annahme, dass das System lokal als homogen betrachtet werden darf (lokale Dichtenäherung). Die Korrekturen führen dann zu einem zusätzlichen Term in der Gross-Pitaevskii Gleichung, was zur *erweiterten* Gross-Pitaevskii führt [39, 40, 45]. Die Tröpfchen treten in dem Bereich auf, in

dem die dipolare Wechselwirkung stärker als die Kontaktwechselwirkung ist, was zur Folge hat, dass die Verwendung der lokalen Dichtenäherung zu den bereits erwähnten Unstimmigkeiten durch die Phononinstabilität führt. Da der Imaginärteil der Korrekturen allerdings klein ist, wird dieser typischerweise einfach ignoriert. Eine selbstkonsistente Beschreibung der Korrekturen zur Molekularfeldtheorie für diese Tröpfchen steht allerdings immer noch aus. In Kapitel 5 untersuchen wir die Korrekturen zur Molekularfeldtheorie für beschränkte Systeme mit Kontaktwechselwirkungen im Kontext eines dimensionellen Übergangs um die Gültigkeit der lokalen Dichtenäherung zu überprüfen.

Obwohl die ersten Tröpfchen in einer Falle beobachtet wurden, sollte nicht vergessen werden, dass durch das Zusammenspiel der repulsiven Kontaktwechselwirkung und dem attraktiven Anteil der dipolaren Wechselwirkung die Tröpfchen selbst-gebunden sind [47, 59–63]. Eine Falle kann jedoch sehr vorteilhaft sein, da diese das Anregungsspektrum durch die Anisotropie der dipolaren Wechselwirkung stark beeinflussen kann. In einer Falle können dipolare Bose-Einstein-Kondensate ein Roton-Spektrum aufweisen [64–66], ähnlich zu dem Spektrum in suprafluiden Helium [67–71]. Während das Roton-Spekrum das typische lineare Verhalten für große Wellenlängen zeigt, besitzt es auch ein Minimum bei endlicher Wellenlänge, dessen Position und Tiefe in dipolaren Kondensaten beeinflusst werden kann. Das Minimum führt damit eine neue Längenskala für die Selbstorganisation ein. Im Jahre 2017 stellte sich heraus, dass auch mehrere Tröpfchen den Grundzustand darstellen können [72, 73]. Das machte dipolare Bose-Einstein-Kondensate zu einem vielversprechenden Kandidaten um die suprasolide Phase zu realisieren [74].

Ein Suprasolid besitzt die Eigenschaften eines Supraleiters, da es einen verlustfreien Strom ermöglicht, und die Dichtemodulation eines Festkörpers [75]. Theoretisch ist das Suprasolid üblicherweise als Zustand definiert, der spontan die $U(1)$ Symmetrie bricht, was zu nebendiagonaler langreichweitiger Ordnung der Einteilchen-Dichtematrix führt [76, 77] und ebenfalls spontan die Translationsinvarianz bricht, was zu diagonaler langreichweitiger Ordnung führt. Es sollte jedoch angemerkt werden, dass dies nicht die allgemeinste Definition dieses Zustandes ist, da in einer räumlichen Dimension die spontane Symmetriebrechung stark durch Quantenfluktuationen beeinflusst wird [78–80]. Es kann aber immer noch zu quasi-diagonaler und quasi-nebendiagonaler Ordnung kommen [81–85], was einen suprafluiden Festkörper, also ein Suprasolid, selbst in einer räumlichen Dimension ermöglicht. Der Einfluss von Quantenfluktuationen auf den suprasoliden Zustand in einer Dimension wird im Detail in Kapitel 7 diskutiert.

Durch seine auf den ersten Blick widersprüchlichen Eigenschaften wurde der suprasolide Zustand 1957 anfänglich für unmöglich gehalten [77], jedoch ohne konkreten Beweis, wodurch das Interesse an diesem exotischen Zustand in den folgenden Jahren ungebrochen war [86–89]. Die Möglichkeit eines suprasoliden Grundzustandes wurde letztendlich von Anthony James Leggett im Jahre 1970 gezeigt, indem er eine obere Grenze für den suprafluiden Anteil des Suprasolids herleitete [90].

Die Suche nach einem Suprasolid fokussierte sich lange auf solides Helium (^{4}He) [75, 91–93]. Während suprasolide Eigenschaften in ^{4}He im Jahre 2004 berichtet wurden [94],

mussten diese Ergebnisse allerdings später wieder zurückgezogen werden [95], sodass es bis heute keinen zwingenden Beweis für Suprasolidität in ^{4}He gibt. Suprasolide Eigenschaften wurden allerdings in Supraflüssigkeiten, in denen Wechselwirkungen durch Resonatoren vermittelt werden [96, 97], als auch in Spin-Bahn gekoppelten Bose-Einstein-Kondensaten beobachtet [98]. In all diesen experimentellen Realisierungen wird die Periodizität jedoch durch das externe Lichtfeld vorgegeben.

Im Gegensatz dazu resultiert die Dichtemodulation in einem dipolaren Quantengas rein aus den Wechselwirkungen zwischen den Teilchen. Während die ersten Aufreihungen von Tröpfchen noch nicht phasenkohärent waren [72], haben spätere Experimente, zunächst in der Gruppe von Giovanni Modugno in Pisa [99] und kurz darauf auch in der Gruppe von Tilman Pfau in Stuttgart [100] und in der Gruppe von Francesca Ferlaino in Innsbruck [101], die globale Phasenkohärenz zwischen den Tröpfchen gezeigt. Die Beobachtung der Goldstone Moden, welche aus den zwei spontan gebrochenen Symmetrieen hervorgehen [102–105], hat dann den echten suprasoliden Charakter dieser Tröpfchen bestätigt [106], während später auch höhere Anregungen untersucht wurden [107–109].

Die experimentellen Anstrengungen den suprasoliden Zustand zu realisieren, wurden durch gründliche theoretische Untersuchungen des Suprasolids und dessen Anregungsspektrums begleitet [74, 85, 100, 101, 110–114, 116–128, 186]. Wie bei den Tröpfchen baut die theoretische Beschreibung hauptsächlich auf die erweiterte Gross-Pitaevskii Gleichung. Numerische Untersuchungen für das experimentelle dreidimensionale System stimmen gut mit den experimentellen Beobachtungen überein [39, 40], jedoch sind Aussagen zum thermodynamischen Limes sowie über die Art des Phasenübergangs von der Supraflüssigkeit zum Suprasolid mit diesen Methoden schwierig zu treffen [74, 127]. In Kapitel 6 präsentieren wir eine analytische Untersuchung des Phasenübergangs und diskutieren das Anregungsspektrum über den Übergang hinweg.

Natürlich hat die erste Beobachtung der suprasoliden Phase in dipolaren Gasen das Interesse an dieser Phase nicht einfach beendet. Die Realisierung und Untersuchung zweidimensionaler Suprasolids [118–120, 129, 130], der Einfluss der endlichen Temperatur auf diese Systeme [123] und das Entwickeln einer selbstkonsistenten Theorie für die Korrekturen zur Molekularfeldtheorie ist nur eine kleine Auswahl an Themen, die derzeit untersucht werden. Dies macht deutlich, dass dipolare Quantengase eine flexible Plattform darstellen, die auch in Zukunft aufregende Möglichkeiten bietet um quantenmechanische Vielteilchenphänomene zu untersuchen.

In dieser Arbeit untersuchen wir die Korrekturen zur Molekularfeldtheorie in beschränkten Systemen und überprüfen die Gültigkeit der lokalen Dichtenäherung mit einem Modellsystem. In einer eindimensionalen Geometrie leiten wir das Anregungsspektrum beim Übergang von einem Suprafluid zu einem Suprasolid her und demonstrieren damit seine Stabilität. Zudem untersuchen wir den Einfluss von Quantenfluktuationen auf die Bildung des eindimensionalen Suprasolids und zeigen, dass für derzeitige experimentelle Parameter die Verwendung der erweiterten Gross-Pitaevskii Gleichung gerechtfertigt

ist. Die Kapitel umfassen die folgenden Inhalte:

- In Kapitel 1 geben wir eine Einführung in das Feld der ultrakalten dipolaren Quantengase
- In Kapitel 2 diskutieren wir die generellen Konzepte der Streutheorie, welche notwendig sind um die Wechselwirkungen in ultrakalten bosonischen Gasen zu beschreiben. Wir führen ein Zwei-Kanal-Modell ein um kurzreichweitige Wechselwirkungen zu beschreiben und diskutieren anschließend kurz die Streuung von dipolaren Teilchen.
- In Kapitel 3 stellen wir zwei fundamentale Methoden mit denen Korrekturen zur Molekularfeldtheorie bestimmt werden können vor und wenden sie exemplarisch auf das dreidimensionale schwach wechselwirkende Bose Gas an. Wir diskutieren kurz die Vor- und Nachteile der jeweiligen Methode und geben eine kurze Übersicht über bereits bekannte Korrekturen in anderen Systemen, welche für diese Arbeit relevant sind.
- In Kapitel 4 verwenden wir das Zwei-Kanal-Modell um die Streuung in beschränkten Systemen zu beschreiben. Wir leiten die *confinement-induced resonance* für eine eindimensionale Geometrie mit periodischen Randbedingungen her und verwenden unsere Methode um die bereits bekannten Resultate für eine zweidimensionale Geometrie mit periodischen Randbedingungen als auch die Resultate für eine harmonische Falle zu reproduzieren.
- In Kapitel 5 untersuchen wir das Verhalten der Korrekturen zur Molekularfeldtheorie eines schwach wechselwirkenden Bose Gases im Kontext eines dimensionellen Übergangs von drei Dimensionen zu einer beziehungsweise zwei Dimensionen. Für eine Box mit periodischen Randbedingungen leiten wir eine analytische Lösung her und zeigen, dass die Korrekturen zur Molekularfeldtheorie die führende Ordnung der confinement-induced resonance beinhalten. Zusätzlich verwenden wir ein Modellsystem in einer harmonischen Falle um die Grenzen der lokalen Dichtenäherung aufzuzeigen. Die Ergebnisse dieses Kapitels entstanden aus einer Zusammenarbeit mit Dmitry Petrov und Luis Sanots.
- In Kapitel 6 verwenden wir einen effektiven Hamiltonian für ein dipolares Bose Gas, der die Korrekturen zur Molekularfeldtheorie in der lokalen Dichtenäherung beinhaltet, um das Anregungsspektrum beim Übergang vom Suprafluid zum Supraosolid in einer eindimensionalen Geometrie zu untersuchen. Wir zeigen, dass das Anregungsspektrum stabil ist und zwei Goldstone Anregungen sowie eine Higgs Anregung für niedrige Energien aufweist. Unsere Resultate deuten darauf hin, dass ein experimentell realisierbarer Parameterbereich existiert, in dem das Supraosolid sowohl ein stabiles Anregungsspektrum aufweist und es sich zudem um einen Phasenübergang zweiter Ordnung handelt, welcher durch die Rotoninstabilität getrieben wird.

- In Kapitel 7 untersuchen wir den Einfluss von Quantenfluktuationen auf die Bildung des eindimensionalen Suprasolids. Unsere Analyse basiert auf einer effektiven Niedrigenergie-Beschreibung des Suprasolids, welche die beiden gekoppelten Goldstone Moden miteinbezieht. Wir zeigen, dass in einer Dimension der Phasenübergang vom Suprafluid zum Suprasolid im Vergleich zur lokalen Entstehung einer periodischen Struktur verschoben ist. Wir zeigen aber auch, dass diese Verschiebung des Phasenübergangs für momentane experimentelle Parameter sehr klein ist, sodass die Nutzung der erweiterten Gross-Pitaevskii gerechtfertigt ist. Die Ergebnisse dieses Kapitel entstanden aus einer Zusammenarbeit mit Chris Bühler.
- In Kapitel 8 stellen wir die Grundideen zweier nicht beendeter Projekte vor, welche weitere numerische Untersuchungen benötigen. Im ersten Teil leiten wir einen Formalismus her der es ermöglicht die Korrekturen zur Molekularfeldtheorie für einen selbst-gebundenen Zustand zu bestimmen. Im zweiten Teil stellen wir die Verbindung zwischen den Parametern des Hubbard Modells und der mikroskopischen Streulänge her und beziehen dabei den Einfluss der confinement-induced resonance mit ein.

Bibliography

[1] Bose, Plancks Gesetz und Lichtquantenhypothese, *Zeitschrift für Physik* **26**, 178–181 (1924).

[2] Einstein, A., Quantentheorie des einatomigen idealen gases, *Sitzungsberichte der Preußischen Akademie der Wissenschaften*, 237–244 (1924).

[3] Einstein, A., Quantentheorie des einatomigen idealen gases: Zweite Abhandlung, *Sitzungsberichte der Preußischen Akademie der Wissenschaften*, 245–257 (1925).

[4] Bogoliubov, N., On the theory of superfluidity, *J. Phys* **11**, 23 (1947).

[5] Beliaev, S., Application of the methods of quantum field theory to a system of bosons, *Sov. Phys. JETP* **7**, 289–299 (1958).

[6] Beliaev, S., Energy spectrum of a non-ideal Bose gas, *Sov. Phys. JETP* **34**, 299 (1958).

[7] Hugenholtz, N.M. and Pines, D., Ground-State Energy and Excitation Spectrum of a System of Interacting Bosons, *Phys. Rev.* **116**, 489–506 (1959).

[8] Gross, E.P., Structure of a quantized vortex in boson systems, *Il Nuovo Cimento* **20**, 454–477 (1961).

[9] Pitaevskii, L.P., Vortex lines in an imperfect Bose gas, *Sov. Phys. JETP* **13**, 451–454 (1961).

[10] Phillips, W.D., Nobel Lecture: Laser cooling and trapping of neutral atoms, *Rev. Mod. Phys.* **70**, 721–741 (1998).

[11] Chu, S., Nobel Lecture: The manipulation of neutral particles, *Rev. Mod. Phys.* **70**, 685–706 (1998).

[12] Cohen-Tannoudji, C.N., Nobel Lecture: Manipulating atoms with photons, *Rev. Mod. Phys.* **70**, 707–719 (1998).

[13] Anderson, M.H., Ensher, J.R., Matthews, M.R., Wieman, C.E., and Cornell, E.A., Observation of Bose-Einstein Condensation in a Dilute Atomic Vapor, *Science* **269**, 198–201 (1995).

[14] Davis, K.B., Mewes, M.O., Andrews, M.R., van Druten, N.J., Durfee, D.S., Kurn, D.M., and Ketterle, W., Bose-Einstein Condensation in a Gas of Sodium Atoms, *Phys. Rev. Lett.* **75**, 3969–3973 (1995).

[15] Bloch, I., Dalibard, J., and Zwerger, W., Many-body physics with ultracold gases, *Rev. Mod. Phys.* **80**, 885–964 (2008).

[16] Courteille, P., Freeland, R.S., Heinzen, D.J., van Abeelen, F.A., and Verhaar, B.J., Observation of a Feshbach Resonance in Cold Atom Scattering, *Phys. Rev. Lett.* **81**, 69–72 (1998).

[17] Inouye, S., Andrews, M.R., Stenger, J., Miesner, H.J., Stamper-Kurn, D.M., and Ketterle, W., Observation of Feshbach resonances in a Bose–Einstein condensate, *Nature* **392**, 151–154 (1998).

[18] Chin, C., Grimm, R., Julienne, P., and Tiesinga, E., Feshbach resonances in ultracold gases, *Rev. Mod. Phys.* **82**, 1225–1286 (2010).

[19] Andrews, M.R., Townsend, C.G., Miesner, H.J., Durfee, D.S., Kurn, D.M., and Ketterle, W., Observation of Interference Between Two Bose Condensates, *Science* **275**, 637–641 (1997).

[20] Madison, K.W., Chevy, F., Wohlleben, W., and Dalibard, J., Vortex Formation in a Stirred Bose-Einstein Condensate, *Phys. Rev. Lett.* **84**, 806–809 (2000).

[21] Tonks, L., The Complete Equation of State of One, Two and Three-Dimensional Gases of Hard Elastic Spheres, *Phys. Rev.* **50**, 955–963 (1936).

[22] Girardeau, M., Relationship between Systems of Impenetrable Bosons and Fermions in One Dimension, *J. Math. Phys.* **1**, 516–523 (1960).

[23] Paredes, B., Widera, A., Murg, V., Mandel, O., Fölling, S., Cirac, I., Shlyapnikov, G.V., Hänsch, T.W., and Bloch, I., Tonks–Girardeau gas of ultracold atoms in an optical lattice, *Nature* **429**, 277–281 (2004).

[24] Kinoshita, T., Wenger, T., and Weiss, D.S., Observation of a One-Dimensional Tonks-Girardeau Gas, *Science* **305**, 1125–1128 (2004).

[25] Greiner, M., Mandel, O., Esslinger, T., Hänsch, T.W., and Bloch, I., Quantum phase transition from a superfluid to a Mott insulator in a gas of ultracold atoms, *Nature* **415**, 39–44 (2002).

[26] Jaksch, D., Bruder, C., Cirac, J.I., Gardiner, C.W., and Zoller, P., Cold Bosonic Atoms in Optical Lattices, *Phys. Rev. Lett.* **81**, 3108–3111 (1998).

[27] Jaksch, D. and Zoller, P., The cold atom Hubbard toolbox, *Ann. Phys.* **315**, 52–79 (2005).

[28] Lewenstein, M., Sanpera, A., Ahufinger, V., Damski, B., Sen(De), A., and Sen, U., Ultracold atomic gases in optical lattices: mimicking condensed matter physics and beyond, *Adv. Phys.* **56**, 243–379 (2007).

[29] Bloch, I., Dalibard, J., and Nascimbène, S., Quantum simulations with ultracold quantum gases, *Nat. Phys.* **8**, 267–276 (2012).

[30] Cronin, A.D., Schmiedmayer, J., and Pritchard, D.E., Optics and interferometry with atoms and molecules, *Rev. Mod. Phys.* **81**, 1051–1129 (2009).

[31] Bongs, K., Holynski, M., Vovrosh, J., Bouyer, P., Condon, G., Rasel, E., Schubert, C., Schleich, W.P., and Roura, A., Author Correction: Taking atom interferometric quantum sensors from the laboratory to real-world applications, *Nature Reviews Physics* **3**, 814–814 (2021).

[32] Hartwig, J., Abend, S., Schubert, C., Schlippert, D., Ahlers, H., Posso-Trujillo, K., Gaaloul, N., Ertmer, W., and Rasel, E.M., Testing the universality of free fall with rubidium and ytterbium in a very large baseline atom interferometer, *New J. Phys.* **17**, 035011 (2015).

[33] Lachmann, M.D., Ahlers, H., Becker, D., Dinkelaker, A.N., Grosse, J., Hellmig, O., Müntinga, H., Schkolnik, V., Seidel, S.T., Wendrich, T., Wenzlawski, A., Carrick, B., Gaaloul, N., Lüdtke, D., Braxmaier, C., Ertmer, W., Krutzik, M., Lämmerzahl, C., Peters, A., Schleich, W.P., Sengstock, K., Wicht, A., Windpassinger, P., and Rasel, E.M., Ultracold atom interferometry in space, *Nat. Commun.* **12** (2021).

[34] Aveline, D.C., Williams, J.R., Elliott, E.R., Dutenhoffer, C., Kellogg, J.R., Kohel, J.M., Lay, N.E., Oudrhiri, K., Shotwell, R.F., Yu, N., and Thompson, R.J., Observation of Bose–Einstein condensates in an Earth-orbiting research lab, *Nature* **582**, 193–197 (2020).

[35] Yi, S. and You, L., Trapped atomic condensates with anisotropic interactions, *Phys. Rev. A* **61**, 041604 (2000).

[36] Yi, S. and You, L., Trapped condensates of atoms with dipole interactions, *Phys. Rev. A* **63**, 053607 (2001).

[37] Lahaye, T., Menotti, C., Santos, L., Lewenstein, M., and Pfau, T., The physics of dipolar bosonic quantum gases, *Rep. Prog. Phys.* **72**, 126401 (2009).

[38] Baranov, M., Theoretical progress in many-body physics with ultracold dipolar gases, *Phys Rep* **464**, 71–111 (2008).

[39] Chomaz, L., Ferrier-Barbut, I., Ferlaino, F., Laburthe-Tolra, B., Lev, B.L., and Pfau, T., Dipolar physics: a review of experiments with magnetic quantum gases, *Rep. Prog. Phys.* **86**, 026401 (2023).

[40] Böttcher, F., Schmidt, J.N., Hertkorn, J., Ng, K.S.H., Graham, S.D., Guo, M., Langen, T., and Pfau, T., New states of matter with fine-tuned interactions: quantum droplets and dipolar supersolids, *Rep. Prog. Phys.* **84**, 012403 (2021).

[41] Griesmaier, A., Werner, J., Hensler, S., Stuhler, J., and Pfau, T., Bose-Einstein Condensation of Chromium, *Phys. Rev. Lett.* **94**, 160401 (2005).

[42] Aikawa, K., Frisch, A., Mark, M., Baier, S., Rietzler, A., Grimm, R., and Ferlaino, F., Bose-Einstein Condensation of Erbium, *Phys. Rev. Lett.* **108**, 210401 (2012).

[43] Lu, M., Burdick, N.Q., Youn, S.H., and Lev, B.L., Strongly Dipolar Bose-Einstein Condensate of Dysprosium, *Phys. Rev. Lett.* **107**, 190401 (2011).

[44] Kadau, H., Schmitt, M., Wenzel, M., Wink, C., Maier, T., Ferrier-Barbut, I., and Pfau, T., Observing the Rosensweig instability of a quantum ferrofluid, *Nature* **530**, 194 (2016).

[45] Ferrier-Barbut, I., Kadau, H., Schmitt, M., Wenzel, M., and Pfau, T., Observation of Quantum Droplets in a Strongly Dipolar Bose Gas, *Phys. Rev. Lett.* **116**, 215301 (2016).

[46] Ferrier-Barbut, I., Schmitt, M., Wenzel, M., Kadau, H., and Pfau, T., Liquid quantum droplets of ultracold magnetic atoms, *J. Phys. B: At., Mol. Opt. Phys.* **49**, 214004 (2016).

[47] Böttcher, F., Wenzel, M., Schmidt, J.N., Guo, M., Langen, T., Ferrier-Barbut, I., Pfau, T., Bombín, R., Sánchez-Baena, J., Boronat, J., and Mazzanti, F., Dilute dipolar quantum droplets beyond the extended Gross-Pitaevskii equation, *Phys. Rev. Research* **1**, 033088 (2019).

[48] Chomaz, L., Baier, S., Petter, D., Mark, M.J., Wächtler, F., Santos, L., and Ferlaino, F., Quantum-Fluctuation-Driven Crossover from a Dilute Bose-Einstein Condensate to a Macrodroplet in a Dipolar Quantum Fluid, *Phys. Rev. X* **6**, 041039 (2016).

[49] Petrov, D.S., Quantum Mechanical Stabilization of a Collapsing Bose-Bose Mixture, *Phys. Rev. Lett.* **115**, 155302 (2015).

[50] Cabrera, C.R., Tanzi, L., Sanz, J., Naylor, B., Thomas, P., Cheiney, P., and Tarruell, L., Quantum liquid droplets in a mixture of Bose-Einstein condensates, *Science* **359**, 301 (2017).

[51] Semeghini, G., Ferioli, G., Masi, L., Mazzinghi, C., Wolswijk, L., Minardi, F., Modugno, M., Modugno, G., Inguscio, M., and Fattori, M., Self-Bound Quantum Droplets of Atomic Mixtures in Free Space, *Phys. Rev. Lett.* **120**, 235301 (2018).

[52] Lee, T.D. and Yang, C.N., Many-Body Problem in Quantum Mechanics and Quantum Statistical Mechanics, *Phys. Rev.* **105**, 1119–1120 (1957).

[53] Lee, T.D., Huang, K., and Yang, C.N., Eigenvalues and Eigenfunctions of a Bose System of Hard Spheres and Its Low-Temperature Properties, *Phys. Rev.* **106**, 1135–1145 (1957).

[54] Lima, A.R.P. and Pelster, A., Beyond mean-field low-lying excitations of dipolar Bose gases, *Phys. Rev. A* **86**, 063609 (2012).

[55] Lopes, R., Eigen, C., Navon, N., Clément, D., Smith, R.P., and Hadzibabic, Z., Quantum Depletion of a Homogeneous Bose-Einstein Condensate, *Phys. Rev. Lett.* **119**, 190404 (2017).

[56] Navon, N., Piatecki, S., Günter, K., Rem, B., Nguyen, T.C., Chevy, F., Krauth, W., and Salomon, C., Dynamics and Thermodynamics of the Low-Temperature Strongly Interacting Bose Gas, *Phys. Rev. Lett.* **107**, 135301 (2011).

[57] Steinhauer, J., Ozeri, R., Katz, N., and Davidson, N., Excitation Spectrum of a Bose-Einstein Condensate, *Phys. Rev. Lett.* **88**, 120407 (2002).

[58] Lopes, R., Eigen, C., Barker, A., Viebahn, K.G., de Saint-Vincent, M.R., Navon, N., Hadzibabic, Z., and Smith, R.P., Quasiparticle Energy in a Strongly Interacting Homogeneous Bose-Einstein Condensate, *Phys. Rev. Lett.* **118**, 210401 (2017).

[59] Schmitt, M., Wenzel, M., Böttcher, F., Ferrier-Barbut, I., and Pfau, T., Self-bound droplets of a dilute magnetic quantum liquid, *Nature* **539**, 259 (2016).

[60] Wächtler, F. and Santos, L., Ground-state properties and elementary excitations of quantum droplets in dipolar Bose-Einstein condensates, *Phys. Rev. A* **94**, 043618 (2016).

[61] Baillie, D., Wilson, R.M., Bisset, R.N., and Blakie, P.B., Self-bound dipolar droplet: A localized matter wave in free space, *Phys. Rev. A* **94**, 021602 (2016).

[62] Baillie, D., Wilson, R.M., and Blakie, P.B., Collective Excitations of Self-Bound Droplets of a Dipolar Quantum Fluid, *Phys. Rev. Lett.* **119**, 255302 (2017).

[63] Cinti, F., Cappellaro, A., Salasnich, L., and Macrì, T., Superfluid Filaments of Dipolar Bosons in Free Space, *Phys. Rev. Lett.* **119**, 215302 (2017).

[64] Santos, L., Shlyapnikov, G.V., and Lewenstein, M., Roton-Maxon Spectrum and Stability of Trapped Dipolar Bose-Einstein Condensates, *Phys. Rev. Lett.* **90** (2003).

[65] Chomaz, L., van Bijnen, R.M.W., Petter, D., Faraoni, G., Baier, S., Becher, J.H., Mark, M.J., Wächtler, F., Santos, L., and Ferlaino, F., Observation of roton mode population in a dipolar quantum gas, *Nat. Phys.* **14**, 442–446 (2018).

[66] Petter, D., Natale, G., van Bijnen, R., Patscheider, A., Mark, M., Chomaz, L., and Ferlaino, F., Probing the Roton Excitation Spectrum of a Stable Dipolar Bose Gas, *Phys. Rev. Lett.* **122**, 183401 (2019).

[67] Landau, L., Theory of the Superfluidity of Helium II, *Phys. Rev.* **60**, 356–358 (1941).

[68] Feynman, R.P., Atomic Theory of the Two-Fluid Model of Liquid Helium, *Phys. Rev.* **94**, 262–277 (1954).

[69] Feynman, R.P. and Cohen, M., Energy Spectrum of the Excitations in Liquid Helium, *Phys. Rev.* **102**, 1189–1204 (1956).

[70] Palevsky, H., Otnes, K., and Larsson, K.E., Excitation of Rotons in Helium II by Cold Neutrons, *Phys. Rev.* **112**, 11–18 (1958).

[71] Henshaw, D.G. and Woods, A.D.B., Modes of Atomic Motions in Liquid Helium by Inelastic Scattering of Neutrons, *Phys. Rev.* **121**, 1266–1274 (1961).

[72] Wenzel, M., Böttcher, F., Langen, T., Ferrier-Barbut, I., and Pfau, T., Striped states in a many-body system of tilted dipoles, *Phys. Rev. A* **96**, 053630 (2017).

[73] Baillie, D. and Blakie, P., Droplet Crystal Ground States of a Dipolar Bose Gas, *Phys. Rev. Lett.* **121**, 195301 (2018).

[74] Roccuzzo, S.M. and Ancilotto, F., Supersolid behavior of a dipolar Bose-Einstein condensate confined in a tube, *Phys. Rev. A* **99**, 041601 (2019).

[75] Boninsegni, M. and Prokof'ev, N.V., Colloquium: Supersolids: What and where are they?, *Rev. Mod. Phys.* **84**, 759–776 (2012).

[76] Penrose, O., CXXXVI. On the quantum mechanics of helium II, *The London, Edinburgh, and Dublin Philosophical Magazine and Journal of Science* **42**, 1373–1377 (1951).

[77] Penrose, O. and Onsager, L., Bose-Einstein Condensation and Liquid Helium, *Phys. Rev.* **104**, 576–584 (1956).

[78] Mermin, N.D. and Wagner, H., Absence of Ferromagnetism or Antiferromagnetism in One- or Two-Dimensional Isotropic Heisenberg Models, *Phys. Rev. Lett.* **17**, 1133–1136 (1966).

[79] Hohenberg, P.C., Existence of Long-Range Order in One and Two Dimensions, *Phys. Rev.* **158**, 383–386 (1967).

[80] Pitaevskii, L. and Stringari, S., Uncertainty principle, quantum fluctuations, and broken symmetries, *J. Low Temp. Phys.* **85**, 377–388 (1991).

[81] Schwartz, M., Off-diagonal long-range behavior of interacting Bose systems, *Phys. Rev. B* **15**, 1399–1403 (1977).

[82] Haldane, F.D.M., Effective Harmonic-Fluid Approach to Low-Energy Properties of One-Dimensional Quantum Fluids, *Phys. Rev. Lett.* **47**, 1840–1843 (1981).

[83] Giamarchi, T., *Quantum physics in one dimension*, International series of monographs on physics, Clarendon Press, 2004.

[84] Petrov, D.S., Shlyapnikov, G.V., and Walraven, J.T.M., Regimes of Quantum Degeneracy in Trapped 1D Gases, *Phys. Rev. Lett.* **85**, 3745–3749 (2000).

[85] Bühler, C., Ilg, T., and Büchler, H.P., Quantum fluctuations in one-dimensional supersolids, *Phys. Rev. Research* **5**, 033092 (2023).

[86] Gross, E.P., Unified Theory of Interacting Bosons, *Phys. Rev.* **106**, 161–162 (1957).

[87] Gross, E., Classical theory of boson wave fields, *Ann. Phys.* **4**, 57–74 (1958).

[88] Andreev, A. and Lifshits, I., Quantum theory of defects in crystals, *Zhur Eksper Teoret Fiziki* **56**, 2057–2068 (1969).

[89] Chester, G.V., Speculations on Bose-Einstein Condensation and Quantum Crystals, *Phys. Rev. A* **2**, 256–258 (1970).

[90] Leggett, A.J., Can a Solid Be "Superfluid"?, *Phys. Rev. Lett.* **25**, 1543–1546 (1970).

[91] Prokof'ev, N., What makes a crystal supersolid?, *Adv. Phys.* **56**, 381–402 (2007).

[92] Balibar, S., The enigma of supersolidity, *Nature* **464**, 176–182 (2010).

[93] Chan, M.H.W., Hallock, R.B., and Reatto, L., Overview on Solid 4He and the Issue of Supersolidity, *J. Low Temp. Phys.* **172**, 317–363 (2013).

[94] Kim, E. and Chan, M.H.W., Probable observation of a supersolid helium phase, *Nature* **427**, 225–227 (2004).

[95] Kim, D.Y. and Chan, M.H.W., Absence of Supersolidity in Solid Helium in Porous Vycor Glass, *Phys. Rev. Lett.* **109**, 155301 (2012).

[96] Léonard, J., Morales, A., Zupancic, P., Esslinger, T., and Donner, T., Supersolid formation in a quantum gas breaking a continuous translational symmetry, *Nature* **543**, 87–90 (2017).

[97] Léonard, J., Morales, A., Zupancic, P., Donner, T., and Esslinger, T., Monitoring and manipulating Higgs and Goldstone modes in a supersolid quantum gas, *Science* **358**, 1415–1418 (2017).

[98] Li, J.R., Lee, J., Huang, W., Burchesky, S., Shteynas, B., Top, F.Ç., Jamison, A.O., and Ketterle, W., A stripe phase with supersolid properties in spin–orbit-coupled Bose–Einstein condensates, *Nature* **543**, 91–94 (2017).

[99] Tanzi, L., Lucioni, E., Famà, F., Catani, J., Fioretti, A., Gabbanini, C., Bisset, R., Santos, L., and Modugno, G., Observation of a Dipolar Quantum Gas with Metastable Supersolid Properties, *Phys. Rev. Lett.* **122**, 130405 (2019).

[100] Böttcher, F., Schmidt, J.N., Wenzel, M., Hertkorn, J., Guo, M., Langen, T., and Pfau, T., Transient Supersolid Properties in an Array of Dipolar Quantum Droplets, *Phys. Rev. X* **9** (2019).

[101] Chomaz, L., Petter, D., Ilzhöfer, P., Natale, G., Trautmann, A., Politi, C., Durastante, G., van Bijnen, R., Patscheider, A., Sohmen, M., Mark, M., and Ferlaino, F., Long-Lived and Transient Supersolid Behaviors in Dipolar Quantum Gases, *Phys. Rev. X* **9**, 021012 (2019).

[102] Nambu, Y., Quasi-Particles and Gauge Invariance in the Theory of Superconductivity, *Phys. Rev.* **117**, 648–663 (1960).

[103] Goldstone, J., Field theories with « Superconductor » solutions, *Il Nuovo Cimento* **19**, 154–164 (1961).

[104] Goldstone, J., Salam, A., and Weinberg, S., Broken Symmetries, *Phys. Rev.* **127**, 965–970 (1962).

[105] Nielsen, H. and Chadha, S., On how to count Goldstone bosons, *Nucl. Phys. B* **105**, 445–453 (1976).

[106] Guo, M., Böttcher, F., Hertkorn, J., Schmidt, J.N., Wenzel, M., Büchler, H.P., Langen, T., and Pfau, T., The low-energy Goldstone mode in a trapped dipolar supersolid, *Nature* **574**, 386–389 (2019).

[107] Tanzi, L., Roccuzzo, S., Lucioni, E., Famà, F., Fioretti, A., Gabbanini, C., Modugno, G., Recati, A., and Stringari, S., Supersolid symmetry breaking from compressional oscillations in a dipolar quantum gas, *Nature* **574**, 382–385 (2019).

[108] Tanzi, L., Maloberti, J.G., Biagioni, G., Fioretti, A., Gabbanini, C., and Modugno, G., Evidence of superfluidity in a dipolar supersolid from nonclassical rotational inertia, *Science* **371**, 1162–1165 (2021).

[109] Natale, G., van Bijnen, R.M.W., Patscheider, A., Petter, D., Mark, M.J., Chomaz, L., and Ferlaino, F., Excitation Spectrum of a Trapped Dipolar Supersolid and Its Experimental Evidence, *Phys. Rev. Lett.* **123**, 050402 (2019).

[110] Hertkorn, J., Böttcher, F., Guo, M., Schmidt, J., Langen, T., Büchler, H., and Pfau, T., Fate of the Amplitude Mode in a Trapped Dipolar Supersolid, *Phys. Rev. Lett.* **123** (2019).

[111] Zhang, Y.C., Maucher, F., and Pohl, T., Supersolidity around a Critical Point in Dipolar Bose-Einstein Condensates, *Phys. Rev. Lett.* **123**, 015301 (2019).

[112] Kora, Y. and Boninsegni, M., Patterned Supersolids in Dipolar Bose Systems, *J. Low Temp. Phys.* **197**, 337–347 (2019).

[113] Roccuzzo, S., Gallemí, A., Recati, A., and Stringari, S., Rotating a Supersolid Dipolar Gas, *Phys. Rev. Lett.* **124**, 045702 (2020).

[114] Gallemí, A., Roccuzzo, S.M., Stringari, S., and Recati, A., Quantized vortices in dipolar supersolid Bose-Einstein-condensed gases, *Phys. Rev. A* **102**, 023322 (2020).

[115] Blakie, P.B., Baillie, D., Chomaz, L., and Ferlaino, F., Supersolidity in an elongated dipolar condensate, *Phys. Rev. Research* **2**, 043318 (2020).

[116] Zhang, Y.C., Pohl, T., and Maucher, F., Phases of supersolids in confined dipolar Bose-Einstein condensates, *Phys. Rev. A* **104**, 013310 (2021).

[117] Ancilotto, F., Barranco, M., Pi, M., and Reatto, L., Vortex properties in the extended supersolid phase of dipolar Bose-Einstein condensates, *Phys. Rev. A* **103**, 033314 (2021).

[118] Hertkorn, J., Schmidt, J.N., Guo, M., Böttcher, F., Ng, K., Graham, S., Uerlings, P., Büchler, H., Langen, T., Zwierlein, M., and Pfau, T., Supersolidity in Two-Dimensional Trapped Dipolar Droplet Arrays, *Phys. Rev. Lett.* **127**, 155301 (2021).

[119] Hertkorn, J., Schmidt, J.N., Guo, M., Böttcher, F., Ng, K.S.H., Graham, S.D., Uerlings, P., Langen, T., Zwierlein, M., and Pfau, T., Pattern formation in quantum ferrofluids: From supersolids to superglasses, *Phys. Rev. Research* **3**, 033125 (2021).

[120] Poli, E., Bland, T., Politi, C., Klaus, L., Norcia, M.A., Ferlaino, F., Bisset, R.N., and Santos, L., Maintaining supersolidity in one and two dimensions, *Phys. Rev. A* **104**, 063307 (2021).

[121] Roccuzzo, S.M., Recati, A., and Stringari, S., Moment of inertia and dynamical rotational response of a supersolid dipolar gas, *Phys. Rev. A* **105**, 023316 (2022).

[122] Roccuzzo, S.M., Stringari, S., and Recati, A., Supersolid edge and bulk phases of a dipolar quantum gas in a box, *Phys. Rev. Research* **4**, 013086 (2022).

[123] Sánchez-Baena, J., Politi, C., Maucher, F., Ferlaino, F., and Pohl, T., Heating a dipolar quantum fluid into a solid, *Nat. Commun.* **14** (2023).

[124] Šindik, M., Recati, A., Roccuzzo, S.M., Santos, L., and Stringari, S., Creation and robustness of quantized vortices in a dipolar supersolid when crossing the superfluid-to-supersolid transition, *Phys. Rev. A* **106**, l061303 (2022).

[125] Bombin, R., Boronat, J., and Mazzanti, F., Dipolar Bose Supersolid Stripes, *Phys. Rev. Lett.* **119**, 250402 (2017).

[126] Bombín, R., Mazzanti, F., and Boronat, J., Berezinskii-Kosterlitz-Thouless transition in two-dimensional dipolar stripes, *Phys. Rev. A* **100**, 063614 (2019).

[127] Smith, J.C., Baillie, D., and Blakie, P.B., Supersolidity and crystallization of a dipolar Bose gas in an infinite tube, *Phys. Rev. A* **107**, 033301 (2023).

[128] Ilg, T. and Büchler, H.P., Ground-state stability and excitation spectrum of a one-dimensional dipolar supersolid, *Phys. Rev. A* **107**, 013314 (2023).

[129] Norcia, M.A., Politi, C., Klaus, L., Poli, E., Sohmen, M., Mark, M.J., Bisset, R.N., Santos, L., and Ferlaino, F., Two-dimensional supersolidity in a dipolar quantum gas, *Nature* **596**, 357–361 (2021).

[130] Bland, T., Poli, E., Politi, C., Klaus, L., Norcia, M., Ferlaino, F., Santos, L., and Bisset, R., Two-Dimensional Supersolid Formation in Dipolar Condensates, *Phys. Rev. Lett.* **128**, 195302 (2022).

[131] Landau, L. and Lifshitz, E., *Quantum Mechanics: Non-Relativistic Theory*, Course of theoretical physics, Elsevier Science, 1991.

[132] Weiner, J., Bagnato, V.S., Zilio, S., and Julienne, P.S., Experiments and theory in cold and ultracold collisions, *Rev. Mod. Phys.* **71**, 1–85 (1999).

[133] Claussen, N.R., Kokkelmans, S.J.J.M.F., Thompson, S.T., Donley, E.A., Hodby, E., and Wieman, C.E., Very-high-precision bound-state spectroscopy near a ^{85}Rb Feshbach resonance, *Phys. Rev. A* **67**, 060701 (2003).

[134] Feshbach, H., Unified theory of nuclear reactions, *Ann. Phys.* **5**, 357–390 (1958).

[135] Feshbach, H., A unified theory of nuclear reactions. II, *Ann. Phys.* **19**, 287–313 (1962).

[136] Fano, U., Sullo spettro di assorbimento dei gas nobili presso il limite dello spettro d'arco, *Il Nuovo Cimento* **12**, 154–161 (1935).

[137] Fano, U., Effects of Configuration Interaction on Intensities and Phase Shifts, *Phys. Rev.* **124**, 1866–1878 (1961).

[138] Petrov, D.S. and Shlyapnikov, G.V., Interatomic collisions in a tightly confined Bose gas, *Phys. Rev. A* **64**, 012706 (2001).

[139] Wódkiewicz, K., Fermi pseudopotential in arbitrary dimensions, *Phys. Rev. A* **43**, 68–76 (1991).

[140] Fermi, E., Sopra lo Spostamento per Pressione delle Righe Elevate delle Serie Spettrali, *Il Nuovo Cimento* **11**, 157–166 (1934).

[141] Fermi, E., Sul moto dei neutroni nelle sostanze idrogenate, *Ricerca Scientifica* **7**, 13–53 (1936).

[142] Breit, G., The Scattering of Slow Neutrons by Bound Protons. I. Methods of Calculation, *Phys. Rev.* **71**, 215–231 (1947).

[143] Huang, K. and Yang, C.N., Quantum-Mechanical Many-Body Problem with Hard-Sphere Interaction, *Phys. Rev.* **105**, 767–775 (1957).

[144] Blatt, J.M. and Weisskopf, V.F., *Theoretical Nuclear Physics*, Springer, 1979.

[145] Thomas, L.H., The Interaction Between a Neutron and a Proton and the Structure of H^3, *Phys. Rev.* **47**, 903–909 (1935).

[146] Köhler, T., Góral, K., and Julienne, P.S., Production of cold molecules via magnetically tunable Feshbach resonances, *Rev. Mod. Phys.* **78**, 1311–1361 (2006).

[147] Moerdijk, A.J., Verhaar, B.J., and Axelsson, A., Resonances in ultracold collisions of ^{6}Li, ^{7}Li and ^{23}Na, *Phys. Rev. A* **51**, 4852–4861 (1995).

[148] Schick, M., Two-Dimensional System of Hard-Core Bosons, *Phys. Rev. A* **3**, 1067–1073 (1971).

[149] Popov, V.N., On the theory of the superfluidity of two- and one-dimensional bose systems, *Theoret. Math. Phys.* **11**, 565–573 (1972).

[150] Cherny, A.Y. and Shanenko, A.A., Dilute Bose gas in two dimensions: Density expansions and the Gross-Pitaevskii equation, *Phys. Rev. E* **64**, 027105 (2001).

[151] Mora, C. and Castin, Y., Extension of Bogoliubov theory to quasicondensates, *Phys. Rev. A* **67**, 053615 (2003).

[152] Pricoupenko, L., Variational approach for the two-dimensional trapped Bose-Einstein condensate, *Phys. Rev. A* **70**, 013601 (2004).

[153] Astrakharchik, G.E., Boronat, J., Casulleras, J., Kurbakov, I.L., and Lozovik, Y.E., Equation of state of a weakly interacting two-dimensional Bose gas studied at zero temperature by means of quantum Monte Carlo methods, *Phys. Rev. A* **79**, 051602 (2009).

[154] Mora, C. and Castin, Y., Ground State Energy of the Two-Dimensional Weakly Interacting Bose Gas: First Correction Beyond Bogoliubov Theory, *Phys. Rev. Lett.* **102**, 180404 (2009).

[155] Lieb, E.H. and Liniger, W., Exact Analysis of an Interacting Bose Gas. I. The General Solution and the Ground State, *Phys. Rev.* **130**, 1605–1616 (1963).

[156] Lieb, E.H., Exact Analysis of an Interacting Bose Gas. II. The Excitation Spectrum, *Phys. Rev.* **130**, 1616–1624 (1963).

[157] Pines, D., Nozieres, P., and Nozieres, P., *Theory of Quantum Liquids (Advanced Book Classics)*, Westview Press, 1999.

[158] Brueckner, K.A. and Sawada, K., Bose-Einstein Gas with Repulsive Interactions: General Theory, *Phys. Rev.* **106**, 1117–1127 (1957).

[159] Ilg, T. Quantum Corrections in Cold Dipolar Gases. Master's thesis, University of Stuttgart, 2017.

[160] Wu, T.T., Ground State of a Bose System of Hard Spheres, *Phys. Rev.* **115**, 1390–1404 (1959).

[161] Fetter, A.L. and Walecka, J.D., *Quantum Theory of Many-Particle Systems*, Dover Publications, 2003.

[162] Abrikosov, A.A., *Methods of quantum field theory in statistical physics*, Dover Publications, 1975.

[163] Dickhoff, W.H., *Many-body theory exposed!*, World Scientific, 2008.

[164] Lammers, S., Boettcher, I., and Wetterich, C., Dimensional crossover of nonrelativistic bosons, *Phys. Rev. A* **93**, 063631 (2016).

[165] Olshanii, M., Atomic Scattering in the Presence of an External Confinement and a Gas of Impenetrable Bosons, *Phys. Rev. Lett.* **81**, 938–941 (1998).

[166] Pricoupenko, L., Resonant Scattering of Ultracold Atoms in Low Dimensions, *Phys. Rev. Lett.* **100**, 170404 (2008).

[167] Ferrier-Barbut, I., Wenzel, M., Böttcher, F., Langen, T., Isoard, M., Stringari, S., and Pfau, T., Scissors Mode of Dipolar Quantum Droplets of Dysprosium Atoms, *Phys. Rev. Lett.* **120**, 160402 (2018).

[168] Bisset, R.N., Wilson, R.M., Baillie, D., and Blakie, P.B., Ground-state phase diagram of a dipolar condensate with quantum fluctuations, *Phys. Rev. A* **94**, 033619 (2016).

[169] Macia, A., Sánchez-Baena, J., Boronat, J., and Mazzanti, F., Droplets of Trapped Quantum Dipolar Bosons, *Phys. Rev. Lett.* **117**, 205301 (2016).

[170] Saito, H., Path-Integral Monte Carlo Study on a Droplet of a Dipolar Bose–Einstein Condensate Stabilized by Quantum Fluctuation, *J. Phys. Soc. Jpn.* **85**, 053001 (2016).

[171] Cinti, F. and Boninsegni, M., Classical and quantum filaments in the ground state of trapped dipolar Bose gases, *Phys. Rev. A* **96**, 013627 (2017).

[172] Cheiney, P., Cabrera, C.R., Sanz, J., Naylor, B., Tanzi, L., and Tarruell, L., Bright Soliton to Quantum Droplet Transition in a Mixture of Bose-Einstein Condensates, *Phys. Rev. Lett.* **120**, 135301 (2018).

[173] Cikojević, V., Dželalija, K., Stipanović, P., Markić, L.V., and Boronat, J., Ultra-dilute quantum liquid drops, *Phys. Rev. B* **97**, 140502 (2018).

[174] Parisi, L., Astrakharchik, G., and Giorgini, S., Liquid State of One-Dimensional Bose Mixtures: A Quantum Monte Carlo Study, *Phys. Rev. Lett.* **122**, 105302 (2019).

[175] Ferioli, G., Semeghini, G., Masi, L., Giusti, G., Modugno, G., Inguscio, M., Gallemí, A., Recati, A., and Fattori, M., Collisions of Self-Bound Quantum Droplets, *Phys. Rev. Lett.* **122**, 090401 (2019).

[176] Ilg, T., Kumlin, J., Santos, L., Petrov, D.S., and Büchler, H.P., Dimensional crossover for the beyond-mean-field correction in Bose gases, *Phys. Rev. A* **98**, 051604 (2018).

[177] Zin, P., Pylak, M., Wasak, T., Gajda, M., and Idziaszek, Z., Quantum Bose-Bose droplets at a dimensional crossover, *Phys. Rev. A* **98**, 051603 (2018).

[178] Edler, D., Mishra, C., Wächtler, F., Nath, R., Sinha, S., and Santos, L., Quantum Fluctuations in Quasi-One-Dimensional Dipolar Bose-Einstein Condensates, *Phys. Rev. Lett.* **119**, 050403 (2017).

[179] Muryshev, A., Shlyapnikov, G.V., Ertmer, W., Sengstock, K., and Lewenstein, M., Dynamics of Dark Solitons in Elongated Bose-Einstein Condensates, *Phys. Rev. Lett.* **89**, 110401 (2002).

[180] Sinha, S., Cherny, A.Y., Kovrizhin, D., and Brand, J., Friction and Diffusion of Matter-Wave Bright Solitons, *Phys. Rev. Lett.* **96**, 030406 (2006).

[181] Mazets, I.E., Schumm, T., and Schmiedmayer, J., Breakdown of Integrability in a Quasi-1D Ultracold Bosonic Gas, *Phys. Rev. Lett.* **100**, 210403 (2008).

[182] Sohmen, M., Politi, C., Klaus, L., Chomaz, L., Mark, M.J., Norcia, M.A., and Ferlaino, F., Birth, Life, and Death of a Dipolar Supersolid, *Phys. Rev. Lett.* **126**, 233401 (2021).

[183] Petter, D., Patscheider, A., Natale, G., Mark, M.J., Baranov, M.A., van Bijnen, R., Roccuzzo, S.M., Recati, A., Blakie, B., Baillie, D., Chomaz, L., and Ferlaino, F., Bragg scattering of an ultracold dipolar gas across the phase transition from Bose-Einstein condensate to supersolid in the free-particle regime, *Phys. Rev. A* **104**, L011302 (2021).

[184] Biagioni, G., Antolini, N., Alaña, A., Modugno, M., Fioretti, A., Gabbanini, C., Tanzi, L., and Modugno, G., Dimensional Crossover in the Superfluid-Supersolid Quantum Phase Transition, *Phys. Rev. X* **12**, 021019 (2022).

[185] Norcia, M.A., Poli, E., Politi, C., Klaus, L., Bland, T., Mark, M.J., Santos, L., Bisset, R.N., and Ferlaino, F., Can Angular Oscillations Probe Superfluidity in Dipolar Supersolids?, *Phys. Rev. Lett.* **129**, 040403 (2022).

[186] Blakie, P.B., Baillie, D., and Pal, S., Variational theory for the ground state and collective excitations of an elongated dipolar condensate, *Commun. Theor. Phys.* **72**, 085501 (2020).

[187] Lima, A.R.P. and Pelster, A., Quantum fluctuations in dipolar Bose gases, *Phys. Rev. A* **84**, 041604 (2011).

[188] Josserand, C., Pomeau, Y., and Rica, S., Coexistence of Ordinary Elasticity and Superfluidity in a Model of a Defect-Free Supersolid, *Phys. Rev. Lett.* **98**, 195301 (2007).

[189] Josserand, C., Pomeau, Y., and Rica, S., Patterns and supersolids, *Eur. Phys. J. Special Topics* **146**, 47–61 (2007).

[190] Yoo, C.D. and Dorsey, A.T., Hydrodynamic theory of supersolids: Variational principle, effective Lagrangian, and density-density correlation function, *Phys. Rev. B* **81**, 134518 (2010).

[191] Bühler, C. Properties of a supersolid in one dimension: Study on the algebraic decay of correlation functions and the stability analysis of the supersolid phase. Master's thesis, University of Stuttgart, 2021.

[192] Kagan, Y., Prokof'ev, N.V., and Svistunov, B.V., Supercurrent stability in a quasi-one-dimensional weakly interacting Bose gas, *Phys. Rev. A* **61**, 045601 (2000).

[193] Büchler, H.P., Geshkenbein, V.B., and Blatter, G., Superfluidity versus Bloch Oscillations in Confined Atomic Gases, *Phys. Rev. Lett.* **87**, 100403 (2001).

[194] Gogolin, A.O., Nersesyan, A.A., and Tsvelik, A.M., *Bosonization and Strongly Correlated Systems*, Cambridge University Press, 2004.

[195] Tsvelik, A.M., *Quantum field theory in condensed matter physics*, Cambridge University Press, 2003.

[196] Altland, A. and Simons, B.D., *Condensed Matter Field Theory*, Cambridge University Press, 2010.

[197] Kane, C.L. and Fisher, M.P.A., Transmission through barriers and resonant tunneling in an interacting one-dimensional electron gas, *Phys. Rev. B* **46**, 15233–15262 (1992).

[198] Ghoshal, S. and Zamolodchikov, A., Boundary S matrix and boundary state in two-dimensional integrable quantum field theory, *Int. J. Modern Phys. A* **9**, 3841–3885 (1994).

[199] Fendley, P., Saleur, H., and Warner, N., Exact solution of a massless scalar field with a relevant boundary interaction, *Nucl. Phys. B* **430**, 577–596 (1994).

[200] Fendley, P., Ludwig, A.W.W., and Saleur, H., Exact Conductance through Point Contacts in the $\nu = 1/3$ Fractional Quantum Hall Effect, *Phys. Rev. Lett.* **74**, 3005–3008 (1995).

[201] Chudzinski, P., Gabay, M., and Giamarchi, T., Orbital current patterns in doped two-leg Cu-O Hubbard ladders, *Phys. Rev. B* **78**, 075124 (2008).

[202] Kundu, S. and Tripathi, V., Competing phases and critical behaviour in three coupled spinless Luttinger liquids, *New J. Phys.* **23**, 103031 (2021).

[203] Sepúlveda, N., Josserand, C., and Rica, S., Nonclassical rotational inertia fraction in a one-dimensional model of a supersolid, *Phys. Rev. B* **77**, 054513 (2008).

[204] Büchler, H.P., Microscopic Derivation of Hubbard Parameters for Cold Atomic Gases, *Phys. Rev. Lett.* **104**, 090402 (2010).

[205] Büchler, H.P., Erratum: Microscopic Derivation of Hubbard Parameters for Cold Atomic Gases [Phys. Rev. Lett. 104, 090402 (2010)], *Phys. Rev. Lett.* **108**, 069903 (2012).

[206] Winkler, K., Thalhammer, G., Lang, F., Grimm, R., Denschlag, J.H., Daley, A.J., Kantian, A., Büchler, H.P., and Zoller, P., Repulsively bound atom pairs in an optical lattice, *Nature* **441**, 853–856 (2006).

[207] Denschlag, J.H. and Daley, A.J., Exotic atom pairs: Repulsively bound states in an optical lattice, arXiv: cond-mat/0610393, (2006).

Acknowledgments

A PhD Thesis does not emerge from the vacuum, but is a result of many fortunate events in a students life which make this exciting journey possible in the first place. At least this was the case for me.

Without the opportunity to do a PhD in physics, this journey does not even begin such that first and foremost I want to thank Hans Peter Büchler. Before working on my master thesis, I intended to leave Stuttgart and work on my PhD somewhere else. Working with you Hans Peter during my master thesis completely changed my mind. From our long discussions I realized that I could learn so much from your intuition and perspective on physics, which I would hardly find anywhere else. In addition, it is not a given that a supervisor dedicates so much time for his students to support them, but still gives them space to toy around with their interests and ideas. Thus, also after my PhD, I never regretted staying in Stuttgart and I am very grateful for working in your group. Thank you!

Of course examining a thesis is a lot of work such that I want to thank Jörg Main and Tilman Pfau for taking this task. Both examiners not only made the examination possible, but also played a role in my scientific career. Thank you again Jörg for supervising me during my Bachelor thesis and I hope you can forgive me for not participating in your relativity exam. I also want to thank Tilman Pfau for many interesting and helpful discussions about dipolar quantum gases during my PhD.

For many helpful discussions about the behavior of beyond-mean-field corrections, I also want to thank Dmitry Petrov and Luis Santos. I still find it amazing how far the collaboration on this project has led us analytically.

I also want to thank Krzysztof Jachymski for taking so much time discussing scattering problems and beyond-mean-field physics during his stay in Stuttgart. These discussions really facilitated the start of my PhD. In this regard, a very special thanks also goes to Jan Kumlin, who always took time for my questions, even after leaving to Aarhus and who became a close friend over the years. I wish you the best for your scientific career!

During my time as a PhD student, I was not only lucky in having a motivating supervisor, but also to be surrounded by a group of like-minded people that were always open to discussions of any kind. For these discussions during lunch or dinner after work, I want to thank Rukmani Bai, Katharina Brechtelsbauer, Nastasia Makki, Kevin Kleinbeck, Felix Roser and Sebastian Weber. Further thanks go to our institute volleyball team "Absteigeoperator" consisting of Chris Bühler, Johannes Mögerle and Yanek Verghis. I hope you will also win future tournaments and defend our honor.

Further, I want to thank Oliver Nagel for relieving all members of the institute of so

much administrative work. I think I cannot stress enough how lucky we are in having you help keep the institute running.

Another member, which keeps the institute running, is Nicolai Lang. Thank you for taking so much care of our IT infrastructure and the many excellent seminar talks in which you managed to explain extremely challenging topics in a way that made them seem simple.

During the past years, I could always rely on friends and family to balance my work. Therefore, I want to thank all of my friends and family for their support. In particular, I could always count on Artur Skjlarow, Sascha Polatkan, and Desirée Rausch if I needed help in any form. In addition, I want to thank Gabi and Dieter for their support and guidance. My final thanks go to my parents Elke and Roland, which never doubted any of my decisions and provided unconditional support throughout my life.